Synthesis and structure-stability relationship of aromatic helical foldamers

Christos Tsiamantas

université de BORDEAUX

THÈSE PRÉSENTÉE

POUR OBTENIR LE GRADE DE

DOCTEUR DE

L'UNIVERSITÉ DE BORDEAUX

ÉCOLE DOCTORALE DES SCIENCES CHIMIQUES

SPÉCIALITÉ CHIMIE ORGANIQUE

Par Christos TSIAMANTAS

Synthesis and structure-stability relationship of Aromatic Helical Foldamers

Sous la direction de : Ivan HUC
(co-directeur : Victor MAURIZOT)

Soutenue le 20 janvier 2015

Membres du jury :

M. TAILLEFUMIER Claude, Professeur, Université Blaise Pascal, Clermont-Ferrand	Président
Mme PALMANS Anja, Professeur associée, Eindhoven University of Technology, Pays-Bas	Rapporteur
M. BARBOIU Mihai, Directeur de recherche CNRS, Université de Montpellier	Rapporteur
M. HUC Ivan, Directeur de recherche CNRS, Université de Bordeaux	Examinateur
M. MAURIZOT Victor, Chargé de recherche CNRS, Université de Bordeaux	Examinateur

Résumé

Les foldamères sont des oligomères artificiels possédant une architecture moléculaire repliée qui présente des similarités structurales avec les biomopolymères. Ils peuvent être composés de blocs élémentaires (monomères) naturels ou non, aliphatiques ou aromatiques. Différents motifs structuraux peuvent être obtenus en fonction de la composition de ces oligomères, le motif hélicoïdal étant le plus répandu. Les foldamères peuvent servir de systèmes modèles pour la compréhension des paramètres qui contrôlent l'architecture hélicoïdale.

Les composés étudiés dans ce manuscrit sont des foldamères aromatiques hélicoïdaux dont les unités sont connectées par des liaisons amides. En principe, quand une liaison amide est placée entre deux unités aromatiques celle-ci adopte, de par sa conjugaison, une conformation plane par rapport aux cycles adjacents. De plus lorsqu'un groupement donneur ou accepteur de liaisons hydrogène se trouve en *ortho* de la liaison amide, des interactions attractives ou répulsives conduisent à la stabilisation d'une des deux conformations possibles. Les hélices de longs oligomères sont stabilisées par un empilement aromatique supplémentaire. Dans le cas des oligomères de quinolines, ces interactions permettent la formation d'une architecture hélicoïdale prévisible et bien définie (Figure 1).

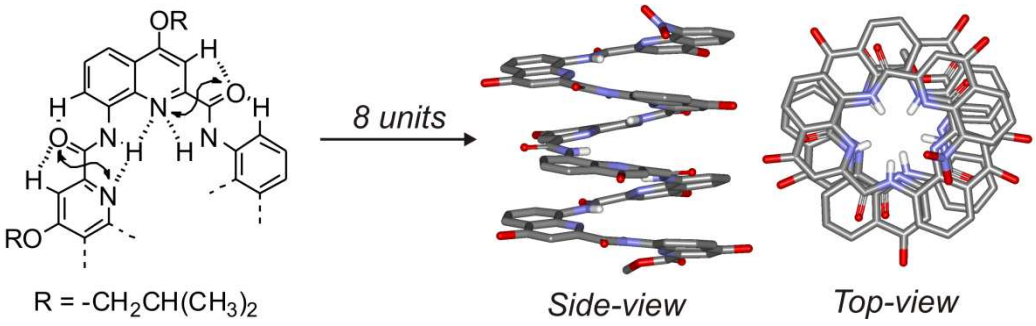

Figure 1: Conformation préférentielle locale de la liaison aryl-amide dans un oligomère de quinolines conduisant à une structure hélicoïdale (exemple de la structure d'un octamère).

Les oligoamides aromatiques ont démontré leur potentiel dans le domaine des mimes biologiques, de la reconnaissance moléculaire et des sciences des matériaux. Leur stabilité hélicoïdale en particulier a fait l'objet de plusieurs études. Notamment les études de l'influence de la longueur de l'oligomère, du solvant et de la présence dans la séquence d'unités monomériques aliphatiques sur la stabilité des hélices ont déjà été menées par notre groupe de recherche afin de mieux comprendre les facteurs influant sur la dynamique de ces systèmes. Afin de poursuivre ces études, dans le cadre de ce travail de thèse, la conception et la synthèse de nouveaux systèmes modèles a été entreprise ainsi que l'étude des paramètres

structuraux conférant son unique stabilité au système. Il est important de noter que, malgré leur grande stabilité, ces architectures hélicoïdales n'en restent pas moins dynamiques et qu'il existe un échange entre hélice droite (P) et gauche (M). Ce qui signifie que si une de ces deux hélices est séparée et isolée, elle évoluera vers un mélange équivalent (50/50) d'hélices P et M. Ce processus de racémisation nécessite le déroulement (au moins partiel) de l'architecture hélicoïdale afin de permettre le changement du sens d'hélicité. La vitesse de ce processus nous informe ainsi directement sur la stabilité de l'hélice. Cette donnée sera largement utilisée dans le reste du travail expérimental présenté dans ce manuscrit.

Le premier chapitre présente une revue sur les foldamères aromatiques avec une attention particulière pour le repliement dirigé par restrictions conformationelles (proches ou éloignées dans la séquence), notamment le cas des foldamères d'oligoamides aromatiques. Plusieurs études sur la stabilité des architectures hélicoïdales de ces composés ont été menées et sont décrites dans ce chapitre afin de présenter le contexte et les bases du travail expérimental entrepris lors de cette thèse.

Dans un premier temps de ce travail (chapitre 2) l'effet sur le repliement de cinq monomères fréquemment utilisés pour la préparation de foldamères d'oligoamides aromatiques et leur contribution dans la stabilité de l'hélice a été évalué. Ces monomères sont la 2,6-diamino-pyridine (**1**), le 1,3-diamino-benzène (**2**), le 2,6-diamino-fluorobenzène (**3**), le 2,6-diamino-chlorobenzène (**4**) et le 2,6-diamino-toluène(**5**). Les composés **1**, **3**, **4** possèdent un accepteur de liaison hydrogène dont le diamètre est différent pour chacun de ces résidus. L'unité diaminobenzène a été sélectionnée car elle ne comporte pas de conformation locale préférentielle et l'unité diaminotoluène a été choisie car elle possède un groupement encombrant méthyl pouvant créer une gêne stérique en lieu et place de l'accepteur de liaison hydrogène. Ces monomères ont été placés au milieu de la séquence de l'oligomère, entre deux blocs composés de quatre unités structurantes quinolines. Cette méthode a déjà été utilisée dans le groupe afin de déterminer la capacité de certains monomères à promouvoir la formation d'une hélice continue. Les structures cristallines des cinq composés synthétisés pour cette étude sont présentées figure 2. Les études RMN et la séparation par chromatographie dynamique (en collaboration avec l'équipe d'O. Trapp, à l'université de Heidelberg en Allemagne) nous ont permis d'obtenir des informations qualitatives et quantitatives concernant la contribution de chaque unité aromatique dans la stabilité de l'architecture hélicoïdale. La RMN nous a fourni des informations sur des processus suffisamment rapides pour être observés à l'échelle des temps de la RMN alors que la chromatographie dynamique nous informe sur des évènements plus lents pour les composés les plus stables.

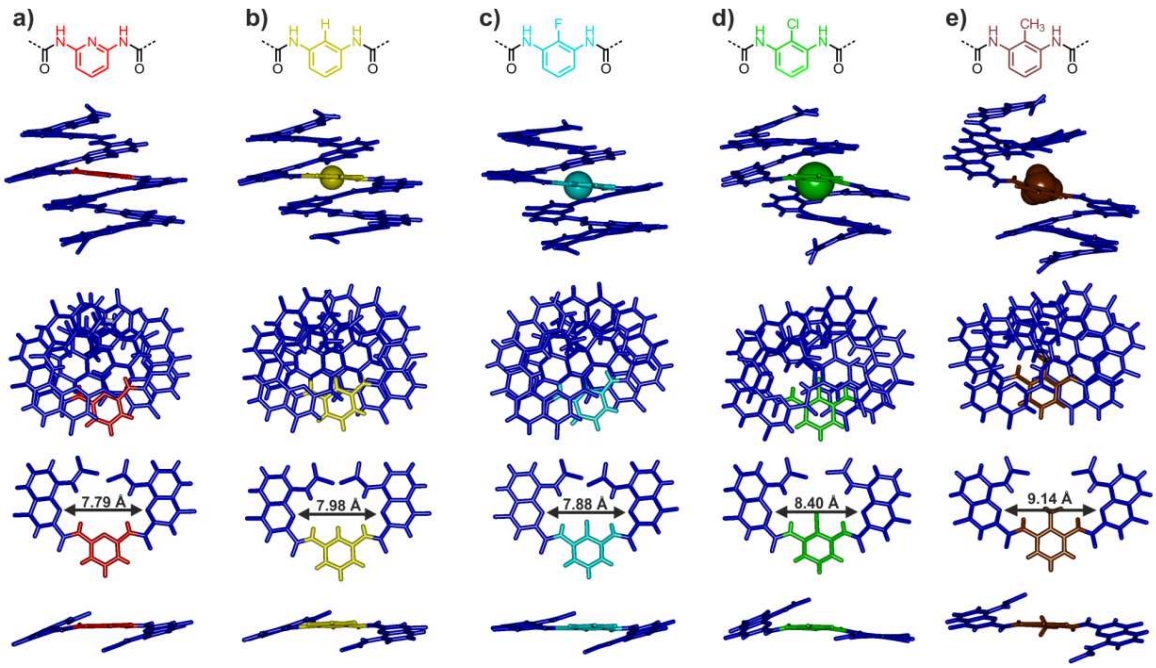

Figure 2: Structure cristalline des composés (a) **1**, (b) **2**, (c) **3**, (d) **4** and (e) **5**. De haut en bas: vue de coté de l'architecture hélicoïdale, vue du dessus, partie central de l'hélice vue de dessus et de côté.

Les résultats de ces deux techniques ont été combinés afin de déterminer la relative stabilité des cinq composés synthétisés. Ces résultats sont résumés dans le schéma 1.

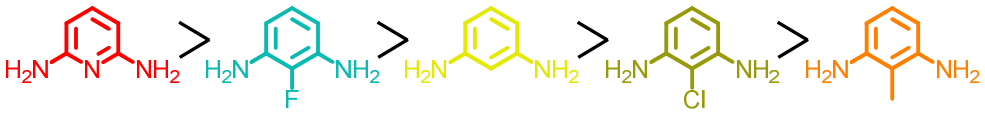

Schéma 1: Représentation de la contribution des cinq monomères dans la stabilité des foldamères d'oligoamide aromatique.

Cette étude a permis de mettre en évidence l'importance des groupements fonctionnels présents sur les unités constituant l'oligomère tels que ceux permettant la formation de liaisons hydrogène ou introduisant des restrictions conformationnelles, mais aussi la mise en évidence que l'encombrement stérique créé par ces groupements devait être pris en compte lors de la conception de telles architectures.

Dans une seconde partie de ce manuscrit (chapitre 3), inspirée par l'implication des ponts disulfure dans la structuration et la fonction des protéines naturelles, des liaisons disulfure ont été introduites à l'extérieur d'une hélice unique ou de façon à connecter deux hélices entre elles (Schéma 2). Le but de ce projet est d'évaluer l'influence d'une telle liaison sur la stabilité de l'architecture hélicoïdale.

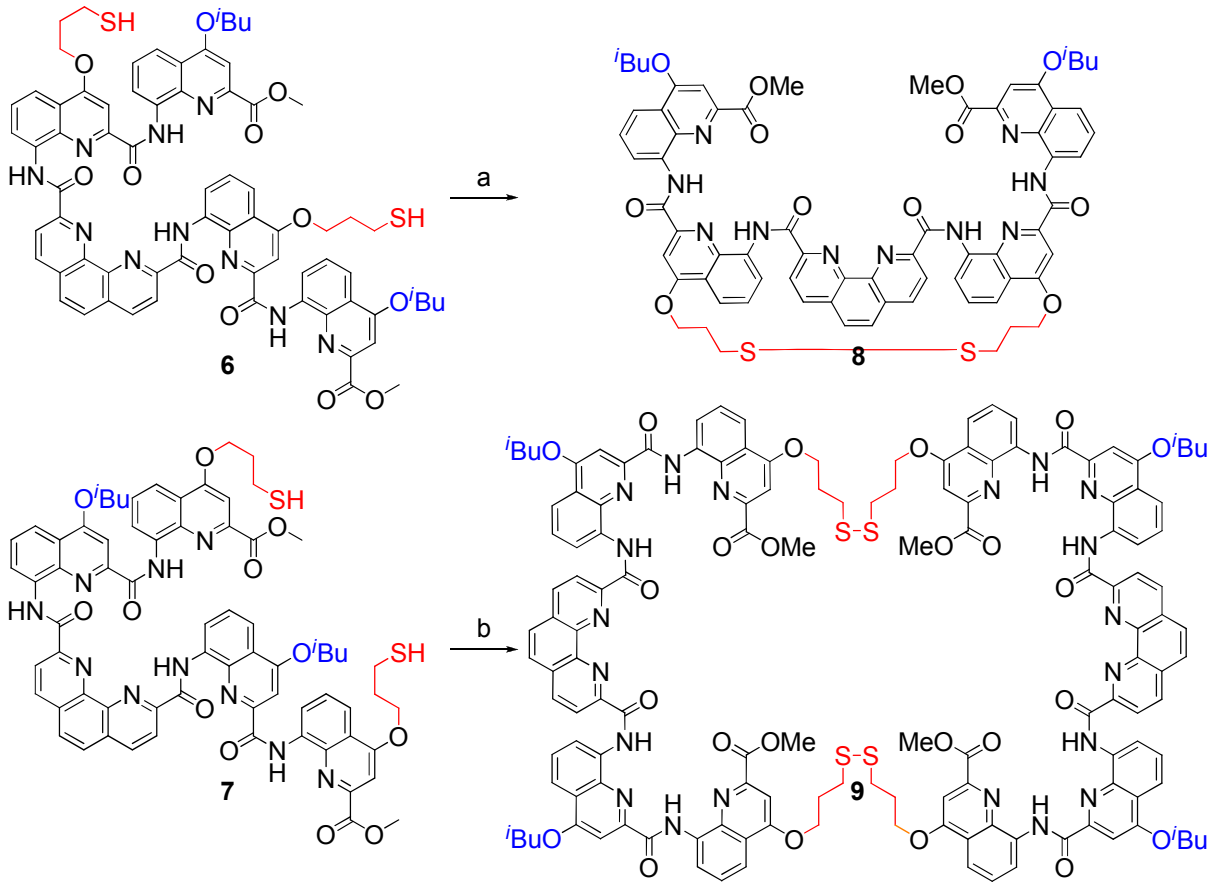

Schéma 2: 5 mM in $CHCl_3$/MeOH (8/2), DIEA (40 µL), 25 C, (a) 48 hours and (b) 72 hours

La stabilité de ces hélices a été déterminée par une méthode déjà décrite par le groupe qui consiste à séparer les deux énantiomères (P et M) et d'étudier la cinétique de racémisation. Les hélices possédant les ponts disulfures (**8** et **9**) sont ensuite comparées à leur précurseur « non ponté » (**6** et **7**) afin de déterminer l'influence de la liaison sur la stabilité du système. Les résultats obtenus indiquent que cette liaison conduit à une stabilisation pour les deux systèmes préparés possédant une connexion intra- et intermoléculaire des hélices. Il est intéressant de noter que, malgré cette rigidification, les hélices sont toujours capables d'opérer une inversion du sens de leur hélicité (tableau 1).

Tableau 1: Temps de demi-vie de racémisation des composés **8** et **9**, ainsi que leur précurseur *tert*-Bu à 30 °C

	$t_{1/2}$ (min)	
	$CHCl_3$	THF
précurseur *tert*-Bu de **6**	4	16
précurseur *tert*-Bu de **7**	4	12
Composé **8**	53	150
Composé **9**	115	ND[a]

[a] non déterminé de par sa faible solubilité

La formation du pont disulfure a été suivi par chromatographie HPLC et ne semble pas indiquer la formation d'autre composé en quantité significative ni la formation d'intermédiaire réactionnel. Il a de plus été démontré qu'il existe une communication entre les deux hélices du système possédant deux ponts disulfures, comme suggéré par HPLC chirale et cristallographie des rayons X

Dans la dernière partie du travail expérimental (Chapitre 4), la formation de fonctions anhydrides a été utilisée comme moyen de synthétiser de longues hélices polymériques. Ces anhydrides avaient précédemment été montrés comme étant résistant à l'hydrolyse une fois insérés dans une hélice. Une stratégie de « triplement de segment » a été proposée et expérimentalement validée pour produire des foldamères amides aromatiques hélicoïdaux d'une longueur de l'ordre de 10 nm en seulement deux étapes (Figure 3). Cette performance a été rendue possible par l'utilisation d'un segment nonamérique terminé par une fonction acide à chaque extrémité comme réactif de départ. Un premier triplement conduit à un segment munis de 27 unités, et un deuxième triplement à un segment de 81 unités. La caractérisation de ces composés a été effectuée par RMN, par spectrométrie de masse, et pour certains par cristallographie des rayons X.

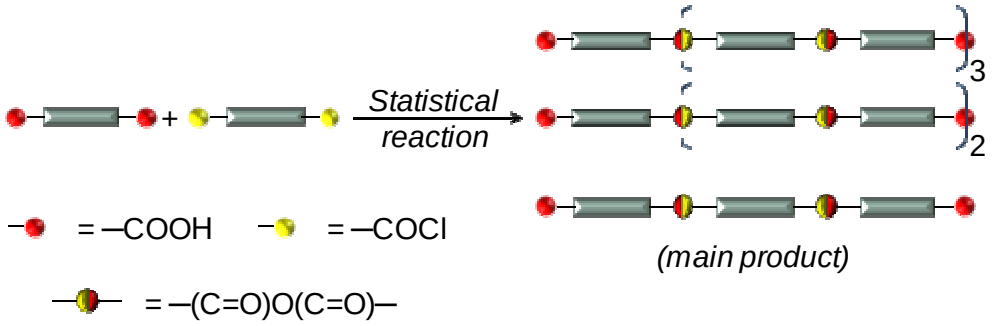

Figure 3: Représentation graphique de la stratégie de triplement de segment.

Acknowledgements

In the past three years, I have not only obtained knowledge in chemistry, but also I received help from many people without whom I could not have finished my project. I feel really grateful to my advisors, because they offer me deeper insights into the field of chemistry, to my friends, for their support throughout my studies and to my family members, because they were always by my side with their love and support.

First and foremost, I would like to offer my sincerest gratitude to my supervisors, Dr. Ivan Huc and Dr Victor Maurizot, who assisted me throughout my thesis with their care, patience and knowledge, providing me with direct and indirect lessons that led to my academic and ultimately personal growth.

I would like to thank Dr Yann Ferrand who assisted me in cultivating my team spirit and assisted me by sharing his valuable insights in relevance with my studies.

I would like to thank Dr. Brice Kauffmann and Dr. Stephan Massip (X-Ray team) for their valuable help in visualizing my work and providing me with their insights in crystallography. Additionally, I would like to thank Dr. Axelle Grélard for her assistance in NMR spectroscopy.

Special thanks to three special people given alphabetically: Dr. Simon Dawson, Dr. Michael Singleton and Dr. Krzysztof Ziach. Being both labmates and good friends, they assisted me and they stood by my side and provided me with their advices in the most difficult moments. Additionally, I would like to thank Maëlle Vallade for frienship and her assistance with the French parts of this manuscript.

I would like to thank all of the people from the Huc group, the Guichard group, the Quideau group and the Oda group for making these three years and amazing experience that finally resulted in this manuscript.

Finally, I would like to thank my family for supporting me and never losing their faith in me!

List of abbreviations

AcOH: Acetic acid

CD: Circular dichroism

COSY: Correlated spectroscopy

CPK: Corey, Pauling, Koltune space filling

DIAD: Diisopropyl azodicarboxylate

DIPEA: N,N-Diisopropylethylamine

DOSY: Diffusion ordered spectroscopy

ESI: Electrospray ionization

EtOAc: Ethyl acetate

EtOH: ethanol

Ghosez reagent: 1-chloro-N,N,2-trimethyl propenylamine

GPC: Gel permeation chromatography

HPLC: High-performance liquid chromatography

HRMS: High resolution mass spectroscopy

MALDI: matrix-assisted laser desorption/ionization

Me: methyl

MeOH: methanol

MTBE: Methyl tert-butyl ether

NMR: Nuclear magnetic resonance

NOESY: Nuclear overhauser effect spectroscopy

NPySCl: 3-nitro-2-pyridinesulfenyl chloride

O^{i}Bu: Isobutoxy

PPh$_3$: Triphenyl phosphine

ppm: parts per million

r.t.: Room temperature

TBP: Tri-*n*-butylphosphine

tBu: *tert*-butyl

THF: Tetrahydrofuran

TLC: Thin layer chromatography

Table of Contents

General Introduction

Helical patterns at the molecular level are of great interest for scientists since such architectures are often involved in delicate functions. An interesting characteristic of helical entities is that if placed in front of a mirror, they are distinguishable from their mirror images. This difference is crucial in Nature and the preference towards handedness is associated with function; α-helices in proteins, as well as the A and B form of DNA in biology, are right-handed and Z DNA left-handed. Isolation of a α-helix from a protein structure results in conformational changes that render it inactive. Principles governing the structure-stability relationship have been addressed by the field of foldamers.

Foldamers are molecular architectures that fold into conformationally ordered states and demonstrate structural and functional similarities with biopolymers. They can be composed of many different building blocks natural or not, aliphatic or aromatic. Depending on the oligomer composition they can give rise to several structural motifs, with helices being dominant. Foldamers can serve as ideal test systems to help scientists obtain better understanding on structural parameters capable of giving rise to well-defined stable helical architectures.

In the Huc group, we are particularly interested in foldamers that are composed of aromatic oligoamides; during the last years several such molecules have demonstrated great potential in the field of biomimetics, molecular recognition and materials science. Their properties in general and their helical stability in particular play a crucial role in their potential applications. For this reason several parameters affecting their stability have been extensively investigated, such as the influence of the length, the solvent effects and the presence of aliphatic monomers linkers within an aromatic sequence.

Following these earlier studies, in this thesis is described the design and syntheses of model test systems followed by investigation of the structural parameters giving rise to unique stability profiles. In particular:

- Chapter 1 consists of a short review about foldamers, with special attention paid towards conformational preferences (local or remote within the sequence) governing their folding, especially in the case of aromatic oligoamide foldamers. Several

parameters that have been investigated in the past and they were shown to affect the helical stability of these entities are also briefly reviewed to provide a better background and facilitate understanding of the experiments described in the following chapters.

- In Chapter 2, a series of aromatic oligoamide helices is presented that differ in just one monomer in the center of the helical sequence. This design is used to evaluate the helical propensity of 5 different commonly used aromatic monomers and quantify their stability.

- In Chapter 3, inspired by the contribution of disulfide bonds in the protein structure and function one covalent linkage is incorporated on the exterior of a single helix, or two of them are used to connect two helices together. The reason for this is to evaluate the ability of disulfide bonds to stabilize synthetic helical architectures.

- In Chapter 4, despite the labile nature of a carboxylic acid anhydride, we envisaged its utilization in a segment tripling strategy for the generation of helical rods of polymeric dimension, mediating head-to-head communication of the helical segments. The reported strategy is the first of its kind and it enables the synthesis of helical polymers in a limited number of synthetic steps and in a mono-disperse manner.

NB: Each chapter constitutes a distinct scientific topic and for this reason they can be considered individually. Therefore, section, figure and reference numbering are restarted in each chapter.

Chapter 1: Aromatic Helical Foldamers: A review

1. Introduction

Over the last 15 years, interest in foldamers has significantly increased due to their structural and functional characteristics that resemble closely those of biomacromolecules. A foldamer is an oligomer that folds into a conformationally ordered state due to non-covalent interactions. They can be constructed from a huge arsenal of building blocks, including α-,β-, γ-and δ-amino acids,[1-4] and can be either aliphatic or aromatic: Foldamer design can give rise to helical, turn-like and sheet-like entities.[1, 2, 4-12] Foldamers consisting of unnatural building blocks often have the ability to resist proteolytic cleavage, compared to their natural analogues; this is a feature which makes them unique and attractive candidates in the field of peptide mimetics.[2] In addition, foldamers have been successfully used in other fields, such as material- and nano-science.[13-19]

Foldamers were initially developed with the aim of mimicking the architecture of biomolecules due to their common structural characteristics. What made the field so attractive was that natural biomolecules consist of a limited number of building blocks: twenty amino acids for proteins and four nucleobases for DNA. On the other hand, foldamers can be designed and synthesized using a wider variety of building blocks only limited by the imagination. This results in an extremely large number of possible combinations (e.g. through the synthesis of hybrids). It is for this reason that foldamers have been investigated ─this arsenal of building blocks can be exploited to explore possibilities not permitted by natural monomer units.

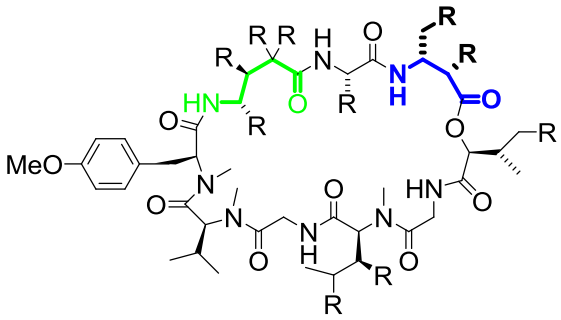

Figure 1: Structural formula of dolastatin 11. The β-peptide residue is highlighted in blue and the γ-residue in green.

During the first years, pioneers in the field were mostly interested in replacing, fully or partially, α-amino acids with their longer analogues such as β- and γ- amino acids. The introduction of such units has been observed in nature; for example in the cyclic depsipeptide dolastatin 11 (Figure 1) isolated from the sea hare (*Dolabella auricularia)*,[20] in which a β-residue and a γ-residue were incorporated within an array of α- residues. Another example in which nature operates in this way is in the case of poly-γ-D-glutamate that has been first isolated from *Bacillus anthracis*.[21, 22]

One of the earliest examples was reported by Karle *et al*. in which a cyclo-tetrapeptide consisting of an α-β-α-β motif was synthesized.[23] The purpose of this study was to explore the synthesis of cylindrical peptides through the linkage of individual cyclic 14-membered oligotetrapeptides by covalent and hydrogen bonds. In a similar manner, Balaram *et al*. thoroughly reviewed the backbone diversification resulting from the incorporation of a single extended amino acid within an α-peptide sequence.[24] It was demonstrated that higher homologues of the α-amino acid residues can be accommodated within well-folded secondary structures. It is noteworthy that even unsubstituted β-, γ- and δ-residues have the ability to adopt folded conformations when located within peptide sequences.[25, 26] This greatly enhances molecular diversity compared to the traditional approach, in which diversity is generated by varying the nature of the side chain in the α-amino acid residues. Structural elements of homologated polypeptide backbones were examined earlier and examples can be found in the 1960s and 70s.[25] It was in 1965 when it was proven that polymeric β-peptides are able to adopt stable helical conformations, even though elucidation of the precise helical geometries was not stated.[27] It was not until 1996 though, that there was a resurgence of interest towards the conformational properties of the higher homologues of α-amino acids, following the observation of well-defined helical architectures in oligopeptides.

Later on, extensive research took place and numerous examples can be found in the literature, with foldamers consisting of fully non-natural backbones or hybrids of β-/γ-amino acids being able to successfully mimic the secondary structures and functions of their natural biopolymeric analogues.[1, 4, 28-31] As an example, numerous studies have been carried out by Gellman *et al*., where it was demonstrated that conformationally rigid, cyclic residues (β-peptides), either alone or when combined with α-residues in an αβ , αββ or ααβ sequence adopt stable helical conformations. Interestingly, it was also demonstrated that slight differences in the cyclic residues of the sequence affect the adopted folding patterns (Figure 2-3).[7]

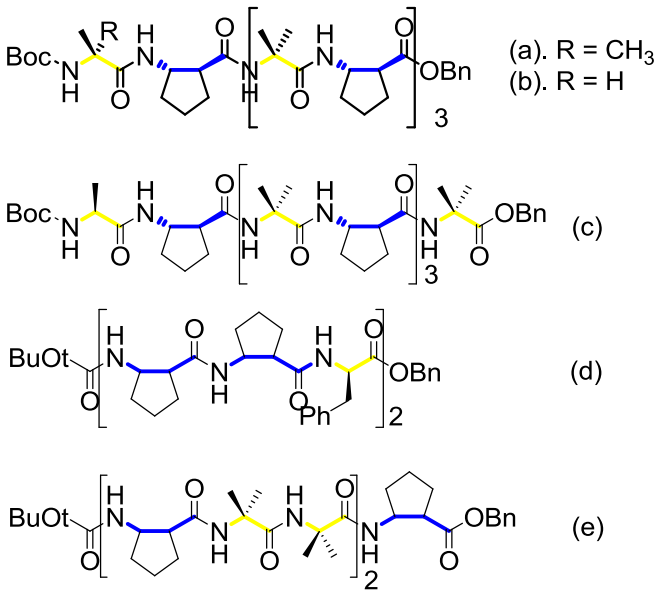

Figure 2: Structural formulas of αβ (a, b, c), αββ (d) and ααβ (e) sequences manufactured by Gellman *et al.*. α-amino acid residues are highlighted in yellow and β- in blue

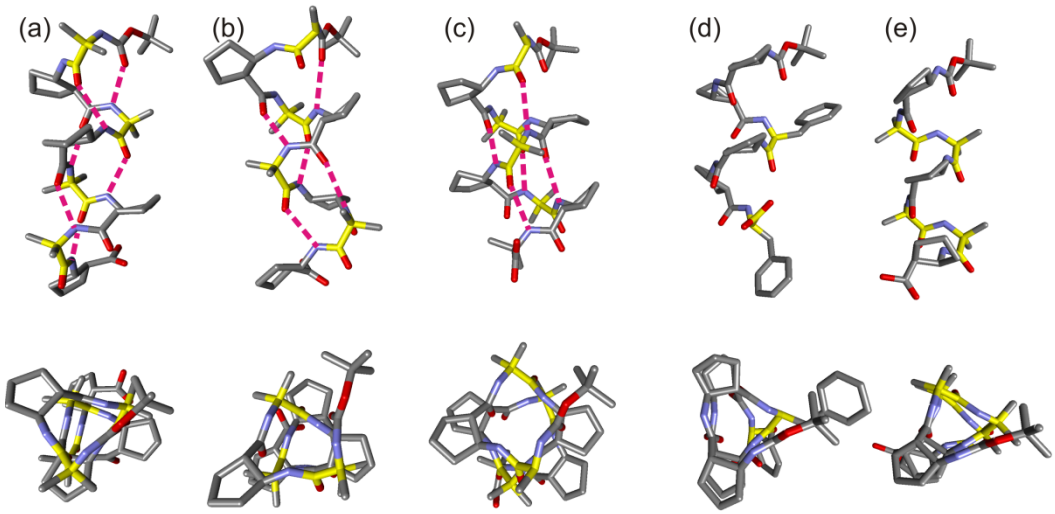

Figure 3: Crystal structures of compounds a-e presented in figure 2. There is a noteworthy change in the hydrogen bonding pattern of the *Boc* group from an $i \rightarrow i + 3$ H-bond in **a** to an $i \rightarrow i + 4$ H-bond in **b.** Some atoms have been omitted for clarity.

As mentioned before, foldamers adopt molecular architectures that resemble the secondary structures of biomolecules, such as helices, sheets and turns. Due to the huge diversity of the building blocks that can be used to design foldameric structures, the present manuscript will focus only on molecules that consist of aromatic building blocks, and especially those that form exclusively helical entities.

2. Aromatic Helical Foldamers

Helices are important structural elements which are pervasive throughout many scientific fields (Figure 4). There are countless examples of helical moieties in nature; this motif plays an important role in controlling the function of DNA and proteins, both key elements in the modulation of cellular processes.

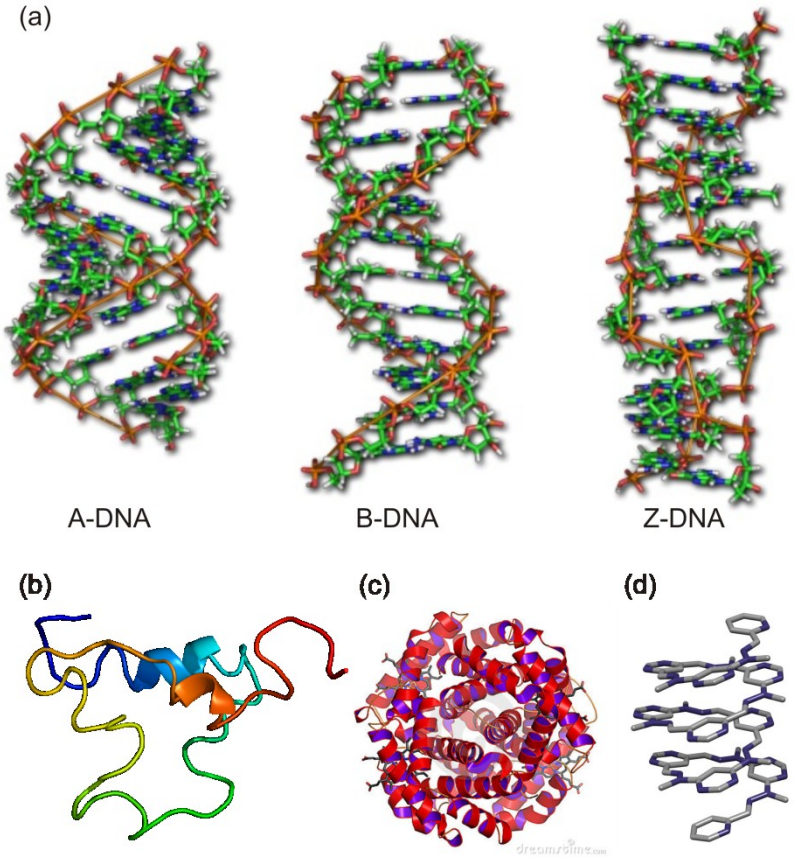

Figure 4: (a) X-ray structures of A-, B- and Z-DNA demonstrating the helical conformation adopted by the DNA strands, (b) PDB structure of IGF1 (Insulin-like growth factor 1) possessing two helical segments, (c) structure of hemoglobin composed of multiple helical segments and (d) abiotic helical architecture reported by Lehn *et al.*

Due to the large number of building blocks that a chemist can use, and the diversity of architectures rising from different combinations of these building blocks, synthetic foldamers that form helices have been thoroughly studied. As previously mentioned, only foldamers that consist of aromatic building blocks are going to be examined.

A common feature to all aromatic foldamers is a certain degree of backbone rigidity that limits the entropic cost of adopting an organized conformation. Additionally, short- and long-range intramolecular interactions can be designed to lead to the formation of well-defined helical conformations.[32] It is noteworthy that a foldamer's structure can also occur from intermolecular interactions. It has been demonstrated that the presence of guest molecules can

induce the folding of molecules that are otherwise linear, or in general have no preferential conformations. Several examples can be found in the literature representing foldamers that owe their folding propensity to host-guest interactions and some will be discussed later on in this manuscript. For ease of presentation the examples listed below are going to be divided into smaller categories depending on the main driving forces that govern their folding. However, it should be stated that foldamers may owe their folding to many different elements and in this way they fall into more than one of the below-mentioned categories.

2.1. Foldamers based on conformational restrictions

These systems are one of the simplest to understand and they are related to extreme backbone rigidity leading to a unique conformation. The first example of such a helical entity was the helicene reported in 1956 by Newman *et al*., composed of 6 aromatic rings connected in the *meta* position with each other.

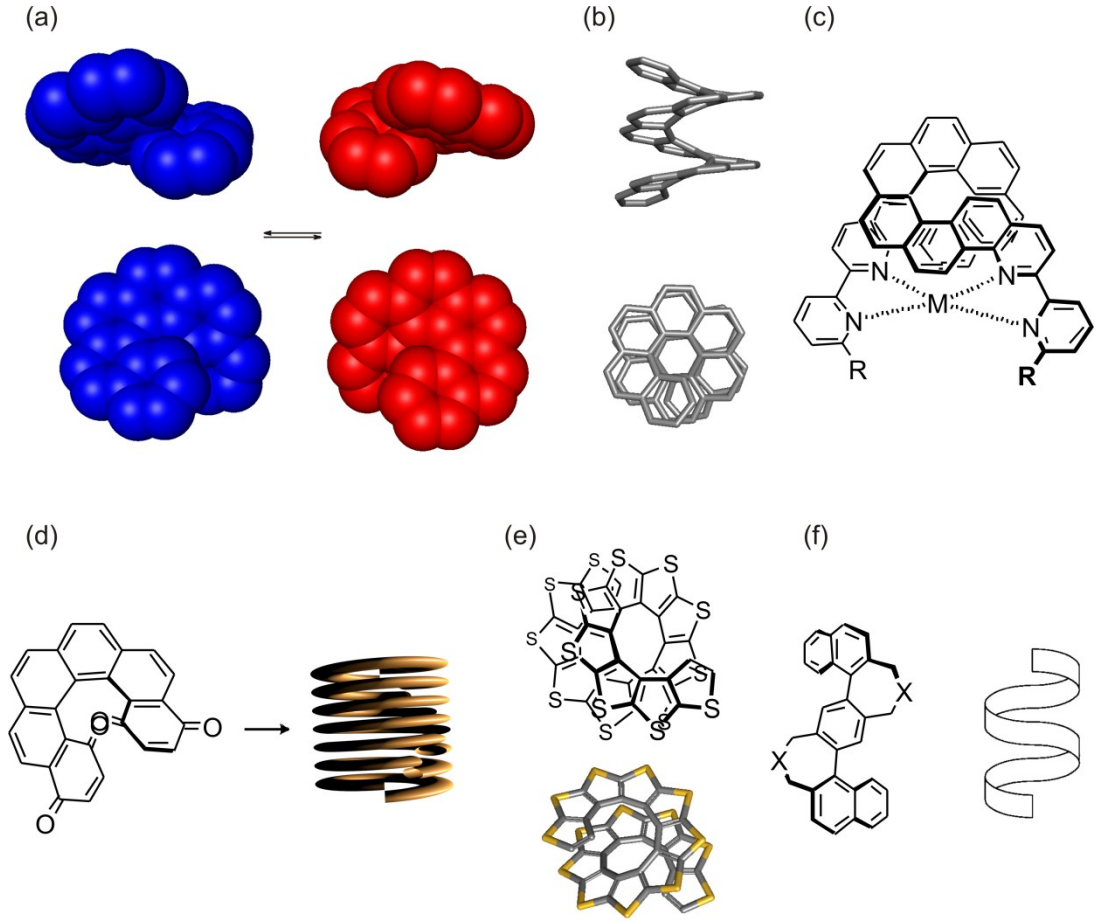

Figure 5: **Examples of foldamers based on conformational restrictions.** (a) CPK models of the two enantiomers of [6]helicene (right-handed in blue and left-handed in red) (b) model structure of [13]helicene, (c) helicopodand reported by Diederich F. *et al*., (d) self-organization of a modified helicene moiety into liquid crystals, (e) polythiophene and (f) Geländer helix.

The steric clash that occurs between the aromatic rings at both the extremities of this molecule forces it out of planarity, giving rise to a helical entity that can be found in two different interconverting enantiomeric forms, possessing opposite axial chirality (Figure 5a).[33] More efforts have been made towards such molecules and a helicene consisted of 13 consecutive aromatic rings was reported just a few years later (Figure 5b).[34] Functionalization of these helicenes by incorporation of a pre-organized cleft that is equipped with convergent coordination bond functionalities gave rise to a chiral entity that was named as helicopodand (Figure 5c).[35, 36] This name is attributed to the fact that helicopodands are nonmacrocyclic (podand) and derived from helicenes. The helicene moiety acts as a rigid backbone to form a cleft of profound asymmetric character at the end of the helical turn. Another modification was introduced by Castellanos *et al.*, in which electron poor rings were used as terminal units in the helicene entity (Figure 5d).[37, 38] The idea was based on the fact that donor-acceptor interactions between the electron rich helicene core of one molecule and electron poor external rings of another molecule could give rise to stable columnar stacks, a concept that was validated experimentally. Another diversification of the helicenes by replacing the benzene rings with thiophene rings has also been described (Figure 5e).[39] The last example of rigid covalently restricted foldamers refers to the compounds reported by Vôgtle *et al.*, also known as Geländer helices[40] which are *ortho*-bridged terphenyls. In contrast to the helicenes that resemble the shape taken by the steps of a spiral staircase, these compounds can be compared to the banisters of such a staircase, which are vertical to the steps (Figure 5f).

2.2. Foldamers based on intramolecular organisation

2.2.1. Foldamers based on close proximity interactions

This type of helical foldamers is obtained by accumulation of preferential conformations at each rotatable bond of a molecule that eventually adopts an overall helical architecture. Driving elements for the structuration of this type of foldamers are mainly electrostatic interactions which can be attractive or repulsive and/or short range π—π stacking interactions. Tanatani *et al.* have designed and synthesized oligourea and oligoguanidine foldamers[41-43] that are based on the *cis-cis* conformational preference of N-methylated urea and guanidino groups (Figure 6a). The folding of these molecules is based on the fact that *N,N′*-dimethyl-*N,N′*-diphenylurea and *N,N′*-dimethyl-*N,N′*- diphenylguanidinium bromide already form folded structures with the two phenyl groups adopting a face-to-face arrangement, both in the solid state and in solution.[44, 45] From the crystal structure it is demonstrated that these compounds have multi-layered aromatic structures possessing large dihedral angles between the benzene ring planes and the planes of the urea/guanidino functionalities. Another

noteworthy characteristic is the tilting of the benzene rings, which is attributed to repulsive, electrostatic interactions of the π electrons. Lehn *et al.* reported the formation of helical structures due to the *trans* conformational preference of 2,2-bipyridine (Figure 6b).[46, 47] As shown in figure 6 the *trans* conformation prevails for two reasons. The first is that in this conformation the endocyclic nitrogen of one ring is hydrogen bonded with the proton in position 3 of the other pyridine ring and secondly, the *cis* conformation is strongly disfavored due to repulsive interactions between the two nitrogen atoms. Expanding the idea of using azaheterocycles to induce conformational preferencesleading to helical conformations was further exploited. Helices consisting of pyridine-pyridazine, pyridine-pyrimidine and pyridine-pyrazine adopting also *trans* conformations have been reported, and characteristic examples are given below (Figure 6c, d).[48, 49] Constable *et al*. reported the synthesis of a similar foldamer consisting of oligo-(2,2'-bipyridyl)pyrazines containing 4 heterocycles per helical turn (Figure 6e).

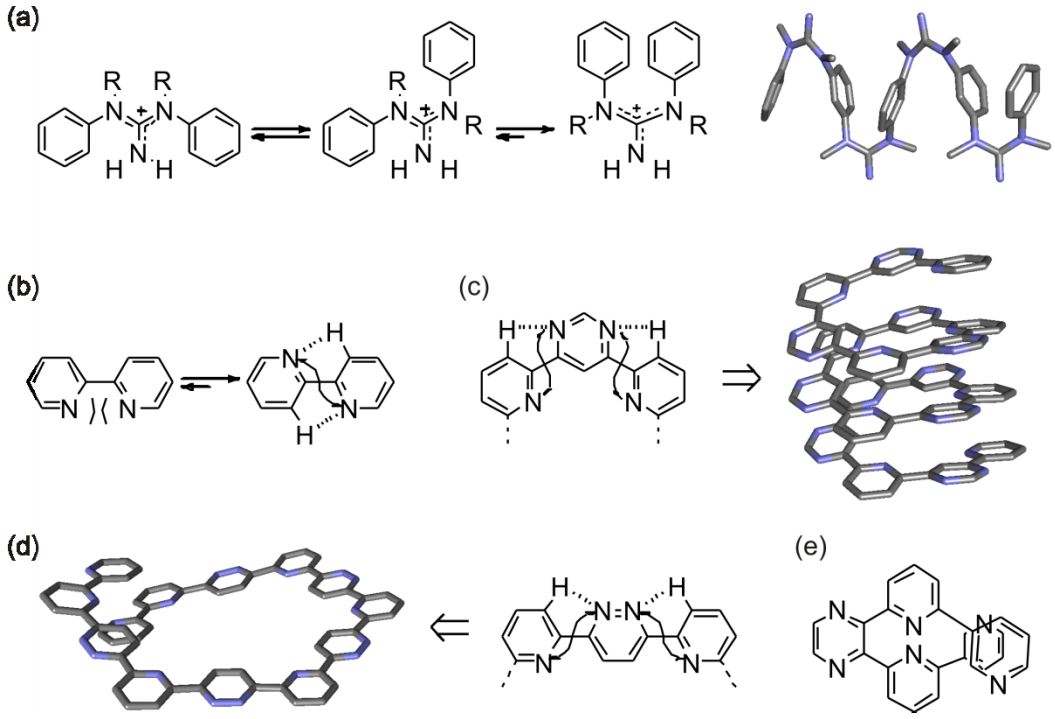

Figure 6: **Examples of foldamers based on close proximity interactions**. (a) oligoguanidine oligomer with its X-ray structure demonstrating large dihedral angles between the benzene plane and the plane of the guanidine functionality, (b) 2,2'-bipyridine adopting a *trans* conformation due to electrostatic interactions, (c) pyridine-pyrimidine oligomer and its expected modeled structure, (d) pyridine-pyridazine oligomer and its expected modeled structure and (e) oligo-(2,2'-bipyridyl)pyrazine.

Although the above mentioned strategies allowed scientists to prepare molecules with helical architectures with up to four turns, the synthesis of longer strands was found to be very challenging. Thus efforts have been made to design foldamers composed of aromatic units

that are connected by easily formed bonds. In this respect, Lehn *et al*. headed towards the generation of extended helical entities consisting of oligopyrimidines connected by facile imine bond formation (Figure 7).[50] These oligomers are prepared from the reaction of oligoheterocyclic aldehydes with bis-hydrazine to yield bis-hydrazones. These adopt a *transoid-transoid* conformation that satisfies both steric and electronic factors governing conformational selection. In more detail, the pyrimidine that is closer to the hydrazone functionality adopts a *transoid* conformation due to hydrogen bonding between the hydrazone NH and the endocyclic pyrimidine nitrogen, and electrostatic repulsions between the latter and the nitrogen atom of the hydrazone. The other pyrimidine ring adopts a *transoid* conformation due to hydrogen bonding between the endocyclic nitrogen and the proton of the sp^2 carbon. Additionally this conformation is favored due to electrostatic repulsions between the pyrimidine endocyclic nitrogen and the nitrogen of the hydrazone functionality.

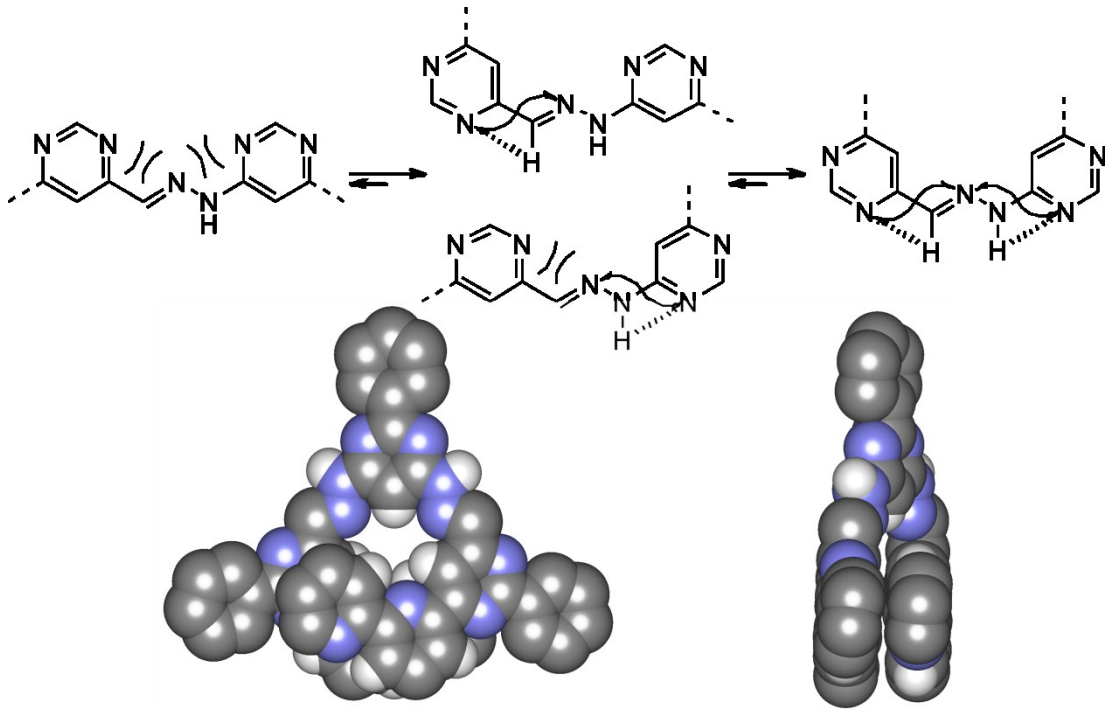

Figure 7: Conformational preferences of the hydrazone functionality leading to the adopted *transoid-transoid* conformation. Top and side view of the X-ray structure reported by Lehn *et al*.. Solvent molecules and side chain atoms have been omitted for clarity.

Hamilton *et al.* in their pioneering work reported the synthesis of an oligomer constituted of a central pyridine dicarboxamide unit and adjacent anthranilamide units giving rise to one of the first examples of oligoamides adopting a helical conformation (Figure 8a).[51-53]

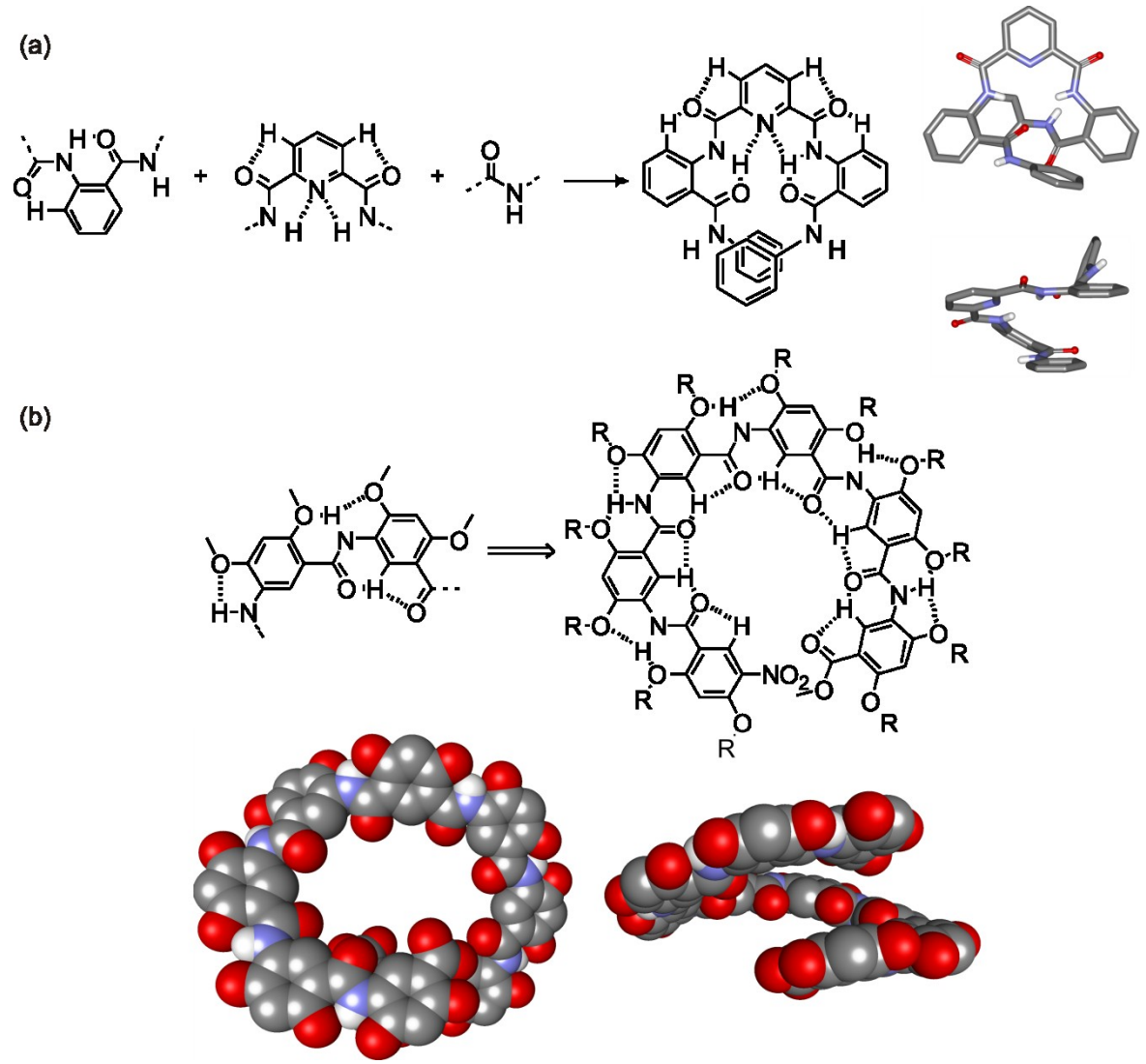

Figure 8: **Conformational preferences of aromatic oligoamide foldamers**. (a) crescent-like motif reported by Hamilton *et al.* owing its well-defined conformation to an extensive hydrogen bond network and electrostatic interactions in the aryl-amide linkage (X-ray structure on the right) and (b) crescent motif reported by Gong *et al.* (top and side view of the obtained X-ray structure at the bottom).

Helical folding is controlled thusly: the NH of the anthranilamide is hydrogen bonded to the oxygen of the carbonyl functionality, within the same building block. Additionally, in the pyridine carboxamide the nitrogen of the pyridine ring undergoes a three-centered hydrogen bond with the adjacent amide NHs. In a similar manner, Gong *et al*. used oligoamides to afford crescent/helical architectures owing their conformational preferences to electrostatic interactions between the amide functionality and substituents on the aromatic ring.[54, 55] As depicted in figure 8b, on each benzene ring the two amide linkages have been placed *meta* to each other leading to backbones that are exclusively consisted of *meta* residues. In this conformation each amide NH is hydrogen bonded with the ether oxygen of its neighboring substituents, thus stabilizing the exterior of the crescent motif. Additionally, each amide carbonyl is hydrogen bonded with the proton of the benzene ring that is located between the

two amide functionalities, leading to stabilization of the interior of the structure. At the same time, Huc *et al.* synthesized an oligomer consisted of alternating pyridine diacids and diamines to yield a helical oligoamide (Figure 9).[56]

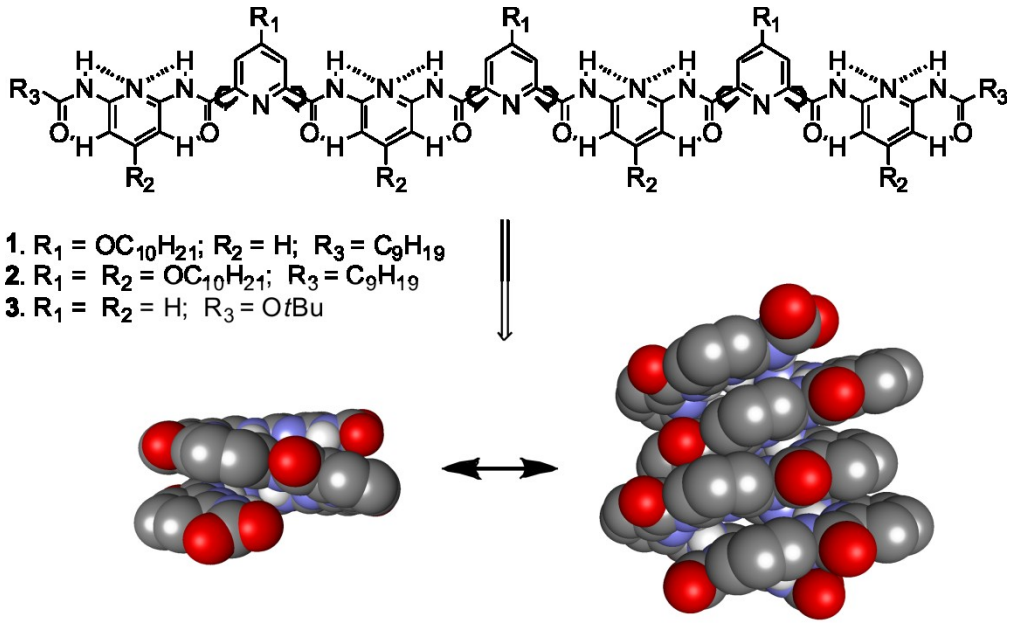

Figure 9: *Above*: Chemical formula of the oligoamide consisted of alternating pyridine diacid and diamine units. *Below*: CPK representations of the oligomeric X-ray structures forming a single helical motif, as well as a hybridized double helical conformation.

Its helicity was a result of extensive hydrogen bonding throughout the oligomeric strand. Later oligomers took advantage of a wide range of quinoline, naphthyridine and anthracene building blocks affording helical architectures with different properties, such as helices with variable diameter, binding properties and solubility profiles due to e.g. different monomer curvature, dipole direction, substitution pattern and potential for hybridization. In every case short proximity interactions along with extensive π—π stacking were the driving elements for the folding capability of these entities (Figure 10a-c). [32, 57-59]

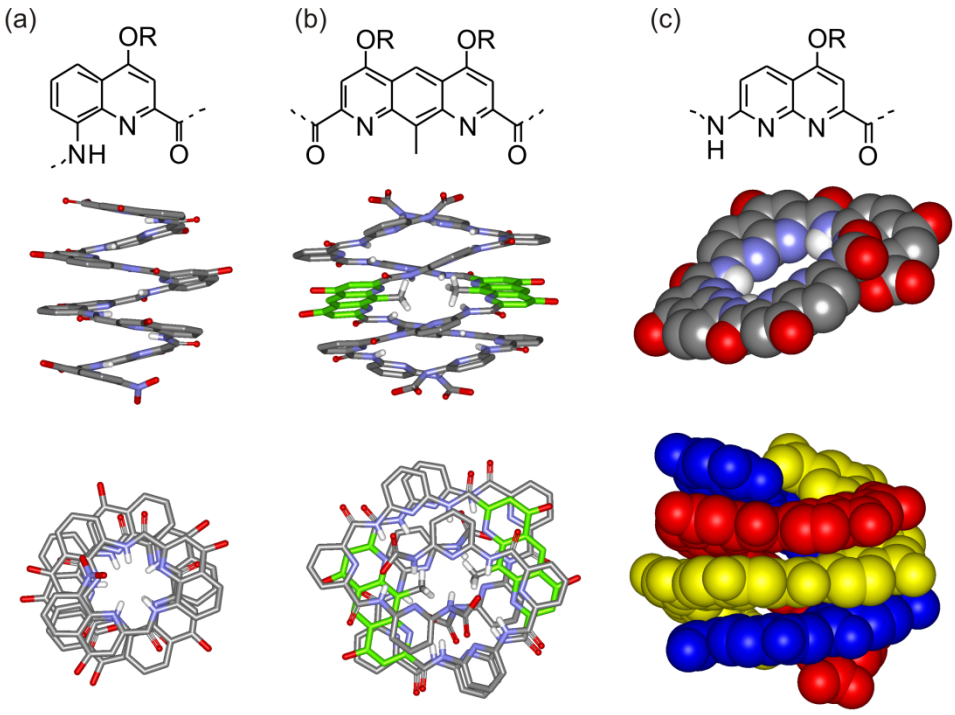

Figure 10: **Crystal structures of oligoamides** (side and top view). (a) 8-mer constituted exclusively from quinoline-based monomers forming a helical motif, (b) 7-mer bearing an anthracene diacid as a central unit coupled with two pyridine 3-mers, yielding a double helical motif and (c) 4-mer consisted of naphthyridine monomers (CPK reperesentations). Solvent molecules and side chains have been omitted for clarity.

2.2.2. Foldamers based on long proximity interactions

In this type of foldamers no interaction or direct conformational restrictions can be found between adjacent units; the folding of the molecule arises from interactions that are remotely located within the sequence of the oligomer. Representative examples of this category of helical foldamers have been developed by Moore and Iverson. Moore firstly reported the synthesis and characterization of oligophenylacetylenes in which there is no rotational restriction at the bonds between aromatic and acetylenic unit. Folding was expected to come from non-specific forces alone (such as Van der Waals and hydrophobic interactions) to guide intramolecular organization (Figure 11a).[60, 61]

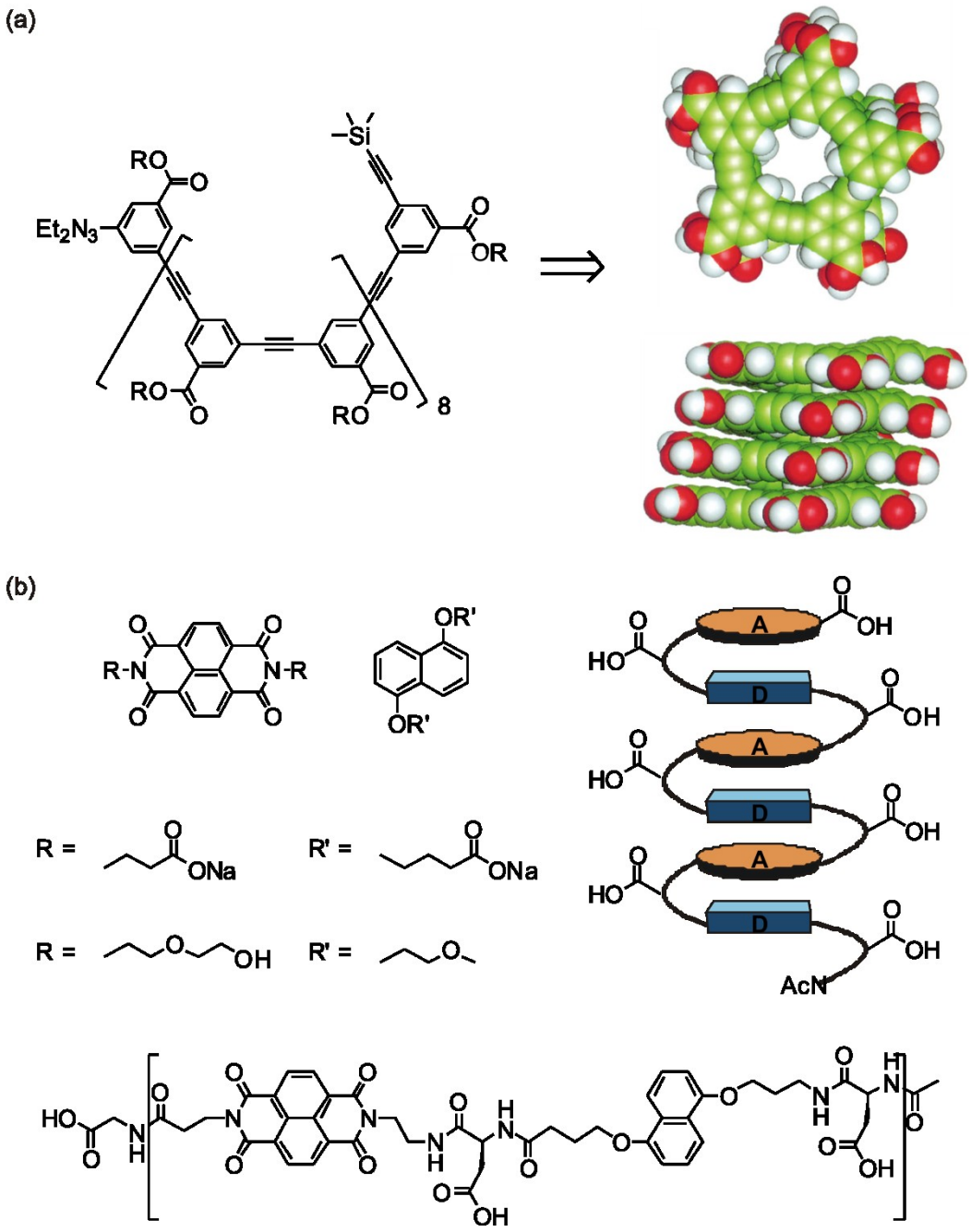

Figure 11: **Foldamers based on long proximity interactions**. (a) Octadecamer consisted of phenylacetylene moieties reported by Moore *et al.*, adopting a helical conformation (*right*: top and side view of molecular models) due to solvophobic effects and (b) oligomer folded due to alternating donor/acceptor units, reported by Iverson.

The hydrophobic aromatic building blocks were equipped with various side-chains, providing solubility in a wide range of solvents. Dissolution in protic solvents led to the formation of oligomeric helical moieties due to solvophobic effects, resembling the behavior of a monomeric micelle. In a comparable manner, Iverson alternated electron-rich donor units with electron-poor acceptor units connected together with L-aspartic acid residues, that enhance the water solubility of these molecules (Figure 11b).[62, 63] Spectroscopic data proved that in

water this molecule folded into a pleated structure in which the aromatic rings are stacked in a parallel, alternating fashion.

2.3. Foldamers based on intermolecular organisation

Two types of foldamers based on the use of intermolecular interactions can be discriminated. The first is based on the structuration of a non-preorganised molecule into a helical segment only in the presence of a template. The second is based on the aggregation via non covalent linkage of monomeric, non-helical building blocks into helical super structures. In the latter case, intrinsic problems come from the absence of control over the aggregation, which eventually give rise to supramolecular helical polymers, possessing a molecular weight distribution. Such an example of foldamer has been reported by Hamilton *et al.* in which they used an isophtalate derivative and dicarboxylic acid to form a helical structure (Figure 12), where the driving force for the formation of the helical entity is hydrogen bond formation between the amino pyridines and the carboxylic acids. [64] In this study, it has been shown that depending on the length of the dicarboxylic acid units that were used, a helical motif or planar ribbon structure could be obtained. A system like this is more properly described by the term polymolecular, instead of (uni-) molecular and unfortunately exceeds the scope of this brief review.

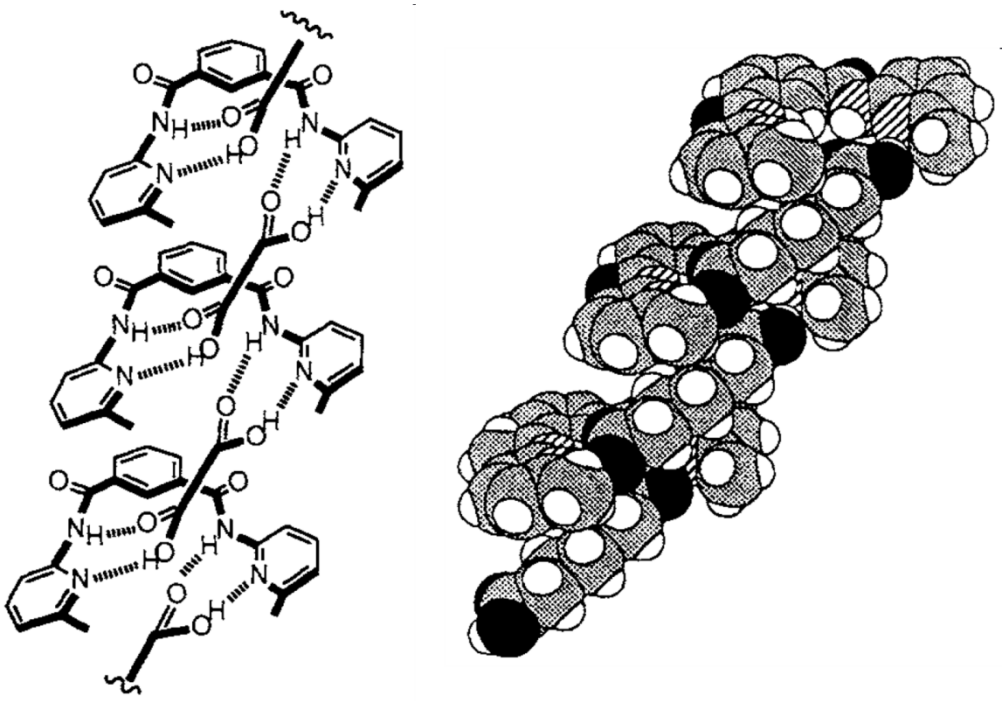

Figure 12: Helix formation by intermolecular hydrogen bonding reported by Hamilton *et al.*

Self-organization of an oligomeric strand can also occur by folding around a template. A representative example on this category is provided by helicates: a metal ion is used as a template which induces the folding of the oligomeric ligand, depending on the coordination sphere of the metal (Figure 13a).[65] Che *et al*. reported the folding capability of a linear quinque(penta)pyridine oligomer in the presence of rhenium metal in different oxidative states. Addition of rhenium 3 or rhenium 1 results in the folding of the strand into two different helical motifs.[66] Moore *et al.* functionalized the internal cavities of the helices formed by oligometaphenyleneacetylene with cyano groups and demonstrated that addition of six cyano groups into a dodecamer gives rise to a coordination cavity inside the helical structure. Upon addition of silver triflate and coordination of the metal by the converging cyano group, the molecule folds into a well-defined helical architecture even in solvents where no solvophobic effect can drive the folding (Figure 13b).[67] The group of Lehn reported the utilization of the previously described hydrazone linkage for the synthesis of a pyridine-hydrazone oligomer that is able to bind Pb^{2+} and subsequently forms a helical entity.[68] ^{1}H NMR and $^{1}H-^{1}H$ NOESY experiments displayed upfield shifts of signals due to increasing $\pi-\pi$ stacking interactions upon metal-complexation and X-ray structure determination demonstrated a complex consisting of a helical strand wrapped around two Pb^{2+} ions (Figure 13c).

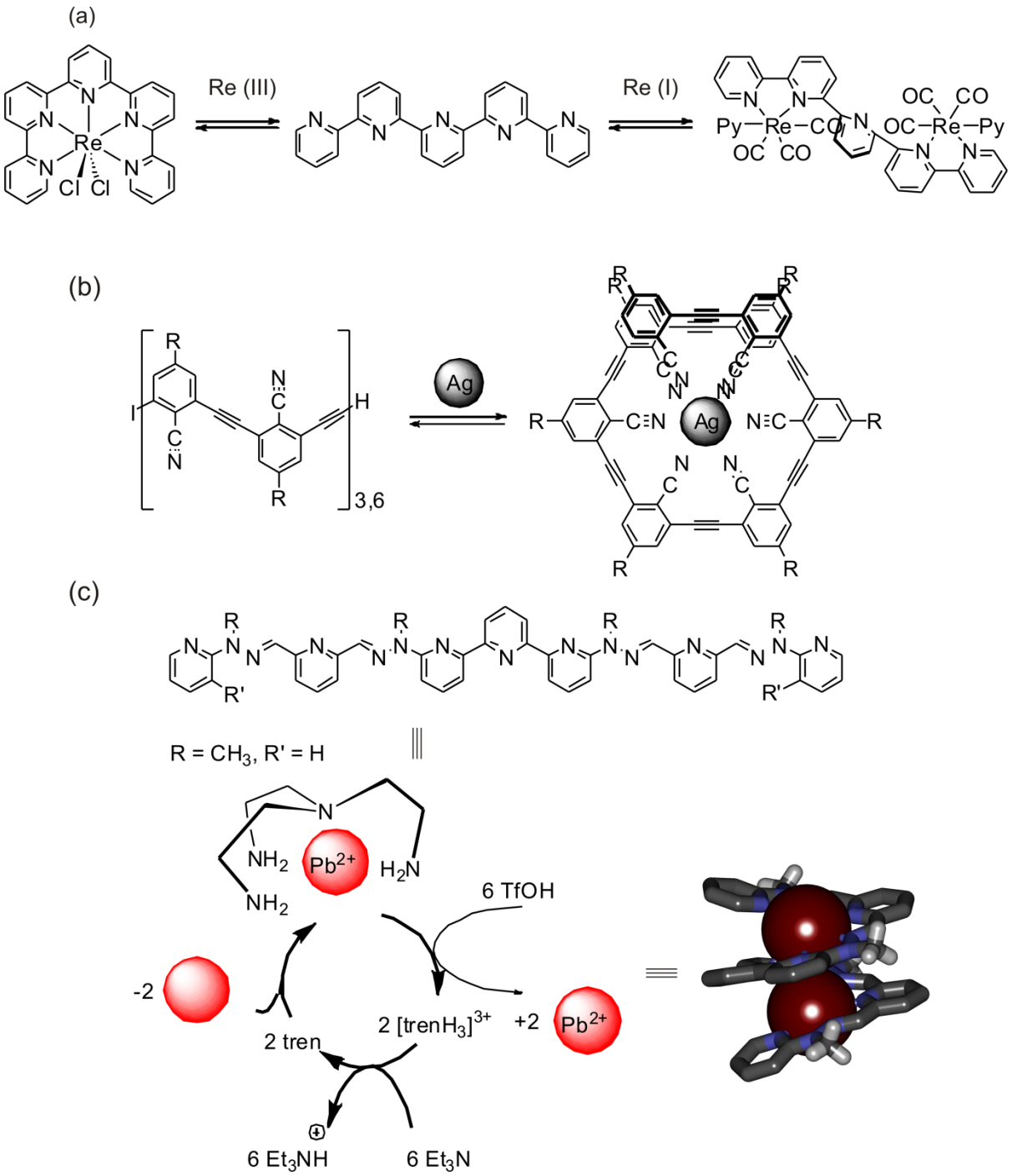

Figure 13: Foldamers based on metal complexation. (a) quinquepyridine affording one helical motif upon complexation with Re(III) and a different motif upon complexation with Re(I), (b) oligometaphenyleneacetylene having its interior equipped with cyano groups leads to a helical conformation upon complexation with Ag, even when solvophobic effects are absent and (c) pyridine-hydrazone oligomer able to bind Pb^{2+} forms a helical entity upon complexation with the latter, process that is reversible when Pb^{2+} binds to a better ligand (X-ray structure of the coordinated foldamer at the bottom right).

The last foldamer described in this category was reported by Fox *et al.* and it involves the synthesis and characterization of a single-stranded molecule that, similarly to the previous examples, adopts a helical conformation in response to metal complexation.[69] The design of the reported moiety is based on salen and salophen ligand derivatives that only upon

complexation to either Ni or Cu forms a well-defined helical structure (Figure 14). X-ray data and ^{1}H NMR were used to validate the structural identity of the molecule. It is noteworthy that an uncomplexed ligand displays various conformers in the ^{1}H NMR.

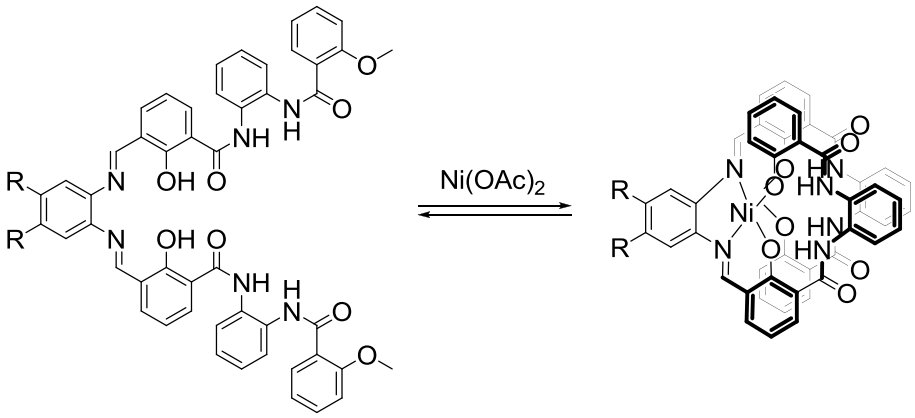

Figure 14: Helical folding upon complexation with Ni(II), as reported by Fox *et al.*

In addition to metal ions, many examples can be found in the literature where anions have been used to template helical folding. A characteristic example can be found in the work of Jeong and co-workers, where the synthesis of oligoindoles consisting of four, six and eight indole units connected with ethynyl linkers has been reported (Figure 15a).[70] ^{1}H NMR spectroscopy demonstrated that addition of chloride to oligoindoles resulted in a large downfield shift of the indole NHs which was attributed to hydrogen bonding to the anion and consequently to helical folding from a previously expanded conformation. Additionally, characteristic upfield shift of the aryl protons was observed as a result of π─π stacking between adjacent helical turns, supporting further that this molecule was folding into a helical motif upon binding of chloride. In a similar manner, Craig *et al*. demonstrated that a flexible oligomer containing aryl-1,2,3-triazole functionalities has the ability to bind chloride, which induces folding of the oligomer into a helical conformation creating an electropositive cavity (Figure 15b).[71] In contrast to the previously describe anion templated folding, no hydrogen bonding to the halogen is involved in the folding of such an oligomer, and the molecule exclusively binds chloride through C─H – chloride contacts.

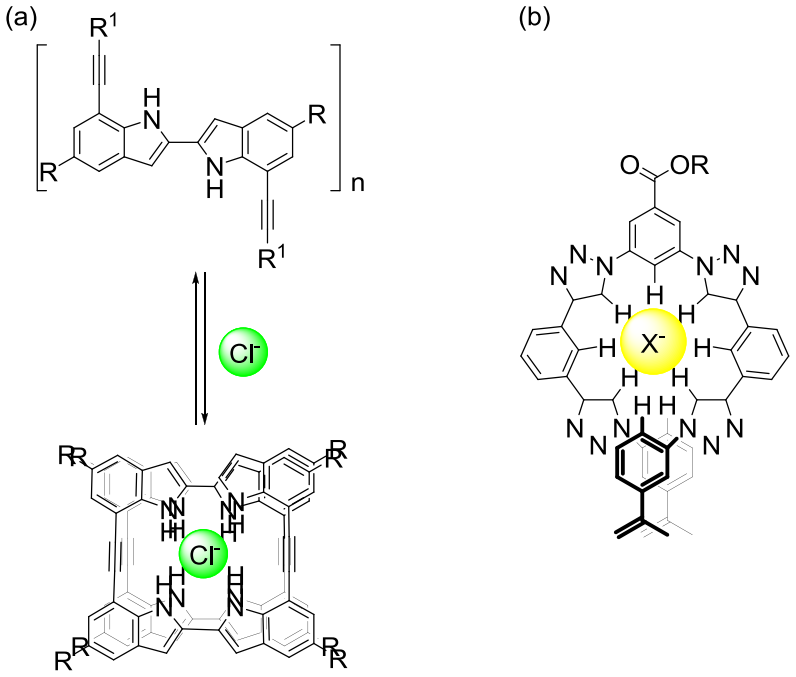

Figure 15: Foldamers based on anion binding. (a) oligoindoles are adopting a helical conformation upon binding chloride and (b) oligomer containing aryl-1,2,3-triazole functionalities folds upon binding anions.

Folding induction driven by molecular recognition can also be done using organic molecules as template. Berl *et al*. have synthesized and studied an oligo(diaminopyridine) that adopts a random coil conformation in solution in the absence of a guest molecule (Figure 16)[72] but folds in the presence of cyanurate to adopt a well-defined helical conformation. Folding comes from the formation of a hydrogen bond network between amidic protons of the strand and the carbonyl groups of the guest, and between protons of the guest and the nitrogen atoms of the pyridine of the oligomeric strand. Sharpening of the previously broad ^{1}H NMR signals is observed upon addition of the guest molecule, indicating a transition from multiple conformational isomers to a specific conformation in solution. ^{1}H–^{1}H Nuclear Overhauser Effect (NOE) cross peaks between the amide NHs and the aryl protons, pointing towards the interior of the cavity indicate close proximity which suggests a helical conformation in presence of the guest.

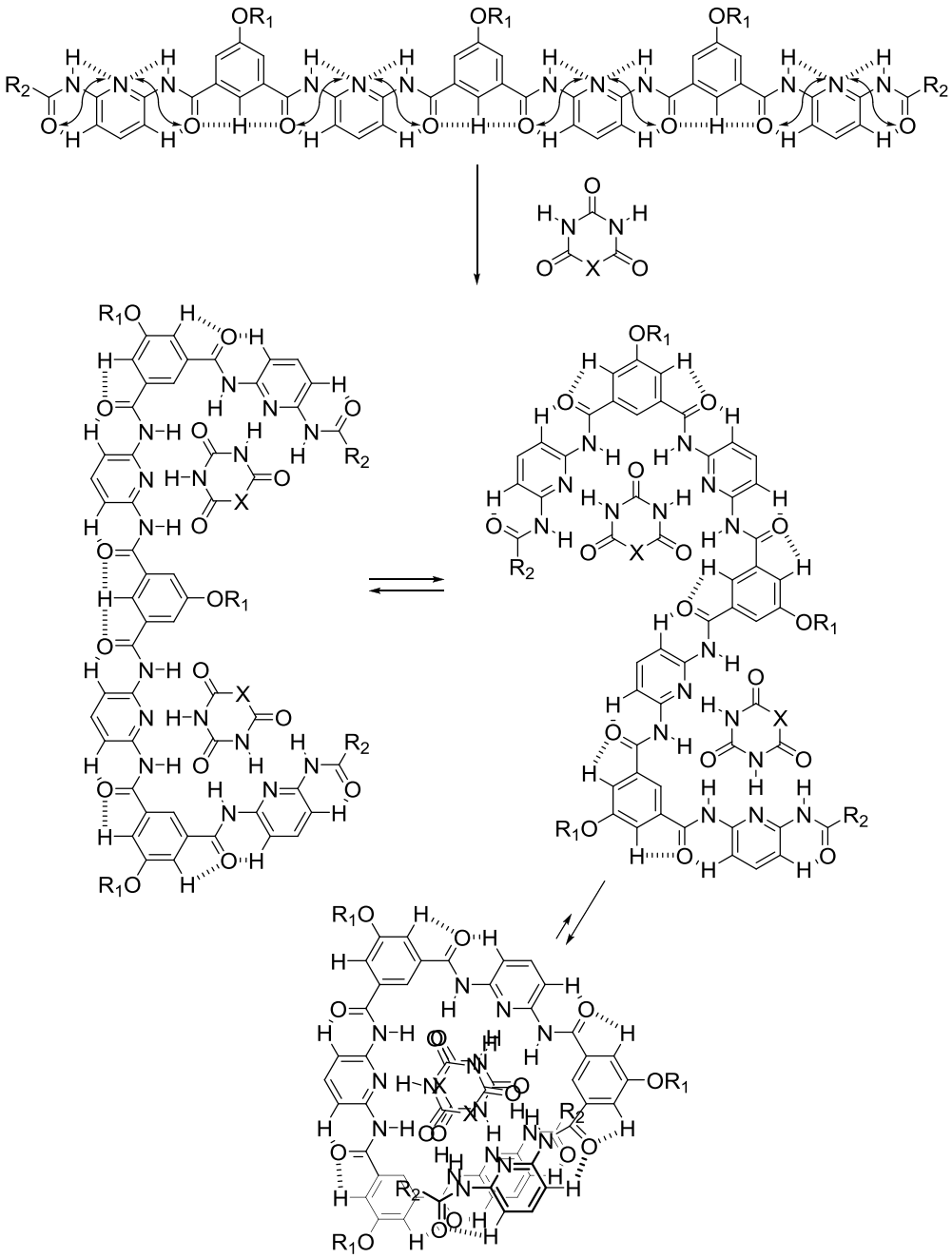

Figure 16: Host-guest induced folding. In the presence of cyanurate the multiple possible rotamers collapse into a single helical conformation.

Later work by Inouye *et al.* developed a foldamer consisting of pyridines and ethynylenes, in which hydrogen bonding to hexoses induces a conformational shift from a random to an ordered helical conformation (Figure 17).[73, 74]

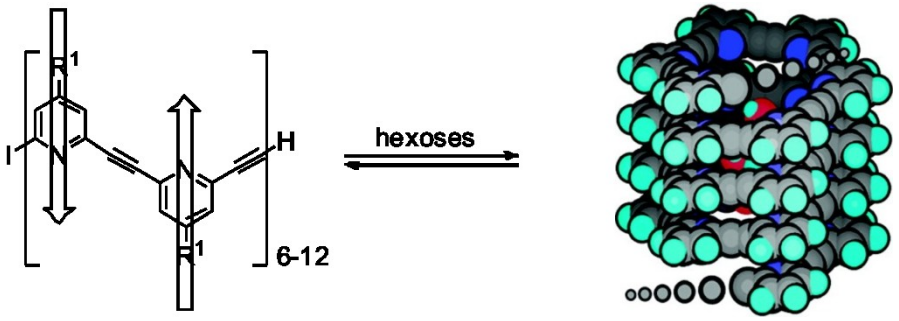

Figure 17: Oligo(pyridine-ethynylene) adopts a helical conformation due to solvophobic effects, as well as saccharide binding, as reported by Inouye *et al.*

Foldamers consisting of aromatic oligoamides will now be discussed in more detail. However it should be mentioned that they can belong to more than one of the above categories, representing a class of foldamers that keeps evolving by incorporating different features leading to new generations of molecules.

3. Aromatic oligoamide foldamers (AOFs)

Aromatic foldamers consisting of oligoamides are an interesting class of foldamers due to their unique characteristics, which can be attributed to the nature of the amide bond. Their synthesis is generally facile and they offer the benefit of bearing both a hydrogen bond donor (the amide NH) and an acceptor (the carbonyl of the amide). This functionality has been undoubtedly exploited by nature in order to control the secondary and higher order structures of polypeptides. Aromatic polyamides were initially reported by Dervan *et al*. in pioneering work where oligo pyrole and imidazole sequences were synthesized as DNA-binding sequences.[75, 76] Later, Hamilton *et al*. explored the design and folding capability of various other aromatic polyamides. Concerning this class of molecules, numerous examples can be found, by Hamilton,[51-53, 64, 77, 78] Gong,[31, 54, 79-87] Huc[88-90] and Li,[88, 91-93] reporting complex molecular architectures mimicking the secondary structures of biomolecules with helices being dominant motifs. Despite being far from what nature has selected during the evolutionary process, these structures have been shown to interact with biomolecules in various ways.[12, 94-100] Additionally there have been numerous examples reporting the utilization of aromatic oligoamide foldamers in catalysis, electron transfer and molecular recognition.

The interest of our group lies in foldamers that consist of aromatic amino acids and in particular quinoline-, pyridine-, anthracene- and naphthyridine- based monomers. Various combinations of these monomers give rise to different molecular motifs with helices being

dominant. The parameters affecting the predictability and stability of the architectures formed by these AOFs will now be described.

3.1. Predictability of AOFs

A key feature of aromatic foldamers is the predictability of the structures, which is defined by Hecht and Huc as: *"oligomeric structures that possess numerous rotatable bonds and that may, in principle, envelop a vast array of conformations, but whose conformational space is narrowed down to a single conformer because a well-defined preference exists at each rotatable bond"*. Helical folding arises from the combination of internal and external parameters such as monomer shape and rigidity, intramolecular attractive and repulsive interactions (local or between units remotely located in a sequence), rotational restrictions, solvophobic effects, and aggregation or the presence of guest molecules. In the case of the AOFs, monomer rigidity is guaranteed by their conjugated nature. Rotational restrictions of the amide bond are guaranteed by local conformational preferences both at the amide bond itself and at the aryl-amide linkage (Figure 18). It was shown by Pauling and Corey that electron delocalization within a peptide confers partial double bond character onto the amidic C–N bond and thus free rotation around that bond is restricted with a rotational barrier of 65-90 kJ/mol. That restriction leads to two possible and non-equal conformations: a *trans*- and a *cis*-configured amide bond with the former being more favorable by about 8 kJ/mol over the latter. Furthermore, when a hydrogen bond donor or acceptor is introduced on an aryl ring in a position adjacent to an amide function, a favored conformation occurs at the aryl-amide linkage due to conjugation and electrostatic interactions that can be either attractive or repulsive. Exploiting and manipulating these interactions can lead to bent conformations that eventually form compact helical moieties.

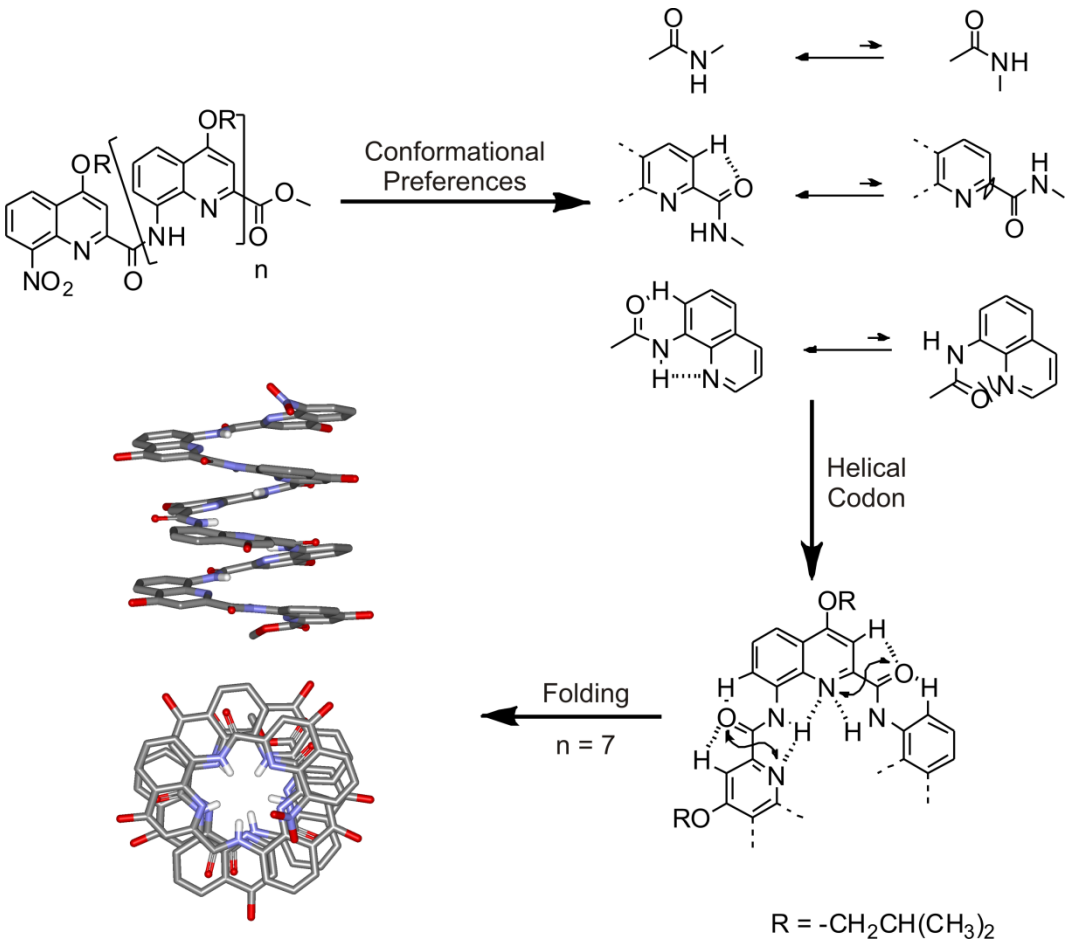

Figure 18: Conformational preferences occurring at the aryl-amide linkage of a quinoline-based oligomer, affording a well-defined helical conformation. Crystal structure of an octameric strand (side and top view). Side chains atoms and hydrogen atoms apart from the NH groups have been omitted for clarity.

The combination of the above mentioned local conformational preferences, promotes helical folding. As an example, quinoline-based oligomers fold into helical architectures where the pitch equals the thickness of one aromatic ring, 3.5 Å, and the number of units per helical turn is almost 2.5. The aromatic backbone of these oligomers gives rise to hydrophobic effects in protic solvents that provide an additional driving force favoring the helical conformation. The behavior of such foldamers has been reported in water and their kinetic inertness towards racemization, due to the solvophobic effect is spectacular. More details concerning this topic will be given later in this manuscript. To conclude, all these factors contribute in different magnitudes to the well-defined and predictable character of aromatic oligoamide foldamers.

3.2. Intrinsic Properties of helical entities

3.2.1. Helical Chirality

Helical entities are chiral, which means that their mirror images are not superimposable, even if they do not have any stereogenic center. They can be found in two distinct enantiomeric forms: left- or right-handed (Figure 5a). Typical examples of molecular helical entities are provided by the helicenes. When these molecules consist of five or more rings, steric hindrance at both ends of the molecule prevents it from adopting a planar conformation, giving rise to helical, enantiomeric structures with C_2 symmetry. Multiple examples can be found in the literature of chiral helical molecules, such as *trans*-cyclooctenes and substituted heptalenes (Figure 19).[101, 102]

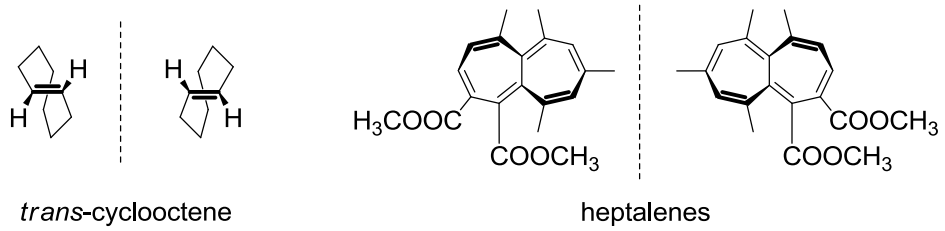

Figure 19: Enantiomeric forms of *trans*-cyclooctene and heptalene.

In the case of aromatic quinoline-based oligoamides with 2.5 units per turn, when the oligomer consists of more than three monomeric units, the molecule is forced to adopt a non-planar conformation due to steric clash occurring between the C- and the N-terminus, giving rise to a helical conformation, which by definition possesses helical chirality (in the absence of stereogenic centers).

At this point it is necessary to mention that in the case of quinoline-based oligoamide helical molecules, racemization takes place. During this process the helix passes through an unfolded (or partially unfolded) intermediate, in order for helix handedness inversion to take place. Thus, racemization kinetics are directly associated with helical stability and their investigation provides a straightforward way to assess this stability. Analysis of racemization kinetics allows evaluation of the Gibbs energy, meaning the actual energy difference between the folded (more stable) structure and a partially unfolded intermediate. More details concerning the correlation of racemization kinetics and helical stability are given below.

3.2.2. Helical Stability of Foldamers

Helical stability is a fundamental property of helix-like entities that governs their potential applications. Parameters which influence helical stability of oligoamide foldamers have been investigated by multiple experimental and theoretical studies.[103-108] The stability of

these helical entities comes partially from conformational preferences taking place at the aryl-amide linkage and by the nature of the amide bond itself. Additionally, in long oligomers aromatic stacking is an additional stabilizing force. These principles are independent of the orientation of the amide bond, as well as on the number of atoms contributing to the hydrogen bonding.

To investigate the effect of hydrogen bonds on folding Gong *et al.* quantified the stability of local three-center H─bonds by determination of the half-lives of amide proton-deuterium exchange. Additionally they used NOESY experiments to investigate the effect of temperature on helical conformation.[82] For the first part of their study, they conducted H─D exchange experiments on a 9-mer and 3 different dimers (Figure 20). Comparison of the half-lives of H─D exchange demonstrated the enhanced stability contributed by three-center H─bonds compared to two-center H─bonds. Additionally they proved that a six-membered H─bond is slightly more stable than a five-membered one.

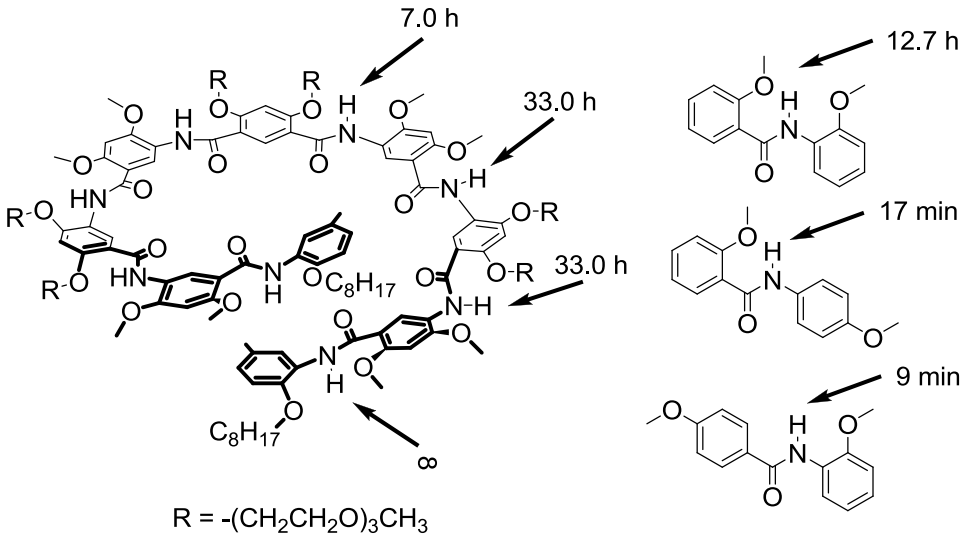

Figure 20: Half-lives of amide H─D exchange for a symmetric nonamer and 3 different dimers with different H─bonding patterns.

In the second part of their study, comparison of amide→R group NOEs with helix terminus→terminus NOEs revealed a much more rapid disappearance of the latter while increasing the temperature, indicating that distortion of the H─bonded rings, that are associated with each amide group, allows the helix to perform a spring-like extension/breathing movement.

To serve as an introduction to the experimental work presented in this manuscript, previous stability studies of quinoline-based foldamers will be briefly reviewed. Different parameters affecting helical stability will be discussed, such as helix length, solvent effects, and the presence of non-quinoline monomer units.

3.2.2.1. Effect of the length in helical stability of quinoline based foldamers

To study the effect of helical stability ten different foldamers constituted of 2 to 16 quinoline monomers were synthesized. NMR characterization suggested their well-folded and predictable helical nature; the presence of sharp signals in all 10 spectra (Figure 21) is consistent with the well-defined and stable helical conformations that are adopted by these oligomers.[109]

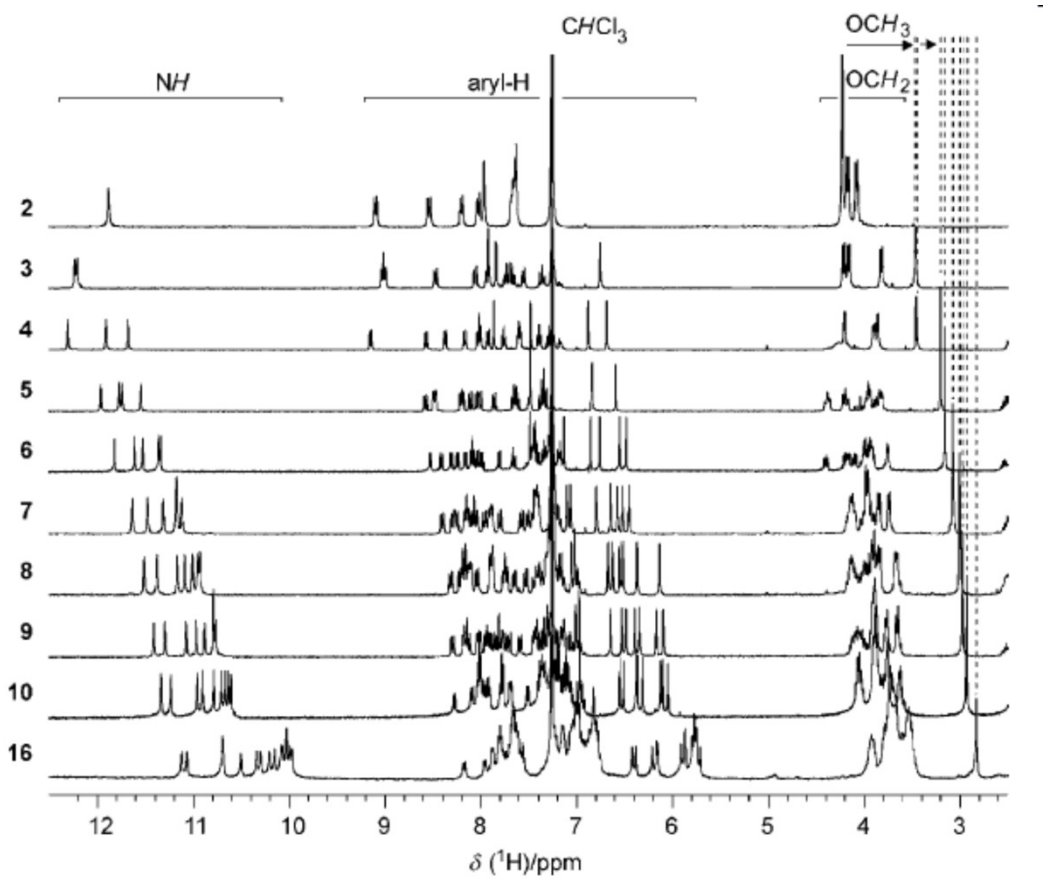

Figure 21: ^{1}H NMR spectra of 2mer–10mer and 16mer in $CDCl_3$. The numbers on the left axis indicate the number of monomers within the sequence.

Amide and aromatic signals are well-dispersed suggesting different micro-environments, even though these oligomers consist of the same repeating building block. It can also be seen that the longer the oligomer is, the more upfield its signals are shifted. It has been assumed that this is probably due to the accumulation of multiple weak ring current effects, as well as intramolecularly stacked quinoline residues. Another observation based on NMR experiments involves the signal of the methyl ester at the C-terminus that can be found at 2.93 ppm for the oligomer containing 10 monomeric units and at 2.83 ppm for the 16mer. What is interesting is that even though the N-terminus is remotely located 10 or 16 monomeric units away, the ester function appears to 'feel' the difference in its microenvironment. This observation has also

been attributed to weak ring current effects, but its actual origins are not totally clear. Another very characteristic characteristic indicating helical folding is the diastereotopicity of the methylene signals of the isobutoxy side chains. In the two shortest oligomers (n = 3 and 4), these signals appear as broad doublets, indicating the average environment for the two protons, even if they belong to an intrinsically chiral entity. It is noteworthy though, that upon cooling the broad peaks eventually split into doublets of doublets, which reflects the equilibrium between the two possible enantiomeric conformations. This behavior is rapid on the NMR timescale at room temperature, but slows down at lower temperatures. For oligomers consisting of 6 or more units, the exchange is slow even at room temperature resulting in diastereotopic patterns for these protons. It is noteworthy that the increase in helical stability is so significant that for oligomers with 6 or more monomeric units the diastereotopic signals do not coalesce upon heating at temperatures up to 100 ^{o}C. At that point it is worth-mentioning that a quinoline-based octameric sequence shows no signs of unfolding in DMSO at 120 ^{o}C, providing an indirect measurement for how stable the resulting conformation is.

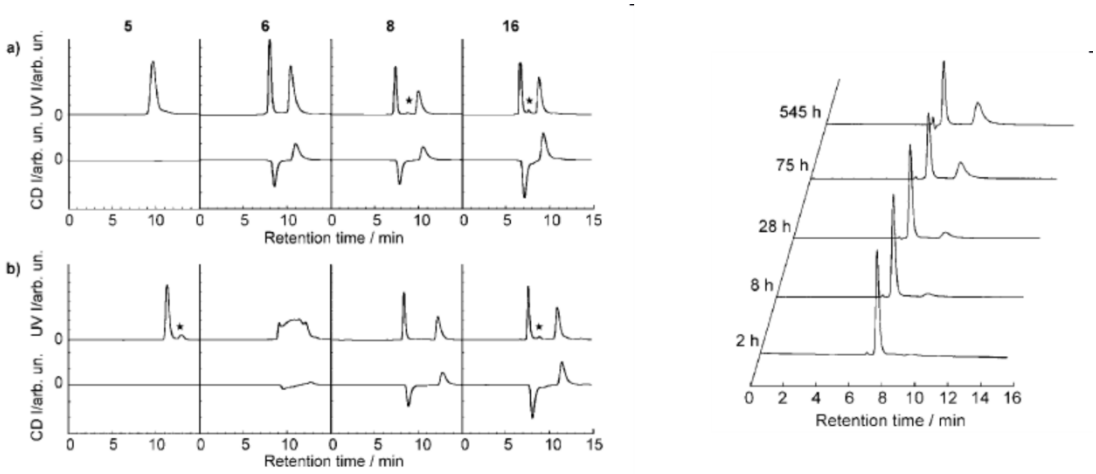

Figure 22: Chromatograms of oligomers consisted of 5, 6, 8 and 16 on a Chiralpack IA recorded at (a) 0 ^{o}C and (b) 30 ^{o}C. Trace of the UV (top) and CD (bottom) detector demonstrating that the left-handed helix elutes first and (c) follow up of the racemization kinetics of 8-mer by chiral HPLC at 10 ^{o}C.

In order to quantify this trend of increasing stability with foldamer length, separation of the two enantiomers by chiral HPLC was carried out, and racemization kinetics of the separate enantiomers were studied (Figure 22). The methodology was based on the fact that racemization kinetics for oligomers bearing more than six monomeric units is slow enough that chromatographic separation of the two enantiomers on a chiral stationary phase becomes feasible.

Table 1: Kinetic and thermodynamic parameters determined by follow-up of the racemization kinetics at variable temperatures. Chromatographic separation was done in *n*-hexane/$CHCl_3$ (75/25 v/v)

n[a]	n_t[b]	T[°C]	k_{rac}[s^{-1}][c]	$t_{1/2}$[h][d]	$\Delta G^{\ddagger}$[kJ mol^{-1}][e]	$\Delta G^{\ddagger}/(n-1)$[kJ mol^{-1}][e]
6	2.4	0	$1.3x10^{-4}$	0.7	87.0	17.4
		10	$6.6x10^{-4}$	0.2	86.4	17.3
		30	–[f]	–[f]	–[f]	–[f]
7	2.8	0	$3.3x10^{-6}$	28.8	95.3	15.9
		10	$1.5x10^{-5}$	6.3	95.3	15.9
		30	$1.6x10^{-4}$	0.5	95.7	16.0
8	3.2	0	$4.9x10^{-7}$	196.4	99.6	14.2
		10	$2.6x10^{-6}$	37.4	99.5	14.2
		30	$4.6x10^{-5}$	2.0	99.3	14.2
9	3.6	0	$1.4x10^{-7}$	684.8	102.5	12.8
		10	$7.7x10^{-7}$	125.0	102.3	12.8
		30	$1.5x10^{-5}$	6.4	102.2	12.8
10	4	0	$6.3x10^{-8}$	1540.0	104.3	11.6
		10	$3.7x10^{-7}$	262.5	104.1	11.6
		30	$7.4x10^{-6}$	13.1	104.0	11.5
16	6.4	0	$10x10^{-10}$[g]	10000[g]	108.6	7.2
		10	$5.1x10^{-8}$	1870.0	108.7	7.2
		30	$1.5x10^{-6}$	66.3	108.1	7.2

[a] number of monomers, [b] number of helical turns, [c] racemization constant, [d] half-life if racemization, [e] Gibbs energy of activation, [f] very fast kinetics and [g] estimation of these values from partial racemization due to extremely slow kinetics

One of the two conformers was thus isolated and its racemization was monitored by chiral HPLC at various temperatures, results that were then fitted to a first order kinetic model to yield the rqcemization constant and the Gibbs energy of activation. This therefore provides a quantitative representation of helical stability. The results of this study are depicted in Table 1, which clearly illustrates the increase of helical stability as the oligomer length increases.

3.2.2.2. Effect of the solvent in helical stability

Another crucial parameter affecting the stability of quinoline-based sequences is the solvent. In order to explore this effect a new quinoline-based octamer was synthesized. This oligomer was decorated with triethylene glycol side chains, to ensure solubility in a wide range of solvents (Figure 23).[110] For the purpose of this study the two enantiomers (*P* and *M*) of the synthesized octamer were separated on chiral HPLC and afterwards their racemization

kinetics was followed by CD (circular dichroism) in different solvents. The decay of the CD intensity that was measured was fitted to a first order kinetics model (Figure 24), which yielded the racemization constant (k_{rac}) and the half-lives of racemization.

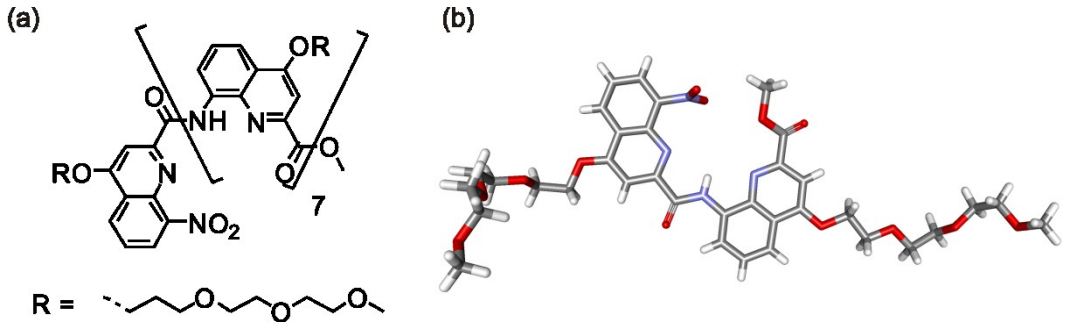

Figure 23: (a) Chemical formula of the octamer equipped with triethylene glycol side chains and (b) crystal structure of the dimeric precursor.

This therefore provides a quantitative measurement of the effect of the solvent on the stability of the helical architecture. The results of this study are summarized on Table 2, which demonstrates an enhancement of helical stability in protic solvents. It was shown that the half-life of helix handedness inversion is increased by two orders of magnitude in alcohols, such as methanol and 2-propanol and was increased by a further order of magnitude when water was present. Marginal racemization was detected after one 1 day at 30 ^{o}C in MeOH/H_2O (50:50) mixture. Overall, this trend can be explained by the solvophobic effects that in protic solvents force the aromatic quinoline-based backbone to form a lipophilic core, surrounded by the hydrophilic side chains that interact with the solvent molecules.

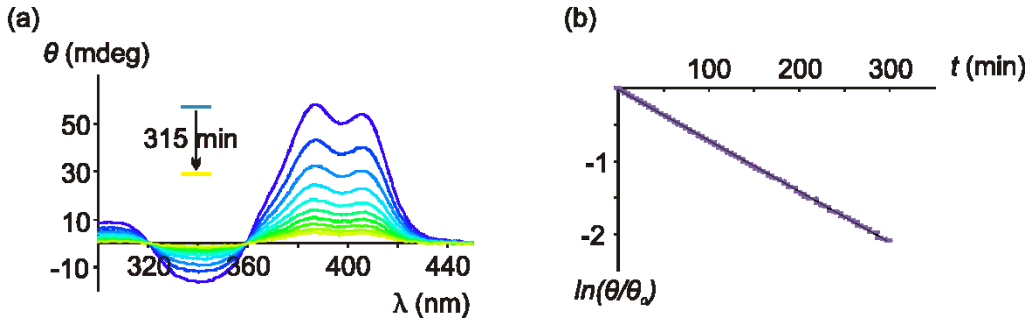

Figure 24: (a) Decay of the CD intensity. Depicted region 300-450 nm, in $CHCl_3$, 30 ^{o}C and (b) linear plot of the CD intensity fitted to a first order decay.

Table 2: First order kinetic constants and half-lives of racemization in various solvents for the triethylene glycol equipped octamer.

Solvent	$k^{[a]}$ [min^{-1}]	$t_{1/2}^{[a]}$ [min]
THF	$4.4x10^{-2}$	16
Toluene	$2.5x10^{-2}$	28
DMF	$1.7x10^{-2}$	40
Et_2O	$9.0x10^{-3}$	77
$CHCl_3$	$7.0x10^{-3}$	99
2-propanol	$2.0x10^{-3}$	350
MeOH	$7.7x10^{-4}$	900
95:5 MeOH/H_2O[b]	$4.8x10^{-4}$	1445
80:20 MeOH/H_2O[b]	$1.7x10^{-4}$	4080
50:50 MeOH/H_2O[b]	*ND*[c]	*ND*[c]

[a] Determined my monitoring the decay of CD intensity of P-1, [b] vol/vol and [c] kinetics too slow to be determined.

In other words, helical stability increases presumably because the partial unfolding of the helical segment, required for helix handedness inversion to take place, would lead to exposure of the aromatic backbone to solvent, which is strongly disfavored. Another interesting finding is that backbone composition seems to be the key element affecting helical stability as far as solvent effects are concerned. An octamer equipped with isobutoxy side chains was tested and the results were compared to those of the triethylene glycol octamer.

3.2.2.3. Effect of aliphatic amino acids within a well-defined helical array

The effect of introducing one or more aliphatic units within a well-defined helical array has been explored[111] addressing the extent to which the combination of two unnatural building blocks, that possess overall different folding propensities, can give rise to a well-defined helical architecture. If the sergeant-soldier effect is applied, a 'dominant' monomer is anticipated to impart conformational patterns to the 'recessive' one, finally templating very large well-defined helical architectures, consisting of both monomers. For this study a series of compounds was synthesized containing oligoquinoline-based arrays (Q) as very stable helically folded conformations and 6-aminomethyl-2-pyridinecarboxylic acid (P) as more flexible units, imparting conformational preferences that differ from those of quinoline units (Figure 25a). The overall aim of this study was focused on exploring whether a tetrameric quinoline sequence that is well folded is able to impart folding to a strand that is made of monomers not able to adopt a helical conformation.

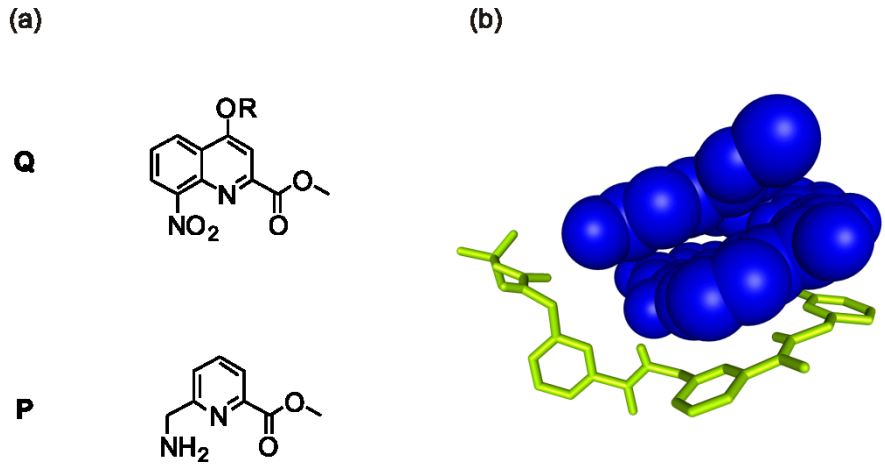

Figure 25: (a) chemical structures of the quinoline tetramer (Q) and the flexible pyridine monomer (P) and (b) crystal structure of *Boc*-P_3Q_4, demonstrating that only the first two pyridine monomers follow the helical pattern implied by the well defined quinoline tetramer. CPK representation in blue for the quinoline tetramer and in green the methylene pyridine monomers.

In the first part of the study 5 compounds were synthesized which consisted of two segments: a fixed quinoline-based tetramer and a segment consisting of a variable number of P units, forming P_nQ_4, with n = 1-5. It was demonstrated that P monomers that are close to the quinoline tetramer adopt a helical conformation which is indicated by the diastereotopic behavior of the methylene protons. Solid state data confirmed the results found in solution. The crystal structure of compound *Boc*-P_3Q_4 indicated that 2 out of 3 P units are well-folded, while the third one hangs out and lies in a plane parallel to the helix axis, due to the flexibility introduced by the methylene moiety (Figure 25b). In the second part, P oligomers with variable lengths were sandwiched between two quinoline tetramers. Since that type of molecule contains two well defined helical segments connected with an aliphatic segment, it can in principle give rise to three different enantiomers: *PP*, *MM* and *PM*. The homochiral species are expected to have identical NMR spectra, but not the heterochiral one. In fact, the NMR experiments indicated one set of sharp signals suggesting the existence of one diastereomeric conformer with strictly defined helix handedness of the two Q_4 segments. Additionally, the pyridine backbone ─CH_2─ signals showed strong diastereotopicity, even in the molecule bearing a P_5 segment, suggesting a stable helical structure of this segment. X-ray diffraction data proved the presence of well-defined helical segments with up to three pyridine monomers and additionally they showed that the contribution of P units in the helical curvature closely resembles that of the quinoline monomers (Figure 26).

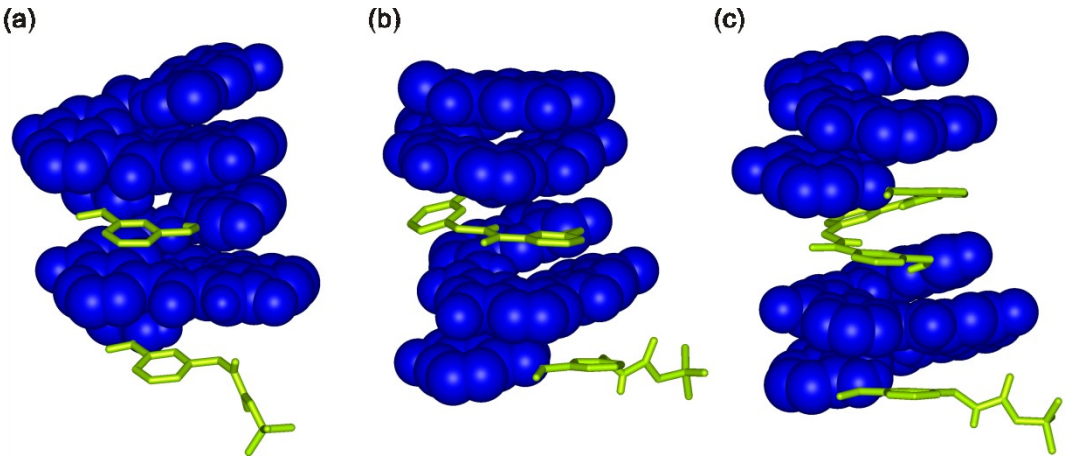

Figure 26: **X-ray structures of *Boc*-$PQ_4P_nQ_4$ oligomers**. (a) n = 1, (b) n = 2 and (c) n = 3. Q_4 segments are colored blue (CPK representation) and P segments are colored in green. Side chains, solvent molecules and non-amidic protons have been omitted for clarity.

In order to quantitatively assess helical stability, HPLC analysis on a chiral stationary phase was carried out. Interestingly, only two diastereomers were observed during the chromatographic separation, indicating that the heterochiral species could not be observed in the timescale of the experiment.

Table 3: First order kinetic constants, half-lives of racemization and values of free energy of activation in various temperatures for the *Boc*-$PQ_4P_nQ_4$ oligomers.

Compound	T [°C]	k_{rac} [s^{-1}]	$t_{1/2}$ [h]	$\Delta G^{\ddagger}$[kJ mol^{-1}]
Boc-PQ_4PQ_4	0	4.8×10^{-6}	20	94
	10	2.0×10^{-5}	4.9	95
	30	2.8×10^{-4}	0.34	95
Boc-$PQ_4P_2Q_4$	0	3.3×10^{-5}	3.0	90
	10	1.2×10^{-4}	0.81	90
	30	1.4×10^{-3}	0.07	91
Boc-$PQ_4P_3Q_4$	0	1.3×10^{-4}	0.76	87
	10	4.0×10^{-4}	0.24	88
	30	1.5×10^{-3}	0.06	91
Boc-$(PQ_4)_4$	0	3.6×10^{-7}	260	100
	10	1.5×10^{-6}	65	101
	30	3.4×10^{-5}	2.8	100

The two enantiomers were then isolated and their racemization kinetics were followed by chiral HPLC at various temperatures. The data were fitted to a first order kinetic model to yield the racemization constant (k_{rac}) and the half-lives of racemization. Additionally, by using the Eyring equation the free energy of activation ($\Delta G^{\ddagger}$) was also evaluated providing a

quantitative measurement of the energy difference between the folded state and the partially unfolded intermediate – this energy difference directly reflects helical stability. The results are summarized in table 3 and they clearly show that upon addition of P units in the sequence the stability of the helical entity is reduced due to the flexibility introduced by these units.

In the last part of this study a series of $(PQ_4)_n$ oligomers were synthesized with n ranging from 1 to 8. NMR experiments demonstrated that despite the numerous P monomers present within the above-mentioned sequences, no inversion of helix handedness occurs at these positions that could result in the appearance of other diastereotopic forms. To confirm this observation, chiral HPLC was carried out that showed that all the Q_4 segments within the helical array possess the same handedness leading to two possible enantiomers, *P* and *M*. Furthermore, it was demonstrated that the half-life of racemization for *Boc*-$(PQ_4)_4$ is approximately 10 days at 0 ^oC, whereas for PQ_4 PQ_4 it was less than a day (20 hours). This suggests that despite the longer sequence possessing two more 'P' units, this is compensated by the extra eight quinoline monomers.

3.2.2.4. Effect of aliphatic linkers in helical stability of AOFs

In two closely related studies, five different aliphatic linkers were evaluated for their contribution in helical folding.[112, 113] 1,2- ethylenediamine, 1,7-diaza-diethyleneglycol, *p*- and *m*-xylyl-diamine and carboxylic acid anhydride linkers (Figure 27) were placed between two quinoline tetramers and the propensity of these units to follow a particular helical scheme was evaluated.

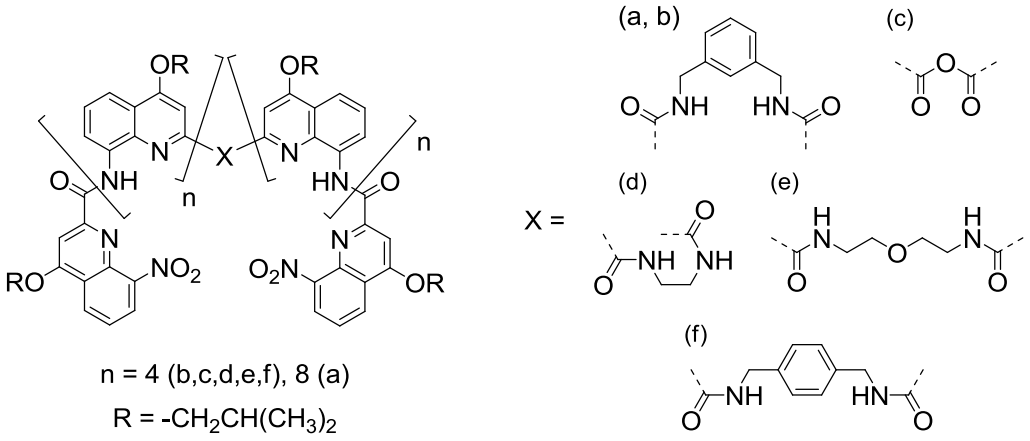

Figure 27: Chemical formulas for the six different compounds tested, consisting of a central diamine coupled with well-defined helical segment of 4mer and 8mer oligoquinolines

The evaluation was based on the fact that all of these oligomers could adopt three possible conformations in solution, since they are composed of two rigid helical segments connected with a potential inversion center. They can be homochiral, meaning that both of the

quinoline-based segments have the same handedness (either *PP* or *MM*) or heterochiral meaning the *meso* species, in which the two segments have opposite chirality. If the linker is promoting folding there should be helical communication between the helical segments, leading to the homochiral species. In order to assess the helical propensity of these units, NMR studies were carried out along with X-Ray structure elucidation (Figure 28). NMR studies evaluating these phenomena were carried out in chloroform and toluene in different temperatures, and it was shown that the latter favors homochiral entities compared to chloroform for all the compounds. These studies concluded that the helical entities containing 1,2- ethylenediamine, 1,7-diaza-diethyleneglycol and carboxylic acid anhydride central units have good helix propensity and they align themselves with the overall helical motif. The anhydride functionality, despite its nature (lacking H─bond donor) provides good communication between the helices favoring homochiral architectures, as proven by the variable temperature NMR experiments and solid state data. The ethylenediamine and diethyleneglycol linkers gave rise to broad peaks in the NMR at room temperature but at lower temperatures signals became sharper and a minor set of signals corresponding to the *meso* compound could be observed.

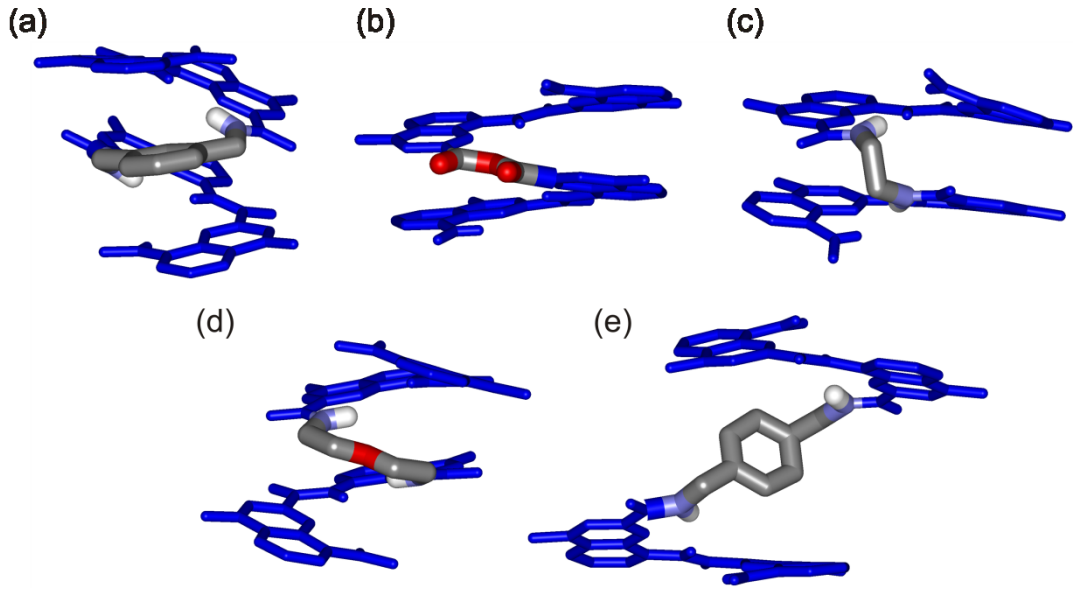

Figure 28: X-ray structures of compounds b,c,d,e and f (Figure 27). Central units are shown in bold. The two external quinoline segments from each side, as well as side chains have been omitted for clarity.

The major species was attributed to the homochiral entity, as indicated by the crystal structure. For both the *m*- and *p*-xylene central units the obtained ratio of homo- to hetero-chiral conformations (by NMR), is pointing towards the fact that these two linkers do not promote intrastrand communication. Additionally, crystallographic data for the *p*-xylene linked foldamer showed the *meso*-conformation in which the phenyl ring of the bridge is

almost perpendicular to the adjacent quinoline rings and is not involved in face-to-face aromatic stacking. In contrast, the *m*-xylene bridge lies flat between two quinoline rings (Figure 28a). It is noteworthy also that the solvent influences the helical propensity of the xylenyl linkers. In chloroform both of them present similar behavior, but in toluene the m-xylene showed a shift of the equilibrium to a ratio of 9:1 in favor of the *PP/MM* conformers, in which extensive intramolecular π—π stacking takes place. Results indicate that relatively simple and flexible aliphatic units have the ability to adopt folded conformations once incorporated in the context of a rigid helically folded aromatic oligoamide.

In another study, two oligomers,[114] bearing either a central pyridine or a benzene 2,6-methylenediamine, were synthesized (Figure 29). Comparison of their helical propensity showed that the oligomer bearing the pyridine is more stable; this unit despite the aliphatic carbons connecting the aromatic ring with the amine functionalities has the ability to form hydrogen bonds between the nitrogen of the pyridine and the hydrogen atoms of the adjacent amides.

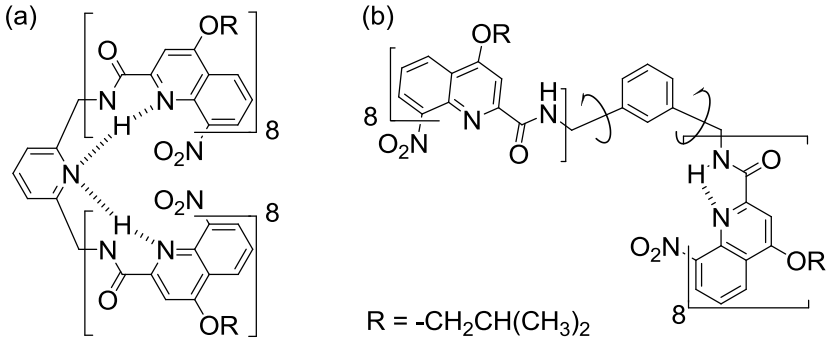

Figure 29: Schematic representation of the two aromatic oligomers tested for their helical stability. A pyridine (a) and a benzene (b) ring demonstrated the importance of conformational preferences in helical folding.

NMR experiments indicated one set of signals for this compound suggesting the existence of the homochiral orientation alone. Additionally to solution state data, the crystal structure of this compound showed a homochiral orientation, in which the central unit adopts the conformation necessary to promote helical communication.

3.2.3. Intermolecular communication and helical stability

This final section details studies on supramolecular complexes consisting of two helical strands connected with a short flexible spacer,[114, 115] connecting not the ends, but the centers of the architectures; interactions between the sides of the oligomers become possible and amenable to investigation (Figure 30). The design was inspired by the tertiary folding of biomolecules that brings together secondary motifs giving rise to more complex architectures.

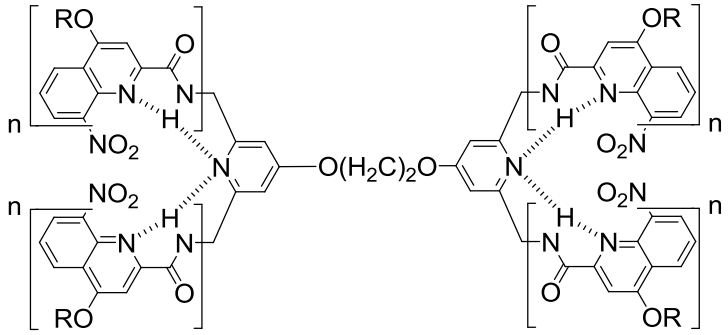

n = 8 (**i**), 4 (**ii**) and 5 (**iii**)

R = -$CH_2CH(CH_3)_2$

Figure 30: Chemical structures of compounds **i-iii**

This type of folding in biomolecules involves multiple cooperative processes, which makes its design and prediction difficult. The individual helical components consisting the tested system [Figure 29, (a)] gives rise to well-defined conformations, thus reducing the degrees of freedom to: (a) the relative handedness of the individual helices that can be homo- or hetero-chiral, (b) the relative orientation of the helices (the actual angle between the axis of the two helical components) that may fluctuate upon rotation of the helices at the spacer and (c) the conformation adopted by the ethylene glycol spacer. Entities inducing a desired conformation are absent, allowing the system to respond to its natural tendency. NMR studies and solid state data highlighted the importance of the 5th quinoline monomer - whose side chain is in very close proximity with the neighboring helix - as a key element for the communication of the two helices. To investigate further two compounds possessing shorter helical segments (**ii** and **iii**) were synthesized.

The results obtained suggested communication of the helices, probably mediated by solvent molecules, allowing tunability of the adopted conformation depending on the solvent (Table 4). The different enantiomeric ratios obtained and their solvent dependence triggered further investigation, e.g. crystals grown in chlorinated solvents were dissolved in aromatic and *vice versa*. NMR spectra were immediately recorded, showing slow interconversion from one species to the other. The data were fitted to a single exponential decay curve and it was demonstrated that the results were similar to those of the solvent dependence study (Section 3.2.2.1), with the helix inversion time of 3.5 hours in toluene hours compared to 10 hours in chloroform.

Table 4: *PM*/(*PP/MM*) ratio based on NMR experiments carried out in different solvents.

	$CDCl_3$	toluene-d_8	$CDCl_3/CD_3OD$ 2:3 vol/vol	DMSO-d_6
i	7/93	70/30	20/80	50/50
ii	74/26[a]	58/42[a]	77/23[a]	50/50
iii	7/93	*insoluble*	16/84	50/50

[a] Assignment of the two sets of signals to either the homo- or the hetero-chiral species was not feasible, but it was possible conclude that the same species dominates in all solvents.

Additionally, NMR of compound **iii** in chloroform afforded the same ratio of conformers as compound **i**, a fact which highlights the importance of the 5th quinoline segment in the interactions that take place at the helix-helix interface and subsequently inter-helical communication and stability. The similarities between the crystal structure of **iii** and that of compound **i**, supported even further the NMR results.

The NMR spectrum of compound **ii** in toluene resulted in a conformer ratio which indicates that helix-helix handedness communication is weaker in the case of the tetrameric oligomers, and that the solvent dependence follows a different trend. The crystal structure of compound **ii** revealed a parallel orientation of the two helices, presumably due to the absence of the 5th quinoline segment, which in the longer oligomer segments results in steric effects (Figure 31).

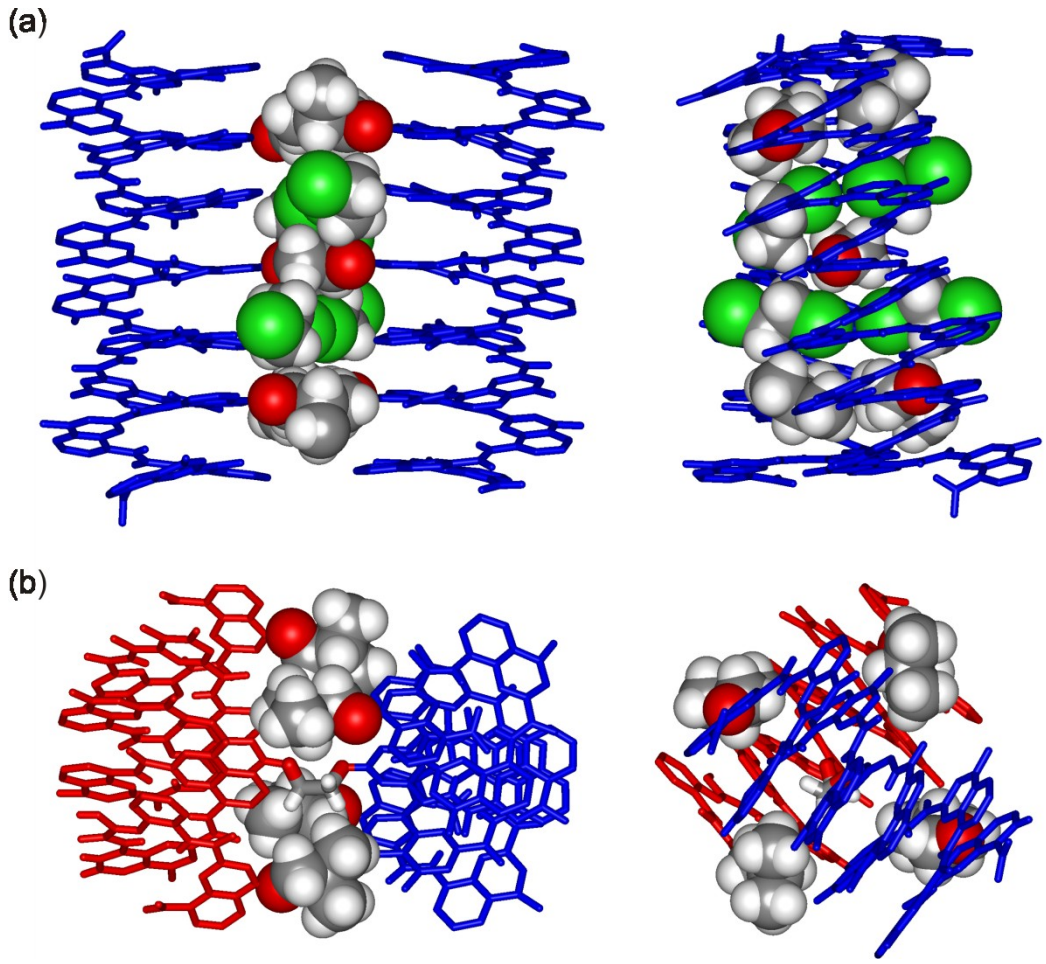

Figure 31: Crystal structures of compound: (a) **i** demonstrating the conformation of the homochiral system and the crucial positioning of 1,2-dichloroethane molecules within the cavities formed by the interacting helices; (b) **iii** showing the heterochiral and perpendicular conformation driven by steric clash between the side chains of the 5th quinoline residues.

In summary, this study demonstrated that interactions between longitudinal sides of the helices are able to induce and control helical communication and ultimately the stability of the system. Such interactions between the side-chains are able to induce conformational preferences, as shown by the analysis of the solid state structure and the solvent dependence of NMR spectra, a process which is probably mediated by solvent molecules.

4. Conclusions

In this chapter a very brief introduction about foldamers was given with particular emphasis on aromatic foldamers. Several examples that have been reported in the literature were listed in order to provide a better understanding of the elements that give rise to helical architectures. The driving forces affecting the helicity of aromatic oligoamide foldamers, as well as factors affecting the helical stability of such architectures have been briefly reviewed.

Additionally, helix-helix side-by-side and head-to-head communication has been introduced to facilitate understanding of the work presented in this manuscript. In the following chapters more parameters affecting helical stability in aromatic oligoamide foldamers will be discussed.

In the second chapter the folding propensity of several aromatic monomers, that have been widely used in oligoamide foldamer synthesis, is studied. In the third chapter, inspired by nature's stabilizing elements, the effect of introducing either intra or inter disulfide bridges in a helical system consisted of aromatic oligoamides is explored. Finally, the last chapter involves the synthesis of very long helical oligomers with a radical segment tripling strategy which is based on the observation that anhydride functionalities are easily formed, compatible with folding and protected within a helical moiety.

5. References

1. D. Seebach and J. L. Matthews, *Chemical Communications (Cambridge)*, 1997, 2015-2022.
2. S. H. Gellman, *Accounts of Chemical Research*, 1998, **31**, 173-180.
3. D. J. Hill, M. J. Mio, R. B. Prince, T. S. Hughes and J. S. Moore, *Chemical Reviews (Washington, D. C.)*, 2001, **101**, 3893-4011.
4. R. P. Cheng, S. H. Gellman and W. F. DeGrado, *Chemical Reviews (Washington, D. C.)*, 2001, **101**, 3219-3232.
5. D. Seebach, A. K. Beck and D. J. Bierbaum, *Chemical Biodiversity*, 2004, **1**, 1111-1239.
6. D. Seebach and J. Gardiner, *Accounts of Chemical Research*, 2008, **41**, 1366-1375.
7. W. S. Horne and S. H. Gellman, *Accounts of Chemical Research*, 2008, **41**, 1399-1408.
8. X. Li and D. Yang, *Chemical Communications*, 2006, 3367-3379.
9. X. Li, Y.-D. Wu and D. Yang, *Accounts of Chemical Research*, 2008, **41**, 1428-1438.
10. C. M. Goodman, S. Choi, S. Shandler and W. F. DeGrado, *Nature Chemical Biology*, 2007, **3**, 252-262.
11. Y.-D. Wu, W. Han, D.-P. Wang, Y. Gao and Y.-L. Zhao, *Accounts of Chemical Research*, 2008, **41**, 1418-1427.
12. G. Guichard and I. Huc, *Chemical Communications (Cambridge, United Kingdom)*, 2011, **47**, 5933-5941.
13. E. Berni, C. Dolain, B. Kauffmann, J.-M. Leger, C. Zhan and I. Huc, *Journal of Organic Chemistry*, 2008, **73**, 2687-2694.
14. C. Grison, S. Geneve, S. Claudel, P. Coutrot and M. Marraud, *Tetrahedron Letters*, 2003, **44**, 2297-2300.
15. H.-Y. Hu, J.-F. Xiang, Y. Yang and C.-F. Chen, *Organic Letters*, 2008, **10**, 1275-1278.
16. G. Maayan, M. D. Ward and K. Kirshenbaum, *Proceedings of the National Academy of Sciences of the United States of America*, 2009, **106**, 13679-13684.
17. R. B. Prince, S. A. Barnes and J. S. Moore, *Journal of the American Chemical Society*, 2000, **122**, 2758-2762.
18. C. Winterboer and S. Hecht, *Polymer Preprints (American Chemical Society, Division of Polymer Chemistry)*, 2008, **49**, 1005.
19. M. Wolffs, N. Delsuc, D. Veldman, V. A. Nguyexn, R. M. Williams, S. C. J. Meskers, R. A. J. Janssen, I. Huc and A. P. H. J. Schenning, *Journal of the American Chemical Society*, 2009, **131**, 4819-4829.
20. M. A. Ali, R. B. Bates, Z. D. Crane, C. W. Dicus, M. R. Gramme, E. Hamel, J. Marcischak, D. S. Martinez, K. J. McClure, P. Nakkiew, G. R. Pettit, C. C. Stessman, B. A. Sufi and G. V. Yarick, *Bioorganic & Medicinal Chemistry*, 2005, **13**, 4138-4152.
21. W. E. Hanby and H. N. Rydon, *Biochemical Journal*, 1946, **40**, 297-307.
22. H. N. Rydon, *Journal of Chemical Society*, 1964, 1328-1333.
23. I. L. Karle, B. K. Handa and C. H. Hassall, *Acta Crystallographica, Section B*, 1975, **B31**, 555-560.
24. S. Chatterjee, R. S. Roy and P. Balaram, *Journal of the Royal Society Interface*, 2007, **4**, 587-606.
25. A. Banerjee and P. Balaram, *Current Science*, 1997, **73**, 1067-1077.
26. K. Ananda, S. Aravinda, P. G. Vasudev, K. M. P. Raja, H. Sivaramakrishnan, K. Nagarajan, N. Shamala and P. Balaram, *Current Science*, 2003, **85**, 1002-1011.
27. J. Kovacs, R. Ballina, R. L. Rodin, D. Balasubramanian and J. Applequist, *J Am Chem Soc*, 1965, **87**, 119-120.
28. D. Seebach and J. Gardiner, *Accounts of Chemical Research*, 2008, **41**, 1366-1375.

29. D. Seebach, A. K. Beck, M. Brenner, C. Gaul and A. Heckel, *Chimia*, 2001, **55**, 831-838.
30. M. G. Woll, J. R. Lai, I. A. Guzei, S. J. C. Taylor, M. E. B. Smith and S. H. Gellman, *Journal of the American Chemical Society*, 2001, **123**, 11077-11078.
31. A. R. Sanford and B. Gong, *Current Organic Chemistry*, 2003, **7**, 1649-1659.
32. I. Huc and L. Cuccia, *Foldamers: Structure, properties and applications,* ed. S. Hecht and I. Huc, Wiley-VCH, Weinheim, 2007, ch. 1, 3–33.
33. M. S. Newman and D. Lednicer, *Journal of the American Chemical Society*, 1956, **78**, 4765-4770.
34. R. H. Martin, G. Morren and J. J. Schurter, *Tetrahedron Letters*, 1969, **10**, 3683-3688.
35. K. Deshayes, R. D. Broene, I. Chao, C. B. Knobler and F. Diederich, *The Journal of Organic Chemistry*, 1991, **56**, 6787-6795.
36. L. Owens, C. Thilgen, F. Diederich and C. B. Knobler, *Helvetica Chimica Acta*, 1993, **76**, 2757-2774.
37. C. Nuckolls, T. J. Katz and L. Castellanos, *Journal of the American Chemical Society*, 1996, **118**, 3767-3768.
38. C. Nuckolls, T. J. Katz, G. Katz, P. J. Collings and L. Castellanos, *Journal of the American Chemical Society*, 1998, **121**, 79-88.
39. A. Rajca, H. Wang, M. Pink and S. Rajca, *Angewandte Chemie International Edition*, 2000, **39**, 4481-4483.
40. B. Kiupel, C. Niederalt, M. Nieger, S. Grimme and F. Vögtle, *Angewandte Chemie International Edition*, 1998, **37**, 3031-3034.
41. A. Tanatani, H. Kagechika, I. Azumaya, R. Fukutomi, Y. Ito, K. Yamaguchi and K. Shudo, *Tetrahedron Letters*, 1997, **38**, 4425-4428.
42. R. Fukutomi, A. Tanatani, H. Kakuta, N. Tomioka, A. Itai, Y. Hashimoto, K. Shudo and H. Kagechika, *Tetrahedron Letters*, 1998, **39**, 6475-6478.
43. A. Tanatani, K. Yamaguchi, I. Azumaya, R. Fukutomi, K. Shudo and H. Kagechika, *Journal of the American Chemical Society*, 1998, **120**, 6433-6442.
44. K. Yamaguchi, G. Matsumura, H. Kagechika, I. Azumaya, Y. Ito, A. Itai and K. Shudo, *Journal of the American Chemical Society*, 1991, **113**, 5474-5475.
45. A. Tanatani, H. Kagechika, I. Azumaya, K. Yamaguchi and K. Shudo, *Chemical and Pharmaceutical Bulletin*, 1996, **44**, 1135-1137.
46. M. Ohkita, J.-M. Lehn, G. Baum and D. Fenske, *Chemistry - A European Journal*, 1999, **5**, 3471-3481.
47. L. A. Cuccia, J.-M. Lehn, J.-C. Homo and M. Schmutz, *Angewandte Chemie International Edition*, 2000, **39**, 233-237.
48. F. R. Heirtzler, M. Neuburger, M. Zehnder and E. C. Constable, *Liebigs Annalen*, 1997, **1997**, 297-301.
49. E. Botek, F. Castet and B. Champagne, *Chemistry – A European Journal*, 2006, **12**, 8687-8695.
50. K. M. Gardinier, R. G. Khoury and J.-M. Lehn, *Chemistry – A European Journal*, 2000, **6**, 4124-4131.
51. Y. Hamuro, S. J. Geib and A. D. Hamilton, *Angewandte Chemie*, 1994, **106**, 465-467.
52. Y. Hamuro, S. J. Geib and A. D. Hamilton, *Journal of the American Chemical Society*, 1996, **118**, 7529-7541.
53. Y. Hamuro, S. J. Geib and A. D. Hamilton, *Journal of the American Chemical Society*, 1997, **119**, 10587-10593.
54. J. Zhu, R. D. Parra, H. Zeng, E. Skrzypczak-Jankun, X. C. Zeng and B. Gong, *Journal of the American Chemical Society*, 2000, **122**, 4219-4220.
55. B. Gong, H. Zeng, J. Zhu, L. Yuan, Y. Han, S. Cheng, M. Furukawa, R. D. Parra, A. Y. Kovalevsky, J. L. Mills, E. Skrzypczak-Jankun, S. Martinovic, R. D. Smith, C. Zheng, T. Szyperski, X. C. Zeng and L. Yua, *Proceedings of the National Academy of Sciences of the United States of America*, 2002, **99**, 11583-11588.
56. V. Berl, I. Huc, R. G. Khoury, M. J. Krische and J.-M. Lehn, *Nature (London)*, 2000, **407**, 720-723.
57. H. Jiang, J.-M. Leger, C. Dolain, P. Guionneau and I. Huc, *Tetrahedron*, 2003, **59**, 8365-8374.
58. H. Jiang, J.-M. Leger and I. Huc, *Journal of the American Chemical Society*, 2003, **125**, 3448-3449.
59. I. Huc, *European Journal of Organic Chemistry*, 2004, 17-29.
60. J. C. Nelson, J. G. Saven, J. S. Moore and P. G. Wolynes, *Science*, 1997, **277**, 1793-1796.
61. M. S. Gin, T. Yokozawa, R. B. Prince and J. S. Moore, *Journal of the American Chemical Society*, 1999, **121**, 2643-2644.
62. R. S. Lokey and B. L. Iverson, *Nature (London)*, 1995, **375**, 303-305.
63. A. J. Zych and B. L. Iverson, *Journal of the American Chemical Society*, 2000, **122**, 8898-8909.
64. S. J. Geib, C. Vicent, E. Fan and A. D. Hamilton, *Angewandte Chemie*, 1993, **105**, 85-85.
65. E. C. Constable, M. G. B. Drew, G. Forsyth and M. D. Ward, *Journal of the Chemical Society, Chemical Communications*, 1988, 1450-1451.
66. P. K.-K. Ho, K.-K. Cheung, S.-M. Peng and C.-M. Che, *Journal of the Chemical Society, Dalton Transactions*, 1996, 1411-1417.
67. R. B. Prince, T. Okada and J. S. Moore, *Angewandte Chemie International Edition.*, 1999, **38**, 233-236.
68. A.-M. Stadler, N. Kyritsakas and J.-M. Lehn, *Chemical Communications (Cambridge, U. K.)*, 2004, 2024-2025.
69. F. Zhang, S. Bai, G. P. A. Yap, V. Tarwade and J. M. Fox, *Journal of the American Chemical Society*, 2005, **127**, 10590-10599.
70. K.-J. Chang, B.-N. Kang, M.-H. Lee and K.-S. Jeong, *Journal of the American Chemical Society*, 2005, **127**, 12214-12215.

71. H. Juwarker, J. M. Lenhardt, D. M. Pham and S. L. Craig, *Angewandte Chemie International Edition England*, 2008, **47**, 3740-3743.
72. V. Berl, M. J. Krische, I. Huc, J.-M. Lehn and M. Schmutz, *Chemistry - A European Journal*, 2000, **6**, 1938-1946.
73. M. Inouye, M. Waki and H. Abe, *Journal of the American Chemical Society*, 2004, **126**, 2022-2027.
74. H. Abe, N. Masuda, M. Waki and M. Inouye, *Journal of the American Chemical Society*, 2005, **127**, 16189-16196.
75. P. B. Dervan, *Science*, 1986, **232**, 464-471.
76. P. B. Dervan and R. W. Burli, *Current Opinion in Chemical Biology*, 1999, **3**, 688-693.
77. A. S. Determan, B. G. Trewyn, V. S. Y. Lin, M. Nilsen-Hamilton and B. Narasimhan, *Journal of Controlled Release*, 2004, **100**, 97-109.
78. I. Saraogi and A. D. Hamilton, *Chemical Society Reviews*, 2009, **38**, 1726-1743.
79. B. Gong, H. Zeng, J. Zhu, L. Yua, Y. Han, S. Cheng, M. Furukawa, R. D. Parra, A. Y. Kovalevsky, J. L. Mills, E. Skrzypczak-Jankun, S. Martinovic, R. D. Smith, C. Zheng, T. Szyperski and X. C. Zeng, *Proceedings of the National Academy of Sciences of the United States of America*, 2002, **99**, 11583-11588.
80. X. Yang, A. L. Brown, M. Furukawa, S. Li, W. E. Gardinier, E. J. Bukowski, F. V. Bright, C. Zheng, X. C. Zeng and B. Gong, *Chemical Communications (Cambridge, U. K.)*, 2003, 56-57.
81. X. Yang, L. Yuan, K. Yamato, A. L. Brown, W. Feng, M. Furukawa, X. C. Zeng and B. Gong, *Journal of the American Chemical Society*, 2004, **126**, 3148-3162.
82. L. Yuan, H. Zeng, K. Yamato, A. R. Sanford, W. Feng, H. S. Atreya, D. K. Sukumaran, T. Szyperski and B. Gong, *Journal of the American Chemical Society*, 2004, **126**, 16528-16537.
83. X. Yang, L. Yuan, K. Yamato, A. L. Brown, W. Feng, M. Furukawa, X. C. Zeng and B. Gong, *Journal of the American Chemical Society*, 2004, **126**, 3148-3162.
84. L. Yuan, A. R. Sanford, W. Feng, A. Zhang, J. Zhu, H. Zeng, K. Yamato, M. Li, J. S. Ferguson and B. Gong, *Journal of Organic Chemistry*, 2005, **70**, 10660-10669.
85. B. Gong, *Accounts of Chemical Research*, 2008, **41**, 1376-1386.
86. B. Gong, *Science China: Chemistry*, 2010, **53**, 45-51.
87. J. Cao, M. Kline, Z. Chen, B. Luan, M. Lv, W. Zhang, C. Lian, Q. Wang, Q. Huang, X. Wei, J. Deng, J. Zhu and B. Gong, *Chemical Communication (Cambridge, U. K.)*, 2012, **48**, 11112-11114.
88. D.-W. Zhang, X. Zhao, J.-L. Hou and Z.-T. Li, *Chemical Reviews (Washington, DC, United States)*, 2012, **112**, 5271-5316.
89. L.-Y. You, S.-G. Chen, X. Zhao, Y. Liu, W.-X. Lan, Y. Zhang, H.-J. Lu, C.-Y. Cao and Z.-T. Li, *Angewandte Chemie, International Edition*, 2012, **51**, 1657-1661.
90. J.-L. Hou, X.-B. Shao, G.-J. Chen, Y.-X. Zhou, X.-K. Jiang and Z.-T. Li, *Journal of the American Chemical Society*, 2004, **126**, 12386-12394.
91. X. Zhao, X.-Z. Wang, X.-K. Jiang, Y.-Q. Chen, Z.-T. Li and G.-J. Chen, *Journal of the American Chemical Society*, 2003, **125**, 15128-15139.
92. Z.-Q. Wu, X.-B. Shao, C. Li, J.-L. Hou, K. Wang, X.-K. Jiang and Z.-T. Li, *Journal of the American Chemical Society*, 2005, **127**, 17460-17468.
93. Z.-T. Li, J.-L. Hou, C. Li and H.-P. Yi, *Chemistry - An Asian Journal*, 2006, **1**, 766-778.
94. J. Iriondo-Alberdi, K. Laxmi-Reddy, B. Bouguerne, C. Staedel and I. Huc, *ChemBioChem*, 2010, **11**, 1679-1685.
95. B. Baptiste, F. Godde and I. Huc, *ChemBioChem*, 2009, **10**, 1765-1767.
96. P. V. Jena, P. S. Shirude, B. Okumus, K. Laxmi-Reddy, F. d. r. Godde, I. Huc, S. Balasubramanian and T. Ha, *Journal of the American Chemical Society*, 2009, **131**, 12522-12523.
97. P. S. Shirude, E. R. Gillies, S. Ladame, F. d. r. Godde, K. Shin-ya, I. Huc and S. Balasubramanian, *Journal of the American Chemical Society*, 2007, **129**, 11890-11891.
98. E. R. Gillies, F. Deiss, C. Staedel, J.-M. Schmitter and I. Huc, *Angewandte Chemie International Edition*, 2007, **46**, 4081-4084.
99. L. Delaurière, Z. Dong, K. Laxmi-Reddy, F. Godde, J.-J. Toulmé and I. Huc, *Angewandte Chemie International Edition*, 2012, **51**, 473-477.
100. J. Buratto, C. Colombo, M. Stupfel, S. J. Dawson, C. Dolain, B. Langlois d'Estaintot, L. Fischer, T. Granier, M. Laguerre, B. Gallois and I. Huc, *Angewandte Chemie International Edition*, 2014, **53**, 883-887.
101. A. C. Cope and R. D. Bach, *Organic Synthesis*, 1969, **49**, 39.
102. K. Abou-Hadeed, Z. A. Molnar, P. Göksaltık, R. W. Kunz, A. Linden and H.-J. Hansen, *Helvetica Chimica Acta*, 2012, **95**, 885-921.
103. C. A. Hunter and D. H. Purvis, *Angewandte Chemie*, 1992, **104**, 779-782.
104. J. F. Malone, C. M. Murray, G. M. Dolan, R. Docherty and A. J. Lavery, *Chemistry of Materials*, 1997, **9**, 2983-2989.
105. V. Pophristic, S. Vemparala, I. Ivanov, Z. Liu, M. L. Klein and W. F. DeGrado, *Journal of Physical Chemistry B*, 2006, **110**, 3517-3526.
106. J. F. Galan, J. Brown, J. L. Wildin, Z. Liu, D. Liu, G. Moyna and V. Pophristic, *Journal of Physical Chemistry B*, 2009, **113**, 12809-12815.
107. Z. Liu, R. C. Remsing, D. Liu, G. Moyna and V. Pophristic, *Journal of Physical Chemistry B*, 2009, **113**, 7041-7044.

108. Z. Liu, A. Teslja and V. Pophristic, *Journal of Computational Chemistry*, 2011, **32**, 1846-1858.
109. N. Delsuc, T. Kawanami, J. Lefeuvre, A. Shundo, H. Ihara, M. Takafuji and I. Huc, *ChemPhysChem*, 2008, **9**, 1882-1890.
110. T. Qi, V. Maurizot, H. Noguchi, T. Charoenraks, B. Kauffmann, M. Takafuji, H. Ihara and I. Huc, *Chemical Communications (Cambridge, United Kingdom)*, 2012, **48**, 6337-6339.
111. D. Sanchez-Garcia, B. Kauffmann, T. Kawanami, H. Ihara, M. Takafuji, M.-H. Delville and I. Huc, *Journal of the American Chemical Society*, 2009, **131**, 8642-8648.
112. N. Delsuc, L. Poniman, J.-M. Leger and I. Huc, *Tetrahedron*, 2012, **68**, 4464-4469.
113. C. Dolain, J.-M. Leger, N. Delsuc, H. Gornitzka and I. Huc, *Proceedings of the National Academy of Sciences of the United States of America*, 2005, **102**, 16146-16151.
114. N. Delsuc, J.-M. Leger, S. Massip and I. Huc, *Angewandte Chemie International Edition*, 2007, **46**, 214-217.
115. N. Delsuc, S. Massip, J.-M. Leger, B. Kauffmann and I. Huc, *Journal of the American Chemical Society*, 2011, **133**, 3165-3172.

Chapter 2: Evaluating the effect of aromatic composition in the stability of aromatic oligoamide foldamers

1. Introduction

In the introductory chapter a wide and diverse range of artificial foldamers consisting of various building blocks has been presented that demonstrates their ability to adopt stable helically folded conformations. Particular emphasis was given to aromatic oligoamide foldamers. Proteins (which also have the ability to populate this particular structural element) consist of a constant repeat unit in their backbone and variable side chains that utterly bequeath the adopted secondary structure to the system. This happens either because they impart local constraints on the backbone folding or due to their participation in intra- or inter-molecular interactions. Examples of both of these cases have been reported in the literature.[1-14] Aromatic oligoamide foldamers have an advantage over proteins in this respect in that predictable folding can be achieved, which is independent to side chain functionality and position.

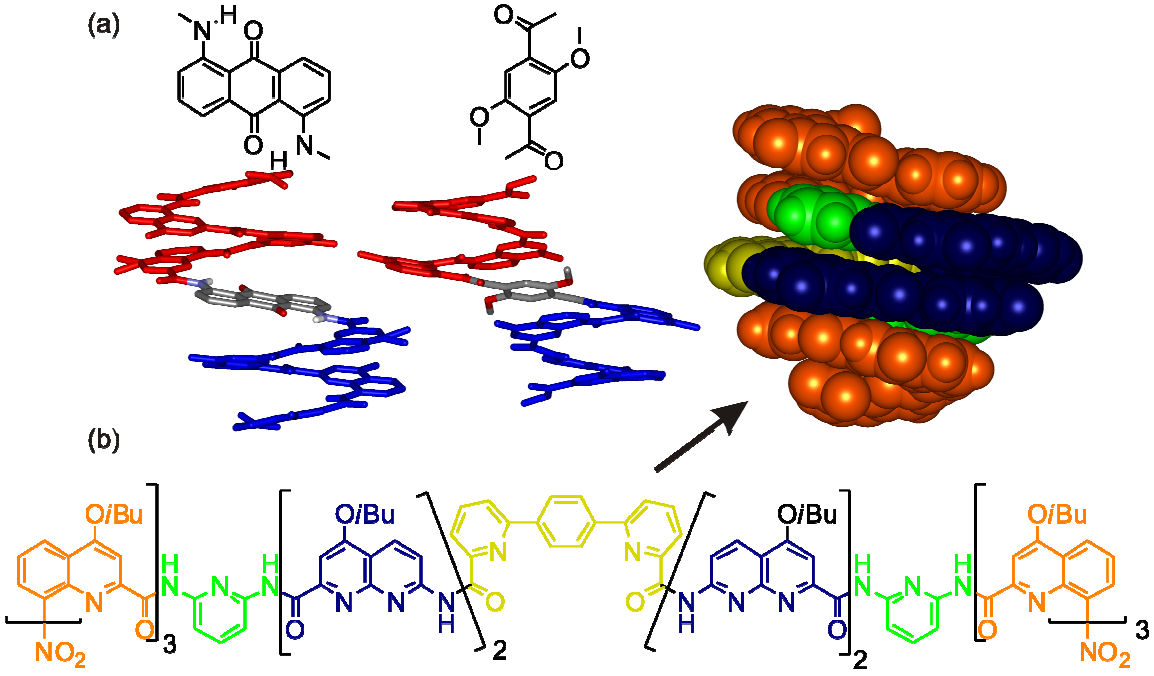

Figure 1: Unnatural helical architectures resulting from heterogeneous backbones. (a) X-ray structures of helical architectures possessing two different helix inversion centers. Right-handed (*P*) helix colored in blue and left-handed (*M*) colored in red and (b) helix with variable diameter resulting from the utilization of different monomers. In all cases Side chains and solvent molecules have been omitted for clarity.

Helix diameter can be altered throughout an AOF sequence by installing building blocks which can impart a particular curvature at any given point (Figure 1b).[15, 16] These architectures have been engaged in the fields of molecular recognition and catalysis. Casting minor alterations in the composition of the sequence can result in radical changes in the structural characteristics; hence better understanding of the unique contribution of each individual monomer within a foldameric sequence can lead to improved design and function. In addition to the resulting curvature attributed by each individual monomer, its directional dipole moment or the generation of a binding site, that will eventually stabilize the desired system, are also important.

However, little is known about the contribution of each monomer on helical stability, which is a crucial property for applications of AOFs. For example, in the case of helical capsules for molecular recognition[15, 17-19] the contribution of each monomer inside the sequence influences the dynamic binding and release of guest molecules and consequently the functional properties of these structures. Since the guest cannot simply slip through the capsule walls binding and release from the host must occur via a partially unfolded conformation.[20] Thus, the higher the stability of the helix, the slower these processes will occur.

Quinoline, naphthyridine and anthracene units form the majority of building blocks used in the synthesis of functional aromatic oligoamide foldamers in the Huc group. The folding ability of these moieties is mainly due to local conformational preferences induced by endocyclic or exocyclic moieties on each aromatic monomer at *ortho* positions to the amide bonds[21], for example, endocyclic nitrogen atoms and exocyclic fluorine, chlorine and methyl groups.[22, 23] By placing such a monomer within a foldamer sequence, electrostatic (either attractive or repulsive) and steric interactions occur within the backbone, leading to a unique folding pattern.

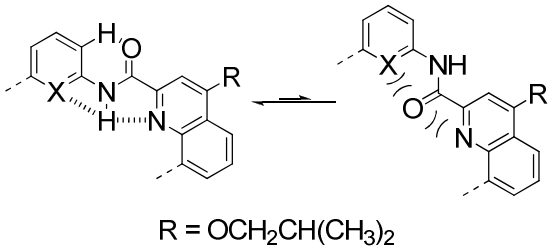

Scheme 1: Schematical representation of electrostatic interactions occurring in the aryl-amide linkage of aromatic oligoamide foldamers.

It is known that in the case of hydrogen bonding, stability increases with the increase of the electronegativity of the acceptors.[24] On the other hand, this principle mostly applies in

the case of nitrogen and oxygen, since halogen atoms are considered weak hydrogen-bond acceptors.[25-27] Even in the case of the most electronegative fluorine the contribution is not great due to its low polarizability and tightly contracted lone pairs.[27] To date, experimental data evaluating the precise contribution of individual aromatic monomers in the overall stability of the helix are limited.

This chapter investigates the contribution of commonly used functionalities[22, 23, 28], located on a benzene ring, on the helical stability of foldamers. In order to evaluate the preorganization of different aromatic units and their propensity to mediate the formation of the helical structure, five oligomers consisting of two quinoline tetramers coupled to a central diamine unit were synthesized and their thermodynamic stability was evaluated.

2. Design

In the context of this study five aromatic central units were chosen to screen the scope of preorganized building blocks that have been used for the construction of aromatic oligoamide foldamers. Evaluation of their contribution to helical stability was assessed by chiral HPLC and NMR experiments. Pyridine, fluorobenzene and chlorobenzene diamino units were chosen due to the hydrogen bonding potential between the amidic proton and the acceptor atom (N, F or Cl) *ortho* to its position. Beside their electronegativity the main difference between these atoms lies in their molecular radius and the steric hindrance that they can potentially create (Scheme 2).

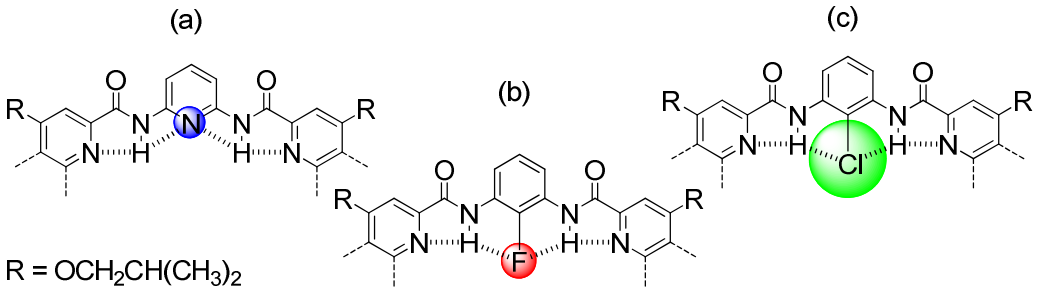

Scheme 2: Schematical representation of the three H–bond acceptors located in the central part of the oligomeric sequences, highlighting the difference in their molecular radii

While planarity of the amide bond should be conserved in all five cases due to the overall conjugation of the system, benzyl and tolyl units do not possess the ability to stabilize local conformations through hydrogen bonding. Thus in the case of the non-substituted benzene free rotation could be expected about the amide bond (Scheme 3a), but in the case of the tolyl bearing foldamer, the methyl group should be positioned

proximal to the hydrogen of the amide to avoid steric clash with its carbonyl moiety (Scheme 3b).

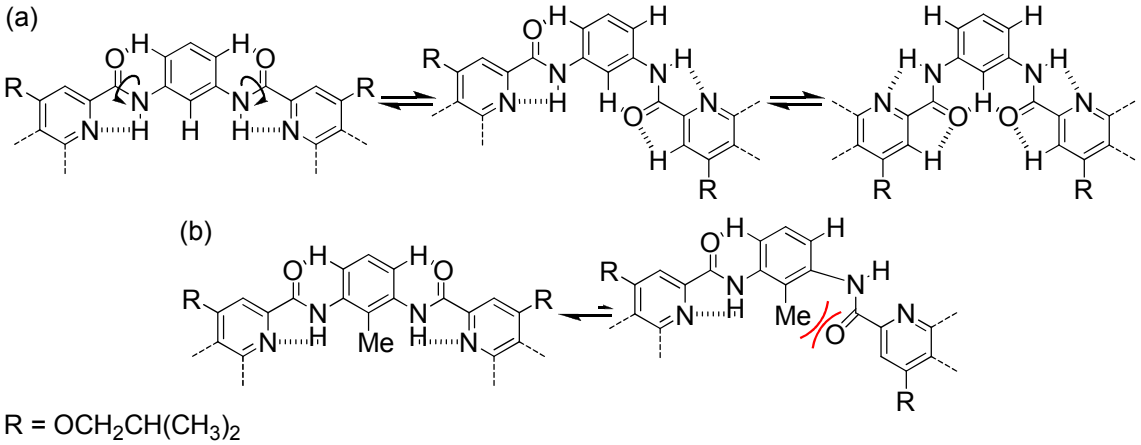

Scheme 3: Schematic representation presenting the conformational preferences impied by the aryl-amide linkages for (a) benzyl and (b) tolyl units.

All of these units were sandwiched between two tetrameric quinoline segments to form five nonameric sequences. A diamine was chosen as a central unit instead of an amino acid analogue, in order to facilitate synthesis. The diamine coupled with the same acid chloride at both sides gives rise to a C_2 symmetrical structure making data interpretation easier. Their length of 9 aromatic units was chosen according to previous studies,[29] which indicated that for this particular length racemization kinetics should not be too fast, enabling separation of the two enantiomers by chiral HPLC and/or analysis by NMR experiments to provide dynamic information. However, racemization was predicted to be sufficiently fast to allow its observation within reasonable experimental time. In these helically folded structures, helical handedness inversion requires total or at least partial unfolding of the oligomer, thus the rate of racemization is directly correlated to the stability of the folded architecture. The effect of introducing a new monomer between two tetrameric quinoline Q_4 segments can therefore be evaluated by measuring the rate of racemization to assess the handedness communication of the two helical segments through the additional unit.

3. Synthesis

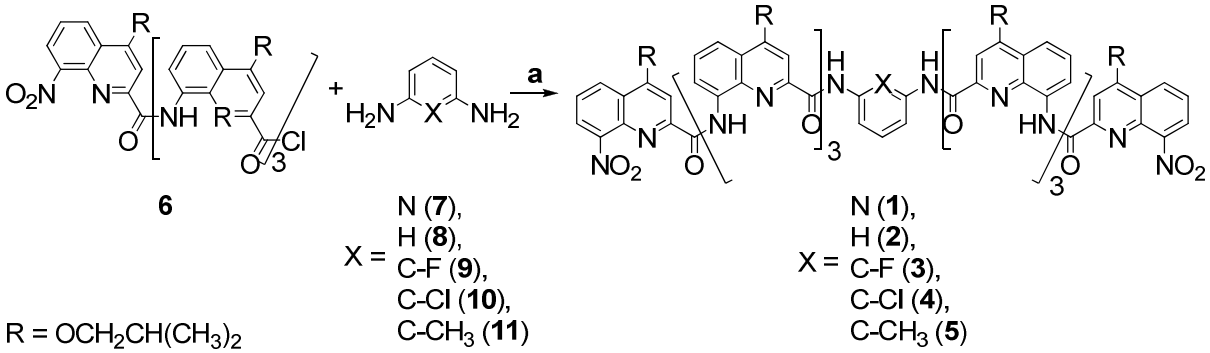

Scheme 4: Synthesis of the 9-mers **1**, **2**, **3**, **4** and **5**; (a) DIPEA, CH_2Cl_2, r.t, overnight.

The choice of isobutoxy side chains was to provide good solubility in organic solvents and crystallinity, with the latter also being enhanced by the presence of the two terminal nitro groups. The synthetic strategy used to obtain these compounds involved the coupling reaction of the central diamine units with two quinoline tetramer acids (Scheme 4). These units were synthesized by a segment doubling strategy as described in the literature,[30] and subsequently coupled to the five different central diamine units, via acid chloride activation of the carboxylic acids. Pyridine, benzene and tolyl diamines were commercially available while fluoro- and chloro-benzene diamines were prepared according to literature procedures.[31, 32] Unoptimized yields for the synthesis of the five compounds ranged from 60-80% (See experimental section).

4. Results

4.1. Solid state data

Crystals suitable for X-ray crystal structure analysis of the five oligomers were obtained by liquid-liquid diffusion of methanol in solutions of nonamers in chlorinated solvent (dichloromethane or chloroform) and are presented in Figure 2. Crystallographic tables for the five oligomers are provided in the experimental section.

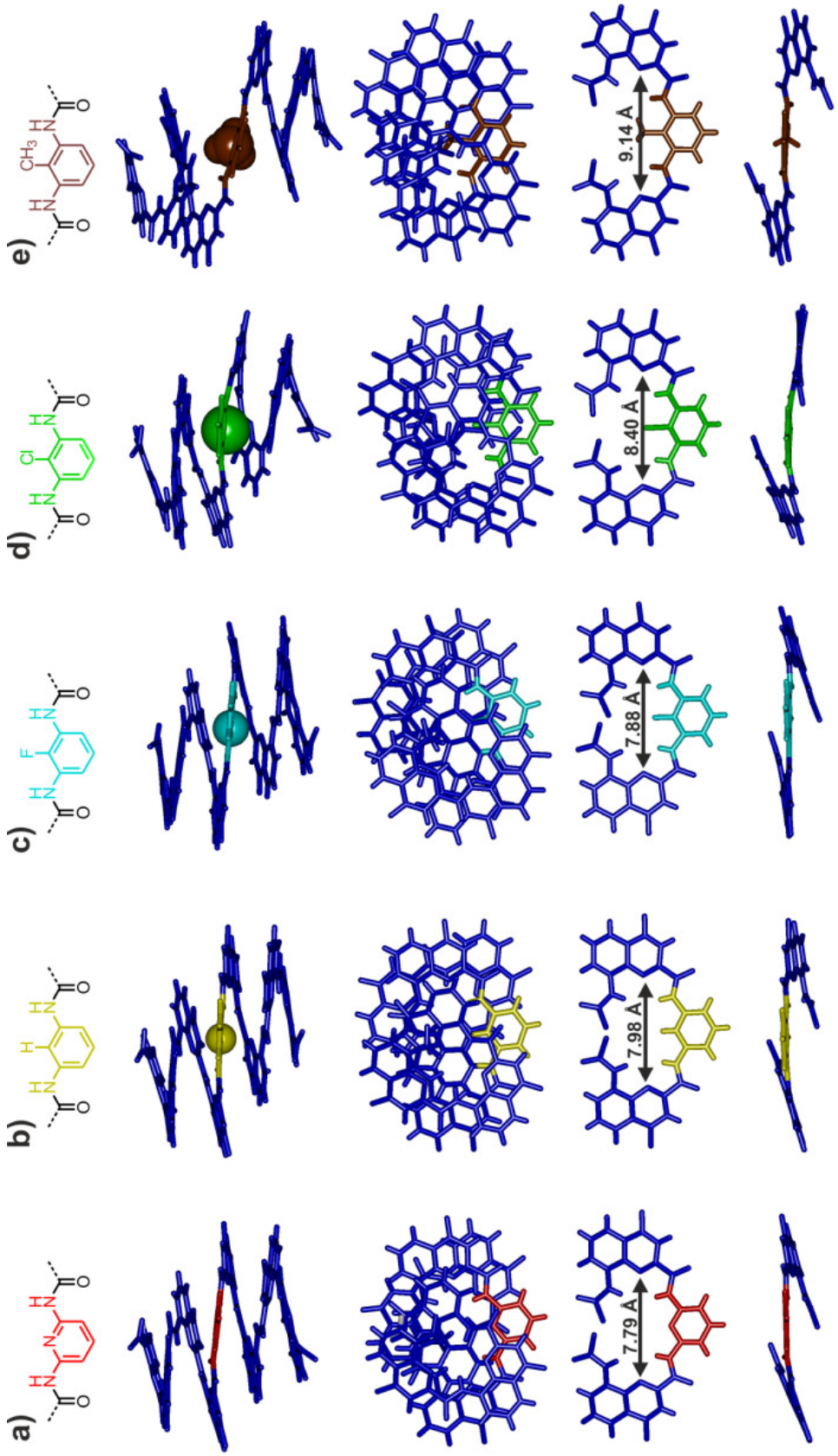

Figure 2: X-Ray structures of compounds (a) **1**(N), (b) **2**(H), (c) **3**(F), (d) **4**(Cl) and (e) **5**(CH_3). From top to bottom: Side view of the helical architecture, top view, slice of the central part of the helical segment highlighting the diamino central unit (side and top view, respectively). Side-chains and solvent molecules have been removed for clarity.

All the obtained structures demonstrate helical architectures, where the central unit adopts a conformation in which the two hydrogen atoms of the amide bond point towards the interior of the helical cavity, thus propagating the helical handedness to the two quinoline tetrameric extremities. These two blocks show a regular curved shape except for **4** where the presence of the chlorine atom creates steric hindrance that eventually distorts the helical pattern. Although the methyl of the tolyl central unit of **5** is even more bulky than chlorine, the shape of the tetrameric blocks is more conserved. The steric hindrance of the central atom can be monitored by the distance between the two endocyclic nitrogen of its neighboring quinolines units. This distance is similar for **1** (7.79 Å) and **3** (7.88 Å) for which a bifurcated hydrogen bond can be formed between the amidic protons and the acceptor (N in **1** and F in **3**) and larger for compound **2** (7.98 Å), where no local conformational preferences are expected. In **4**, the chlorine atom is involved in the same hydrogen bond pattern but due to its larger size, it gives rise to steric repulsions that elongate this distance to 8.40 Å. This distance is even longer in **5** (9.14 Å), due to the fact that the methyl group is larger than chlorine and not a hydrogen bond acceptor. This size difference has an impact on the overall size of the molecular architecture. The length of the structure between the two nitro termini, is 10.86 Å for **2**, 10.92 Å for **3**, 12.41 Å for **4** and 14.22 Å for **5**, in agreement with the increasing hindrance of the central unit. But this observation can not be extrapolated to compound **1** (11.56 Å) for which the presence of the hydrogen bond between the amide NH and the endocyclic nitrogen, and the absence of any central atom, increases the curvature of the central part of the oligomer. This creates a gap in the aromatic stacking that eventually results in the elongation of the molecule. Although these five X-ray structures show propagation of the helical architecture with conservation of handedness, it is important to note that they only represent a snapshot of all the possible conformations which may exist in solution.

4.2. Solution state data

4.2.1. NMR experiments

In order to afford dynamic information about the structural stability of these oligomers, NMR studies were carried out. ^{1}H NMR spectra recorded at 25 °C showed sharp signals for compound **1**, **3** and **4**, with sharp diastereotopic signals of the methylene side chain protons indicating that no helical handedness inversion occured

during the course of the spectrum recording (Figure 3). Due to the chiral nature of the helix, the two protons carried by the first carbon of the side chain are in different environment and therefore should give two distinct signals. However if helical inversion occurs during the course of the measurement the environment of each geminal proton would be inverted, resulting in an averaging of the NMR signals (i.e. observed as broadness).

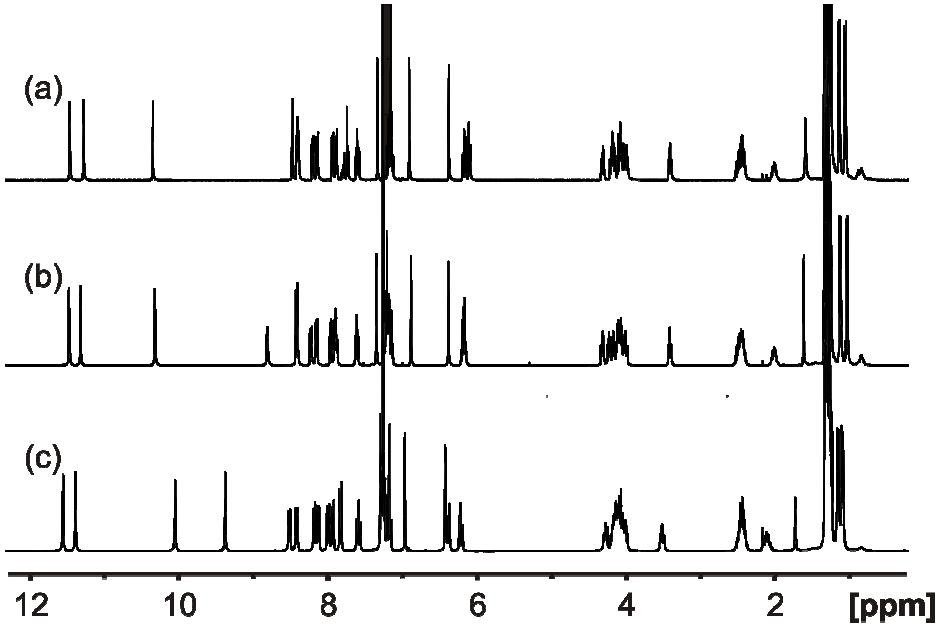

Figure 3: NMR spectra of compound **1**(N) (a), **3**(F) (b) and **4**(Cl) (c) recorded at 25 °C in $CDCl_3$, demonstrating sharp signals.

Indeed, upon heating at 50 °C, broadening of these signals can be noticed for compound **4** (Figure 4) indicating that helical handedness inversion becomes fast on the NMR timescale at this temperature. In contrast the rest of the spectrum remains sharp, indicating that at this higher temperature the overall structure is not destabilized.

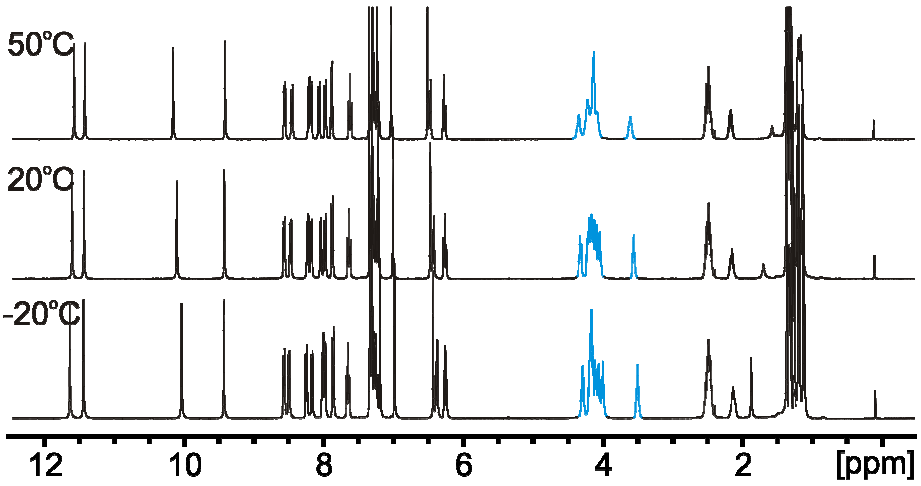

Figure 4: Temperature dependant NMR experiment (in $CHCl_3$) for compound **4**(Cl). CH_2 signals are highlighted in blue.

In contrast, compound **1** and **3**, did not show any change in their spectra (Figures 5 & 6, respectively) at 50 °C suggesting stable helical architecture, which results in slow handedness inversion on an NMR timescale.

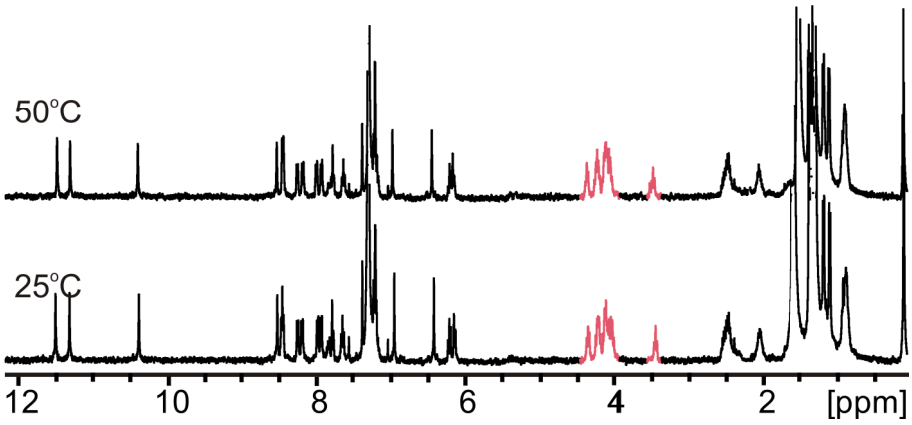

Figure 5: Temperature dependant NMR experiment (in $CHCl_3$) for compound **1**(N)**.** CH_2 signals are highlighted in fuchsia.

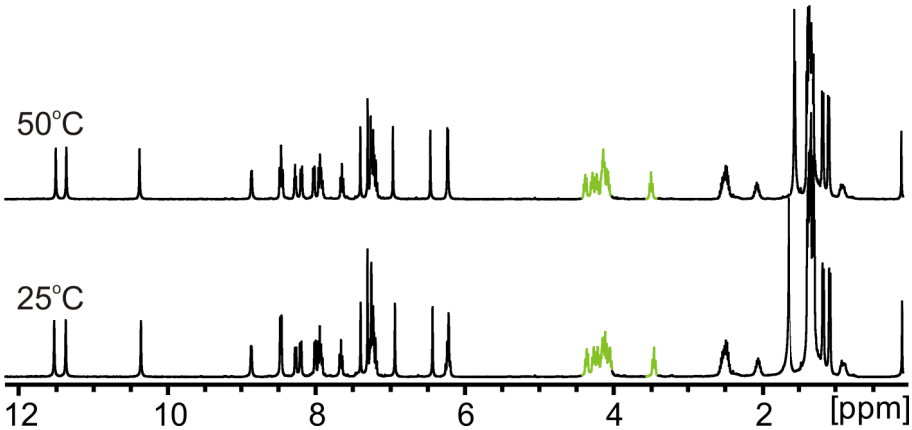

Figure 6: Temperature dependant NMR experiment (in $CHCl_3$) for compound **3**(F). CH_2 signals are highlighted in green.

On the other hand, compound **5** (Figure 7), for which no hydrogen bonds stabilize the local amide bond conformation around the central unit, afforded broad NMR signals at 25 °C, reflecting high internal dynamics of the molecule and a poor folded organization. Upon cooling, all signals sharpen and the isobutoxy methylene signals become diastereotopic (-20 °C), indicating stabilization of the architecture and causing helical inversion kinetics to become slow on an NMR timescale.

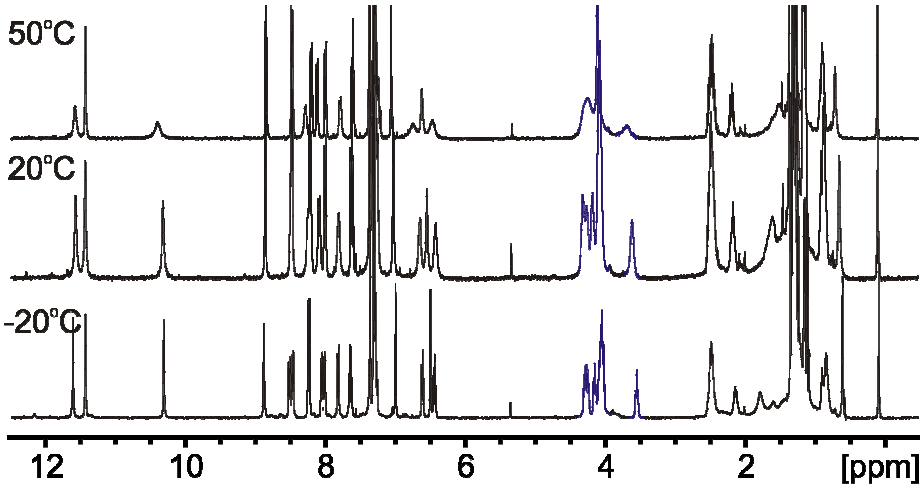

Figure 7: Temperature dependant NMR experiment (in $CHCl_3$) for compound **5**(CH_3). CH_2 signals are highlighted in blue.

Compound **2** (Figure 8) has an intermediate behavior meaning that sharp diasterotopic signals of the side chain could be observed at 25 °C and even at 50 °C indicating slow helical handedness inversion on an NMR timescale. However, some aromatic signals were broad reflecting a dynamic environment around these protons.

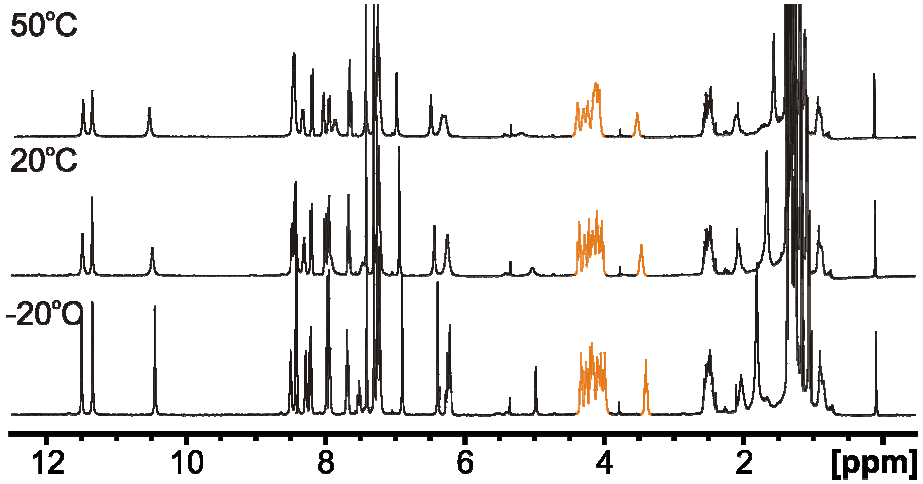

Figure 8: Temperature dependant NMR experiment (in $CHCl_3$) for compound **2**(H). CH_2 signals are highlighted in orange.

Upon cooling to -20 °C this motion appeared to become slower, resulting in sharp signals which were assigned to the protons of the central benzene unit, using COSY NMR experiments (Figure 9). It is interesting to note the strong upfield shift of the internal hydrogen (in between the two amino groups of the benzene unit) at 5 ppm at -20 °C, which is a consequence of the strong current effect of the stacked quinoline rings in the helix. The destabilization in **2** is localized to the central part of the molecule since the rest of the oligomer shows sharp NMR signals even at higher temperature. This observation reflects the fact that there is no strong structuration of the central part of the oligomer when using the benzenediamine unit, due to the absence of a hydrogen bond acceptor on this ring. A similar remark can be made for **5** (possessing the central diaminotoluene unit). Indeed, when the internal hydrogen of **2** is replaced by the bulky methyl group, additional steric hindrance is encountered that further reduces the stability of the entire helical architecture, making this oligomer the least stable of the tested compounds.

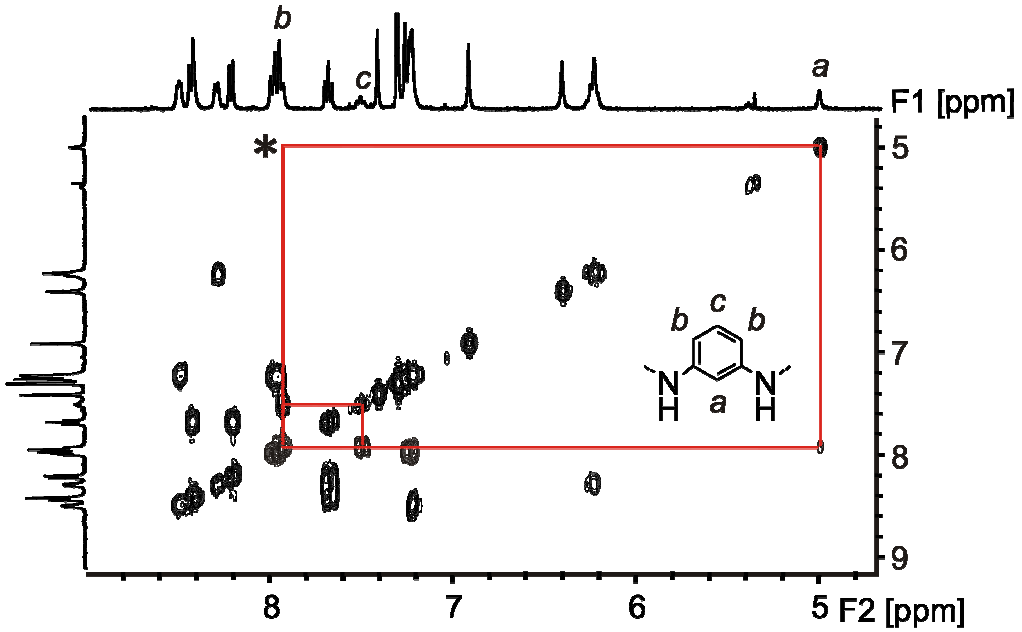

Figure 9: COSY NMR of compound **2** (in $CHCl_3$) demonstrating the correlation between the protons of the central benzene ring. The spectrum was recorded at 0°C. The asterisk represents a signal that is visible at lower threshold.

This NMR study afforded dynamic information about internal molecular motion and helical handedness inversion kinetics for compounds **2**, **4** and **5**, behaviour which was observable on an NMR timescale. However, for compound **1** and **3** (which show higher stability) no sign of destabilization or racemisation could be observed even at higher temperature using NMR spectroscopy. For this reason, a different technique was

used in order to quantitatively assess the stability imparted by the pyridine and the fluorobenzene central units.

4.2.2. Chiral HPLC analysis

Dynamic chiral HPLC was carried out in order to evaluate the racemisation kinetics and thermodynamic parameters of the more stable compounds. These experiments were performed by Oliver Trapp and his colleagues in the institute of Organic Chemistry in Heidelberg. Separation of the two *P* and *M* conformational enantiomers of this class of compounds can be achieved using a chiral (CHIRALPAK IA) stationary phase as previously described,[29] if no helical handedness inversion occurs during the HPLC experiment. If racemisation is fast helix inversion occurs and only one peak showing an average retention time should be observed. However if partial interconversion occurs during the separation process, characteristic batman's® head plateau between the well separated peaks of the *P* and *M* enantiomers should be seen. From peak profiles *i.e.* the relative height of this plateau and the retention time at different temperature, racemisation kinetics and interconversion phenomena can be extracted by using the unified equation.[33]

Briefly, the unified equation allows the direct calculation of reaction rate constants and Gibbs activation energies ($\Delta G^{\ddagger}$) for all types of first-order reactions taking place in chromatographic or electrophoretic systems, regardless of the initial concentrations of the interconverting analytes A and B and the equilibrium constant $K_{A/B}$. The following figure shows the mathematical separation of dynamic and on-column reaction chromatographic elution profiles into non-interconverted peaks, represented by time-dependent Gaussian distribution functions ΦA(t) and ΦB(t), and the interconverted part, represented by the stochastic distribution functions Ψ(t) (Figure 10).

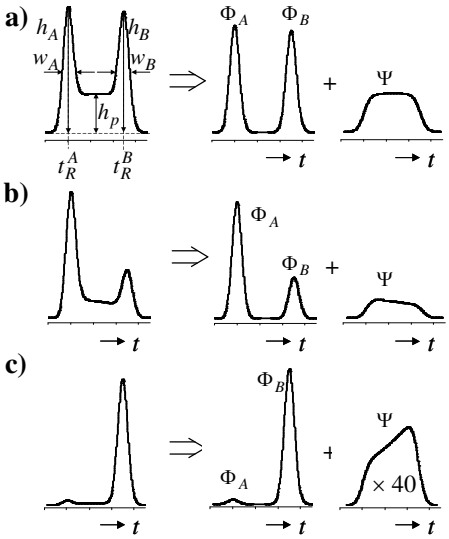

Figure 10: a) Degenerated reversible (pseudo-) first-order reaction with an equilibrium constant $K_{A/B}$ =1, b) reversible (pseudo-) first-order reaction with $K_{A/B}$ >1 and c) reversible (pseudo-) first-order reaction with $K_{A/B}$ <1.

A detailed description of the derivation has been reported by Trapp *et al.*[33] The analytical solutions of the unified equation are implemented in the computer program DCXplorer.[34] The program DCXplorer can be downloaded from the homepage of the corresponding author (http://trapp.uni-hd.de/downloads.html).

4.2.2.1. Dynamic chiral HPLC results

The methodology of Trapp and co-workers was applied to the different studied oligomers and HPLC chromatograms recorded in a temperature range from -30 °C to 65 °C. HPLC of compounds **4** and **5** did not show any separation of *P* and *M* enantiomers even at low temperatures which was attributed to a fast helix handedness inversion even at -30 °C. Lower temperatures could not be used due to the high viscosity of the eluant and the increasing pressure in the HPLC apparatus at this temperature. Chromatograms of compounds **1** and **3** recorded at 5 °C showed two sharp peaks corresponding to the *P* and *M* enantiomers indicating a slow racemisation rate at this temperature. Upon increasing the temperature the helical inversion rate was increased, resulting in the appearance of a plateau (batman's® head). The peaks that finally coalesced to one broad peak at 65 °C and 35 °C respectively for **1** and **3** [Figure 11 (a) & (b)].A similar observation could be made for **2** [Figure 11 (c)] but at 5 °C complete separation was not obtain and lower temperatures (-30 °C) were required in order to reduce the inversion rate, resulting in two distinct peaks on the chromatogram.

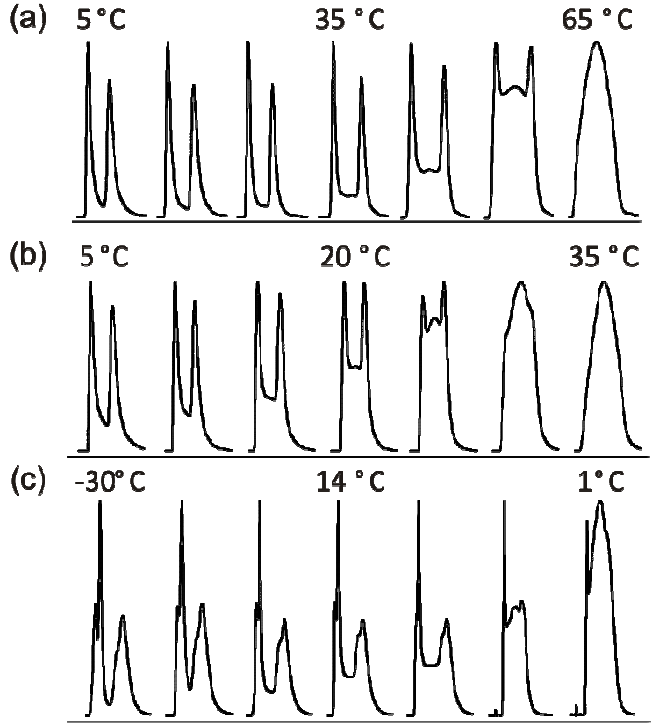

Figure 11: Variable temperature chiral HPLC chromatogram of compound **1**(N) (a), **3**(F) (b) and **2**(H) (c), with experimental temperatures ranging from 5 - 65 ^{o}C, 5 - 35 ^{o}C and -30 - 1 ^{o}C, respectively.

This observation indicates that compound **2** has greater conformational flexibility than **1** and **3** resulting in a faster helix inversion. This can be attributed to the less restricted benzene central unit to which no intramolecular hydrogen bond can be made from the amide. Processing of these HPLC chromatogram data at variable temperatures gave the enantiomerization barrier, $\Delta G^{\neq}$, with the activation enthalpy $\Delta H^{\neq}$ and the activation enthropy $\Delta S^{\neq}$. $\Delta G^{\neq}$ is the Gibbs energy which represents the energy difference between the most stable, fully folded conformation and the partially unfolded intermediate that allows handedness inversion to occur. Values are reported in Table 1. At 25 °C, it can be seen that **2** has the lowest enantiomerization barrier (78.9 kJ.mol^{-1}) which is in agreement with the lower stability previously discussed. It can also be noted that this low barrier does not seem to come from its enthalpic factor (57.9 kJ.mol^{-1}) since this is similar to that of **3**(F) (58.3 kJ.mol^{-1}) and higher than that of **1** (52.5 kJ.mol^{-1}). The lower enthalpic activation of **1** is surprising considering the additional hydrogen bond which can be formed to the pyridine. The main thermodynamic difference in the racemization of these compounds is the entropic parameter that is more important in **1** (-123 J.K^{-1}.mol^{-1}) than for **3** (-89 J.K^{-1}.mol^{-1}) and **2** (-70 J.K^{-1}.mol^{-1}) but in all cases exhibits a high negative value. Such high entropic parameters are usually considered an evidence for a dissociative mechanism of the inversion process. In these compounds no such mechanism can occur (as it would require covalent bond cleavage) and such observation may reflect the strong stabilization brought by the extensive π—π stacking

and hydrogen bonds in the folded state.

Table 1: $\Delta G^{\ddagger}$, $\Delta H^{\ddagger}$ and $\Delta S^{\ddagger}$ values for compounds **1**, **2** and **3**

Compound	**1**	**2**	**3**
$\Delta G^{\ddagger}_{(298K)}$ (KJ.mol^{-1})	89.1	78.9	84.7
$\Delta H^{\ddagger}$ (KJ.mol^{-1})	52.5±1.0	57.9±4.0	58.3±1.5
$\Delta S^{\ddagger}$ (J.K^{-1}.mol^{-1})	-123±5	-70±9	-89±4

5. Conclusions

Combining the results of dynamic NMR and HPLC experiments allowed us to evaluate the helical stability of oligomers containing different aromatic diamino central units and their propensity to mediate helical communication. Qualitative data were obtained from temperature dependant NMR experiments which showed that compounds **1** and **3** are the most stable compounds probably due to the conformational restriction brought by the central fluorine and endocyclic nitrogen atoms. When the central unit contains the more bulky chlorine atom **4**, although an internal hydrogen bond can be formed with the amide proton, steric hindrance appears to perturb the internal stacking of the aromatic units resulting in faster inversion kinetics. A similar observation was made for compound **5** where the methyl group of toluene is bulky and also not a hydrogen bond acceptor, making this oligomer the least stable of the study. Compound **2** which has no local conformation preference in its central part showed slow racemization due to efficient aromatic stacking in the helical shape, but was also shown to be dynamic in the center of the helix. Dynamic chiral HPLC afforded quantitative information about the stability of oligomers **1**, **2** and **3** and provided inversion thermodynamics. It revealed that the compound bearing a pyridine unit in the center, **1**, is more stable than the oligomer containing a fluorobenzene ring, **3**, as observed by NMR. More interestingly it shows that the high handedness inversion energy barrier of these oligomers results from the strong π—π stacking between the aromatic monomer units. This study highlights the importance of considering the impact of including functional groups, not only in terms of beneficial effects such as hydrogen bond formation and conformational restriction, but also in terms of the steric hindrance which is also incorporated.

6. Experimental Section

Materials and Methods. All reactions were carried out under a dry nitrogen atmosphere. Commercial reagents were purchased from Sigma-Aldrich or Alfa-Aesar and were used without further purification unless otherwise specified. Chloroform, *N,N'*-diisopropylethylamine (DIPEA) were distilled from calcium hydride (CaH_2) prior to use. DCM was dried using a solvent purification system (Mbraun). Reactions were monitored by thin layer chromatography (TLC) on Merck silica gel 60-F254 plates and observed under UV light. Silica gel chromatography was carried out on Merck GEDURAN Si60 (40-63 μm). ^{1}H NMR and ^{13}C NMR spectra were recorded in $CDCl_3$ on 300 MHz Bruker Avance 2 and 400 MHz Bruker Avance spectrometers. Chemical shifts are reported in ppm, (δ) relative to the signal of the NMR solvent used. ^{1}H NMR splitting patterns with observed first-order coupling are designated as singlet (s), doublet (d), triplet (t), or quartet (q). Coupling constants (*J*) are reported in hertz (Hz). Splitting patterns that could not be interpreted or easily visualized are designated as multiplet (m) or broad (br). Electrospray ionization mass spectrometric low and high resolution data (ES-MS, HRMS) were obtained from the Mass Spectrometry Laboratory at the European Institute of Chemistry and Biology (IECB), Pessac, France.

Nuclear Magnetic Resonance

NMR Spectra were recorded with a Bruker Avance 400 NB US NMR spectrometer by means of a 5 mm direct QNP 1H/X probe with gradient capabilities or on a Bruker 300 Avance.

Crystallography

Data were collected using a Rigaku FRX microfocus rotating anode generator with Cu-K_α radiation (1.54178 Å) and varimax HF optics. The data collection, unit cell refinement and data reduction were performed using the CrystalClear software package. The positions of non-H atoms were determined by the program SHELX D and the position of the H atoms were deduced from coordinates of the non-H atoms and confirmed by Fourier Synthesis. H atoms were included for structure factor calculations but not refined. Selected single crystal were mounted on a cryoloop under oil and frozen into a N_2 stream at 100 K.

Crystallographic tables

	Compound 1*	Compound 2*	Compound 3*	Compound 4*	Compound 5*
chemical	$C_{117}H_{115}N_{19}O_{20}$	$C_{118}H_{116}N_{18}O_{20}$	$C_{118}H_{115}FN_{18}O_{20}$	$C_{118}H_{115}ClN_{18}O_{20}$	$C_{119}H_{118}N_{18}O_{20}$
Fw	1164.71	1102.00	2344.19	2140.74	2120.32
Crystal	orthorhombic	triclinic	triclinic	monoclinic	monoclinic
Space group	Pbcn	P-1	P-1	C2/c	C2/c
a, Å	18.649(4)	13.8800(5)	13.9751(9)	34.6218(9)	54.7651(7)
b, Å	31.677(6)	17.9601(5)	17.9501(13)	23.9215(3)	33.8211(6)
c, Å	21.873(4)	24.4392(13)	24.2730(18)	29.9656(5)	25.4434(3)
α, deg	90.00	82.099(6)	98.464(4)	90.00	90.00
β, deg	90.00	90.034(5)	90.244(4)	96.0090(10)	92.1730(10)
γ, deg	90.00	82.324(4)	97.202(3)	90.00	90.00
V, Å^3	12921(4)	5979.3(4)	5973.6(7)	24681.3(8)	47092.8(12)
Z	8	4	2	8	8
D (calcd.),	1197	1.224	1.303	1.219	1.366
temp. (K)	100	113(2)	113(2)	113(2)	113(2)
uniq, refl. / total no. of refl. coll.	11741/58989	21968/84787	17804/17804	20755/56917	41720/41720
abs. coeff.	0.713	0.901	1.547	1.086	2.176
*R*1 ($I > 2\sigma(I)$)	0.0909	0.1128	0.1312	0.1436	0.1592
w*R*2 (all data)	0.2356	0.2770	0.3108	0.3004	0.3239
data/restraints/ parameters	11741/83/716	21968/12/1411	17804/0/1430	20755/0/1430	41720/0/2830
GooF on F2 [c]	1.189	1.025	1.309	1.005	1.282

[a] $R1 = \Sigma||F_0|-|F_c||/\Sigma|F_0|$

[b] $wR2 = [\Sigma[w(F_0^2-F_c^2)^2]/\Sigma[w(F_0^2)_2]^{1/2}$, where $w = 1/\sigma^2(F_0^2)+(aP)^2+bP$, $P = (F_0^2+2F_c^2)/3$

[c] $GooF = [\Sigma[w(F_0^2-F_c^2)^2]/(n-p)]^{1/2}$ where n = no. of reflections and p = no. of refined parameters.

[*] including solvents molecules

HPLC experiments

HPLC measurements were performed on an Agilent Technologies 1200 HPLC (Agilent Technologies, Palo Alto, California, USA), equipped with a binary solvent pump, an autosampler, membrane solvent degasser, DAD detector and a quadrupole mass spectrometer Agilent 6120, equipped with an APCI source. All operations were

controlled by the Agilent ChemStation software (Agilent Technologies, Palo Alto, California, USA). Enantioselective separations were performed on a Chiralpak® IA-3 column (150 mm, i.d. 4.6 mm, particle size 3 μm), which was bought from Chiral Technologies, Illkirch, France. The solvents used (*n*-hexane, 2-propanol and dichloromethane) were obtained from Sigma-Aldrich (HPLC-grade quality). Dynamic HPLC measurements of all compounds were performed with solutions of the substances in dichloromethane.

Compound **1**: To a solution of 2,6-diamino pyridine (3.5 mg, 0.032 mmol) and anhydrous DIEA (0.05 mL, 0.28 mmol) in dry DCM (1 mL) was added via a cannula, under N_2 atmosphere, tetramer acid chloride (0,098 mmol) in anhydrous DCM (2 mL) and the reaction was left to react overnight at room temperature. The reaction mixture was then extracted in DCM and the organic layer was washed with 5% citric acid solution (10 mL) and saturated solution of NaCl (10 mL). The organic layer was dried over Na_2SO_4 for 1 hour and evaporated. The crude solid was purified by flash silica gel column chromatography (EtOAc/DCM) 5:95 to 40:60. The resulting compound was purified further by liquid-liquid diffusion crystallization using DCM/MeOH and afforded a yellow solid with 78% yield (48 mg). ^{1}H NMR ($CDCl_3$): δ 11.47 (2H, s), 11.28 (2H, s), 10.35 (2H, s), 8.47 (2H, s), 8.43–8.37 (4H, m), 8.21 (2H, dd, *J* = 7.5, 1.3 Hz), 8.14 (2H, dd, *J* = 8.3, 1.2 Hz), 7.94 (2H, dd, *J* = 7.5, 1.1 Hz), 7.89 (2H, dd, *J* = 8.3, 1.2 Hz), 7.82–7.71 (3H, m), 7.60 (2H, t, *J* = 8.0 Hz), 7.34 (2H, s), 7.22–7.11 (8H, m), 6.91 (2H, s), 6.38 (2H, s), 6.17 (2H, t, *J* = 7.8 Hz), 6.10 (2H, dd, *J* = 8.3, 1.3 Hz), 4.31 (2H, dd, *J* = 8.8, 6.7 Hz), 4.22–3.96 (12H, m), 3.41 (2H, t, *J* = 8.1 Hz), 2.55–2.36 (6H, m), 2.01 (2H, m), 1.35–1.23 (36H, m), 1.14 (6H, d, *J* = 6.8 Hz), 1.06 (6H, d, *J* = 6.8 Hz). ^{13}C NMR ($CDCl_3$): 163.49, 163.25, 163.11, 162.72, 161.31, 161.21, 160.60, 159.91, 153.76, 150.98, 148.69, 147.95, 147.92, 145.31, 139.48, 139.05, 138.39, 138.15, 137.97, 134.71, 133.63, 133.49, 127.80, 126.74, 126.64, 126.43, 125.68, 124.20, 123.96, 122.35, 122.09, 121.39, 117.35, 117.23, 116.97, 116.87, 116.35, 114.45, 109.28, 100.48, 99.60, 98.16, 97.27, 76.02, 75.71, 75.66, 74.81, 30.05, 28.67, 28.60, 28.58, 28.34, 20.13, 19.84, 19.82, 19.79, 19.77, 19.74, 19.67, 1.37. HRMS (ES^+): *m/z* calcd for $C_{117}H_{115}N_{19}O_{20}$ $[M+H]^+$ 2106.8644 found 2106.8788.

Compound **2**: To a solution of diaminobenzene (3.2 mg, 0.030 mmol) and anhydrous DIEA (0.05 mL, 0.28 mmol) in dry DCM (1 mL) was added via a cannula, under N_2 atmosphere, tetramer acid chloride (0,090 mmol) in anhydrous DCM (1.8 mL) and the

reaction was left to react overnight at room temperature. The reaction mixture was then extracted in DCM and the organic layer was washed with 5% citric acid solution (10 mL) and saturated solution of NaCl (10 mL). The organic layer was dried over Na_2SO_4 for 1 hour and evaporated. The crude solid was purified by flash silica gel column chromatography (EtOAc/DCM) 15:85 to 40:60. The resulting compound was purified further by liquid-liquid diffusion crystallisation using DCM/MeOH and afforded a yellow solid with 72% yield (45 mg). ^{1}H NMR ($CDCl_3$): δ 11.44 (2H, bs), 11.30 (2H, s), 10.45 (2H, bs), 8.50–8.33 (6H, m), 8.26 (2H, bs), 8.16 (2H, d, *J* = 8.1 Hz), 7.96 (2H, d, *J* = 7.6 Hz), 7.91 (2H, d, *J* = 8.2 Hz), 7.89 (2H, bs), 7.62 (2H, t, *J* = 7.9 Hz), 7.41 (1H, bs), 7.37 (2H, s), 7.24–7.14 (8H, m), 6.90 (2H, s), 6.40 (2H, s), 6.21 (4H, bs), 4.99 (1H, bs), 4.38–3.93 (14H, m), 3.43 (2H, t, *J* = 7.6 Hz), 2.56–2.36 (6H, m), 2.03 (2H, m), 1.36–1.22 (36H, m), 1.13 (6H, d, *J* = 6.8 Hz), 1.05 (6H, d, *J* = 6.4 Hz). ^{13}C NMR ($CDCl_3$): 163.60, 163.46, 163.12, 162.99, 161.52, 160.84, 160.52, 158.99, 153.79, 151.03, 148.33, 148.29, 145.38, 139.01, 138.10, 138.02, 137.72, 137.25, 134.27, 133.52, 133.21, 129.73, 127.82, 126.92, 126.58, 125.64, 124.24, 123.94, 122.41, 121.95, 121.51, 117.55, 117.47, 117.42, 117.00, 116.39, 114.78, 114.40, 110.64, 100.51, 99.90, 98.02, 97.37, 76.05, 75.77, 74.97, 30.05, 28.65, 28.58, 28.53, 28.34, 20.07, 19.82, 19.80, 19.79, 19.73, 19.64, 1.36. HRMS (ES^+): *m/z* calcd for $C_{118}H_{116}N_{18}O_{20}$ $[M+H]^+$ 2105.8692 found 2105.8811.

Compound **3**: To a solution of 2,6-diaminofluorobenzene (4.2 mg, 0.033 mmol) and anhydrous DIEA (0.05 mL, 0.28 mmol) in dry DCM (1 mL) was added via a canula, under N_2 atmosphere, tetramer acid chloride **6** (0,101 mmol) in anhydrous DCM (2.3 mL) and the reaction was left to react overnight at room temperature. The reaction mixture was then extracted in DCM and the organic layer was washed with 5% citric acid solution (10 mL) and saturated solution of NaCl (10 mL). The organic layer was dried over Na_2SO_4 for 1 hour and evaporated. The crude solid was purified by flash silica gel column chromatography (EtOAc/DCM) 5:95 to 50:50. The resulting compound was purified further by liquid-liquid diffusion crystallisation using DCM/MeOH and afforded a yellow solid with 80% yield (51 mg). ^{1}H NMR ($CDCl_3$): δ 11.47 (2H, s), 11.32 (2H, s), 10.32 (2H, s), 8.81 (2H, d, *J* = 3.9 Hz), 8.42 (4H, d, *J* = 7.8 Hz), 8.23 (2H, dd, *J* = 7.1, 1.7 Hz), 8.15 (2H, dd, *J* = 8.2, 0.8 Hz), 7.96 (2H, dd, *J* = 7.7, 1.0 Hz), 7.91 (2H, dd, *J* = 8.3, 1.1 Hz), 7.89 (2H, t, *J* = 7.5 Hz), 7.61 (2H, t, *J* = 7.9 Hz), 7.35 (2H, s), 7.24–7.11 (9H, m), 6.89 (2H, s), 6.38 (2H, s), 6.19 (2H, t, *J* = 8.3 Hz), 6.16 (2H, dd, *J* = 8.4, 1.9 Hz), 4.31 (2H, dd, *J* = 8.6, 6.5 Hz), 4.23 (2H, dd, *J* = 8.9, 6.5 Hz), 4.17 (2H, dd, *J* = 9.0, 6.7 Hz), 4.14–3.97 (8H, m), 3.41 (2H, t, *J* = 8.3 Hz), 2.55–

2.37 (6H, m), 2.01 (2H, m), 1.35–1.23 (36H, m), 1.12 (6H, d, *J* = 6.7 Hz), 1.03 (6H, d, *J* = 6.7 Hz). ^{13}C NMR ($CDCl_3$): 163.58, 163.44, 163.11, 162.74, 161.43, 161.33, 160.59, 159.25, 153.73, 150.94, 148.07, 145.33, 139.08, 138.14, 137.79, 134.50, 133.64, 133.47, 123.96, 122.42, 122.08, 121.32, 116.87, 76.03, 75.74, 28.67, 28.60, 28.57, 28.33, 20.10, 19.84, 19.81, 19.78, 19.75, 19.64, 143.44, 141.02, 138.56, 127.85, 126.76, 126.67, 126.49, 125.73, 125.66, 125.59, 124.24, 117.52, 117.36, 116.94, 116.41, 114.69, 114.52, 100.46, 99.70, 97.96, 97.19, 75.76, 74.90, 30.05, 1.36. HRMS (ES^+): *m/z* calcd for $C_{118}H_{115}FN_{18}O_{20}$ $[M+H]^+$ 2123.8597 found 2123.8740.

Compound **4**: To a solution of 2,6-diaminochlorobenzene (4.4 mg, 0.031 mmol) and anhydrous DIEA (0.05 mL, 0.28 mmol) in dry DCM (1 mL) was added via a cannula, under N_2 atmosphere, tetramer acid chloride (0,090 mmol) in anhydrous DCM (1.8 mL) and the reaction was left to react overnight at room temperature. The reaction mixture was then extracted in DCM and the organic layer was washed with 5% citric acid solution (10 mL) and saturated solution of NaCl (10 mL). The organic layer was dried over Na_2SO_4 for 1 hour and evaporated. The crude solid was purified by flash silica gel column chromatography (EtOAc/DCM) 5:95 to 50:50. The resulting compound was purified further by liquid-liquid diffusion crystallisation using DCM/MeOH and afforded a yellow solid with 72% yield (46 mg). ^{1}H NMR ($CDCl_3$): δ 11.56 (2H,s), 11.39 (2H, s), 10.05 (2H, s), 9.38 (2H, s), 8.52 (2H, dd, *J* = 7.7, 0.8 Hz), 8.42 (2H, dd, *J* = 8.2, 1.5 Hz), 8.18 (2H, dd, *J* = 8.3, 1.1 Hz), 8.13 (2H, dd, *J* = 7.6, 1.1 Hz), 8.00 (2H, dd, *J* = 7.7, 1.0 Hz), 7.94 (2H, dd, *J* = 8.4, 1.1 Hz), 7.83 (2H, d, *J* = 8.1 Hz), 7.59 (2H, t, *J* = 8.0 Hz), 7.31–7.14 (11H, m), 6.96 (2H, s), 6.42 (2H, s), 6.38 (2H, dd, *J* = 8.5, 1.1 Hz), 6.22 (2H, d, *J* = 8.0 Hz), 4.28 (2H, dd, *J* = 8.9, 6.5 Hz), 4.22–3.95 (12H, m), 3.51 (2H, t, *J* = 7.6 Hz), 2.44 (6H, m), 2.11 (2H, m), 1.36–1.21 (36H, m), 1.15 (6H, d, *J* = 6.7 Hz), 1.09 (6H, d, *J* = 6.7 Hz). ^{13}C NMR ($CDCl_3$): 163.49, 163.31, 162.98, 162.79, 161.84, 161.18, 160.59, 159.37, 153.61, 150.61, 148.55, 148.26, 145.30, 139.11, 138.91, 138.16, 137.91, 134.61, 133.73, 133.66, 133.64, 127.94, 127.10, 126.76, 126.58, 126.55, 125.92, 124.33, 123.83, 122.37, 122.25, 121.32, 118.24, 117.58, 117.17, 117.06, 116.56, 114.77, 114.20, 112.67, 100.33, 99.43, 98.19, 97.28, 75.94, 75.73, 75.58, 74.82, 31.36, 30.15, 28.62, 28.57, 28.54, 28.49, 19.95, 19.77, 19.74, 19.71, 1.35. HRMS (ES^+): *m/z* calcd for $C_{118}H_{115}ClN_{18}O_{20}$ $[M+H]^+$ 2139.8302 found 2139.8421.

Compound **5**: To a solution of 2,6-diaminotoluene (3.9 mg, 0.032 mmol) and anhydrous DIEA (0.05 mL, 0.28 mmol) in dry DCM (1 mL) was added via a cannula, under N_2

atmosphere, tetramer acid chloride (0,098 mmol) in anhydrous DCM (2 mL) and the reaction was left to react overnight at room temperature. The reaction mixture was then extracted in DCM and the organic layer was washed with 5% citric acid solution (10 mL) and saturated solution of NaCl (10 mL). The organic layer was dried over Na_2SO_4 for 1 hour and evaporated. The crude solid was purified by flash silica gel column chromatography (EtOAc/DCM) 2:98 to 40:60. The resulting compound was purified further by liquid-liquid diffusion crystallisation using $CHCl_3$/MeOH and afforded a yellow solid with 60% yield (38 mg). ^{1}H NMR ($CDCl_3$): δ 11.52 (2H, s), 11.38 (2H, s), 10.27 (2H, s), 8.81 (2H, s), 8.43 (2H, d, *J* = 7.4 Hz), 8.20 (2H, bs), 8.16 (2H, d, *J* = 8.3 Hz), 8.05 (2H, d, *J* = 7.1 Hz), 7.96 (2H, d, *J* = 8.3 Hz), 7.76 (2H, bd, *J* = 4.2 Hz), 7.57 (2H, t, *J* = 8.0 Hz), 7.36–7.16 (9H, m), 6.99 (2H, s), 6.61 (2H, bs), 6.51 (2H, bs), 6.38 (2H, bs), 4.37–3.93 (14H, m), 3.58 (2H, bs), 2.44 (6H, m), 2.14 (2H, m), 1.34–1.23 (36H, m), 1.11 (12H, bs). ^{13}C NMR ($CDCl_3$): 163.63, 163.36, 163.08, 163.02, 161.49, 161.38, 160.61, 159.03, 153.73, 150.68, 149.54, 148.57, 145.34, 139.17, 138.55, 138.22, 138.07, 135.34, 134.24, 133.64, 133.45, 127.98, 127.17, 126.77, 126.39, 126.27, 125.00, 124.43, 123.86, 122.54, 122.27, 121.56, 121.52, 118.14, 117.90, 117.76, 117.19, 116.73, 115.09, 115.01, 100.37, 99.76, 98.52, 97.38, 75.99, 75.73, 75.65, 75.02, 31.27, 30.03, 28.63, 28.59, 28.49, 19.78, 19.75, 10.38, 1.34. HRMS (ES^+): *m/z* calcd for $C_{119}H_{118}N_{18}O_{20}$ $[M+H]^+$ 2119.8848 found 2119.8979.

7. References

1. M. Ramirez-Alvarado, F. J. Blanco and L. Serrano, *Nature Structural Biology*, 1996, **3**, 604-612.
2. E. de Alba, M. A. Jiménez and M. Rico, *Journal of the American Chemical Society*, 1997, **119**, 175-183.
3. A. J. Maynard and M. S. Searle, *Chemical Communications*, 1997, 1297-1298.
4. A. J. Maynard, G. J. Sharman and M. S. Searle, *Journal of the American Chemical Society*, 1998, **120**, 1996-2007.
5. S. R. Griffiths-Jones, G. J. Sharman, A. J. Maynard and M. S. Searle, *Journal of Molecular Biology*, 1998, **284**, 1597-1609.
6. H. E. Stanger and S. H. Gellman, *Journal of the American Chemical Society*, 1998, **120**, 4236-4237.
7. J. F. Espinosa, F. A. Syud and S. H. Gellman, *Protein Science*, 2002, **11**, 1492-1505.
8. A. G. Cochran, N. J. Skelton and M. A. Starovasnik, *Proceedings of the National Academy of Sciences*, 2001, **98**, 5578-5583.
9. S. M. Butterfield and M. L. Waters, *Journal of the American Chemical Society*, 2003, **125**, 9580-9581.
10. R. Mahalakshmi, S. Raghothama and P. Balaram, *Journal of the American Chemical Society*, 2006, **128**, 1125-1138.
11. U. A. Ramagopal, S. Ramakumar, D. Sahal and V. S. Chauhan, *Proceedings of the National Academy of Sciences*, 2001, **98**, 870-874.
12. Rudresh, S. Ramakumar, U. A. Ramagopal, Y. Inai, S. Goel, D. Sahal and V. S. Chauhan, *Structure*, 2004, **12**, 389-396.
13. D. Haldar, H. Jiang, J.-M. Léger and I. Huc, *Angewandte Chemie International Edition*, 2006, **45**, 5483-5486.
14. D. Haldar, H. Jiang, J.-M. Léger and I. Huc, *Tetrahedron*, 2007, **63**, 6322-6330.
15. Y. Ferrand, A. M. Kendhale, B. Kauffmann, A. Grelard, C. Marie, V. Blot, M. Pipelier, D. Dubreuil and I.

Huc, *Journal of the American Chemical Society*, **132**, 7858-7859.
16. V. Maurizot, C. Dolain, Y. Leydet, J.-M. Leger, P. Guionneau and I. Huc, *J. Am. Chem. Soc.*, 2004, **126**, 10049-10052.
17. E. Berni, J. Garric, C. Lamit, B. Kauffmann, J.-M. Leger and I. Huc, *Chemical Communications (Cambridge, United Kingdom)*, 2008, 1968-1970.
18. C. Bao, B. Kauffmann, Q. Gan, K. Srinivas, H. Jiang and I. Huc, *Angewandte Chemie, International Edition*, 2008, **47**, 4153-4156.
19. J. Garric, J.-M. Leger and I. Huc, *Chemistry - A European Journal*, 2007, **13**, 8454-8462.
20. Y. Ferrand, N. Chandramouli, A. M. Kendhale, C. Aube, B. Kauffmann, A. Grelard, M. Laguerre, D. Dubreuil and I. Huc, *Journal of the American Chemical Society*, **134**, 11282-11288.
21. I. Huc, *European Journal of Organic Chemistry*, 2004, 17-29.
22. C. Li, S.-F. Ren, J.-L. Hou, H.-P. Yi, S.-Z. Zhu, X.-K. Jiang and Z.-T. Li, *Angewandte Chemie, International Edition*, 2005, **44**, 5725-5729.
23. J. J. Mousseau, L. Xing, N. Tang and L. A. Cuccia, *Chemistry - A European Journal*, 2009, **15**, 10030-10038.
24. L. Pauling, *Journal of the American Chemical Society*, 1932, **54**, 988-1003.
25. G. Jeffrey, *Acta Crystallographica Section B*, 2000, **56**, 333-334.
26. J. D. Dunitz and R. Taylor, *Chemistry - A European Journal*, 1997, **3**, 89-98.
27. J. D. Dunitz, *ChemBioChem*, 2004, **5**, 614-621.
28. L. Wang, Z.-Y. Xiao, J.-L. Hou, G.-T. Wang, X.-K. Jiang and Z.-T. Li, *Tetrahedron*, 2009, **65**, 10544-10551.
29. N. Delsuc, T. Kawanami, J. Lefeuvre, A. Shundo, H. Ihara, M. Takafuji and I. Huc, *ChemPhysChem*, 2008, **9**, 1882-1890.
30. T. Qi, T. Deschrijver and I. Huc, *Nature Protocols*, 2013, **8**, 693-708.
31. C. Dolain, J.-M. Leger, N. Delsuc, H. Gornitzka and I. Huc, *Proceedings of the National Academy of Sciences of the United States of America*, 2005, **102**, 16146-16151.
32. C. M. Hall, J. B. Wright, H. G. Johnson and A. J. Taylor, *Journal of Medicinal Chemistry*, 1977, **20**, 1337-1343.
33. O. Trapp, *Analytical Chemistry*, 2006, **78**, 189-198.
34. O. Trapp, *Journal of Chromatography B*, 2008, **875**, 42-47.

Chapter 3: Disulfide bond formation and helical stability

1. Introduction

1.1. Disulfide bonds in nature

The tertiary structure of proteins is governed by a large number of weak interactions, such as hydrogen bonding,[1] hydrophobic interactions,[2] salt bridges and less polar interactions.[3] In addition to these noncovalent forces, certain proteins are stabilized with disulfide bonds.[4] A disulfide bond is the second most common covalent linkage between amino acids in proteins after the peptide bond itself. Such an entity occurs between two cysteine residues or between a thiolate and an already existing disulfide bridge (Equation 1 & 2). In principle, this functionality is dominant in proteins released from the cell or exposed on the cell surface.

$$2\text{R-SH} \xrightarrow{\text{oxidation}} \text{R-S-S-R} + 2\text{H}^+ + 2\text{e}^- \qquad \text{(Equation 1)}$$

$$\text{R}_1\text{S}^- + \text{R}_2\text{SSR}_3 \longrightarrow \text{R}_2\text{S}^- + \text{R}_1\text{SSR}_3 \qquad \text{(Equation 2)}$$

Disulfide bonds are well-known as functionalities enhancing protein stability against the harsh extracellular environment providing resistance against proteases. In general, disulfide bonds could be considered as staples that fully or partially (depending on the case) restrict proteins into particular folds or configurations. At the same time, they can provide several degrees of freedom to the system because of the rotation around the cysteine side chain and the disulfide bond itself, allowing several conformational changes to occur.[5, 6] Recent findings have indicated that these bonds serve as switches of protein structure and function by confining certain conformational changes, triggered by external stimuli. Such an example is provided by the viral capsids (Figure 1). The capsids can be defined as protein coats that enclose and protect the viral genetic material during the process in which the virus leaves the infected cell and is transferred to a healthy host cell. In different viruses it has been shown that the function of disulfide bonds is to hold together the capsid after its assembly and carry the viral genome through the extracellular matrix to a healthy cell. The latter contains sufficient reducing potential to initiate the disassembly of the capsid by reduction of the disulfide bonds,[7, 8] leading to the release of the former to the healthy cell.

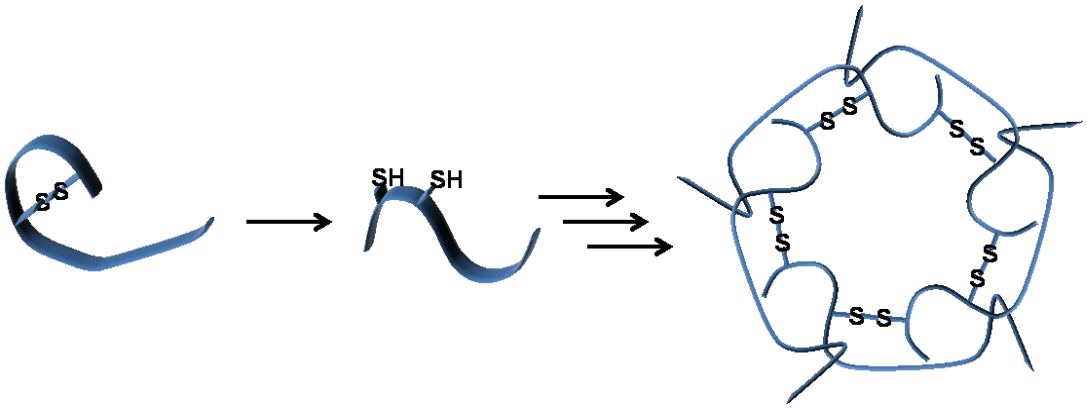

Figure 1: Capsid formation in simian virus 40 after reversible cross-linking.

Small proteins (< 100 residues) lacking an extensive hydrophobic core and possessing few secondary structure elements, are stabilized by the formation of disulfide bonds. It is believed that such proteins could not hold their tertiary structures without the contribution of disulfide bonds. An example is provided by *Ascaris Suum* chymotrypsin/elastase inhibitor, which is a 60-residue protein with a structural fold governed by five conserved disulfide bonds. Due to the fact that this protein contains few secondary elements and lacks a hydrophobic core,[9] it has been assumed that it is highly unlikely that a non-disulfide analog would exist in nature.[10] Another example highlighting the importance of disulfide bond in protein fold is lymphotactin. Lymphotactin is a chemokine that belongs to a fold family whose members normally contain two disulfide bonds. This particular protein contains only one and can be found in two distinct conformational states. One which resembles the monomeric form of the other family members[11] and another one that results in a dimeric form after adopting major structural rearrangements.[12] Addition of a disulfide bond at a position where it appears in other chemokines locks lymphotactin to its monomeric form rendering it unable to dimerize.[11] To summarize, folding of small and especially very small proteins (<35 residues) is often intolerant of even one cysteine mutation as far as this is involved in a disulfide bond. [10]

1.1.1. Characteristics of disulfide bonds

One of the most striking characteristics of disulfide bond reactions is their reversibility. Under relatively mild redox conditions a disulfide bridge can be formed by or cleaved to two cysteine groups, processes known as oxidative folding and reductive unfolding respectively. Both of these have been described as localized, two-state and structurally well-defined changes. Furthermore, due to the covalent nature of the intermediates that are involved into the process of disulfide bond formation and reshuffling, they can be isolated and structurally characterized. As mentioned before, their rate of formation and cleavage can be modified in

the absence of harsh conditions that could cause significant alterations of other interactions within a protein. Additionally, they are known to stabilize the protein in more or less well-understood ways.[13]

From a more chemical point of view, studies have been conducted with thiols and disulfides which indicated that: a) free thiols in the presence of oxygen and catalytic amounts of base yield readily disulfides; b) as soon as catalytic amounts of free thiols are present under mild conditions (pH 7-9) disulfide exchange can occur; c) under acidic conditions disulfide exchange is almost fully quenched; d) disulfides are stable toward many different functional groups.[14]

.

1.1.2. Factors affecting disulfide bond formation and cleavage

Disulfide bond reactions are commonly inhibited by burial of the reactive groups into stable tertiary structures. In this respect, accessibility of the reactive groups is an essential feature for disulfide bond formation to occur. One of the pioneers in proving how important are positional effects in disulfide engineering was Hodges *et al*.,[15] by demonstrating that enhancement of protein stability by insertion of a disulfide bridge is directly related to its position and that the most 'effective' disulfide bridges are those located in the hydrophobic core of the protein without disruption of the protein tertiary structure. On the other hand, limited amount of data on disulfide engineering leads to lack of firmly established rules for choosing appropriate positions for disulfide cross-linking. This characteristic has also been used by scientists as a tool to monitor the accessibility of the reactive groups, ultimately providing indirect evidence for the stability of the protective tertiary structure.

A very crucial parameter associated to the formation of disulfide bonds is the proximity of the cysteine residues. Additionally, the reactivities of the thiolate and the disulfide bond itself which depend on their electrostatic environment (such as the pH of the solvent or the pK_a of the thiols groups involved) are of major importance for the formation/cleavage of a disulfide bond.

1.2. Disulfide bond contribution in protein stability

Two different approaches have been used in order to explore the impact of disulfide bridges in protein stability: 1) by introduction of a novel disulfide within the protein sequence and 2) by disrupting an already existing disulfide linkage.

Multiple examples have been reported in the literature in which disulfide bonds have been successfully introduced into a variety of proteins including among others dihydrofolate reductase,[16, 17] phage T4 lysozyme,[18-23] subtilisin,[24-27] λ repressor,[28] ribonuclease H,[29] LamB

protein[30] and β/α barrel protein.[31] In phage T4 lysozyme, which has no disulfide bridges in its native form, five different disulfide bonds have been introduced and three of them demonstrated additive stabilizing potential. The other two revealed that disulfide bridges can also have a destabilizing role within a protein sequence.[4] What becomes clear from such an example is that introduction of disulfide bridges does not always enhance protein stability. This can mainly be attributed to unwanted phenomena in the surrounding amino acids within the folded protein or because of elimination of an already existing favorable interaction.

Disruption of an already existing disulfide bridge is the alternative approach for evaluating its contribution in the overall stability of a protein structure. RNase A provides a well-studied example in this respect, since it is a typical disulfide-bonded protein. This term indicates that this protein does not fold to its native structure until nearly all of its four native disulfide bonds (at positions 26─84, 58─110, 40─95 and 65─72, Figure 2) have been formed.

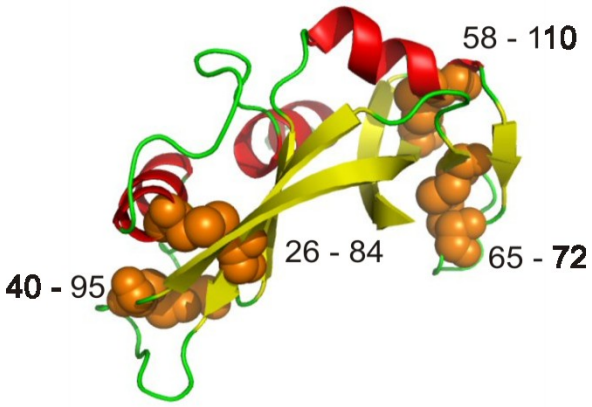

Figure 2: Structure of RNase A. The four disulfide bridges have been highlighted in orange using CPK representation.

Studies on RNase A highlighted the contribution of individual disulfide bonds in the thermodynamic stability of the protein. It was shown that out of the four disulfide bonds in the structure, two (65—72 and 40—95) can be selectively reduced, presumably due to burial of the other two within the protein's tertiary structure. Furthermore, regeneration of protein folding from the fully reduced sequence proceeds initially through the formation of unstructured ensembles that can have one or more disulfide bridges in any location.[32, 33] However, folding to the native structure can only proceed through the stable conformations where only one disulfide (either 65─72 or 40─95) remains in the reduced state.

Interestingly the presence of disulfide bonds does not only contribute in the thermodynamic stability of proteins, but also in their mechanical stability. Such an example can be seen in Nature in *Hydra*. *Hydra* is a small predatory freshwater organism equipped with a harpoon-like structure that is able to unleash a projectile towards a prey in an explosive

manner. The projectile component rests inside an organelle that is called nematocyst which when in the resting state is under extreme osmotic pressure. When it discharges, a miniature harpoon is launched with accelerations up to 40000g.[34] The nematocyst contains short collagen molecules that after their syntheses are equipped with intramolecular disulfide bonds.[35, 36] During a maturation process the minicollagens substitute intramolecular disulfide bonds with intermolecular cross-links[35] and the resulting organelle shows tensile strength as great as steel,[34] making it able to withstand the extreme conditions under which it functions.

1.3. Utilization of disulfide bond formation

Disulfide chemistry has been successfully exploited in some synthetic peptides, for example in the stabilization of α-helical peptides,[37-40] or in the capture of one handedness from a *P*-*M* mixture of 3_{10} helices.[41] Extension of this concept includes various stapling methods between amino acid side chains with other chemical functions than disulfides.[42-47] Disulfide bridges have also been used for the dynamic covalent assembly of macrocycles from several dithiol units.[14, 48-51] In these systems as well, the formation of a particular macrocycle reflects its intrinsic stability and the preorganization of the linear dithiol precursor for cyclization.

1.3.1. Stabilization of helical peptides

α-helical sequences are considered responsible for interactions of proteins with nucleic acids or with other proteins due to the accurate positioning of amino acid residues on the surface of these entities. This makes them ideal recognition elements but their utilization is limited because they are usually unstable when isolated from the native protein structure. Multiple methodologies have been investigated in order to stabilize these structural elements, such as metal binding,[39, 43] lactam-,[52] salt-,[53] hydrazone-bridges,[54] hydrogen bond[55] surrogate and hydrocarbon cross-links.[56] Schultz *et al*., inspired by the bee venom peptide apamin,[37] an 18-residue peptide possessing a remarkably stable three dimensional structure attributed to the two native disulfide bonds ([1—3] and [11—15]), synthesized a sequence of peptides being able to form intrastrand disulfide bonds. Their results demonstrated increased α-helical character for the bridged compounds even at 60 ^{o}C, a temperature at which their non-bridged analogues demonstrated random-coil behavior. This was one of the first studies highlighting the utility of using intramolecular disulfide bonds to stabilize helical conformations in short peptidic sequences. Similar results were reported by Allemann *et al*.[38] who demonstrated that an apamin-like N-terminal helical foldamer, in its oxidized form, adopts a well-defined three-dimensional structure and high stability over a wide pH and temperature range, compared

again to the reduced analogue. In a similar manner, Arora *et al*. expanded the idea of hydrogen bond surrogate helices (which contain a covalent bond replacing an intrastrand hydrogen bond between main chain atoms in canonical α-helices) by replacing the main chain hydrogen bond with a disulfide bond.[40] This enabled easy access to reversibly stabilized α-helices (Scheme 1) through consecutive oxidation of the thiol species and reduction of the resulting disulfide.

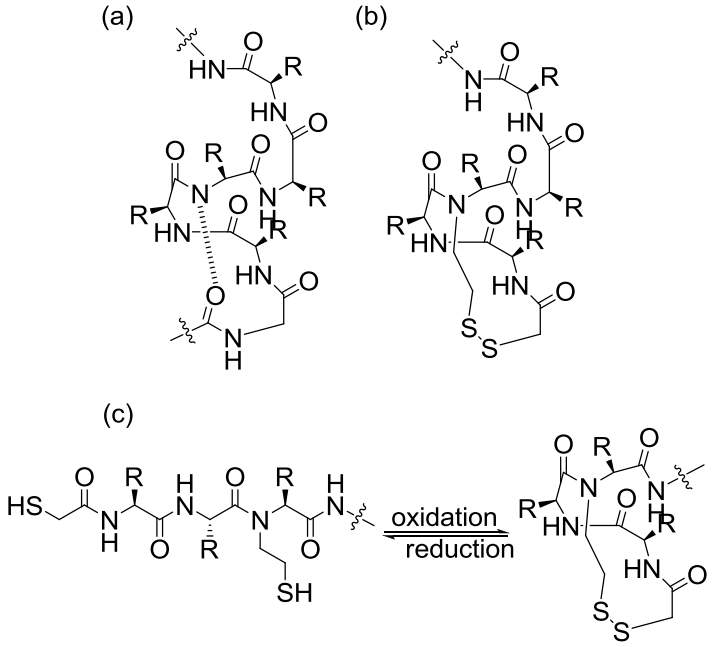

Scheme 1: (a) Schematic representation of a peptide sequence giving rise to α-helical architecture, (b) representation of a disulfide bridge containing hydrogen bond surrogate (HBS) helix and (c) reversible helix stabilization with consecutive oxidation to/reduction of disulfide bond.

Kuroda *et al*. in their pioneering work captured one handedness from a *P*-*M* mixture of 3_{10} helices. Their study was based on the fact that almost in all cases α- and 3_{10}-helices in proteins prefererably adopt right handedness (*P*), attributed to the chirality of the amino acid units. In their experiments they used a peptidic strand containing only two stereogenic centers (two cysteine residues), which after oxidation induced only one-handed helicity on the peptide backbone, as indicated by CD experiments. The crystal structure of the disulfide stapled helical peptide is depicted below (Figure 3).

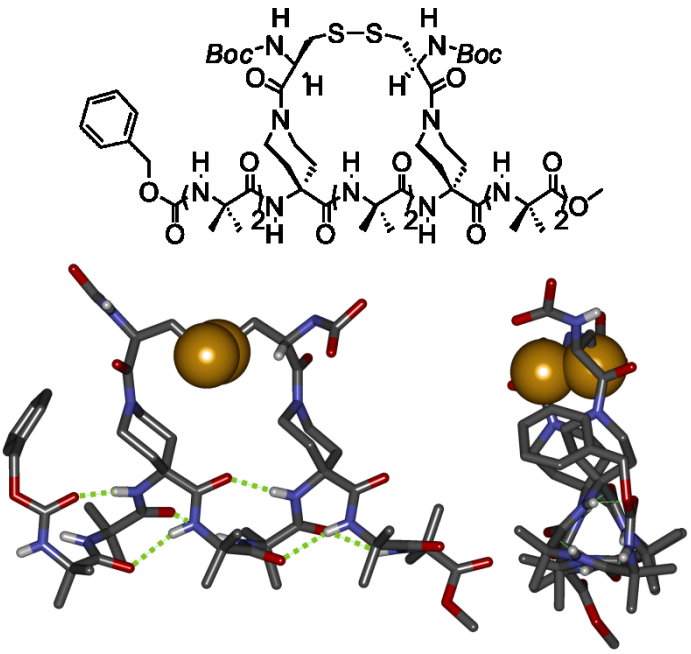

Figure 3: *Above*: Chemical structure of stapled peptide reported by Kuroda *et al.*. *Below*: X-ray structure (side and top view). Backbone hydrogen bonds are highlighted in green. Sulfur atoms have been highlighted using CPK representation. Hydrogen atoms apart from those participating in H-bonding have been removed for clarity.

This is one of the first examples in which stapling between positions *i* and *i*+3 locks selectively the *P* helicity from an interconverting dynamic mixture.

1.3.2. Disulfides in Dynamic Combinatorial Libraries (DCL)

A dynamic combinatorial library contains members which are constantly interconverting, which means that the library is under thermodynamic control. In principle a template molecule induces the stabilization of a class of molecules which bind to the template.[14] Several reversible reactions have been introduced to the field of dynamic combinatorial chemistry during its development. Initial work by Sanders and Lehn used a transesterification[57-59] reaction and Schiff base exchange,[60] respectively. Due to the harsh conditions required for the former and termination via hydrogenation for the latter, reversible reactions requiring milder conditions have been introduced such as the hydrazone exchange reaction[61] and reversible C=N bond formation that can give rise to libraries of oximes.[62] DCL generation through olefin metathesis as well as enzymatic transamination has also been reported. In the year 2000, Sanders *et al*.[14] and Lehn *et al*.[63] (independantly) reported the first examples of disulfide bonds in the generation of DCLs. At that time studies Still *et al*. had already demonstrated that an equilibrium system of different thiols can have its composition altered by host-guest interactions.[64] Starting from that time, disulfide bonds were introduced into the arsenal of reversible reactions, used widely in Dynamic Combinatorial Chemistry (DCC). Covalent cages for molecular

recognition[51] and self replicators[49] are some of the examples exploiting the advantages of disulfide assisted DCC.

Disulfide bonds are gaining more and more attention in multiple scientific fields due to special characteristics that they possess, ranging from protein engineering to redox-triggered polymeric drug and gene delivery agents.[65] The following section describes the first example of disulfide bond introduction into a fully abiotic helical system with the aim of bolstering its stability.

2. Design

The aim of this project was to demonstrate the contribution of disulfide bridges in the thermodynamic stability of an artificial, helical biomimetic system. For this reason two different compounds were synthesized bearing thiol protected side chains in different positions of the sequence. By applying this modification a helix with an intramolecular disulfide bridge and two helices connected with two intermolecular disulfide bridges were obtained. Their stability was assessed by a validated method based on the separation of the two enantiomers, followed by monitoring of the racemization kinetics.[66] The disulfide bridged compounds could be thus compared with their non-bridged precursors, to provide quantitative data of the contribution of disulfide bridge formation in the stability of the system.

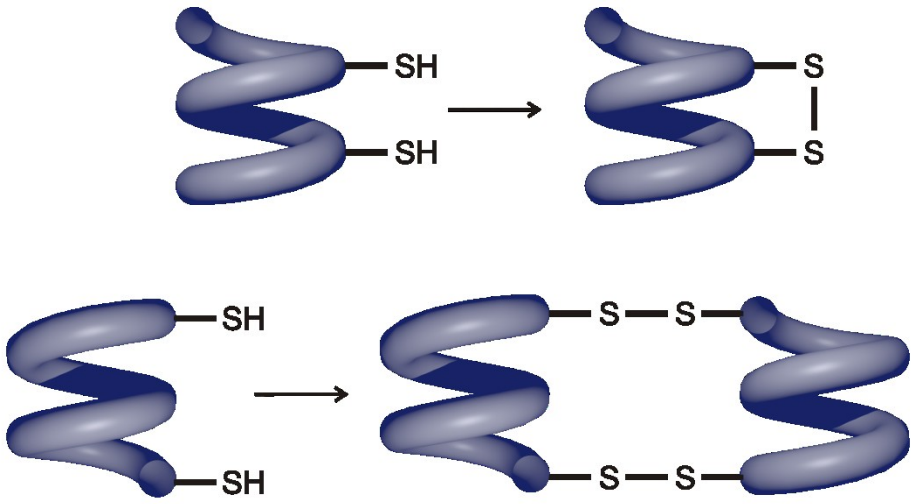

Figure 4: Illustration of the two different pentamers that, depending on the position of the thiol bearing side chains, give rise to different architectures. *Above*: monomeric macrocycle. *Below*: dimeric macrocycle

In order to assess the structural stabilization offered by the presence of either inter- or intra-molecular disulfide bridges in aromatic oligoamide foldamers, two different entities

were designed and synthesized (Figure 4) consisting of two quinoline-based dimers (bearing a methyl ester functionality at the C-terminus and an amine functionality at the N-terminus) coupled to a central phenanthroline diacid unit. In these two different compounds the positioning of the side chains able to undergo disulfide bonding is altered in order to give rise selectively to an intra- and an inter-molecularly bonded compound. If the thiol bearing side chains were placed in close proximity with each other, adjacent to the phenanthroline, this was predicted to afford the short macrocycle (Figure 4, *Top*). However, if the thiol groups were remotely located at the extremities of the helix, an intramolecular disulfide-bridge was not expected due to the constraints that would be introduced to the system by ring closure. This was thus predicted to favor intermolecular disulfide bridging. The reason for choosing the phenanthroline moiety as a central unit was to facilitate the data analysis by limiting possible complications that could rise in the case the molecule possessed N-C polarity, such as parallel and anti-parallel assemblies. Additionally, oligomers bearing 1,10-phenantroline diacid have already been shown to fold into well-defined helical structures in solution, through intramolecular H-bonding and aromatic stacking interactions.[67]

3. Synthesis

Two different monomers bearing different side chains have been used for the synthesis of two different pentamers, one bearing the isobutoxy, $-OCH_2CH(CH_3)_2$, (monomer A) side chain and the other a protected thiol, $-O(CH_2)_3SC(CH_3)_3$ (monomer B). The side chain installation on the quinoline monomers was carried out via a Mitsunobu reaction according to procedures previously reported in the literature.[68] The isobutoxy side chain was chosen to improve solubility in organic solvents and enhance crystallinity. The thioether side chain was chosen for enabling disulfide bridge formation and exchange after deprotection. The side chain was synthesized according to literature procedures from the reaction of 3-chloropropan-1-ol with sodium 2-methylpropane-2-thiolate in refluxing methanol.[69]

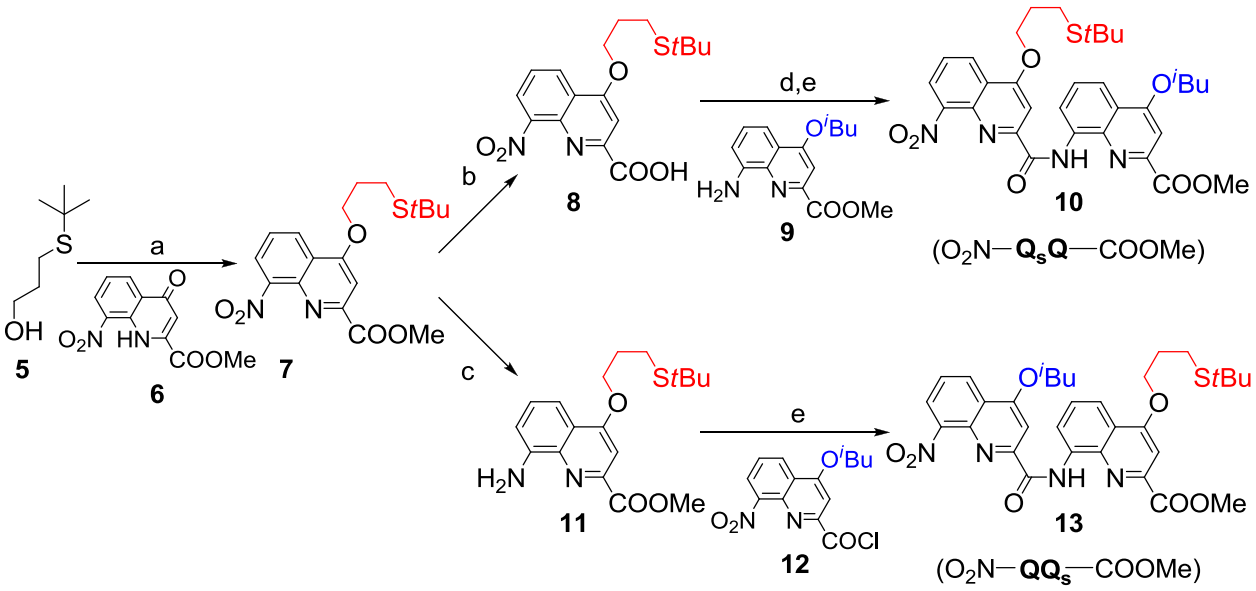

Scheme 2: Synthesis of the dimers **10** and **13**; (a) DIAD, PPh_3, THF, r.t., 4 hours; (b) $LiOH.H_2O$, THF/H_2O, r.t., 1 hour, (c) Pd/C, NH_4VO_3, NH_4HCO_2, $EtOAc/EtOH/H_2O$, 95 °C, 4 h, (d) oxalyl chloride, CH_2Cl_2, r.t., 2 h; (e) DIPEA, CH_2Cl_2, r.t., 18 hours.

After obtaining the two monomers the corresponding nitro acids are formed, as well as the amino esters, followed by acid chloride activation of the acids and coupling with the necessary amine in the presence of base to yield the two ('BA' **11** and 'AB' **14**) quinoline dimers. While Pd-catalyzed hydrogenation of the nitro group is usually carried out with H_2 gas, in the case of the thioether monomer, these conditions were found to be inadequate, presumably due to Pd poisoning by traces of sulphur compounds. However, *in situ* generation of hydrogen with NH_4HCO_2 in the presence of NH_4VO_3 was found to be a more powerful method, leading to quantitative amine formation from the corresponding nitro compound. The two dimers (AB and BA) were then purified by recrystallization and their nitro groups were reduced to the corresponding amine via the NH_4HCO_2 method. After coupling of these two amines to 1,10-phenanthroline-2,9-dicarbonyl dichloride (formed using $SOCl_2$) the two pentameric precursors were obtained.

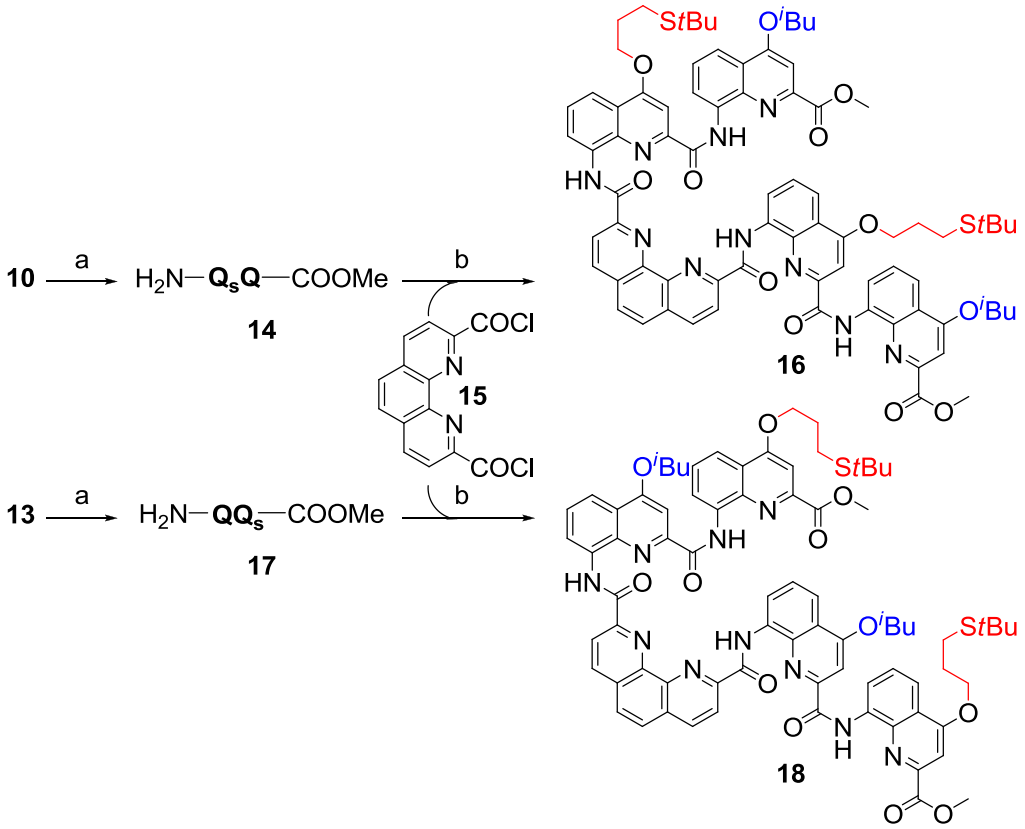

Scheme 3: Coupling of the dimer amines **14** and **17** to 1,10-phenanthroline-2,9-dicarbonyl dichloride **15**; (a) Pd/C, NH_4VO_3, NH_4HCO_2, EtOAc/MeOH/H_2O, 95 °C, 20 hours; (b) DIPEA, CH_2Cl_2, r.t., 18 hours.

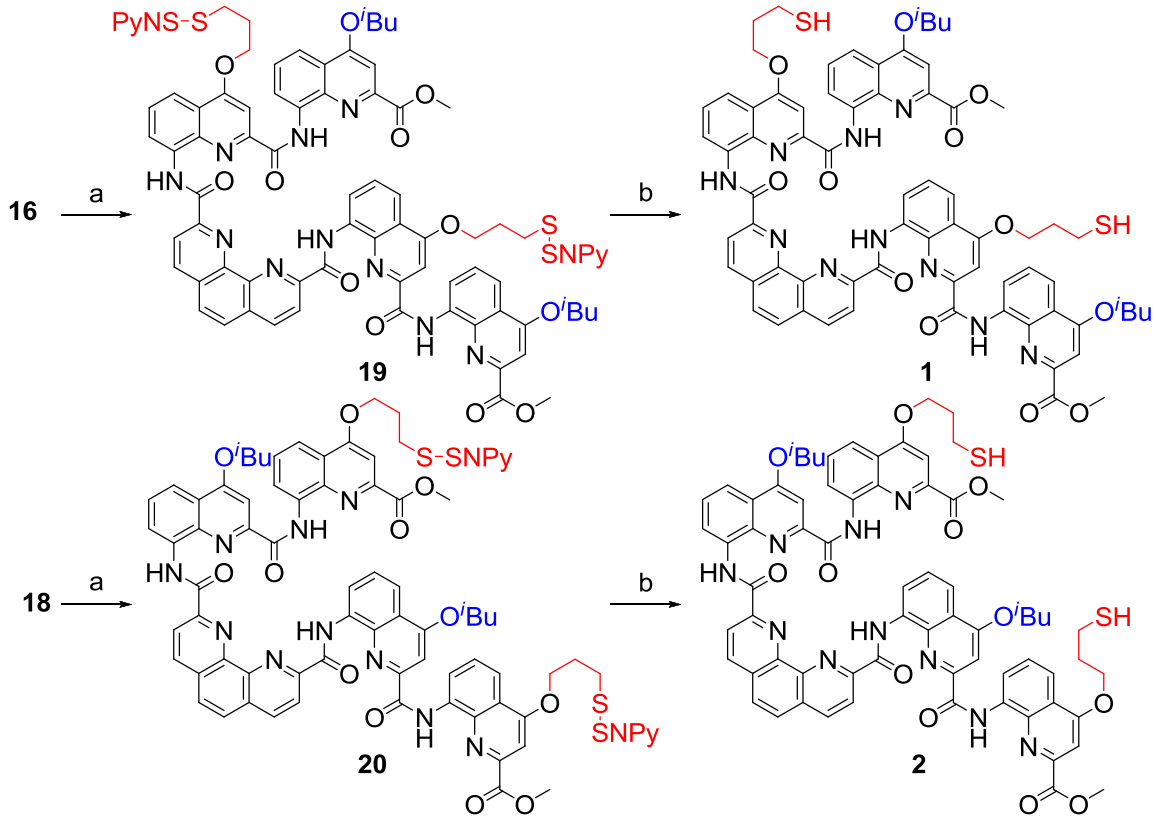

Scheme 4: Removal of S-*tert*-butyl protective group; (a) NPySCl, AcOH, r.t., 20 hours; (b) TBP, $(CH_3)_2CO/H_2O$, r.t., 24 hours.

The *tert*-butyl protected thiols were reacted with NPySCl to yield the NPyS– protected thiols. The *tert*-butyl was initially chosen due to its stability that keeps the thiol intact during all of the previously mentioned steps. Reprotection of the thiol with NPySCl guarantees quantitative yields in the next steps. After reduction of the resulting disulfides in the presence of TBP, clean bis-thiol precursors were obtained after a precipitation step in MTBE. Oxidation of these two pentameric bis-thiol compounds in the presence of air and catalytic amounts of base led to the quantitative formation of the macrocyclic species.

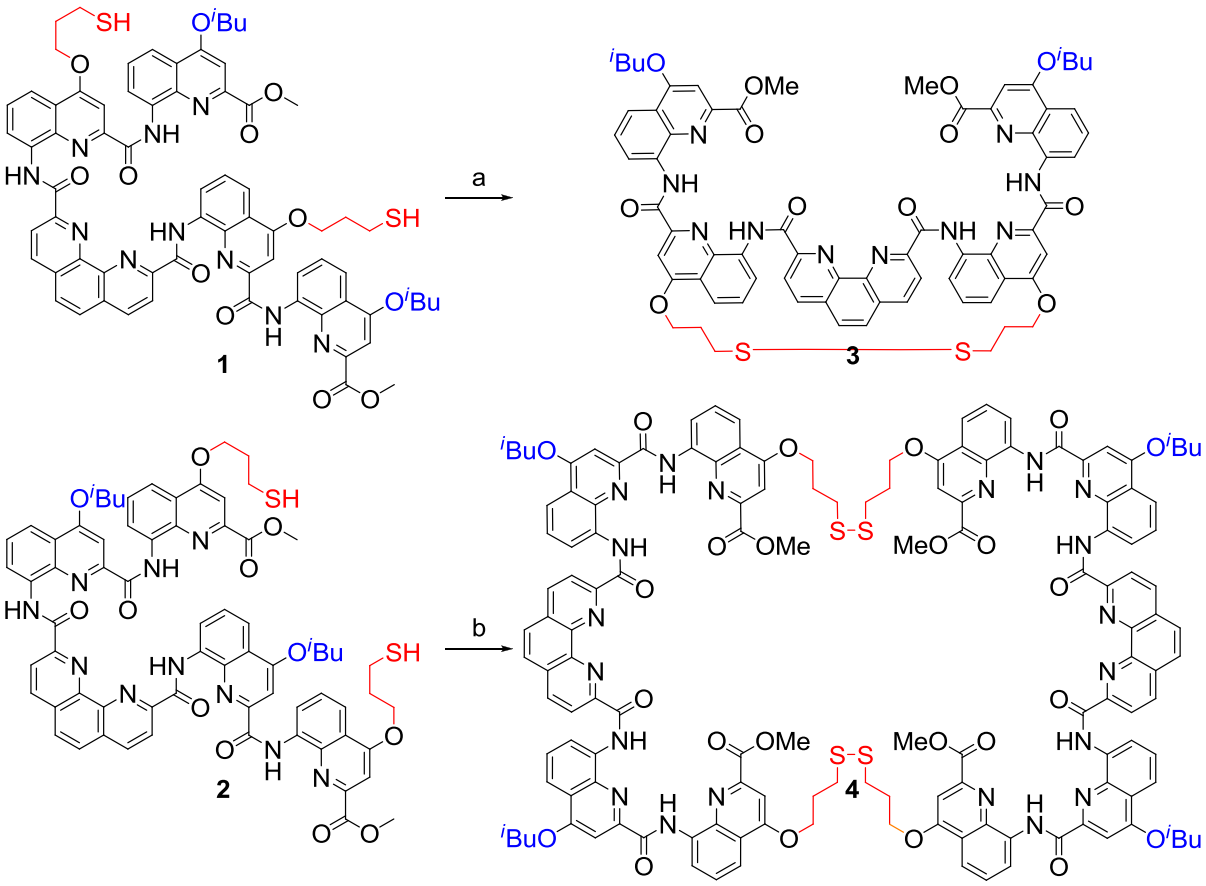

Scheme 5: 5 mM in $CHCl_3$/MeOH (4/1), DIEA (40 µL), 25 C, (a) 48 hours and (b) 72 hours

3.1. Characterization techniques

Different techniques were used in order to confirm the formation and provide the structural characteristics of the two compounds bearing the disulfide bridges, such as mass spectrometry, NMR studies, gel permeation chromatography (GPC) and finally X-ray crystallography. Data related to those studies are presented in more detail in the following sections.

3.1.1. NMR experiments

Solution studies and in particular 1D and 2D NMR were used in order to monitor the formation of both the intra- and the inter-molecular bridged species. Full assignment of the two disulfide bridged compound was also carried out.

The ^{1}H NMR spectrum of the intramolecular bridged compound demonstrated no significant changes in the amide and aromatic region during its formation. For the compound bearing the intermolecular disulfide bridge there was an upfield shift ($\Delta\delta$ = 0.14 ppm) of the most downfield proton, compared to its non-bridged precursor (Figure 5).

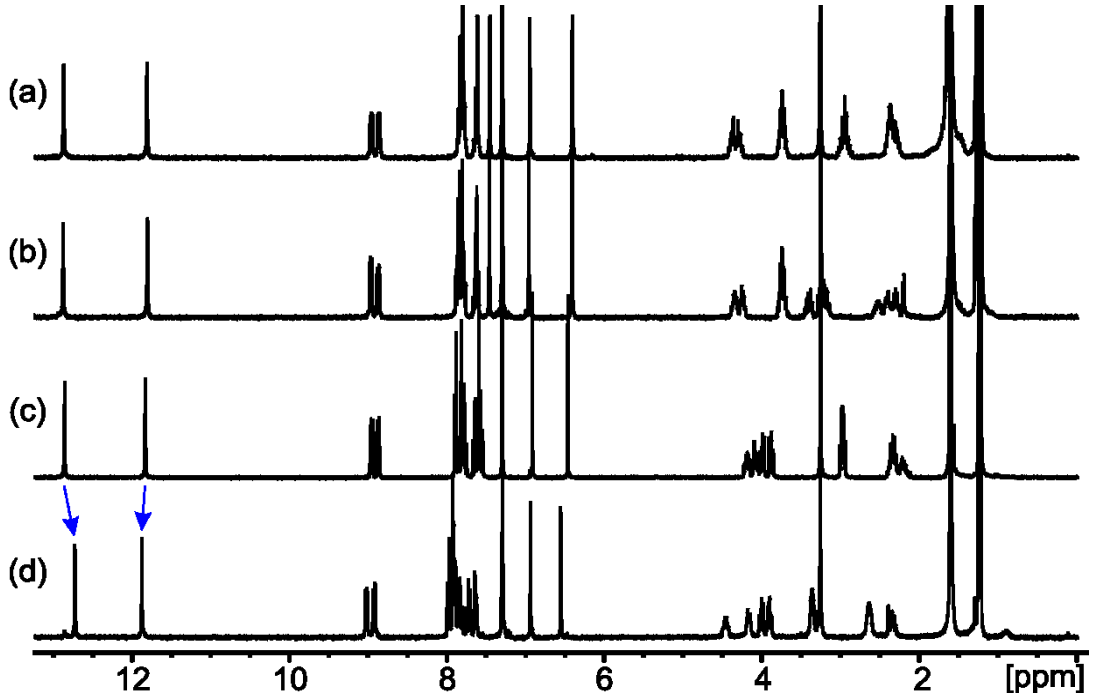

Figure 5: NMR spectra of (a) **1**; (b) **3**; (c) **2**; and (d) **4**, showing no significant differences between the compound **3** and its precursor. Between compounds **2** and **4**, slight differences in the chemical shift values of the amide protons can be observed, as indicated by the blue arrows.

The most striking effect of disulfide bond formation is shown in the aliphatic region, where all methylene signals appear to be diastereotopic and provide a clear indication of the disappearance of the starting free thiol and the formation of the bridged species. In particular, a significant shift in the thioether methylene can be observed for both compounds after the formation of the bridge(s) as depicted in Figure 6. ^{1}H NMR spectra of compounds **1** and **3** demonstrate a downfield shift ($\Delta\delta$ = 0.29 ppm) of the thioether methylene protons and an increase in the chemical shift difference of these diastereotopic protons ($\Delta\delta$ = 0.22 ppm in **3** and close to 0.02 ppm in compound **1**) (Figure 6). ^{1}H NMR experiments were also conducted at lower temperatures (data not shown) and these showed no significant differences of the methylene protons at temperatures, ranging from 25 to 0 ^{o}C. Limited solubility prevented us from recording NMR spectra at lower temperatures.

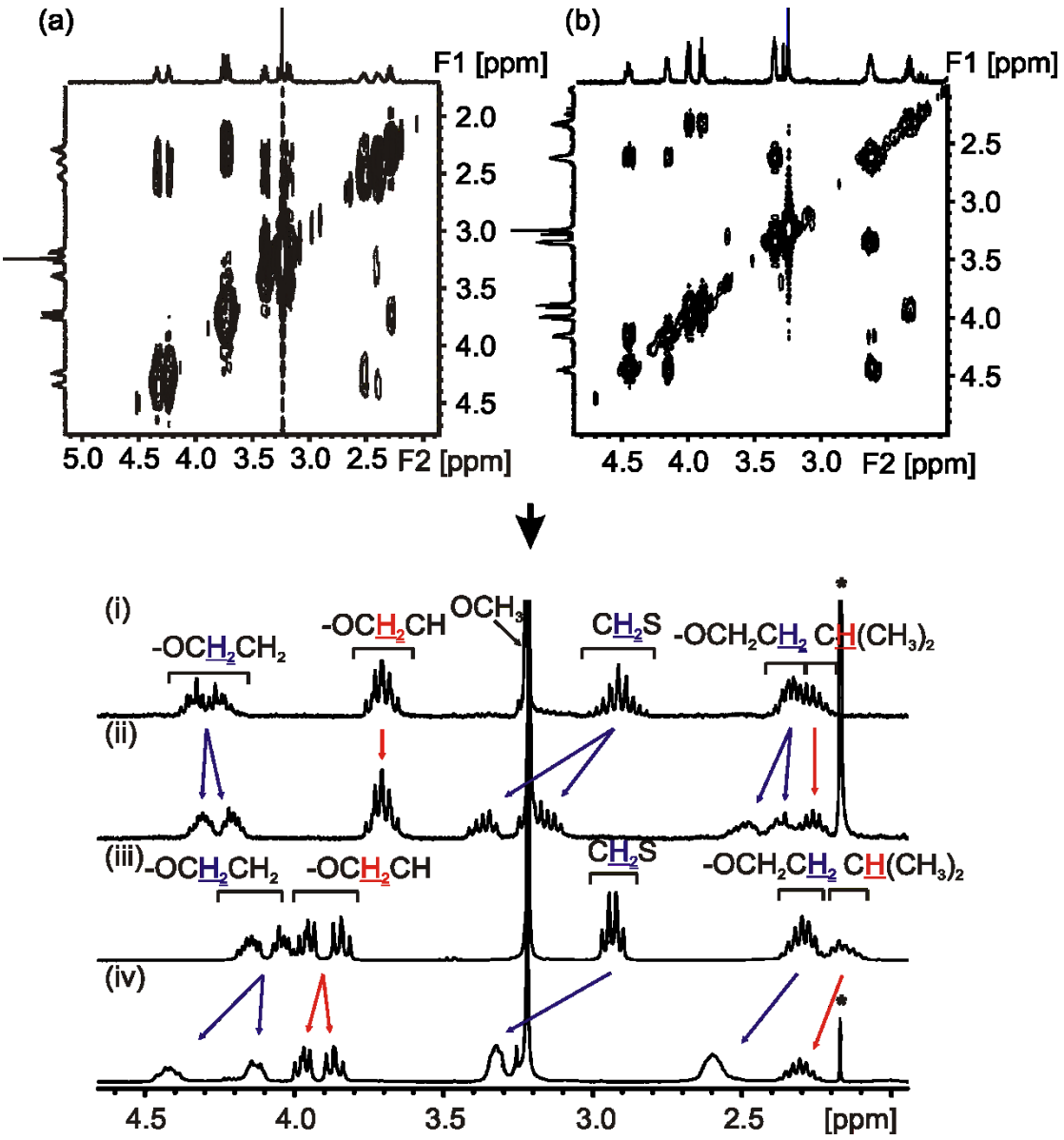

Figure 6: COSY spectra for compounds **3** (a) and **4** (b) assigning the protons of the side chains and NMR spectra of (i) **1**; (ii) **3**; (iii) **2**; and (iv) **4** demonstrating the differences between the bridged compounds and their non-bridged precursors.

Additionally, DOSY (Diffusion Ordered Spectroscopy) NMR (Figure 6) was conducted that confirmed the size difference between compounds **3** and **4**. Diffusion NMR enables the resolution of mixtures of different compounds spectroscopically based on the difference in their diffusion coefficients, which depends on structural characteristics of the molecules, such as size and shape. The general principle is that the larger the molecule is, the faster it diffuses in a given solution. From the diffusion coefficients acquired from this technique and after utilization of the Stokes-Einstein equation for diffusion of spherical particles, the hydrodynamic radii of the molecules of interest can be extracted.

Data interpretation clearly indicates the size difference between the dimeric species when compared to the intramolecularly bridged compound (Figure 7).

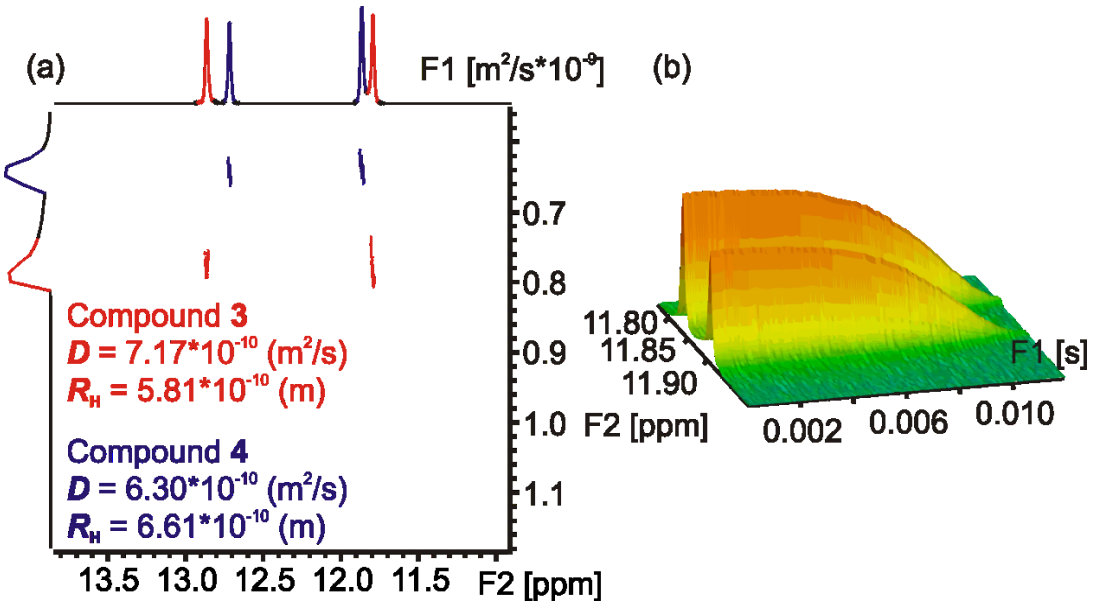

Figure 7: (a) Part of DOSY NMR spectrum illustrating the difference in the diffusion coefficient between compound **3** and **4**. The hydrodynamic radius of each is shown; (b) 3D representation of the decay of the two peaks belonging to **3** and **4**.

3.1.2. GPC profile

Gel Permeation Chromatography (GPC) is another method which was used to characterize the dimeric species. In GPC, compounds with different sizes are expected to interact in a different way with the stationary phase, resulting in retention times that are directly related to their size. In theory, co-injection of a large molecule with a smaller one will result in a unique chromatographic profile, which will reflect their size difference. For this reason, an equimolar solution of the two bridged compounds (**3** and **4**) was injected in a recycling GPC apparatus and resulted in two distinct peaks (Figure 8) even after the first chromatographic cycle, demonstrating a significant size difference between the two species. This technique did not provide quantitative data for the size of its particular compound but qualitatively demonstrated that the two compounds have a significant difference in size.

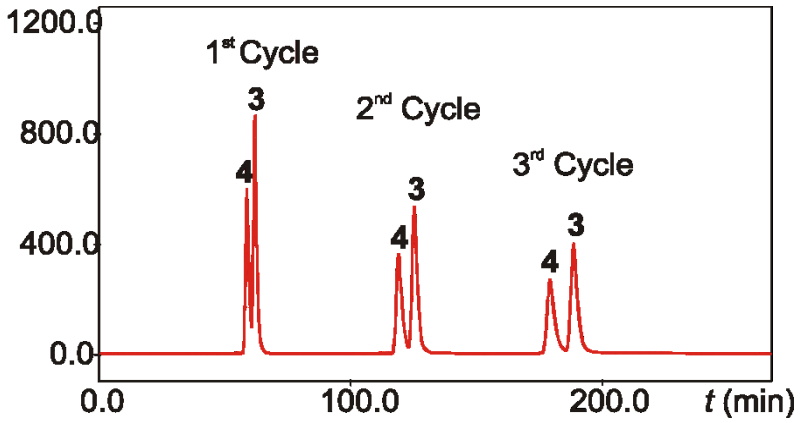

Figure 8: Chromatogram showing the separation of compounds **3** and **4** using GPC. The size difference becomes clear even after the first cycle of the separation.

4. Structural analysis

X-ray crystallography provided data (Table 1) that gave an indication of the orientation and distance between the two sulfur atoms for both of the (*tert*-butyl protected) precursors. This validated the initial design whose aim was to result in appropriate distances between the sulfur atoms, enabling the formation of both an inter- and an intra-molecular disulfide bridged compound.

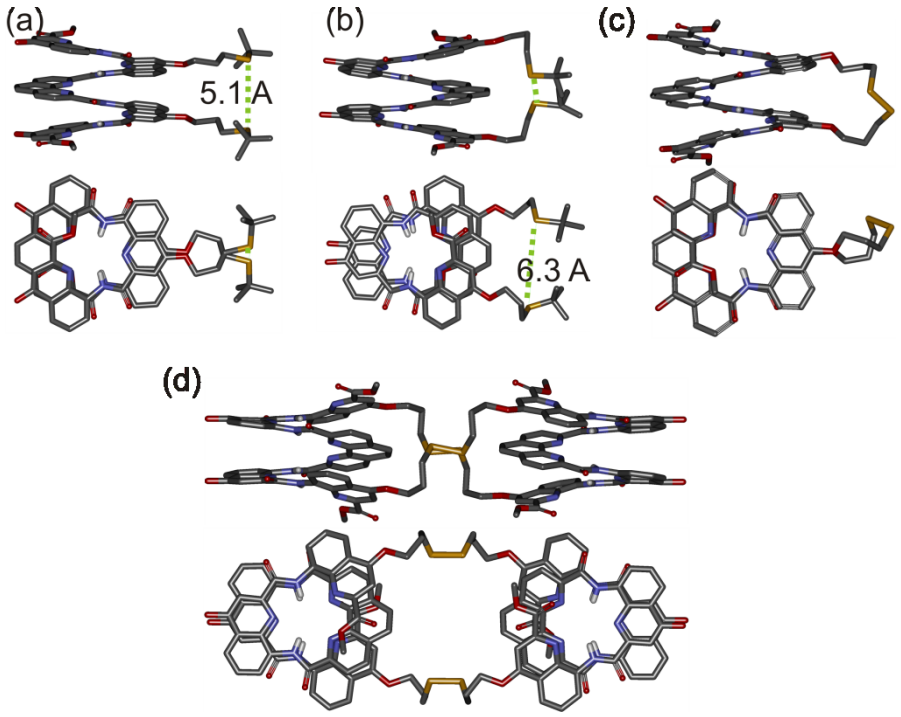

Figure 9: Crystal structures of the *tert*-Bu-protected precursors of (a) **1** and (b) **2**. Energy minimized (Maestro version 6.5 using the MM3 force field) conformation of the structure of **3** and (d) crystal structure of **4**. In all cases, both side views and top views are shown. Hydrogen atoms other than NH, as well as solvent molecules and isobutoxy side chains have been removed for clarity.

Single crystals of the two *tert*-butyl precursors suitable for X-ray analysis, were obtained by crystallization based on vapor/liquid diffusion of methanol in toluene. The crystal structure of the *tert*-Bu precursor of **1** (Figure 9a) shows the resulting helical structure, spanning over two turns. Its two centrally-located thiol-bearing side chains are in close proximity and diverge from one side of the helix, hinting at the possibility to form an intramolecular disulfide bridge. Additionally, the X-ray structure indicates that the two sulphur atoms are 5.1 Å away from each other. This value is significantly larger that the ideal S─S length in a disulfide bridge, which is 2.05 Å. On the other hand the side view of the crystal structure shows that the two side chains are lying parallel to each other. Hence, by taking into account side chain flexibility disulfide bridge formation becomes possible, as suggested by an energy minimized model of compound **3** (Figure 9c), which demonstrates the cyclic folded conformation. As a

distinct element, all bonds of the side chains bearing the disulfide bridge adopt a *gauche* conformation, the disulfide bond itself having a dihedral angle close to 90°.

In contrast, the crystal structure of the *tert*-Bu-protected precursor of **2** (Figure 9b) shows that its thiol-bearing chains also protrude from the same side of the helix, but at distance too large (6.1 Å) to allow intrastrand disulfide bridge formation, even when taking into account side chain flexibility.

Slow evaporation of chloroform resulted in the successful crystallization of the dimeric species leading to better understanding of its structural characteristics. The crystal structure of **4** revealed a C_2 symmetrical bundle of two helices with their axes parallel (Figure 9d). Both helices have the same handedness (*PP* or *MM*) and are linked by two pairs of side chains. The dihedral angles at the disulfide bridges are near 90°.

In order to obtain better understanding of compound **4**, concerning structural parameters and modifications that were not experimentally feasible, molecular modeling was conducted. The X-ray data of the dimeric structure (**4**) indicated that no *meso* compound could be found in the solid state, observation that was confirmed also in solution (see the following chapter). The question that arises is what kind of destabilizing forces occur within the heterochiral dimeric architecture that render it relatively unstable compared to its homochiral analogue. Molecular modeling obtained by Monte Carlo conformational search, starting from a random *PM* conformation of dimer **4**, indicated that the helical shape of each pentamer is well conserved but no specific relative orientation of the *P* and the *M* helices are observed expressing no specific interactions between helices and no preferred conformation (Figure 10).

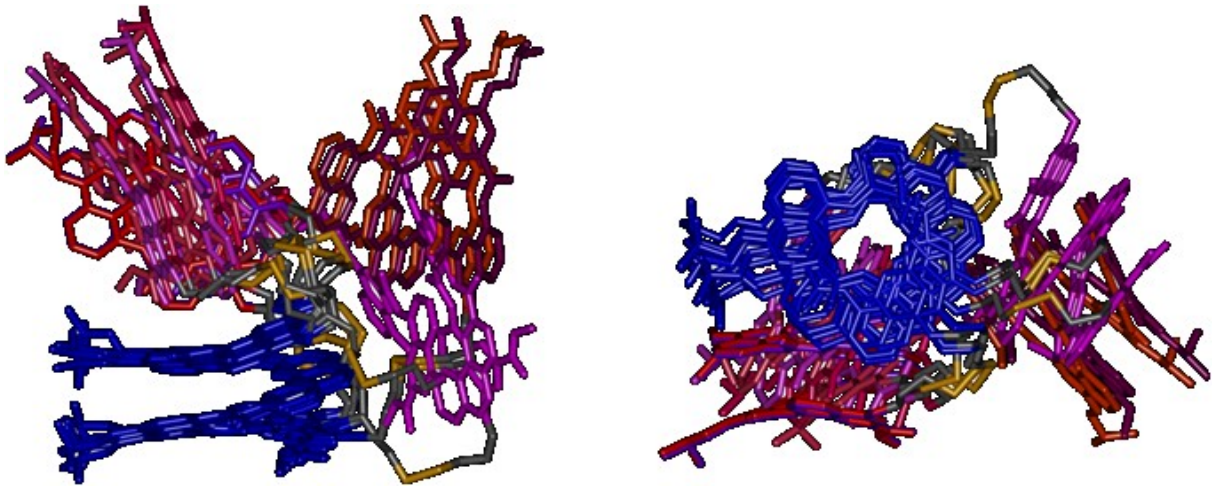

Figure 10: side and top view of the 6 minimum energy conformations (within 0.5% energy) found by Monte Carlo conformational search from a random *PM* conformation of dimer **4.**

Given the quantitative formation of the dimeric species after oxidation of precursor **2** and the absence of intermediate compounds, such as the formation of an intra-molecular bridged compound, made us wonder to what extent the formation of this compound was feasible, so molecular modeling of an intramolecular, linked oligomer was carried out. The resulting models (Figure 11) generated by Monte Carlo conformational search demonstrated that in the case of an intramolecular bridged compound too much constraint was introduced into the system. Over-imposition of the minimum energy structure of the intramolecularly cyclised compound and one of the helices of the dimer **4** in the crystal structure clearly demonstrated that for the intra cyclised compound to occur the helix needed to be contracted about 4.24 Å, a contraction that according to our experience is unlikely to occur due to high energy cost.

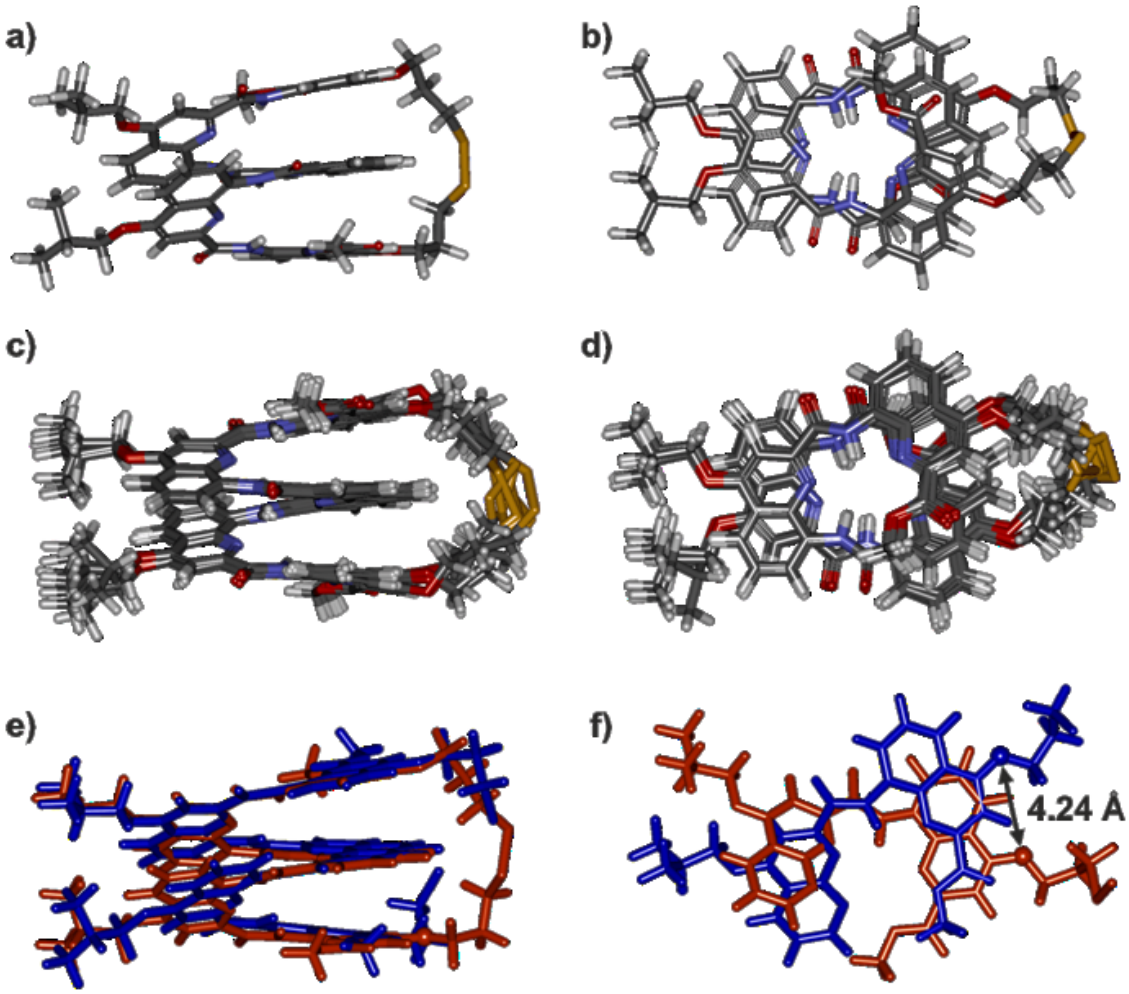

Figure 11: Molecular models of the intramolecular cyclised compound from pentamer **2**. **a)** side view and **b)** top view of the minimum energy structure **c)** and **d)** superposition of 6 of the 10 minimum energy structures (same helical handedness), the 4 non-presented structures were subject to helical handedness inversion during the computational conformational search. **e)** Superposition of the minimum energy structure of the intramolecularly cyclised compound (*in red*) and one of the helices of the dimer **4** in the crystal structure (*in blue*), overlapping the first quinoline of the oligomer. **f)** top view of the 2 last quinolines of the inter and intra cyclised compound showing the 4.24 Å contraction needed for the intramolecular cyclised compound to occur.

Additionally, we wanted to explore what would be the overall effect on the dimeric structure when having the disulfide bond replaced with a C─C bond. Based on the molecular models (Figure 12) replacement of the disulfide bridge introduces diversity of the relative orientations to the system that clearly differs from the S─S parent linker.

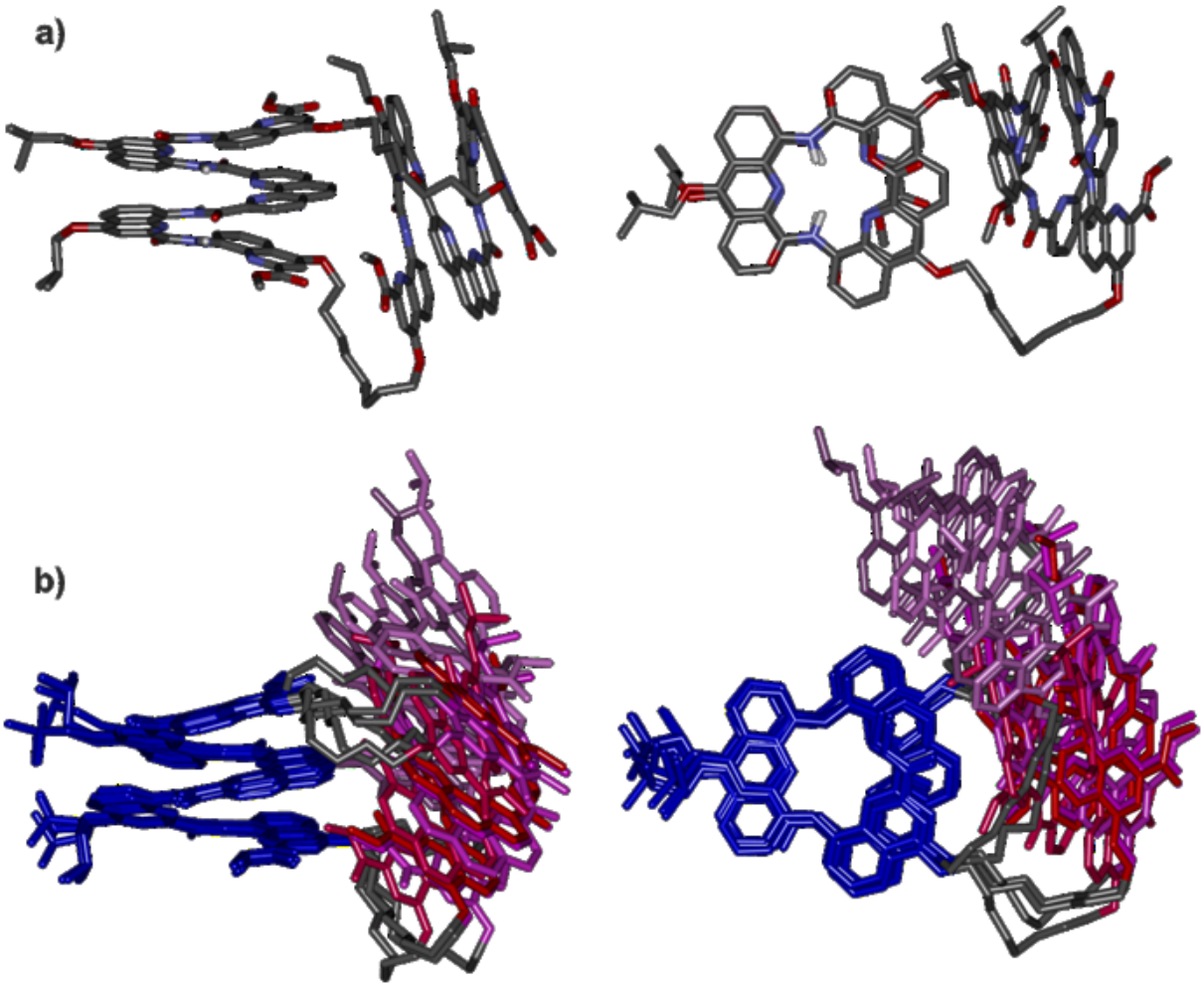

Figure 12: Molecular models using Monte Carlo conformational search (as described in the materials and methods section) for a dimer where each S─S bond has been replaced by a C─C bond. Molecular modeling was initiated from simple S to C exchange in Maestro from the crystal structure of dimer **4**. **a)** minimum energy structure. **b)** Superposition of the 10 structures of minimum energy.

The final question that arose concerning our dimeric system was related to the effect of removing one more carbon in the aliphatic side chain. Molecular modeling indicated that in this case both conformations, *PP*/*MM* or *PM*, gave rise to a large diversity of relative orientations of the helices expressing no specific interactions between helices and no preferred conformation (Figure 13), highlighting the importance of the length of the aliphatic linker in the formation of a well-defined architecture.

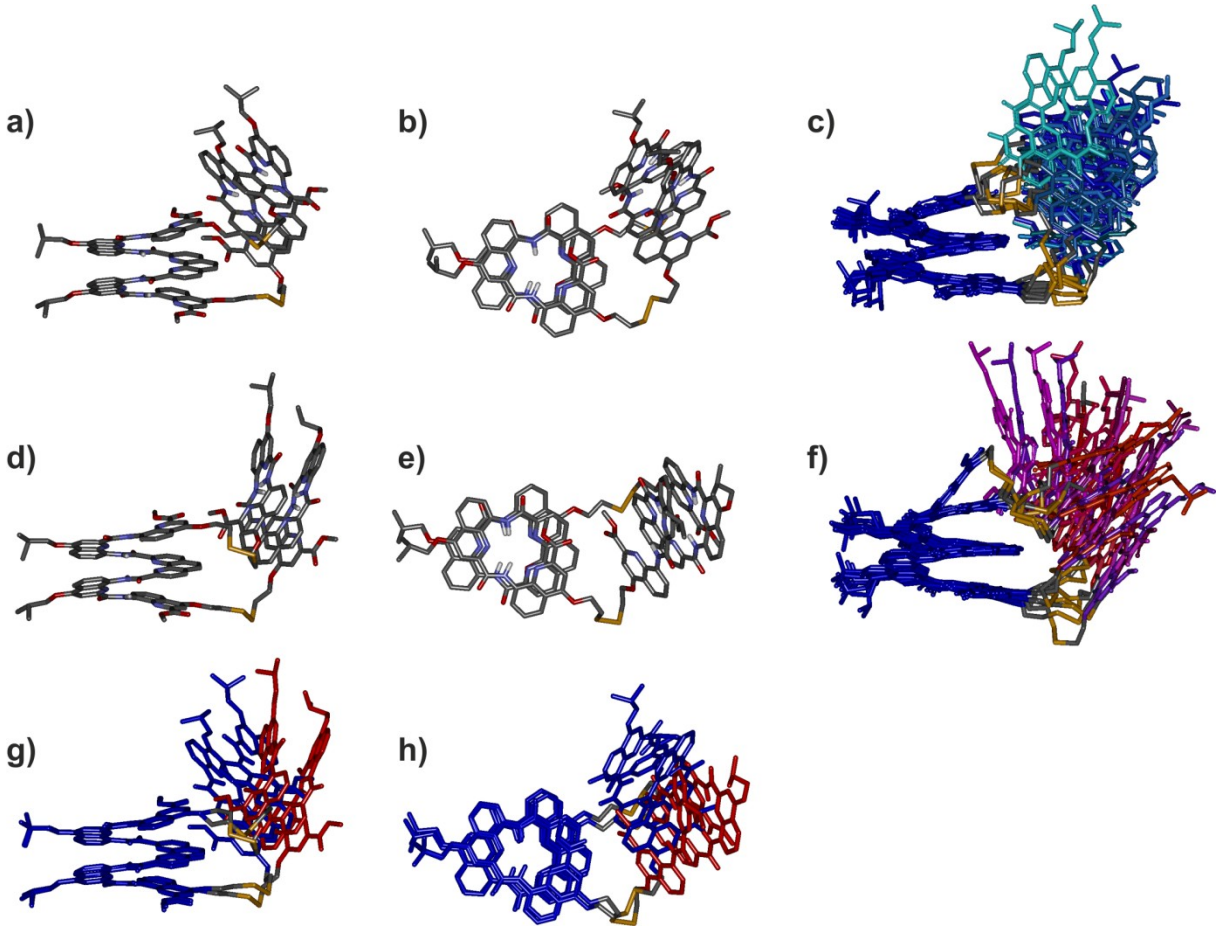

Figure 13: Molecular models using Monte Carlo conformational search of dimers where side chain linkers have been shortened by one CH_2. **a)** and **b)** minimum energy structure of a dimer constituted of two *P* helices, **c)** superposition of the 10 structures of minimum energy of the *PP* dimer, **d)** and **e)** minimum energy structure of a *PM* dimer, **f)** superposition of the 10 structures of minimum energy of the *PM* dimer. **g)** and **h)** superposition of the *PP* dimer and the *PM* dimer structures.

5. Assessing thermodynamic stability

The aim of this project was to assess the contribution of disulfide bonds in the thermodynamic stability of the helical systems. Our initial hypothesis was that upon formation of the disulfide bridges the enantiomers would be locked in either *P* or *M* conformation and interconversion would not be possible. Thus separation of those locked conformations would lead to pure enantiomers that are either right- or left-handed which do not racemize.

5.1. Chiral HPLC separations

Helix thermodynamic stability was quantitatively assessed for **3**, **4**, and the *tert*-Bu protected precursors of **1** and **2** (**16** and **18**, respectively) using a previously described method

which consisted of measuring the rate of interconversion between *P* and *M* helices, and assuming that the activation energy required for this process reflects the energy difference between a folded ground state and an (at least partly) unfolded transition state.[66, 70] Conditions were first optimized to separate *P* and *M* helical conformers of compounds **3**, **4**, **16** and **18** on a chiral HPLC using a CHIRALPAK IA column.

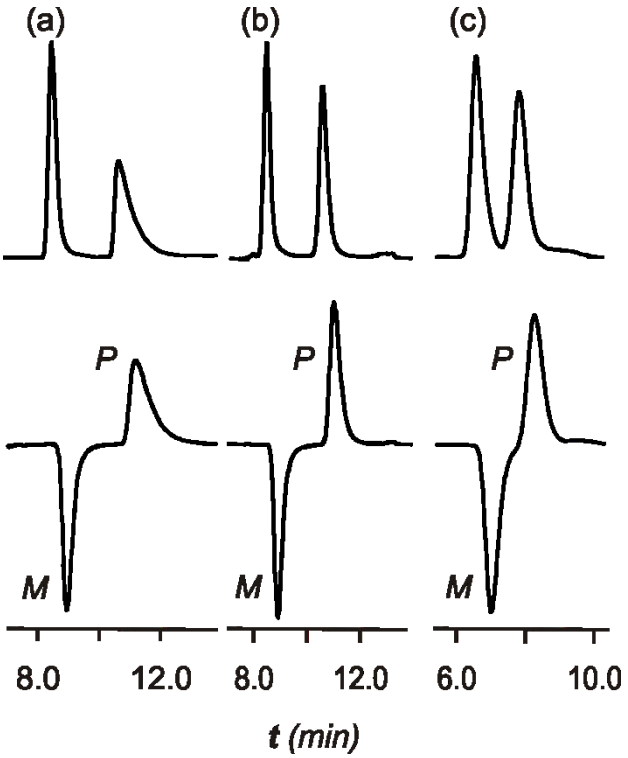

Figure 14: Chromatographic separation (–5 °C, ChiralPak IA column) of *P* and *M* helices of: (a) the *tert*-Bu-protected precursor of **1** (**16**) (THF/Hexane, 40/60, *v*/*v*); (b) **3** (THF/Hexane, 50/50, *v*/*v*); and (c) **4** ($CHCl_3$/EtOAc 30/70, *v*/*v*). UV detector traces (300 nm) are shown at the top, CD detector traces (360 nm) are shown at the bottom.

All the HPLC analyses were performed at -5 °C to enhance the separation of the different enantiomers, by preventing the racemization process during the course of the separation. For compounds **3**, **16** and **18**, the separations were carried out in a mixture of THF and hexane as the mobile phase and for compound **4**, a mixture of chloroform and ethyl acetate was used due to the extremely limited solubility of the macrocyclic compound **4** in the former mobile phase (Figure 14a, b, c). Even for the mobile phase used, the solubility was limited due to the low temperature at which the separation was carried out. The two precursors (**16** and **18**) were separated using 40/60 THF/Hexane, compound **3** was eluted using the same eluting system but with a ratio of 50/50 and finally compound **4** was eluted by using $CHCl_3$/EtOAc in 30/70 ratio. 1-2 mg of each compound were solubilised in 1mL of the eluent (concentrations ranging from 0.7 mM –1.5 mM) for compounds **3**, **16** and **18**. For compound **4** 0.5-1 mg were used for

each injection due to the limited solubility that was mentioned previously (concentration ranging from 0.2 mM – 0.4 mM). The solutions of each isolated compound were evaporated under low temperature in order to prevent further racemization. For this reason, the solutions were placed into an ice-NaCl bath (-10 ^{o}C) during the evaporation process. It is noteworthy that sample **4** gave rise to only two peaks during the enantiomeric separation. One would expect that compound **4** can be found in three different enantiomeric forms: two in which the two helices are homochiral (either *PP* or *MM*) and a heterochiral species, *PM*. The heterochiral species is not expected to give any CD trace, since the opposite CD signals generated from the heterochiral helices cancel each other. However this species was not observed on the chromatogram (UV detector trace), supporting the hypothesis that either it is not favored or its kinetics are extremely fast and it cannot be isolated.

5.2. Monitoring racemization kinetics by circular dichroism

The two enantiomers of each compound **3**, **16** and **18** were dissolved in $CHCl_3$ and THF and the decay of CD intensity over time was measured and fitted to a first order kinetic model. For compound **4** the CD experiments were only conducted in $CHCl_3$ due to the extremely low solubility of this compound in THF. The temperature in which the CD experiments were recorded was 30 ^{o}C, in order to have a convenient time frame for following the racemization kinetics. The UV spectra of *P/M*-**3**, *P/M* -**4**, *P/M* -**16** and *P/M* -**18** were measured before and after monitoring of racemization, to confirm that no precipitation occurred during the racemization time (data not shown). The racemization rate constants (k_{rac}) of these compounds were obtained by curve fitting to an exponential decay, followed by calculation of the half-lives of racemization, that provide a quantitative indication of helical stability.

CD data for the *P/M*-**3**, *P/M* -**4**, *P/M* -**16** and *P/M* -**18** in $CHCl_3$ and THF are presented below (Figure 15, 16, 17 and 18) (Data referring to M helices are colored in blue and data referring to P helices are colored in red).

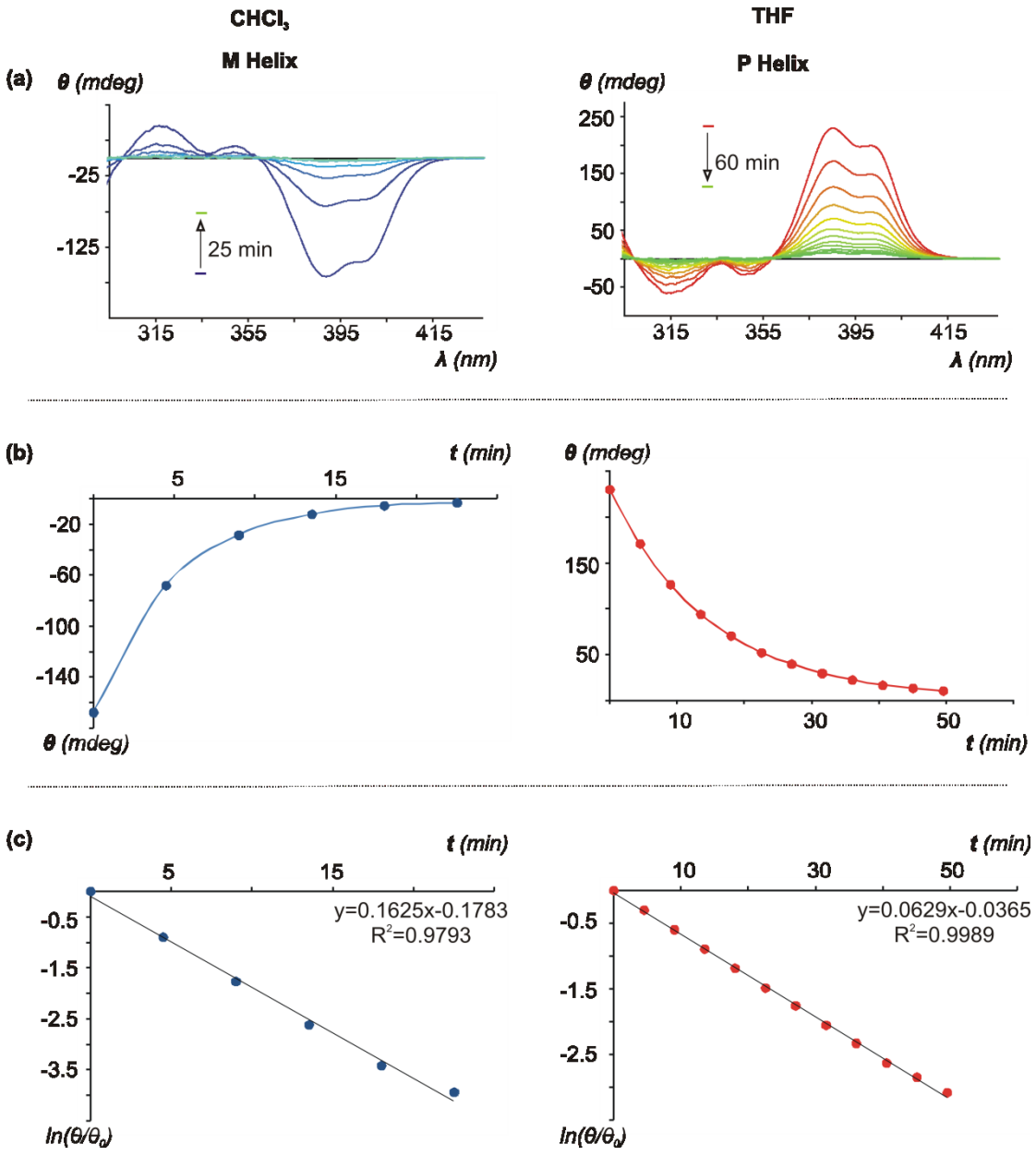

Figure 15: CD data providing the half-life of racemization for compound **16**. On the left data were obtained in $CHCl_3$ (*M* helix) and on the right in THF (*P* helix). (a) decay of the CD spectrum over time for compound **16**, (b) logarithmic fit of CD intensity plotted versus time, (c) linear plot of CD intensity at 381 nm fitted to a first order decay.

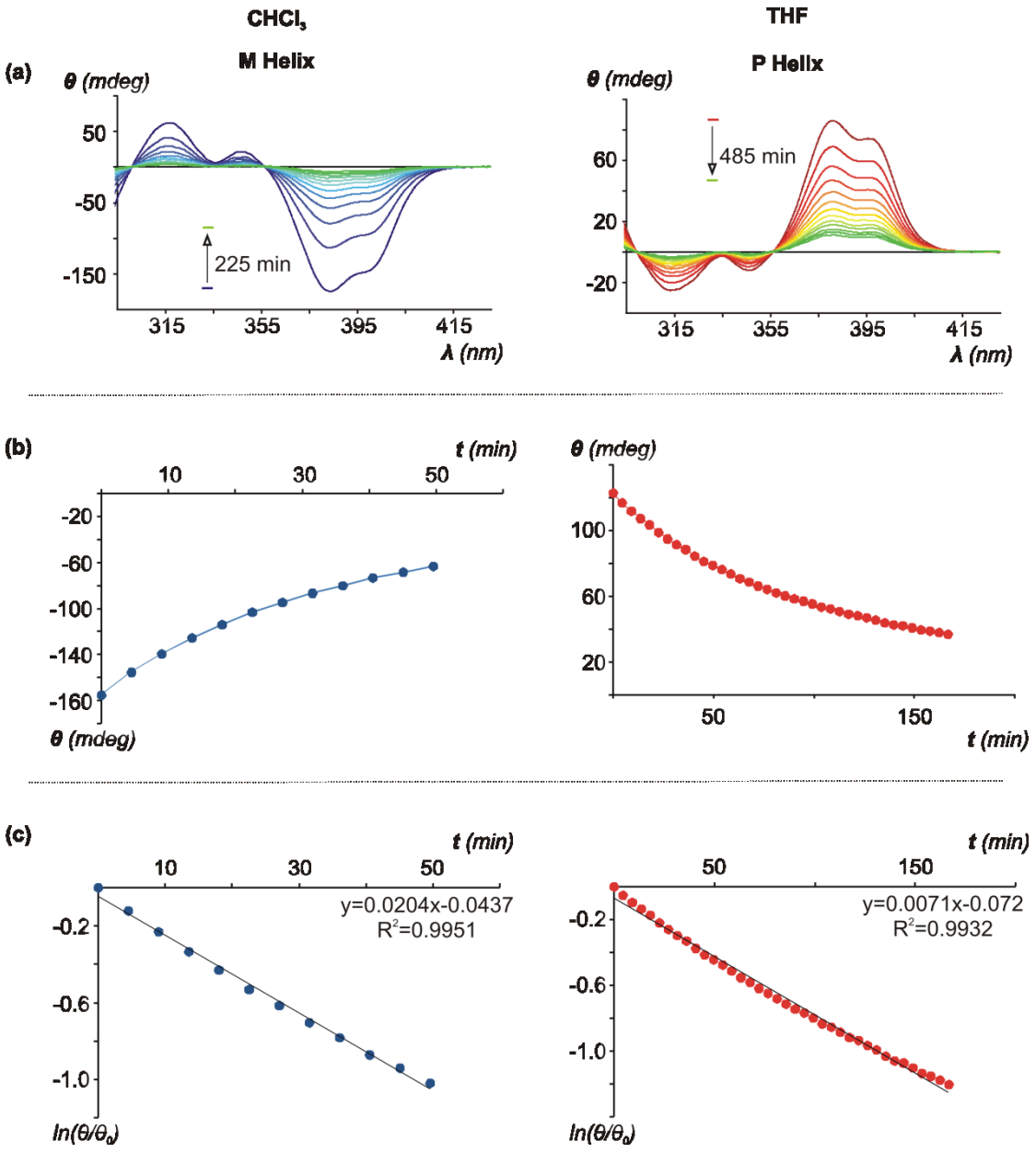

Figure 16: CD data providing the half-life of racemization for compound **3**. On the left data were obtained in $CHCl_3$ (*M* helix) and on the right in THF (*P* helix). (a) decay of the CD spectrum over time for compound **3**, (b) logarithmic fit of CD intensity plotted versus time, (c) linear plot of CD intensity at 381 nm fitted to a first order decay.

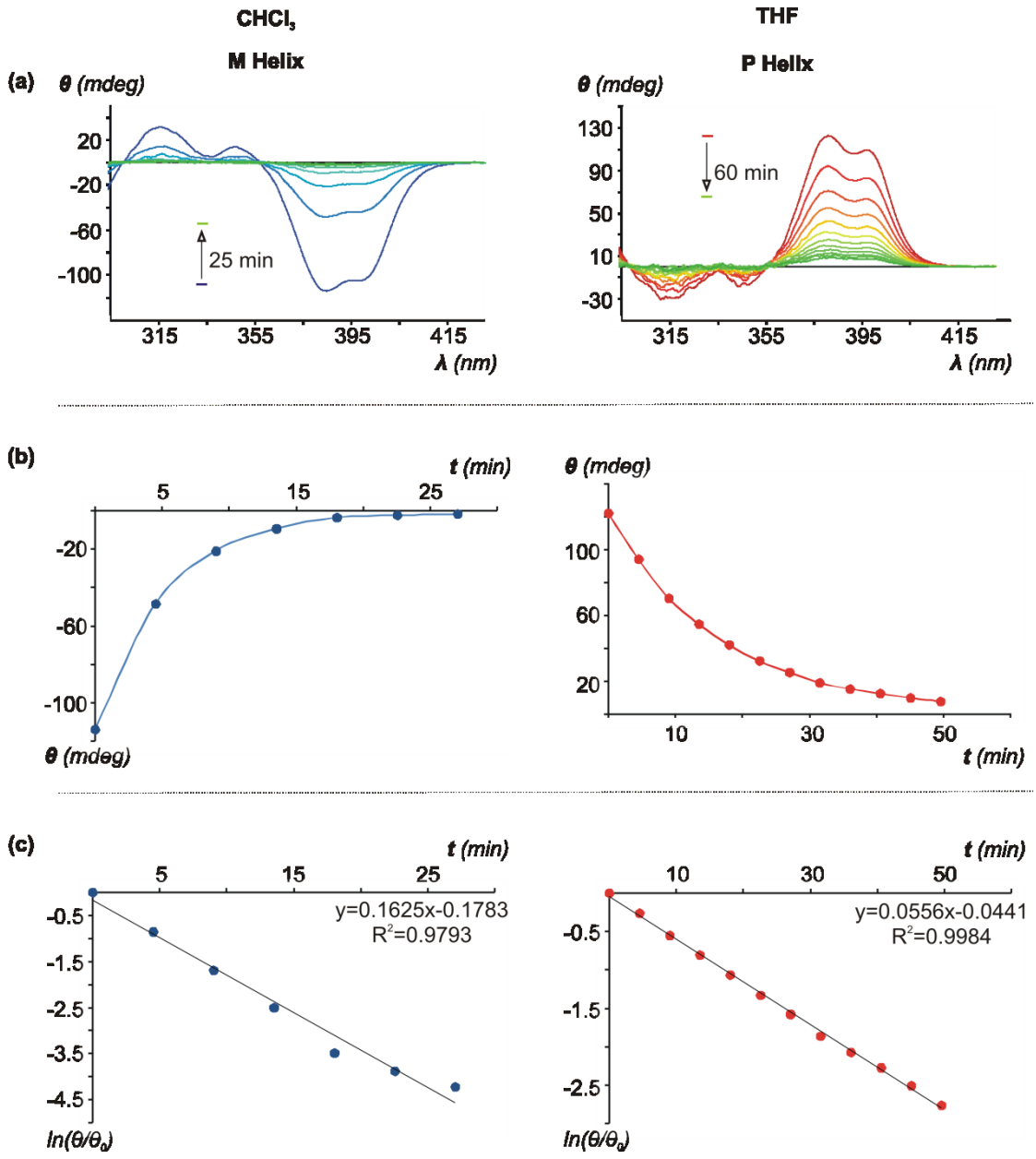

Figure 17: CD data providing the half-life of racemization for compound **18**. On the left data were obtained in $CHCl_3$ (*M* helix) and on the right in THF (*P* helix). (a) decay of the CD spectrum over time for compound **18**, (b) logarithmic fit of CD intensity plotted versus time, (c) linear plot of CD intensity at 381 nm fitted to a first order decay.

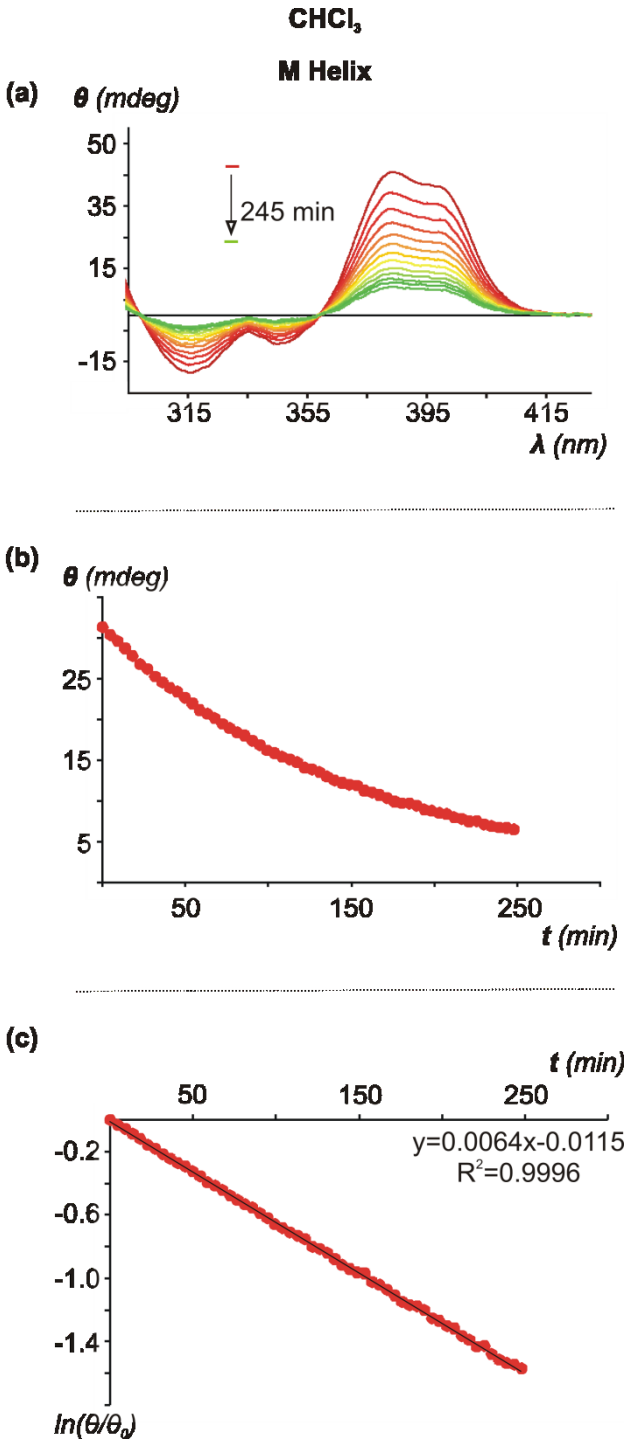

Figure 18: CD data providing the half-life of racemization for compound **4**. Data were obtained in $CHCl_3$ (*P* helix). (a) decay of the CD spectrum over time for compound **4**, (b) logarithmic fit of CD intensity plotted versus time, (c) linear plot of CD intensity at 381 nm fitted to a first order decay.

The calculated half-lives of helix inversion are reported in Table 1. Results show relatively fast kinetics for the non-bridged *tert*-Bu-protected precursors (**16** and **18**), which behave in a similar manner, indicating that the position of the thiol-bearing side chains does not by itself significantly influence helix stability.

Table 1: Half-lives of racemization for compounds **3** and **4**, as well as their *tert*-Bu-precursors at 30 °C.

	$t_{1/2}$ (min)	
	$CHCl_3$	THF
tert-Bu-precursor of **1** (**16**)	4	16
tert-Bu-precursor of **2** (**18**)	4	12
Compound **3**	53	150
Compound **4**	115	ND[a]

[a] not determined due to low solubility

One thing that is noteworthy in these experiments is the fact that the pentamers containing a phenanthroline moiety as a central unit follow a different trend to the quinolines, since the former are more stable in THF than in chloroform.[70] Interestingly, the half-lives of handedness inversion are about one order of magnitude larger for intrastrand disulfide bridged helix **3**, compared to its precursor. This confirms that macrocyclization enhances helix stability and validates the initial design. Nevertheless, one may have expected an even greater effect considering that the small ring size should cause severe strain in the partly unfolded transition state. A possible explanation for this may be that the side chains are not in an optimal orientation for disulfide bridge formation, and that some strain already exists within the ground state disulfide-containing macrocycle of **3**. The half-life of helix handedness inversion of interstrand disulfide bridged helix **4** in $CHCl_3$ is even larger than that of **3**. Again, disulfide bridges bring about significant stabilization. In principle, the very large ring size of macrocycle **4** should make helix inversion easier than in **3**. However, one has to consider that *PP*-*MM* handedness inversion in **4** spans not one but two helix segments that invert in a concerted manner, if not simultaneously. The *PM* intermediate, if it exists, must be strained as well and quickly rearranges to a *PP* or *MM* conformer.

6. Follow-up of disulfide bond formation

As described in the introduction, disulfide bond formation is a dynamic process. In the presence of a thiolate, disulfide exchange reactions occur and given its availability thermodynamic control is granted, meaning that the more thermodynamically stable compound will dominate over possible kinetic intermediates. In this part of our study, we decided to follow the disulfide formation by HPLC and identify intermediates of the macrocyclization reaction.

For this reason the formation of both macrocycles was carried out under both dilute and concentrated conditions to investigate if such a modification could favor the accumulation of different products e.g. dimer during the cyclization of compound **1** and monomer for compound **2**. Compounds **1** and **2** where dissolved in a mixture of chloroform/methanol (80/20), in three different concentrations: 0.2, 1 and 5 mM. 4 eq. of DIPEA was added to initiate the oxidation of the thiols. Additionally, a reaction containing a mixture of the two thiols at 2 mM concentrations was launched. The reaction vessels were equipped with an air-containing balloon to provide the oxygen required and ensure slower evaporation of the organic solvents. The reaction progress was followed by HPLC, by direct injection of the reaction mixture. The mobile phase used was an isocratic mixture of EtOAc/chloroform (70/30) on a normal silica column.

Our results suggested (Figure 19) that no significant amounts of any intermediate could be detected in the tested concentration range, apart from some dimeric species in the case of precursor **1**, as confirmed by mass spectroscopy (results not shown). On the other hand, the rate of the reaction, as well as the overall yield was increased when the concentration was increased.

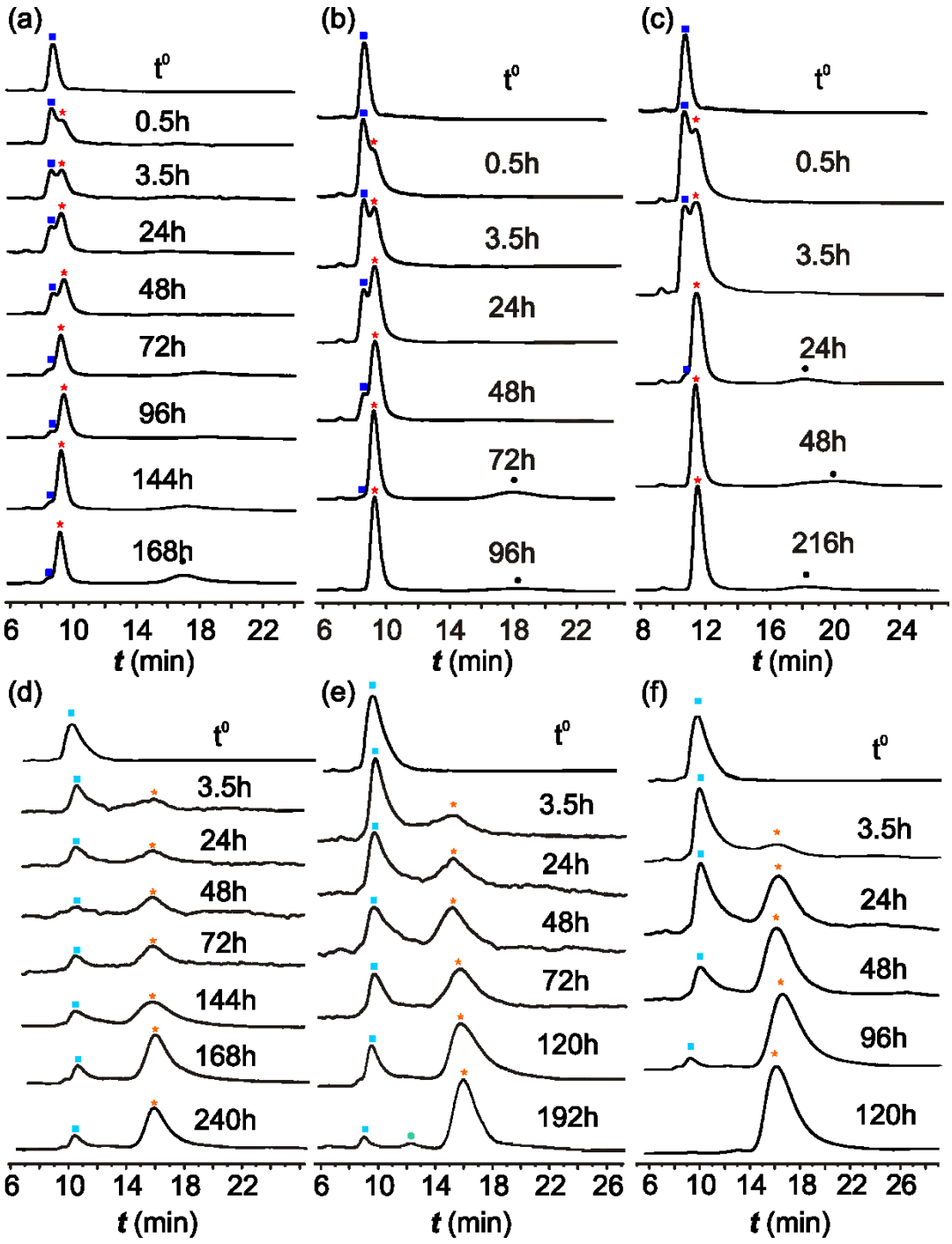

Figure 19: Monitoring of disulfide bridge formation over time. For compound **3** at: (a) 0.2, (b) 1 and (c) 5 mM concentrations in $CHCl_3$/MeOH (80/20) and for compound for **4** (d), (e) and (f) at the same concentrations, respectively. In both cases the desired product has been marked with a star and the starting material with a square.

In a second experiment, inspired by the wide range of different products present in dynamic combinatorial libraries, we decided to mix equimolar solutions of the two free thiol precursors (**1** and **2**) and follow the reaction again by HPLC (Figure 20). With this experiment we expected the formation of several intermediates arising from different combinations of the two precursors eventually leading to the accumulation of thermodynamically stable products. Unfortunately, due to the broadness of the chromatographic peaks detection becomes

difficult, but no intermediate could be observed in significant amounts. The only peaks observed belong to the starting material and the two desired products.

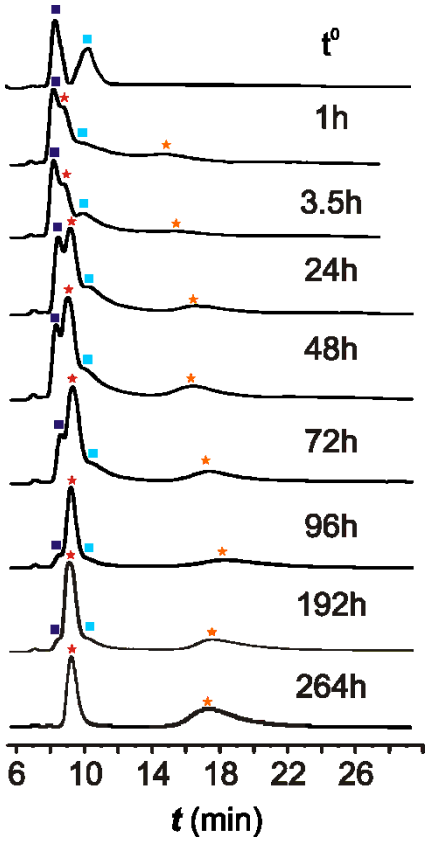

Figure 20: Monitoring over time of disulfide bridge formation in an equimolar mixture of the two free thiols precursors **1** and **2** in $CHCl_3$/MeOH (80/20). Compounds **1** and **2** are marked with dark and light blue square, respectively. Compounds **3** and **4** are marked with a red and an orange star respectively.

7. Conclusions

Depending on the positions of thiol bearing side chains on aromatic oligoamide foldamers, we found that disulfide formation may selectively occur intramolecularly or intermolecularly, yielding structurally well-defined large folded macrocycles. In particular, in the case of intermolecular bridging, X-ray data demonstrated a two-helix bundle-like structure showing complete helix-helix handedness communication. Macrocyclization via disulfide bond formation provides considerable and quantifiable stabilization of the folded conformations. Surprisingly, in the larger macrocycle **4** helix handedness inversion occurs slower than in the case of compound **3**. Additionally, monitoring of the reaction progress by HPLC suggested the absence of significant amounts of intermediates, demonstrating the stability of the desired compounds compared to other possible macrocyclic species. It is interesting to note that the presence of the phenanthroline moiety led to increased stability in

THF compared to chloroform, (a trend which is reversed compared to oligomers consisting of only quinoline monomers) suggesting that different backbones result in different stability profiles.

8. Experimental Section

Materials and Methods: All reactions were carried out under a dry nitrogen atmosphere. Commercial reagents were purchased from Sigma-Aldrich or Alfa-Aesar and were used without further purification unless otherwise specified. Chloroform and DIPEA were distilled from calcium hydride (CaH_2) prior to use. DCM was dried over solvent purification system (MBRAUN SPS-400). Reactions were monitored by thin layer chromatography (TLC) on Merck silica gel 60-F254 plates and observed under UV light. Silica gel chromatography was carried out on Merck GEDURAN Si60 (40-63 μm). Electrospray ionization mass spectrometric low and high resolution data (ESI MS, HRMS) were obtained from the Mass Spectrometry Laboratory at the European Institute of Chemistry and Biology (IECB), Pessac, France.

Nuclear Magnetic Resonance

^{1}H and ^{13}C NMR spectra were recorded in $CDCl_3$ solutions using a Bruker 300 Ultrashield Advance II spectrometer, ^{1}H operating at 300.13 MHz and ^{13}C operating at 75.46 MHz. Chemical shifts are reported in parts per million (ppm, δ) relative to the signal of the NMR solvent used. ^{1}H NMR splitting patterns with observed first-order coupling are designated as singlet (s), doublet (d), triplet (t), or quartet (q). Coupling constants (J) are reported in hertz. Splitting patterns that could not be interpreted or easily visualized are designated as multiplet (m) or broad (br).

Crystallography

X-ray crystallographic data collected on compounds **16**, **18** and **2** were collected at the IECB X-ray facility on a Rigaku MM07 rotating anode (800 kW) at the Cu kα wavelength equipped with a RAPID SPIDER image plate for detection and varimax HF optics. All the data were processed with the Rigaku CrystalClear 1.36 suite. Structures have been solved using direct methods with SHELXD and refined with SHELXL. The Squeeze procedure from the platon suite has been used on all three structures for solvent flattening. Only non disordered solvent molecules were kept in the final models.

Data for compound **4** were collected at 100 K using a Rigaku FRX microfocus rotating anode generator with Cu-K_α radiation (1.54178 Å) and varimax HF optics and a Dectris Pilatus 200K for detection. The data collection, unit cell refinement and data reduction were performed using the CrystalClear software package version 2.25. The positions of non-H atoms were determined by the program SHELXD and the position of the H atoms were deduced from coordinates of the non-H atoms and confirmed by Fourier Synthesis. H atoms were included for structure factor calculations but not refined.

All refinement and data statistics are compiled in the Crystallographic Data Table below (Table 2).

Table 2: Crystallographic data for compounds **2**, **4**, **18** and **19**

	16*	**18***	**2***	**4***
chemical formula	$C_{92}H_{96}N_{10}O_{12}S_2$	$C_{85}H_{85}N_{10}O_{14}S_2$	$C_{87.5}H_{82}N_{10}O_{12}S_2$	$C_{148}H_{132}N_{20}O_{24}Cl_{24}S_4$
Fw	1597.90	1534.78	1529.75	3553.77
Crystal system	Monoclinic	Triclinic	Orthorombic	Monoclinic
Space group	$P2_1/c$ (No 4)	P-1	Pbcn (No 60)	C 2/c
a, Å	11.2360(2)	10.2250(10)	41.6850(1)	35.234(7)
b, Å	20.1960(4)	19.2250(2)	20.2560(1)	21.950(4)
c, Å	39.8870(8)	20.879(2)	20.1800(1)	23.087(5)
α, deg	90	90.154(6)	90	90
β, deg	92.001(3)	103.738(6)	90	118.03(3)
γ, deg	90	90.149(5)	90	90
V, Å^3	9046(3)	4186.5(6)	17039.4	15761(7)
Z	4	2	8	4
D (calcd.), g/cm^3	1.173	1.310	1.193	1.498
temp. (K)	213(2)	213(2)	213(2)	100
uniq, refl. / total no. of refl. coll.	10668 / 77979	9808 / 48116	16452 / 110067	6776/13047
abs. coeff. (mm^{-1})	1.016	1.129	1.091	4.847
$R1$ ($I > 2\sigma(I)$) [a]	0.1227	0.1082	0.2063	0.1608
w$R2$ (all data) [b]	0.3584	0.3372	0.4968	0.3761
restraints/ parameters	60/ 1022	0 / 1001	3 / 995	39/725
GooF on F2 [c]	1.267	1.141	1.495	0.975

[a] $R1 = \Sigma||F_0|-|F_c||/\Sigma|F_0|$

[b] w$R2 = [\Sigma[w(F_0^2-F_c^2)^2]/\Sigma[w(F_0^2)_2]]^{1/2}$, where $w = 1/\sigma^2(F_0^2)+(aP)^2+bP$, $P = (F_0^2+2F_c^2)/3$

[c] GooF $= [\Sigma[w(F_0^2-F_c^2)^2]/(n-p)]^{1/2}$ where n = no. of reflections and p = no. of refined parameters.

[*] including solvents molecules

Circular Dichroism

CD spectra of were recorded on a J-815 Jasco spectropolarimeter (Jasco France, Nantes, France). Data are expressed in *mdeg*. CD spectra of oligomers were acquired in spectrometer grade $CHCl_3$ or THF between 250 and 450 nm using a rectangular quartz cell with a path length of 1 mm (Hellma 110-QS 1mm, Paris, France). As the concentration of each isolated enantiomer was not known after chiral HPLC separation, the CD spectra are reported in *mdeg*.

Chiral HPLC

HPLC separations were performed on a stainless-steel CHIRALPAK IA column (250 mm x 4.6 mm I.D., 5 μm particle-size) [Daicel Chemical Industries, Ltd., Tokyo, Japan]. HPLC-grade solvents were supplied by Sigma-Aldrich. The HPLC system consisted of a JASCO 3-Line Degasser DG-2080-53, two JASCO Intelligent HPLC pumps PU-2080Plus equipped with a Rheodyne injector (Rohnert Park, CA, USA), a 20-μL sample loop, a JASCO Intelligent UV/VIS detector UV-2075Plus and a JASCO CD detector CD1595. The column temperature was controlled in a refrigerated circulator Julabo EH. The software used for the data collection was JASCO Chromonav, version 1.08.02. For all the chiral separations that were conducted the flow rate was set to 0.5 mL min^{-1} at a regulated temperature of -5 °C.

Molecular Modeling

Molecular Models calculation were done using MacroModel version 8.6 (Schrödinger Inc.) with the modified MM3 force-field as implemented in this software. Energy minimized structures were obtained by conformational search using Monte Carlo Torsional Sampling Method (MCMM) using 10000 steps, no implicit solvent was used.

Gel Permeation Chromatography (GPC)

For the GPC experiment an LC-9130G NEXT (Japan Analytical Industry Co., Ltd.) setup was used, equipped with two preparative columns (Inner diameter of 20mm and length of 600 mm): a JAIGEL 2.5H and a JAIGEL 3H, in conjugation with UV-600 NEXT UV detector and an FC-3310 fraction collector. The setup is equipped with a column oven that is set at 37 ^{o}C. Chloroform (HPLC grade, ethanol stabilized) was used for the separations.

Preparation of the different monomers

Methyl 4-(3-(*tert*-butylthio)propoxy)-8-nitroquinoline-2-carboxylate (**7**): In a 250 mL round bottom-flask placed under inert atmosphere, methyl 1,4-dihydro-8-nitro-4-oxoquinoline-2-carboxylate[1] (**6**) (5.08 g, 20.5 mmol), freshly distilled 3-(*tert*-butylthio)propan-1-ol (**5**)[2] (2.09 mL, 22.5 mmol) and PPh_3 (59.0 g, 22.5 mmol) were dissolved in 45 mL of anhydrous THF. The flask was then hermetically closed and remained under inert atmosphere during the reaction time. The reaction mixture was then cooled down to 0° C and DIAD was added (0.444 mL, 22.5 mmol). Resulting slurry was stirred at 0 °C for 30 min and then at room temperature for additional 4 hours. Solvent was removed by evaporation and the crude mixture was subsequently precipitated from cold methanol. The yellow crystalline powder

was collected by filtration and **7** was isolated in 87% yield (6.7 g). ^{1}H NMR ($CDCl_3$):δ 8.46 (1H, d, J = 8.4 Hz, $CH_{ar\text{-}ortho}$), 8.10 (1H, d, J = 7.5 Hz, $CH_{ar\text{-}para}$), 7.69–7.62 (2H, m, $CH_{ar\text{-}quinoline}$ and $CH_{ar\text{-}meta}$), 4.44 (2H, t, J = 6.1 Hz, CH_2-), 4.04 (3H, s, $CH_{3\text{-}ester}$), 2.80 (1H, t, J = 7.0 Hz, CH_2-), 2.26 (1H, q, J = 6.5 Hz, CH_2-), 1.34 (9H, s, $CH_{3\text{-}t\text{Bu}}$). ^{13}C NMR ($CDCl_3$): δ 166.0, 162.9, 151.7, 148.8, 140.4, 126.6, 126.3, 125.4, 123.5, 102.6, 68.5, 53.7, 42.7, 31.3, 29.4, 25.0. Elemental analysis calc. for $C_{18}H_{22}N_2O_5S$: C, 57.13; H, 5.86; N, 7.40; found: C, 57.11; H, 5.86; N, 7.36. HRMS (ES^+): *m/z* calcd for $C_{18}H_{22}N_2O_5S$ $[M+H]^+$ 379.1328 found 379.1342.

4-(3-(*tert*-butylthio)propoxy)-8-nitroquinoline-2-carboxylic acid (**8**)*:* To a solution of Methyl 4-(3-(*tert*-butylthio)propoxy)-8-nitroquinoline-2-carboxylate (**7**) (0.6 g, 1.58 mmol) in THF/H_2O (4:1, v/v, 110 mL), $LiOH.H_2O$ (132 mg, 3.14 mmol) was added and the resulting mixture was stirred for 30 min. Apparition of slurry indicates that the reaction was occurring. The reaction was then quenched by addition of an aqueous solution of citric acid 5%, until the slurry disappeared. The reaction mixture was subsequently diluted with DCM (200 mL). The resulting organic layer was then washed with distilled water and saturated NaCl. Combined aqueous layers were back extracted once with DCM (20 mL). Combined organic layers were finally dried over Na_2SO_4 and filtered. After evaporation, carboxylic acid **8** was obtained as an off-white solid. Yield: 99% (571 mg). ^{1}H NMR ($CDCl_3$): δ 8.54 (1H, dd, J = 8.5, 1.4 Hz, $CH_{ar\text{-}ortho}$), 8.23 (1H, dd, J = 7.5, 1.4 Hz, $CH_{ar\text{-}para}$), 7.77 (1H, s, $CH_{ar\text{-}quinone}$), 7.73 (1H, t, J = 8.5 Hz, $CH_{ar\text{-}meta}$), 4.49 (2H, t, J = 6.2 Hz, $CH_{2\text{-}\alpha}$), 2.80 (1H, t, J = 6.9 Hz, $CH_{2\text{-}\gamma}$), 2.29 (1H, q, J = 6.3 Hz, $CH_{2\text{-}\beta}$), 1.34 (9H, s, $CH_{3\text{-}t\text{Bu}}$). ^{13}C NMR ($CDCl_3$): δ 164.4, 163.8, 149.7, 147.5, 138.7, 127.5, 127.0, 126.6, 123.9, 100.7, 68.3, 42.8, 31.3, 29.3, 24.9. HRMS (ES^+): *m/z* calcd for $C_{17}H_{21}N_2O_5S$ $[M+H]^+$ 365.1171 found 365.1179.

4-(3-(*tert*-butylthio)propoxy)-8-nitroquinoline-2-carbonyl chloride (**8a**): To a solution of 4-(3-(*tert*-butylthio)propoxy)-8-nitroquinoline-2-carboxylic acid (**8**) (457 mg, 1.25 mmol) in freshly distilled DCM (5 mL), oxalyl chloride (12.5 mmol, 1 mL) was added. The reaction mixture was stirred at room temperature for 2 hours. The residue was thoroughly dried at reduced pressure to yield **8a** as yellowish solid in 100% yield. ^{1}H NMR ($CDCl_3$): δ 8.47 (1H, d, J = 8.5 Hz, $CH_{ar\text{-}ortho}$), 8.13 (1H, d, J = 7.4 Hz, $CH_{ar\text{-}para}$), 7.73 (1H, t, J = 8.0 Hz, $CH_{ar\text{-}meta}$), 7.56 (1H, s, $CH_{ar\text{-}quinone}$), 4.45 (2H, t, J = 6.1 Hz, $CH_{2\text{-}\alpha}$), 2.80 (1H, t, J = 6.9 Hz, $CH_{2\text{-}\gamma}$), 2.28 (1H, q, J = 6.5 Hz, $CH_{2\text{-}\beta}$), 1.34 (9H, s, $CH_{3\text{-}t\text{Bu}}$).

Methyl 8-amino-4-(3-(*tert*-butylthio)propoxy)quinoline-2-carboxylate (**11**): Methyl 4-(3-(*tert*-butylthio)propoxy)-8-nitroquinoline-2-carboxylate (**7**) (0.5 g, 1.32 mmol) was dissolved in

ethyl acetate/MeOH (4:1, 25 mL). A catalytic amount of Pd/C (10%) catalyst (50 mg) and ammonium metavanadate (ca 20 mg) were then added. The mixture was stirred at 80 °C, ammonium formate (560 mg dissolved in 1 mL of distilled water) was subsequently added and the reaction was refluxed for 4 hours. The reaction mixture was then filtered through celite and diluted with DCM (10 mL) then washed with saturated NaCl solution (10 mL). Layers were separated and the organic layer was dried over Na_2SO_4, filtered and evaporated to yield **11** as a greenish solid. Yield: 99% (456 mg). ^{1}H NMR (DMSO-d_6): δ 7.47 (1H, s), 7.39 (1H, t, *J* = 7.90 Hz), 7.29 (1H, dd, *J* = 7.3, 1.4 Hz), 6.94 (1H, dd, *J* =, 7.6, 1.4 Hz), 6.05 (2H, bs), 4.37 (2H, t, *J* = 6.1 Hz), 3.95 (3H, s), 2.77 (2H, t, *J* = 7.2 Hz), 2.10 (2H, q), 1.29 (9H, s). ^{13}C NMR (DMSO-d_6): δ 166.5, 162.5, 147.0, 146.0, 138.1, 130.1, 123.1, 110.7, 107.8, 101.6, 68.1, 53.5, 42.9, 31.6, 30.1, 25.0. HRMS (ES^+): *m/z* calcd for $C_{18}H_{25}N_2O_3S$ $[M+H]^+$ 349.1586 found 349.1596.

Synthesis of the dimer intermediates

Methyl-8-(4-(3-(*tert*-butylthio)propoxy)-8-nitroquinoline-2-carboxamido)-4-isobutoxy-quinoline-2-carboxylate (**10**): In a 100 mL round bottomed flask under argon atmosphere, methyl 8-amino-4-isobutoxyquinoline-2-carboxylate[1] (**9**) (326 mg, 1.19 mmol) and DIPEA (8.62 mmol, 1.5 mL) were dissolved in freshly distilled DCM (5 mL). The flask was then cooled down to 0 °C. In a separate flask, 4-(3-(*tert*-butylthio)propoxy)-8-nitroquinoline-2-carbonyl chloride **8a** (1.05 eq.; 1.25 mmol, 478 mg) was dissolved in freshly distilled DCM (5 mL) in an argon atmosphere and subsequently added via a stainless steel canula to the solution of **9** over a period of 30 min at 0 °C. The resulting reaction mixture was stirred at room temperature overnight. After dilution with DCM (10 mL), the organic layer was successively washed with distilled water (20 mL), saturated $NaHCO_3$ (20 mL), and 0.1 M HCl solution (20 mL). The organic layer was then dried over Na_2SO_4, filtered and rotary evaporated. After re-crystallization from cold MeOH / $CHCl_3$ mixture, **10** was obtained as yellow needles. Yield: 86% (635 mg). ^{1}H NMR ($CDCl_3$): δ 11.88 (1H, bs), 9.09 (1H, d, *J* = 7.6 Hz), 8.53 (1H, d, *J* = 8.2 Hz), 8.20 (1H, d, *J* = 7.1 Hz), 8.02 (1H, dd, *J* = 8.5, 1.2 Hz), 7.98 (2H, m), 7.60 (3H, m), 4.52 (2H, t, *J* = 6.0 Hz), 4.23 (3H, s), 4.08 (2H, d, *J* = 6.4 Hz), 2.83 (2H, t, *J* = 7.0 Hz), 2.29 (3H, m), 1.36 (9H, s), 1.16 (6H, d, *J* = 6.6 Hz). ^{13}C NMR ($CDCl_3$): δ 167.3, 163.1, 162.8, 154.4, 148.7, 148.2, 140.1, 139.8, 135.2, 128.2, 127.0, 125.8, 125.7, 123.7, 122.7, 119.1, 117.1, 101.9, 100.7, 75.5, 68.7, 54.0, 42.7, 31.3, 29.5, 28.6, 25.0, 19.6. Elemental analysis calc. for $C_{32}H_{36}N_4O_7S$: C, 61.92; H, 5.95; N, 9.03; found: C, 62.03; H, 5.89; N, 9.18. HRMS (ES^+): *m/z* calcd for $C_{32}H_{37}N_4O_7S$ $[M+H]^+$ 621.2383 found 621.2401.

Methyl 4-(3-(*tert*-butylthio)propoxy)-8-(4-isobutoxy-8-nitroquinoline-2-carboxamido)-quinoline-2-carboxylate (**13**): In a 250 mL round bottomed flask under argon atmosphere, methyl 4-(3-(*tert*-butylthio)propoxy)-8-aminoquinoline-2-carboxylate **11** (517 mg, 1.55 mmol) and DIPEA (4.6 mmol, 0.8 mL) were dissolved in freshly distilled DCM (7 mL). The flask was then cooled down to 0 °C. In a separate flask, 4-isobutoxy-8-nitroquinoline-2-carbonyl chloride[1] (**12**) (1.55 mmol, 4.77 mg) was dissolved in freshly distilled DCM (4 mL) in an argon atmosphere and subsequently added via a stainless steel canula to the solution of **11** over a period of 30 min at 0 °C. The resulting reaction mixture was stirred at room temperature overnight. After dilution with DCM (10 mL), the organic layer was successively washed with distilled water (12 mL), saturated $NaHCO_3$ (12 mL), and 0.1 M HCl solution (12 mL). The organic layer was then dried over Na_2SO_4, filtered and rotary evaporated. After re-crystallization from cold MeOH/$CHCl_3$ mixture, **13** was isolated as yellow needles. Yield: 74% (710 mg). ^{1}H NMR ($CDCl_3$): δ 11.88 (1H, bs), 9.10 (1H, dd, *J* = 7.8, 1.2 Hz), 8.54 (1H, dd, *J* = 8.4, 1.3 Hz), 8.20 (1H, dd, *J* = 7.4, 1.4 Hz), 8.00 (1H, dd, *J* = 8.4, 1.2 Hz), 7.96 (1H, s), 7.66 (3H, m), 4.42 (2H, t, *J* = 6.0 Hz), 4.23 (3H, s), 4.18 (2H, d, *J* = 6.5 Hz), 2.83 (2H, t, *J* = 7.1 Hz), 2.40–2.20 (3H, m), 1.35 (9H, s), 1.17 (6H, d, *J* = 6.8 Hz). ^{13}C NMR ($CDCl_3$): δ 167.2, 163.6, 162.9, 162.8, 154.3, 148.7, 148.2, 140.1, 139.7, 135.3, 128.3, 127.0, 125.8, 123.8, 122.5, 119.1, 116.9, 101.9, 100.6, 76.9, 68.0, 54.0, 42.6, 31.3, 29.7, 28.5, 25.1, 19.5. Elemental analysis calc. for $C_{32}H_{36}N_4O_7S$: C, 61.92; H, 5.95; N, 9.03; found: C, 61.59; H, 6.06; N, 8.96. HRMS (ES^+): *m/z* calcd for $C_{32}H_{37}N_4O_7S$ $[M+H]^+$ 621.2383 found 621.2380

Methyl 8-(8-amino-4-(3-(*tert*-butylthio)propoxy)quinoline-2-carboxamido)-4-isobutoxy 4quinoline-2-carboxylate (**14**): Methyl 8-(4-(3-(*tert*-butylthio)propoxy)-8-nitroquinoline-2-carboxamido)-4-isobutoxy quinoline-2-carboxylate **10** (568 mg, 0.91 mmol) was dissolved in EtOAc/MeOH solvent mixture (4:1, 35 mL). A catalytic amount of Pd/C (10%) catalyst (60 mg) and ammonium metavanadate (31 mg) were then added. The mixture was stirred at 80 °C. Ammonium formate (1.1 g) dissolved in distilled water (1.1 mL) was subsequently added the reaction mixture was refluxed overnight. The reaction mixture was then filtered through celite, diluted with DCM (40 mL) and washed with saturated NaCl (40 mL). The organic layer was dried over Na_2SO_4, filtered and rotary evaporated to yield **14** as green solid. Yield: 99% (532 mg). ^{1}H NMR ($CDCl_3$): δ 12.69 (1H, s), 9.05 (1H, d, *J* = 7.7 Hz), 7.96 (1H, d, *J* = 7.5 Hz), 7.79 (1H, s), 7.67 (1H, t, *J* = 8.1 Hz), 7.58–7.50 (2H, m), 7.39 (1H, t, *J* = 8.0 Hz), 7.01 (1H, d, *J* = 7.4 Hz), 5.53 (1H, bs) 4.44 (2H, t, *J* = 6.1 Hz), 4.10 (3H, s), 4.07 (2H, d, *J* = 6.4 Hz), 2.83 (2H, t, *J* = 7.2 Hz), 2.31–2.19 (3H, m), 1.35 (9H, s), 1.17 (6H, d, *J* = 6.7 Hz). ^{13}C

NMR ($CDCl_3$): δ 165.29, 162.96, 162.91, 162.82, 148.21, 146.70, 144.94, 139.48, 137.34, 135.25, 128.37, 128.25, 122.89, 122.13, 117.11, 115.59, 110.93, 109.33, 101.34, 98.29, 75.13, 67.55, 52.97, 42.36, 31.12, 30.30, 29.61, 28.35, 27.03, 24.99, 19.41. Elemental analysis calc. for $C_{32}H_{38}N_4O_5S$: C, 65.06; H, 6.48; N, 9.48; found: C, 64.47; H, 6.39; N, 9.99. HRMS (ES^+): *m/z* calcd for $C_{32}H_{39}N_4O_5S$ $[M+H]^+$ 591.2641 found 591.2637.

Methyl 8-(8-amino-4-isobutoxyquinoline-2-carboxamido)-4-(3-(*tert*-butylthio)propoxy) quinoline-2-carboxylate (**17**): Methyl 4-(3-(*tert*-butylthio)propoxy)-8-(4-isobutoxy-8-nitroquinoline-2-carboxamido) quinoline-2-carboxylate (**13**) (685 mg, 1.1 mmol) was dissolved in ethyl acetate/MeOH solvent mixture (4:1, 40 mL). A catalytic amount of Pd/C (10%) catalyst (70 mg) and ammonium metavanadate (37 mg) were then added. The mixture was stirred at 80 °C. Ammonium formate (1.32 g) dissolved in distilled water (1.4 mL) was subsequently added and the resulting mixture was refluxed overnight. The reaction mixture was then filtered through celite, diluted with DCM (50 mL) and washed with saturated NaCl (50 mL). The organic layer was dried over Na_2SO_4, filtered and rotary evaporated to yield **17** as a green solid. Yield: 99% (640 mg). ^1H NMR ($CDCl_3$): δ 12.71 (1H, bs), 9.06 (1H, dd, *J* = 7.6, 1.0 Hz), 7.94 (1H, dd, *J* = 7.5, 0.9 Hz), 7.76 (1H, s), 7.66 (1H, t, *J* = 8.1 Hz), 7.58–7.50 (2H, m), 7.39 (1H, t, *J* = 7.8 Hz), 7.01 (1H, dd, *J* = 7.5, 0.8 Hz), 5.54 (2H, bs) 4.42 (2H, t, *J* = 6.0 Hz), 4.11–4.06 (5H, m), 2.84 (2H, t, *J* = 7.0 Hz), 2.35–2.20 (3H, m), 1.35 (9H, s), 1.15 (6H, d, *J* = 6.7 Hz). ^{13}C NMR ($CDCl_3$): δ 165.43, 163.44, 163.30, 162.86, 148.41, 146.96, 144.95, 139.76, 137.55, 135.47, 128.73, 128.31, 123.22, 122.26, 117.37, 115.65, 111.05, 109.66, 101.60, 98.40, 75.20, 67.74, 53.12, 42.52, 31.13, 29.50, 28.41, 24.93, 19.48. Elemental analysis calc. for $C_{32}H_{38}N_4O_5S$: C, 65.06; H, 6.48; N, 9.48; found: C, 64.26; H, 6.49; N, 10.22. HRMS (ES^+): *m/z* calcd for $C_{32}H_{39}N_4O_5S$ $[M+H]^+$ 591.2641 found 591.2639.

*Synthesis of pentamer intermediates **1** and **2***

1,10-phenanthroline-2,9-dicarbonyl dichloride (**15**)*:* 1,10-phenanthroline-2,9-dicarboxylic acid (145 mg; 0.54 mmol) was dissolved in 10 mL of thionyl chloride ($SOCl_2$). The reaction mixture was refluxed at 120 ^oC for 1 hour. Solvents were then removed under high vacuum to yield 1,10-phenanthroline-2,9-dicarbonyl dichloride as a white solid in quantitative yield. $C_{14}H_6O_2Cl_2$= 305.11 $g.mol^{-1}$. ^1H NMR ($CDCl_3$): δ 8.49 (4H, dd, *J* = 11.1, 8.4 Hz), 8.08 (2H, s).

Methylester-isobutoxy-*tert*-butylthiopropoxy-phenantroline-*tert*-butylthiopropoxy-isobutoxy-methylester (**16**): To a solution of 1,10-phenanthroline-2,9-dicarbonyl dichloride, (**15**) (143 mg, 0.47 mmol) in anhydrous DCM (3.5 mL) was added via a cannula, under N_2 atmosphere a solution of methyl 4-(3-*tert*-butylthio)propoxy)-8-(4-isobutoxy-8-aminoquinoline-2-carboxamido)quinoline 2-carboxylate (**14**) (522 mg, 0.88 mmol) and DIPEA (0.6 mL, 3.5 mmol) in anhydrous DCM (5 mL). The reaction mixture was stirred overnight at room temperature. The organic layer was then washed two times with a 1 N solution of HCl, one time with brine, dried over Na_2SO_4, and evaporated to give a residue, which was submitted to flash silica gel silica gel column chromatography, eluting with EtOAc/cyclohexane (1/4, v/v), to furnish **16** as a yellow solid. Yield: 73% (460 mg). $C_{78}H_{80}N_{10}O_{12}S_2$ = 1413.66 g.mol^{-1}. Elemental analysis calc. for $C_{78}H_{80}N_{10}O_{12}S_2$: C, 66.27; H, 5.70; N, 9.91; found: C, 65.97; H, 5.68; N, 10.05. ^{1}H NMR ($CDCl_3$): δ 12.77 (2H, s), 11.80 (2H, s), 8.93 (2H, d, *J* = 7.0 Hz), 8.82 (2H, dd, *J* = 6.5, 1.9), 7.85–7.72 (8H, m), 7.63–7.53 (4H, m), 7.43 (2H, s), 6.88 (2H, s), 6.36 (2H, s), 4.29 (4H, m), 3.70 (4H, m), 3.22 (6H, s), 2.95–2.73 (4H, m), 2.41–2.19 (6H, m), 1.41 (18H, s), 1.23 (6H, d, *J* = 10.0 Hz), 1.17 (6H, d, *J* = 6.7 Hz). ^{13}C NMR ($CDCl_3$): δ 164.3, 162.8, 161.9, 161.8, 161.2, 149.1, 149.0, 144.9, 138.6, 136.1, 134.7, 134.4, 128.8, 128.0, 127.0, 121.5, 120.6, 119.8, 118.9, 116.0, 115.6, 100.4, 98.0, 75.4, 67.3, 52.7, 42.8, 31.4, 29.7, 28.5, 25.0, 19.7, 19.6. HRMS (ES$^+$): *m/z* calcd for $C_{78}H_{81}N_{10}O_{12}S_2$ $[M+H]^+$ 1413.5477 found 1413.5492.

Methylester-*tert*-butylthiopropoxy-isobutoxy-phenanthroline-isobutoxy-*tert*-butylthiopropoxy-methylester (**18**): To a solution of 1,10-phenanthroline-2,9-dicarbonyl dichloride, (**15**) (165 mg, 0.54 mmol) in anhydrous DCM (4 mL) was added via a canula, under N_2 atmosphere, a solution of methyl-4-(3-(*tert*-butylthio)propoxy)-8-(4-isobutoxy-8-aminoquinoline-2-carboxamido)quinoline-2-carboxylate, (**17**) (644 mg, 1.09 mmol) and DIPEA (0.7 mL, 4.22 mmol) in anhydrous DCM (6 mL) and left to react overnight at room temperature. The reaction mixture was then evaporated under reduced pressure before to be purified by flash silica gel column chromatography with EtOAc/cyclohexane (1/4, v/v) as eluting system, followed by precipitation in MeOH to yield **18** as a yellow solid. Yield: 72% (545 mg). ^{1}H NMR ($CDCl_3$): δ 12.79 (2H, s), 11.81 (2H, s), 8.93 (2H, dd, *J* = 7.3, 1.4 Hz), 8.81 (2H, dd, *J* = 7.3, 1.3 Hz), 7.88–7.71 (8H, m), 7.64–7.52 (4H, m), 6.87 (2H, s), 6.40 (2H, s), 4.12–3.91 (6H, m), 3.89–3.79 (2H, m) 3.21 (6H, s), 2.98–2.89 (2H, m), 2.84–2.75 (2H, m), 2.36–2.14 (6H, m), 1.45 (18H, s), 1.18 (12H, dd, J = 6.8, 3.9 Hz). ^{13}C NMR ($CDCl_3$): δ 164.4, 162.8, 162.0, 161.8, 161.3, 149.2, 149.1, 142.6, 145.0, 138.6, 136.2, 134.8, 134.4, 128.8, 128.0, 127.0, 121.6, 120.7, 119.9, 119.1, 119.0, 119.0, 116.0, 115.6, 100.4, 98.0, 75.5, 67.3,

52.8, 31.5, 29.7, 28.5, 25.1, 19.8, 19.6. Elemental analysis calc. for $C_{78}H_{80}N_{10}O_{12}S_2$: C, 66.27; H, 5.70; N, 9.91; found: C, 65.91; H, 5.57; N, 10.00. HRMS (ES^+): *m/z* calcd for $C_{78}H_{81}N_{10}O_{12}S_2$ $[M+H]^+$ 1413.5477 found 1413.5487.

Methylester-isobutoxy-*(NpyS)*thiopropoxy-phenantroline-*(NpyS)*thiopropoxy-isobutoxy-methylester (**19**): To a solution of Methylester-isobutoxy-terbutylthiopropoxy-phenanthroline-terbutylthiopropoxy-isobutoxy-methylester (**16**) (100 mg, 62.5 µmol) in AcOH (4 mL) a slight excess of NpySCl (311 µmol, 54 mg) was added. The reaction was stirred for 24 hours at room temperature, resulting in the formation of yellow precipitate. The AcOH was then removed under vacuum in presence of toluene and the crude was purified by flash silica gel column chromatography first with EtOAc/cyclohexane (7/3, v/v) solvent mixture followed by DCM/MeOH (98/2) to yield **19** as a yellow solid. Yield: 65% (60 mg). ^{1}H NMR ($CDCl_3$): δ 12.79 (2H, s), 11.77 (2H, s), 8.91 (2H, d, *J* = 6.6 Hz), 8.85 (2H, d, *J* = 6.4 Hz), 8.84 (2H, d, *J* = 6.5 Hz), 8.50 (2H, d, *J* = 8.3 Hz), 7.86–7.70 (8H, m), 7.65–7.54 (4H, m), 7.43 (2H, s), 7.37 (2H, dd, *J* = 8.4, 8.1 Hz), 6.88 (2H, s), 6.36 (2H, s), 4.44–4.26 (4H, m), 3.79–3.61 (4H, m), 3.33–3.12 (10H, m), 2.44 (4H, m), 2.25 (2H, m), 1.23 (6H, d, *J* = 6.6 Hz), 1.17 (6H, d, *J* = 6.6 Hz). ^{13}C NMR ($CDCl_3$): δ 164.3, 162.3, 161.7, 161.7, 161.5, 157.4, 154.1, 149.1, 149.0, 144.9, 142.5, 138.8, 138.5, 134.6, 134.4, 134.1, 128.6, 128.5, 128.3, 121.3, 121.2, 120.7, 119.9, 119.0, 115.8, 100.4, 98.0, 75.1, 67.4, 52.7, 34.9, 28.6, 28.5, 19.8, 19.6. HRMS (ES^+): *m/z* calcd for $C_{80}H_{69}N_{14}O_{16}S_4$ $[M+H]^+$ 1609.3899 found 1609.3952.

Methylester-*(NpS)*thiopropoxy-isobutoxy-phenantroline-isobutoxy-(*NpS)*thiopropoxy-methylester (**20**): To a solution of methylester-*tert*-butylthiopropoxy-isobutoxy-phenantroline-isobutoxy-*tert*-butylthiopropoxy-methylester (**18**) (100 mg, 62.5 µmol) in AcOH (4 mL) an excess of para-nitropyridine sulfenyl chloride (NpySCl) was added (311 µmol, 54 mg) and the reaction was stirred 24 hours at room temperature resulting in the apparition of a precipitate. The AcOH was then removed under reduced pressure in presence of toluene and the crude was purified by flash silica gel column chromatography first with EtOAc/cyclohexane (7/3, v/v) solvent mixture followed by DCM/MeOH (98/2) to yield **20** as a yellow solid. Yield: 67% (66 mg). $C_{80}H_{68}N_{14}O_{16}S_4$ = 1609.74 g.mol^{-1}. MS (ESI+): *m/z* = 1609.38 $[M + H]^+$, 1631.37 $[M + Na]^+$. ^{1}H NMR ($CDCl_3$): δ 12.83 (2H, s), 11.79 (2H, s), 8.96–8.83 (6H, m), 8.55 (2H, dd, *J* = 8.0, 1.5 Hz), 7.88 (2H, d, *J* = 8.1 Hz), 7.88–7.71 (6H, dqu, *J* = 7.4, 1.5 Hz), 7.62 (2H, s), 7.58 (2H, t, *J* = 7.6 Hz), 7.49 (2H, d, *J* = 8.0 Hz), 7.41 (2H, dd, *J* = 8.2, 3.4 Hz), 6.88 (2H, s), 6.43 (2H, s), 4.31–4.22 (2H, m), 4.14–4.05 (2H, m), 4.02–

3.94 (2H, m), 3.90–3.82 (2H, m), 3.27–3.17 (10H, m), 2.40–2.25 (6H, m), 1.23 (6H, d, *J* = 6.5 Hz), 1.20 (6H, d, *J* = 6.4 Hz). ^{13}C NMR ($CDCl_3$): δ 164.2, 162.8, 162.0, 161.8, 161.1, 157.3, 154.1, 149.2, 149.1, 144.9, 142.5, 138.8, 138.6, 134.8, 134.4, 134.3, 128.8, 128.7, 128.0, 121.5, 121.5, 120.6, 118.9, 116.0, 98.1, 75.5, 52.8, 34.8, 28.5, 28.0, 19.7, 19.6. HRMS (ES^+): *m/z* calcd for $C_{80}H_{69}N_{14}O_{16}S_4$ $[M+H]^+$ 1609.3899 found 1609.3965.

Methylester-isobutoxy-thiopropoxy-phenantroline-thiopropoxy-isobutoxy-methylester (**1**): To a solution of methylester-*(NpyS)*thiopropoxy-isobutoxy-phenantroline-isobutoxy-*(NpyS)*thiopropoxy-methylester (**19**) (100 mg; 62 μmol) in acetone (5 mL) and water (0.7 mL), was added TBP (35 μL, 0.14 mmol) and the resulting mixture was stirred overnight at room temperature. After removal of the solvent under reduced pressure, the residue was precipitated with MTBE to yield **1** as yellowish solid. Yield: 97% (78 mg). ^{1}H NMR ($CDCl_3$): δ 12.83 (2H, s), 11.77 (2H, s), 8.92 (2H, d, *J* = 6.2, 2.6 Hz), 8.82 (2H, d, *J* = 6.2, 2.2 Hz), 7.85–7.71 (8H, m), 7.64–7.53 (4H, m), 7.43 (2H, s), 6.91 (2H, s), 6.37 (2H, s), 4.33 (2H, m), 4.26 (2H, m), 3.71 (4H, m), 3.22 (6H, s), 2.91 (4H, m), 2.42–2.19 (6H, m), 1.23 (6H, d, *J* = 6.6 Hz), 1.17 (6H, d, *J* = 6.6 Hz). ^{13}C NMR ($CDCl_3$): δ 164.5, 162.5, 162.0, 161.9, 161.6, 149.3, 149.2, 145.0, 142.6, 138.7, 136.2, 134.8, 134.6, 128.8, 128.6, 128.4, 126.8, 121.4, 120.9, 119.2, 115.9, 100.5, 98.2, 75.3, 67.3, 52.9, 33.6, 28.6, 21.7, 20.0, 19.7. HRMS (ES^+): *m/z* calcd for $C_{70}H_{65}N_{10}O_{12}S_2$ $[M+H]^+$ 1301.4225 found 1301.4257.

Methylester-thiopropoxy-isobutoxy-phenantroline-isobutoxy-thiopropoxy-methylester (**2**): To a solution of methylester-*(NpyS)*thiopropoxy-isobutoxy-phenantroline-isobutoxy-*(NpyS)*thiopropoxy-methylester (**20**) (120 mg; 74 μmol) in acetone (6 mL) and water (0.8 mL), TBP (75 μL, 0.16 mmol) was added and the resulting mixture was stirred for 24 hours at room temperature. After removal of the solvent under reduced pressure, the residue was precipitated in MTBE to yield **2** as yellowish solid. Yield: 98% (94 mg). ^{1}H NMR ($CDCl_3$): δ 12.82 (2H, s), 11.80 (2H, s), 8.92 (2H, dd, *J* = 7.3, 1.4 Hz), 8.83 (2H, dd, *J* = 7.6, 1.0 Hz), 7.91–7.46 (16H, m), 6.88 (2H, s), 6.42 (2H, s), 4.21–3.79 (8H, m), 3.21 (6H, s), 2.93 (4H, dd, *J* = 7.2, 7.0 Hz), 2.39–2.01= (6H, m), 1.55 (2H, t, *J* = 7.9 Hz), 1.19 (12H, dd, J = 6.8, 4.4 Hz). ^{13}C NMR ($CDCl_3$): δ 164.4, 162.8, 162.0, 161.8, 161.2, 149.2, 149.2, 144.9, 138.6, 136.1, 134.9, 134.4, 128.9, 128.7, 128.0, 126.9, 121.6, 120.6, 119.9, 119.2, 118.5, 116.0, 115.5, 100.4, 75.5, 66.3, 52.8, 32.0, 31.3, 28.5, 27.3, 21.5, 19.8, 19.6. HRMS (ES^+): *m/z* calcd for $C_{70}H_{65}N_{10}O_{12}S_2$ $[M+H]^+$ 1301.4225 found 1301.4274.

Disulfide Bond formation

Compound **3**: To a solution of Methylester-isobutoxy-thiopropoxy- phenantroline-thiopropoxy-isobutoxy-methylester **1** (60 mg, 0.046 mmol) in $CHCl_3$/MeOH (4/1, v/v) (9.2 mL), DIPEA (40 µL) was added. The reaction mixture was stirred for two days at room temperature. Solvents were then removed under reduced pressure and compound **3** was obtained after precipitation in MTBE, as a yellow-white solid in 98% yield (58 mg). ^{1}H NMR ($CDCl_3$): δ 12.84 (2H, s), 11.77 (2H, s), 8.92 (2H, d, *J* = 7.6 Hz), 8.83 (2H, d, *J* = 6.6 Hz), 7.87–7.71 (8H, m), 7.62–7.56 (4H, m), 7.43 (2H, s), 6.92 (2H, s), 6.37 (2H, s), 4.32 (2H, m), 4.25 (2H, m), 3.70 (4H, m), 3.37 (2H, m) 3.21 (6H, s), 3.15 (2H, m) 2.90 (4H, m), 2.56–2.32 (6H, m), 1.23 (6H, d, *J* = 6.8 Hz), 1.18 (6H, d, *J* = 6.6 Hz). ^{13}C NMR ($CDCl_3$): δ 164.4, 162.4, 162.0, 161.8, 161.6, 149.4, 149.1, 144.9, 142.5, 138.7, 136.1, 134.7, 134.4, 128.7, 128.5, 128.3, 121.3, 120.8, 120.0, 119.2, 116.0, 100.4, 98.1, 75.2, 66.8, 52.8, 37.3, 29.2, 28.5, 19.9, 19.6. HRMS (ES^+): *m/z* calcd for $C_{70}H_{63}N_{10}O_{12}S_2$ $[M+H]^+$ 1299.4068 found 1299.4099

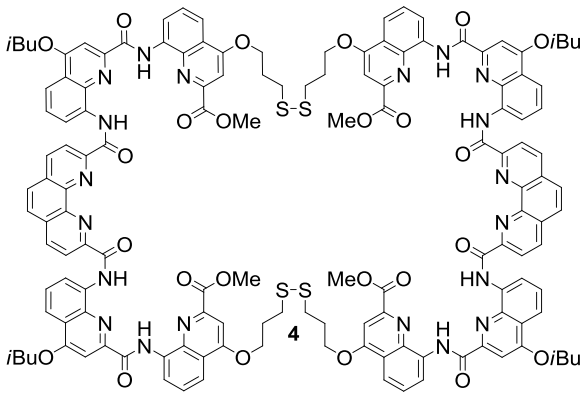

Disulfide bridge formation **4**: To a solution of Methylester-thiopropoxy-isobutoxy-phenantroline-isobutoxythiopropoxy-methylester **2** (60 mg, 0.046 mmol) in $CHCl_3$/MeOH (4/1, v/v) (9.2 mL), DIPEA (40 µL) was added. The reaction mixture was stirred for 72 hours at room temperature. Solvents were then removed under reduced pressure and the residue was purified by precipitation from cold DCM and centrifugation at 4 °C. Solvents were then removed under high vacuum and compound **4** was finally obtained after precipitation in *MTBE*, as an off-white solid. Yield: 71% (40 mg). ^{1}H NMR ($CDCl_3$): δ 12.69 (4H, s), 11.84 (4H, s), 8.99 (4H, d, *J* = 7.3 Hz), 8.89 (4H, d, *J* = 7.4 Hz), 7.98–7.56 (28H, m), 6.90 (4H, s), 6.52 (4H, s), 4.42 (4H, m), 4.13 (4H, m), 3.97 (4H, m), 3.87 (4H, m), 3.32 (4H, m), 3.22 (12H, m), 2.60 (4H, m), 2.31 (4H, s), 1.20 (12H, d, *J* = 1.6 Hz), 1.18 (12H, d, *J* = 1.4 Hz). ^{13}C NMR ($CDCl_3$): δ 164.5, 163.0, 162.0, 161.9, 161.1, 149.3, 149.2, 145.2, 143.0, 139.1, 138.9, 136.1, 135.1, 134.6, 129.4, 129.2, 128.3, 127.6, 121.9, 120.7, 120.1, 119.3, 116.2, 116.1,

115.4, 100.3, 98.2, 75.7, 65.0, 52.8, 32.9, 30.1, 28.6, 19.8, 19.6. HRMS (ES^+): *m/z* calcd for $C_{140}H_{125}N_{20}O_{24}S_4$ $[M+H]^+$ 2597.8058 found 2598.8222.

9. References

1. D. F. Stickle, L. G. Presta, K. A. Dill and G. D. Rose, *Journal of Molecular Biology*, 1992, **226**, 1143-1159.
2. P. L. Privalov and S. J. Gill, *Advances in Protein Chemistry*, 1988, **39**, 191-234.
3. S. K. Burley and G. A. Petsko, *Advances in Protein Chemistry*, 1988, **39**, 125-189.
4. S. F. Betz, *Protein Science*, 1993, **2**, 1551-1558.
5. D. Fass, *Annual Review of Biophysics*, **41**, 63-79.
6. O. A. Ozhogina and E. L. Bominaar, *Journal of Structural Biology*, 2009, **168**, 223-233.
7. T. Inoue and B. Tsai, *PLoS Pathog*ens **7**, e1002037.
8. M. Schelhaas, J. Malmström, L. Pelkmans, J. Haugstetter, L. Ellgaard, K. Grünewald and A. Helenius, *Cell*, 2007, **131**, 516-529.
9. K. Huang, N. C. Strynadka, V. D. Bernard, R. J. Peanasky and M. N. James, *Structure*, 1994, **2**, 679-689.
10. S. Cheek, S. S. Krishna and N. V. Grishin, *Journal of Molecular Biology*, 2006, **359**, 215-237.
11. R. L. Tuinstra, F. C. Peterson, E. S. Elgin, A. J. Pelzek and B. F. Volkman, *Biochemistry*, 2007, **46**, 2564-2573.
12. R. L. Tuinstra, F. C. Peterson, S. Kutlesa, E. S. Elgin, M. A. Kron and B. F. Volkman, *Proceedings of the National Academy of Sciences USA*, 2008, **105**, 5057-5062.
13. W. J. Wedemeyer, E. Welker, M. Narayan and H. A. Scheraga, *Biochemistry*, 2000, **39**, 4207-4216.
14. S. Otto, R. L. E. Furlan and J. K. M. Sanders, *Journal of American Chemical Society*, 2000, **122**, 12063-12064.
15. N. E. Zhou, C. M. Kay and R. S. Hodges, *Biochemistry*, 1993, **32**, 3178-3187.
16. J. E. Villafranca, E. E. Howell, D. H. Voet, M. S. Strobel, R. C. Ogden, J. N. Abelson and J. Kraut, *Science*, 1983, **222**, 782-788.
17. J. E. Villafranca, E. E. Howell, S. J. Oatley, N. H. Xuong and J. Kraut, *Biochemistry*, 1987, **26**, 2182-2189.
18. L. J. Perry and R. Wetzel, *Science*, 1984, **226**, 555-557.
19. L. J. Perry and R. Wetzel, *Biochemistry*, 1986, **25**, 733-739.
20. R. Wetzel, L. J. Perry, W. A. Baase and W. J. Becktel, *Proceedings of the National Academy of Sciences USA*, 1988, **85**, 401-405.
21. M. Matsumura, G. Signor and B. W. Matthews, *Nature*, 1989, **342**, 291-293.
22. M. Matsumura, W. J. Becktel, M. Levitt and B. W. Matthews, *Proceedings of the National Academy of Sciences USA*, 1989, **86**, 6562-6566.
23. M. Matsumura and B. W. Matthews, *Science*, 1989, **243**, 792-794.
24. J. A. Wells and D. B. Powers, *Journal of Biological Chemistry*, 1986, **261**, 6564-6570.
25. C. Mitchinson and J. A. Wells, *Biochemistry*, 1989, **28**, 4807-4815.
26. M. W. Pantoliano, R. C. Ladner, P. N. Bryan, M. L. Rollence, J. F. Wood and T. L. Poulos, *Biochemistry*, 1987, **26**, 2077-2082.
27. H. Takagi, T. Takahashi, H. Momose, M. Inouye, Y. Maeda, H. Matsuzawa and T. Ohta, *Journal of Biological Chemistry*, 1990, **265**, 6874-6878.
28. R. T. Sauer, K. Hehir, R. S. Stearman, M. A. Weiss, A. Jeitler-Nilsson, E. G. Suchanek and C. O. Pabo, *Biochemistry*, 1986, **25**, 5992-5998.
29. S. Kanaya, C. Katsuda, S. Kimura, T. Nakai, E. Kitakuni, H. Nakamura, K. Katayanagi, K. Morikawa and M. Ikehara, *Journal of Biological Chemistry*, 1991, **266**, 6038-6044.
30. M. Luckey, R. Ling, A. Dose and B. Malloy, *Journal of Biological Chemistry*, 1991, **266**, 1866-1871.
31. J. Eder and M. Wilmanns, *Biochemistry*, 1992, **31**, 4437-4444.
32. Y. Konishi, T. Ooi and H. A. Scheraga, *Biochemistry*, 1982, **21**, 4734-4740.
33. D. M. Rothwarf and H. A. Scheraga, *Biochemistry*, 1993, **32**, 2680-2689.
34. T. W. Holstein, M. Benoit, G. von Herder, G. Wanner, C. N. David and H. E. Gaub, *Science (Washington, D. C.)*, 1994, **265**, 402-404.
35. S. Oezbek, U. Engel and J. Engel, *Journal of. Structural. Biology*, 2002, **137**, 11-14.
36. E. Pokidysheva, A. G. Milbradt, S. Meier, C. Renner, D. Haeussinger, H. P. Baechinger, L. Moroder, S. Grzesiek, T. W. Holstein, S. Oezbek and J. Engel, *Journal of Biological Chemistry*, 2004, **279**, 30395-30401.
37. D. Y. Jackson, D. S. King, J. Chmielewski, S. Singh and P. G. Schultz, *Journal of American Chemical Society*, 1991, **113**, 9391-9392.
38. A. J. Nicoll, C. J. Weston, C. Cureton, C. Ludwig, F. Dancea, N. Spencer, O. S. Smart, U. L. Guenther and R. K. Allemann, *Organic and Biomolecular Chemistry*, 2005, **3**, 4310-4315.

39. A. J. Nicoll, D. J. Miller, K. Fuetterer, R. Ravelli and R. K. Allemann, *Journal of American Chemical Society*, 2006, **128**, 9187-9193.
40. S. E. Miller, N. R. Kallenbach and P. S. Arora, *Tetrahedron*, 2012, **68**, 4434-4437.
41. N. Ousaka, T. Sato and R. Kuroda, *Journal of American Chemical Society*, 2009, **131**, 3820-3821.
42. A. M. Spokoyny, Y. Zou, J. J. Ling, H. Yu, Y.-S. Lin and B. L. Pentelute, *Journal of American Chemical Society*, 2013, **135**, 5946-5949.
43. N. Ousaka, N. Tani, R. Sekiya and R. Kuroda, *Chemical Communications (Camb)*, 2008, 2894-2896.
44. N. Ousaka, T. Sato and R. Kuroda, *Journal of American Chemical Society*, 2008, **130**, 463-465.
45. C. E. Schafmeister, J. Po and G. L. Verdine, *Journal of American Chemical Society*, 2000, **122**, 5891-5892.
46. J. Liu, D. Wang, Q. Zheng, M. Lu and P. S. Arora, *Journal of American Chemical Society*, 2008, **130**, 4334-4337.
47. K. Fujimoto, M. Kajino and M. Inouye, *Chemistry - A European Journal*, 2008, **14**, 857-863.
48. S. Hamieh, V. Saggiomo, P. Nowak, E. Mattia, R. F. Ludlow and S. Otto, *Angewandte Chemie, International Edition*, 2013, **52**, 12368-12372.
49. J. M. A. Carnall, C. A. Waudby, A. M. Belenguer, M. C. A. Stuart, J. J. P. Peyralans and S. Otto, *Science (Washington, DC, U. S.)*, 2010, **327**, 1502-1506.
50. S. Otto, R. L. E. Furlan and J. K. M. Sanders, *Science (Washington, DC, U. S.)*, 2002, **297**, 590-593.
51. K. R. West, K. D. Bake and S. Otto, *Organic Letters*, 2005, **7**, 2615-2618.
52. J. W. Taylor, *Peptide Science*, 2002, **66**, 49-75.
53. S. Marqusee and R. L. Baldwin, *Proceedings of the National Academy of Sciences U S A*, 1987, **84**, 8898-8902.
54. E. Cabezas and A. C. Satterthwait, *Journal of American Chemical Society*, 1999, **121**, 3862-3875.
55. D. Wang, M. Lu and P. S. Arora, *Angewandte Chemie, International Edition*, 2008, **47**, 1879-1882.
56. L. D. Walensky, A. L. Kung, I. Escher, T. J. Malia, S. Barbuto, R. D. Wright, G. Wagner, G. L. Verdine and S. J. Korsmeyer, *Science (Washington, DC, U. S.)*, 2004, **305**, 1466-1470.
57. S. J. Rowan, P. A. Brady and J. K. M. Sanders, *Angewandte Chemie, International Edition*, 1996, **35**, 2143-2145.
58. S. J. Rowan, P. A. Brady and J. K. M. Sanders, *Tetrahedron Letters*, 1996, **37**, 6013-6016.
59. P. A. Brady, R. P. Bonar-Law, S. J. Rowan, C. J. Suckling and J. K. M. Sanders, *Chemical Communications (Cambridge)*, 1996, 319-320.
60. I. Huc and J.-M. Lehn, *Proceedings of the National Academy of Sciences U. S. A.*, 1997, **94**, 2106-2110.
61. G. R. L. Cousins, S.-A. Poulsen and J. K. M. Sanders, *Chemical Communications (Cambridge)*, 1999, 1575-1576.
62. V. A. Polyakov, M. I. Nelen, N. Nazarpack-Kandlousy, A. D. Ryabov and A. V. Eliseev, *Journal of Physical Organic Chemistry*, 1999, **12**, 357-363.
63. O. Ramstrom and J. M. Lehn, *Chembiochem*, 2000, **1**, 41-48.
64. H. Hioki and W. C. Still, *Journal of Organic Chemistry*, 1998, **63**, 904-905.
65. L. Brunsveld, B. J. B. Folmer, E. W. Meijer and R. P. Sijbesma, *Chemical Reviews (Washington, D. C.)*, 2001, **101**, 4071-4097.
66. N. Delsuc, T. Kawanami, J. Lefeuvre, A. Shundo, H. Ihara, M. Takafuji and I. Huc, *ChemPhysChem*, 2008, **9**, 1882-1890.
67. Z.-Q. Hu, H.-Y. Hu and C.-F. Chen, *The Journal of Organic Chemistry*, 2006, **71**, 1131-1138.
68. T. Qi, T. Deschrijver and I. Huc, *Nature Protocols*, 2013, **8**, 693-708.
69. H. C. Brown, M. Zaidlewicz, P. V. Dalvi and G. K. Biswas, *Journal of Organic Chemisty*, 2001, **66**, 4795-4798.
70. T. Qi, V. Maurizot, H. Noguchi, T. Charoenraks, B. Kauffmann, M. Takafuji, H. Ihara and I. Huc, *Chemical Communications (Cambridge, United Kingdom)*, 2012, **48**, 6337-6339.

Chapter 4: Anhydrides, polyanhydrides and anhydride-connected foldameric rods

1. Introduction

In principle an anhydride functional group is formed by a condensation reaction between two carboxylic acids. Anhydrides can be either symmetric or asymmetric, depending on the carboxylic acids used for their synthesis and in terms of reactivity they have many similarities with acyl chlorides. This is one of the reasons why they are commonly used in chemistry, as activated carbonyl groups. An example can be found in the synthesis of aspirin.[1] Aspirin derives from 2-hydroxybenzoic acid (salicylic acid), which is then acetylated to yield the desired product. Even though this acylation can be carried out using acetyl chloride, pharmaceutical companies conduct this reaction in the presence of acetic anhydride at 90 ^{o}C (Scheme 1).

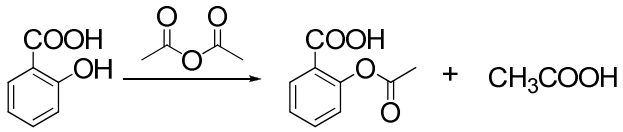

Scheme 1: Schematic representation of the synthesis of aspirin from 2-hydroxybenzoic acid with acetic anhydride.

This preference has several advantages (especially when working on a large scale), such as the lower cost of the anhydride compared to the chloride, it is safer and less corrosive and finally it doesn't produce hazardous HCl fumes. The reactivity of anhydrides towards nucleophiles is related to the electronegativity of the leaving group activating the carbonyl. Less electronegative than chlorine but more than an ester or an amide function, anhydrides constitute milder acylation agents than acyl chlorides. However, anhydrides can react with amines, alcohols and water to yield the corresponding amides, esters and acids respectively, accompanied in all three cases by the generation of an additional acid molecule.

Because of such properties anhydrides have been used extensively as protecting [e.g. Ac_2O] or activating agents (e.g. T3P)[2] in organic synthesis and composite materials/coatings (e.g. maleic anhydride)[3-6] in material science. They also find minor applications in the food industry[7, 8] and pharmaceuticals.[9-11] A very interesting class of molecules that is directly

associated with the anhydride functionality are the polyanhydrides, which will now be discussed.

2. Polyanhydrides

2.1. Characteristics of polyanhydrides

Polyanhydride molecules fall into the category of biodegradable polymers in which anhydride functionalities connect the repeat units throughout the polymer backbone (Scheme 2).[12] The synthesis of polyanhydrides was first reported in 1909 by Bucher and Slade[13] and since then many attempts have been made to enhance the synthesis and functionalization of these molecules.

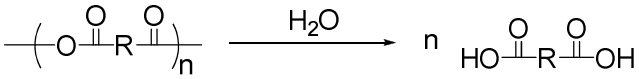

Scheme 2: Schematic representation of polyanhydrides and their hydrolysis products.

In the last three decades interest has significantly increased towards their utilization as biomaterials, due to their biocompatibility (depending on the building blocks used), biodegradability and ease of synthesis.[12] Polyanhydrides are commonly synthesized by melt polycondensation reactions, as well as solution polymerization, including ring opening polymerization, dehydrochlorination and dehydrative coupling agents.[14] Polyanhydrides undergo hydrolytic bond cleavage to form water-soluble degradation products (depending on the nature of the monomer composing the polymer chains) that can dissolve in an aqueous environment, thus resulting in polymer erosion.[15]

2.2. Polyanhydrides in biomaterial applications

Polyanhydrides can be aliphatic, aromatic or mixtures.[16] In the latter case, adjusting the relative ratios of the two can result in materials with tunable properties (e.g. a tunable rate of biodegradability). Research carried out by Langer *et al.*,[15, 17] in which they used carboxyphenoxy propane (CPP) as a hydrophobic residue and sebatic acid (SA) as a less hydrophobic residue (Scheme 3), demonstrated that in a hydrophobic polyanhydride consisting of 100% CPP, 8% of the polymer matrix was dissolved after 14 weeks. On the contrary, a polyanhydride consisting of 15% SA dissolved significantly faster; at a 79% ratio of SA the polymer matrix was completely dissolved in two weeks. Such behavior makes polyanhydrides ideal candidates for the development of controlled drug delivery systems.

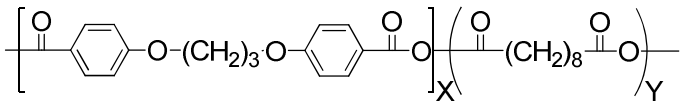

Scheme 3: Structure of the polyanhydride composed of carboxyphenoxy propane (CPP) and sebasic acid (SA).

A drug uniformly distributed inside the matrix of such a polymeric material would result in the release of the drug at the same rate to which the polymer dissolves. This was proved experimentally when the same researchers placed BCNU (carmustine, one of the most toxic anticancer drugs) inside a SA/CPP matrix. BCNU has a very short half-life (12 minutes) but when incorporated into the polymer matrix, the drug lasted as long as the polymer lasted, which suggested that it is protected from degradation. To understand the impact of such molecules in the field of medicine, it needs to be mentioned that after being tested *in vitro*[18] and *in vivo*,[19-23] the FDA has approved the utilization of this treatment for patients with brain cancer.[24]

Apart from the incorporation of BCNU, several molecules of biological importance have been placed inside polymer matrices for multiple drug delivery applications, such as insulin,[25] enzymes[26] and growth factors, and their *in vitro* and *in vivo* release characteristics were evaluated.[27, 28] Polyanhydrides have also been successfully employed in polymer coatings for medical devices[29, 30] and in tissue engineering –e.g. bone growth[31, 32] and nerve regeneration.[29, 33-35]

2.3. Poly(anhydrides-imides/esters)

Incorporation of amino acids (e.g. alanine and glycine) into the polymer backbone has been demonstrated to enhance the mechanical properties compared to the polyanhydride alone. As an example, these amino acids have been introduced into the sequence via an imide bond at the N terminus by reaction with pyromelitic anhydride, leaving the carboxylic acid functionality available for activation by acetic anhydride (Scheme 4a).[36] Esters are another functionality that has been successfully introduced in polyanhydrides affording poly(anhydride-esters).[37] These molecules are of particular interest due to the two types of hydrolytically cleavable bonds which compose the polymer backbone. Overall, they display a two stage degradation profile in which the first step includes the rapid hydrolysis of the anhydride bonds followed by the slow hydrolysis of the ester prepolymers.[38] This has been exploited and polymers that degradade into salicylic acid have been manufactured (Scheme 4b).[39]

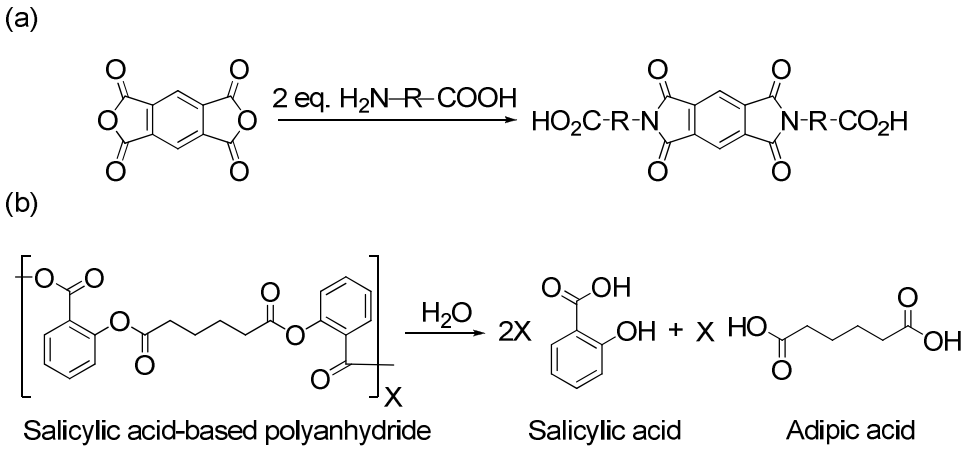

Scheme 4: (a) Monomer for polyanhydride synthesis with amino acids resulting in poly(anhydride-imides), R = glycine or alanine residues; (b) poly(anhydride-esters) that upon hydrolysis generates salicylic acid, an anti-inflammatory agent

This is a brief highlight of anhydrides and polyanhydrides in the field of synthetic chemistry. In addition it needs to be noted that many molecules of biological importance containing anhydride functionalities are based on heteroatoms, such as sulfur and phosphorus. One example is ATP which contains P-anhydride functionalities that are selectively hydrolyzed and reformed, depending on different stimuli. Unfortunately anhydrides containing heteroatoms exceed the scope of this manuscript and will not be discussed further.

3. Foldamers consisting of anhydride functionalities

To date, the anhydride bond is not widely reported in the field of foldamers, which may be attributed to the overall labile nature of this functionality. In the field of aromatic oligoamide foldamers the first reported example of an anhydride 'linker' connecting two well-defined helical segments involves the reaction of an oligomeric acid chloride with an oligomeric acid in the presence of base. Evaluation of its propensity to form helical architectures (Chapter 1, Section 5.2.4) demonstrated its ability to promote folding and intrahelical communication in a head-to head orientation.[40, 41] The homochiral conformation was assumed to be stabilized by conformational preferences. As far as the aryl amide linkages are concerned, they adopt an *anti* conformation as a result of the endocyclic nitrogen atoms *ortho* to each carboxamide. In addition, electrostatic repulsions occur between the endocyclic quinoline nitrogen atoms (adjacent to the anhydride function) with the sp^2 and sp^3 oxygen atoms of the anhydride functionality (Scheme 5). However, due to the fact that repulsions

with the sp^2 oxygen are stronger than those of the sp^3 oxygen the *s-trans* conformation of the aryl-carbonyl linkage is highly favored, despite the absence of a H-bond donor.

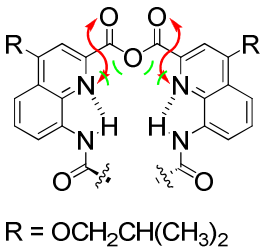

Scheme 5: Schematic representation of the conformational preferences occuring in positions adjacent to the anhydride functionality.

The second example of stable anhydride formation in aromatic oligoamide foldamers was reported while exploring the photochemical properties of diazanthracene-containing oligomers.[42] During the synthesis of a heptamer from the reaction of anthracene diacid chloride with a pyridine trimer amine (Figure 1a), a side product with two tetrameric segments connected head-to-head through an anhydride functionality was observed in 4% yield.

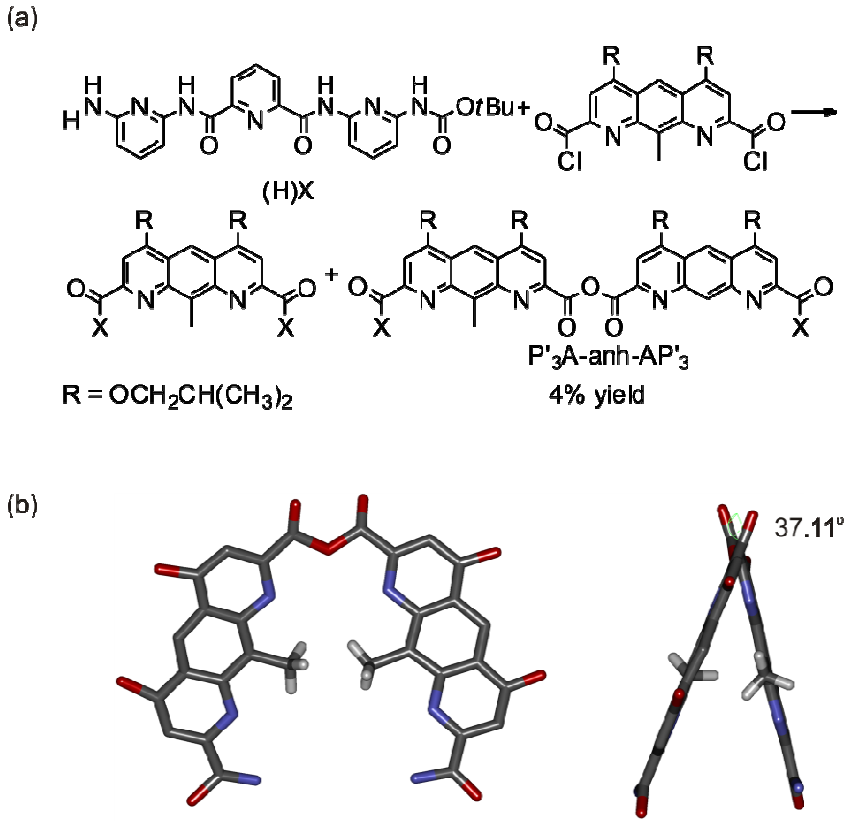

Figure 1: (a) coupling reaction that yielded the desired product (on the left) and the anhydride side product, (P'_3A—anh—AP'_3). (b) X-ray structure of the central part of the anhydride-containing helix. The dihedral angle between the two carbonyl oxygen atoms is 37.11°.

This was shown to be P'$_3$A—anh—AP'$_3$ (where P' stands for the pyridine monomer and A for the anthracene monomer). This finding validated the compatibility of anthracene containing sequences to form stable molecules bearing an anhydride linker, as additionally suggested by X-ray data (Figure 1b). To summarize, the anhydride functionality was found to mediate intrahelical communication and is itself shielded between the two well-defined helical strands. At least one complete helical turn is required on each side of the anhydride group to provide resistance to hydrolysis. The stability of these conformations to nucleophilic attack was also confirmed, as they were isolated using silica gel chromatography without any precautions, even when methanol was used as a co-eluent.

3.1. Origins of anhydride formation in AOFs

In principle anhydride formation in quinoline based oligoamide foldamers occurs during coupling reactions of acid chlorides to amines. This can be explained by the presence of residual water in the reaction, which hydrolyzes the acid chloride. The acid chloride then reacts with an acid functionality, instead of the amine, giving rise to helical segments connected head-to head with a stable anhydride functionality. Due to its stability, cleavage of the anhydride functionality requires refluxing in a mixture of pyridine and water overnight, which yields quantitative recovery of the starting acid.

3.2. Synthesis of long AOFs

Both solid phase and solution phase synthesis have been used for the formation of aromatic oligoamide foldamers.[43, 44] Aromatic oligoamide foldamer synthesis was initially carried out in solution but due to the increasing complexity of the synthesized molecules (in terms of monomer, side chain and sequence diversity), solid phase synthesis became necessary for purposes of rapidity. On the other hand, solution phase synthesis has an advantage over SPS in the synthesis of very long foldameric architectures, since a convergent strategy can be used to access long sequences in only a few steps, whereas SPS involves the addition of separate monomer units individually. In addition a solution phase strategy can be scaled-up more reliably, The synthesis of long aromatic helical segments has thus been established, using a segment doubling strategy, which has afforded oligomers as long as 64 quinoline units.

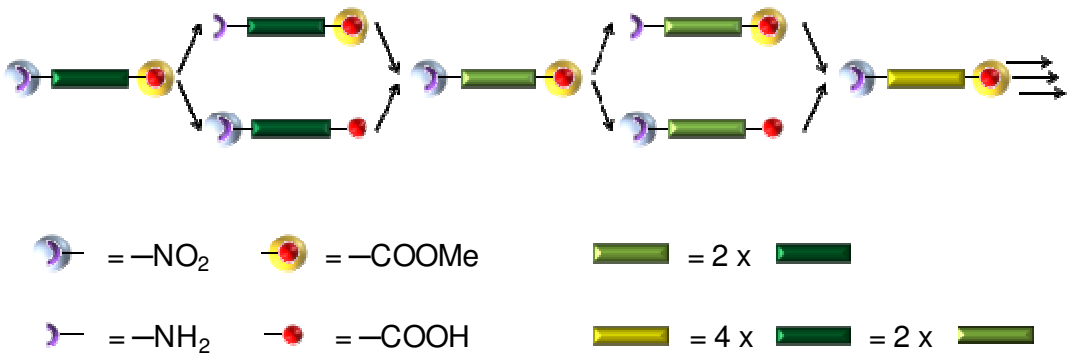

Scheme 6: Schematic representation of the segment doubling strategy.

This segment doubling strategy is convergent and is based on the reaction of a quinoline amino ester with a quinoline nitro acid chloride to yield the desired protected amino acid (Scheme 6). Beyond the 4mer level this reaction becomes susceptible to anhydride formation, since coupling is slower and there is thus greater likelihood of acid chloride hydrolysis by residual moisture. For this reason, in the initial steps the route "*4+2+2*" is preferred to "*4+4*" for the synthesis of the quinoline octamer.[45] The quinoline dimer cannot form a stable anhydride since it would not be protected from hydrolysis, as it requires 2.5 quinoline units to form a complete helical turn. Of course, for longer foldamers, larger and larger building blocks must be used, and thus the risk of anhydride formation is greater, resulting in lower coupling yields.

4. Design & aim of the project

The aim of this project was to make use of the unusual stability of the anhydride function in AOFs. In this respect, a facile method for the synthesis of long aromatic helical rods connected with anhydride functionalities was envisaged. In particular a segment tripling strategy based on the utilization of diacids could potentially afford access to very long AOFs in a few synthetic steps. The strategy is based on the reaction of a doubly activated diacid with two other diacids to yield, after one step, a diacid molecule that is three times larger than the starting material and contains two anhydride functions. In a second step the resulting molecule is 9 times larger that the initial monomer and contains six anhydride functionalities. This convergent technique is very powerful due to the fact that the starting diacid can already be a long oligomer! Additionally, since the desired molecule is still a diacid, there is no need for protection-deprotection steps.

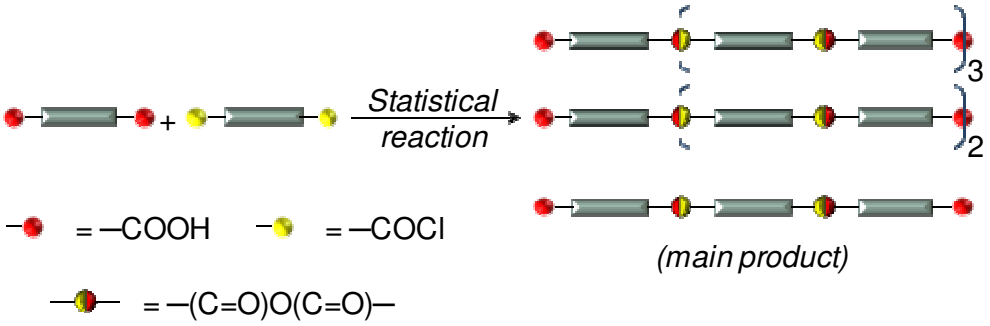

Scheme 7: Schematic representation of the segment tripling strategy.

For this project, symmetrical building blocks consisting of an odd number of monomers and two terminal acid groups were used. After activation of the diacid to form the corresponding diacid dichloride, this block was reacted with excess diacid to statistically form the desired product in excess, compared to the undesired products (Scheme 7). Purification of the different compounds was achieved using size exclusion chromatography, taking advantage of the large size difference between the different products. All undesired products could be recycled by simple hydrolysis of the anhydride function to quantitatively recover the starting diacid building blocks. The building blocks were designed to ensure that there was at least one helical turn to protect the resulting anhydride fuctionality from unwanted hydrolysis.

5. Synthesis

Two different symmetrical building blocks were designed and synthesized in order to validate the segment tripling strategy; one composed of five, and one of nine monomers. Both of them were equipped with 4-isobutoxypyridine-2,6-dicarboxylic acid as the central unit, which provides symmetry to the system, and a quinoline dimer or tetramer at each extremity. For ease of presentation, the two different attempts are discussed separately, under the headings “Series 5” and “Series 9” relating to the composition of the starting diacid.

5.1. Pentameric and nonameric building blocks

Dimeric and tetrameric quinoline blocks were prepared according to previously described methodologies. It is noteworthy that the quinoline tetramer comes from the segment doubling of the dimeric unit. These oligomers (obtained with nitro-ester end functionalities) were first reduced and then reacted with the central pyridine diacid *via* the diacid dichloride intermediate (**3**) (Scheme 7). Purification of the 5mer building block was

carried out by column chromatography affording the product in good yield. Crystallization of the crude nonamer (**5**) by liquid-liquid diffusion of ethyl acetate in dichloromethane resulted in pure material without the use of column chromatography. The pure diesters were then quantitatively saponified (Scheme 8). A large excess of base was used in these reactions (20eq. for **4** and 80 eq. for **5**) in order to increase the rate of reaction. This was because it had been observed that when the duration of saponification reactions was increased, side reactions, presumably amide bond cleavage, occured. After quenching with an aqueous acidic solution and evaporation of the THF, the desired product could be afforded by precipitation from the remaining aqueous solution in good purity.

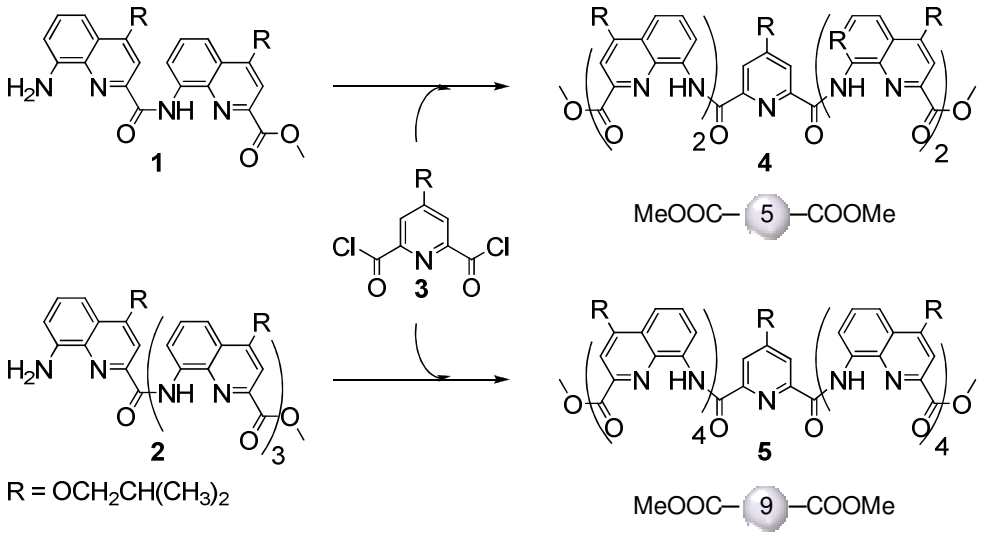

Scheme 7: Synthesis of penta- and nona-meric protected precursors. (a) DIPEA, $CHCl_3$, r.t., 24 hours.

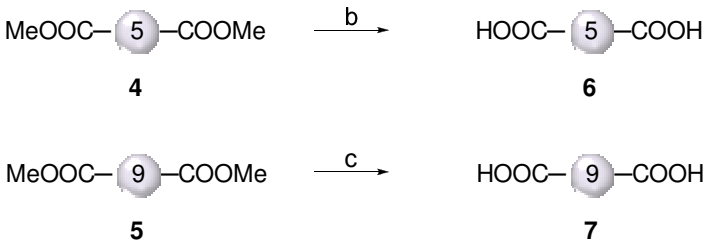

Scheme 8: Deprotection of penta- and nona-meric precursors: THF/H_2O, (b) 20 eq. and (c) 80 eq. KOH

5.2. 'Series 5'

Several optimization attempts were initially carried out to optimize anhydride formation. This was anticipated to be relatively difficult due to the nature of the reactants: long, aromatic and water sensitive molecules, reacting in a statistical way to yield products of polymeric dimensions. The proportion of the starting reactants therefore was identified as an important factor to control. However there were two parameters that could make the reaction drift away from its expected statistical distribution of products. These

are: hydrolysis of the activated diacid or the already formed anhydride and the reactivity drop associated with the increasing oligomer length. In this respect, reaction concentration was important in tuning the reaction rate.

The first parameter that was modulated was the ratio of diacid to diacid chloride. It could be expected that increasing the excess of diacid, would be beneficial, since this would increase the number of molecules that could properly terminate the reaction by yielding the desired compound. This would thus prevent already elongated molecules from reacting further. In order to test this hypothesis four different conditions were tested: using 2, 4, 6 and 8 eq. of acid compared to the acid chloride. Our results (Table 1) confirmed the initial hypothesis: excess diacid slightly improved the reaction yield by minimizing the formation of longer analogues. Providing a larger amount of the compound that terminates the reaction leads eventually to a cleaner reaction e.g. the chances that a mono-activated segment will react with a starting building block, rather than a longer chain are much greater if the former is in large excess.

Table 1: Optimization attempt of the ratio of diacid to diacid chloride*‡

	10mer	15mer	20mer	25mer+≠
2 eqs of acid	0.23	0.57	0.11	0.09
4 eqs of acid	0.23	0.66	0.11	0
6 eqs of acid	0.24	0.69	0.07	0
8 eqs of acid	0.25	0.75	0	0

*The values in this table are the % product compared to the overall amount of products formed, as indicated by NMR experiments.

‡The concentration of all reactions for this study was 20 mM

≠All the longer sequences are included here

However, in our experiments it was decided that 3 equivalents of diacid should be used (compared to diacid dichloride) as this was the best compromise between the price (complexity) of the starting material, the yield of the reaction and the purification difficulties, associated with having a high excess of starting materials present at the end of the reaction.

Additionally, the effect of adjusting reaction concentration was evaluated. Five different concentrations were tested ranging from 5 to 40 mM and our results (Table 2) demonstrated that upon dilution of the reaction, moisture appeared to be introduced with solvent that was not completely anhydrous and/or the reaction rate decreased resulting in

moisture entering the reaction over time. In either case this was shown to lead to a drop in the reaction yields. The impurities observed are composed of an even number of starting building blocks, which suggests that significant hydrolysis took place.

Table 2: Optimization of reaction concentration*‡

	10mer	15mer	20mer
40 mM	0.25	0.72	0.03
20 mM	0.24	0.73	0.03
10 mM	0.28	0.69	0.03
6 mM	0.44	0.56	0
5 mM	0.44	0.56	0

*The values in this table are the % product compared to the overall amount of products formed, as indicated by NMR experiments.

‡The ratio of acid to acid chloride was the same (3 eq) in all reactions

Finally, the amount of base added in the coupling reaction was also investigated but no significant effect was observed.

5.2.1. Synthesis of 15mer (1st coupling step)

The 5mer diacid (**6**) was activated as the acid chloride via oxalyl chloride and added to a solution containing pentamer diacid (3 eq.) and base under inert atmosphere (Scheme 8). The reaction was then stirred at room temperature for 24 hours. ^{1}H NMR of the reaction mixture suggested the presence of the desired 15-mer, along with several side products (Figure 3a). Gel permeation chromatography (GPC) was used for the purification of the 15-mer (Figure 3b). From the chromatogram, the 10mer and 20mer (even number of building blocks) were observed which meant that hydrolysis of the diacid chloride occurred during the course of the reaction, leading to its premature termination. Note that the chromatogram below comes from a recycling GPC setup, which means that the solution circulates in the apparatus passing through the column multiple times. This is carried out until optimum separation is afforded, and the products are then eluted.

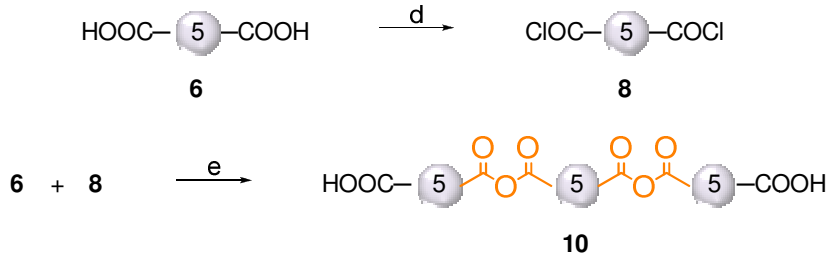

Scheme 8: 1st tripling step in 'Series 5': (d) oxalyl chloride, $CHCl_3$, r.t., 2 hours and (e) DIPEA, $CHCl_3$, r.t., 24 hours. Newly formed bonds are highlighted in orange.

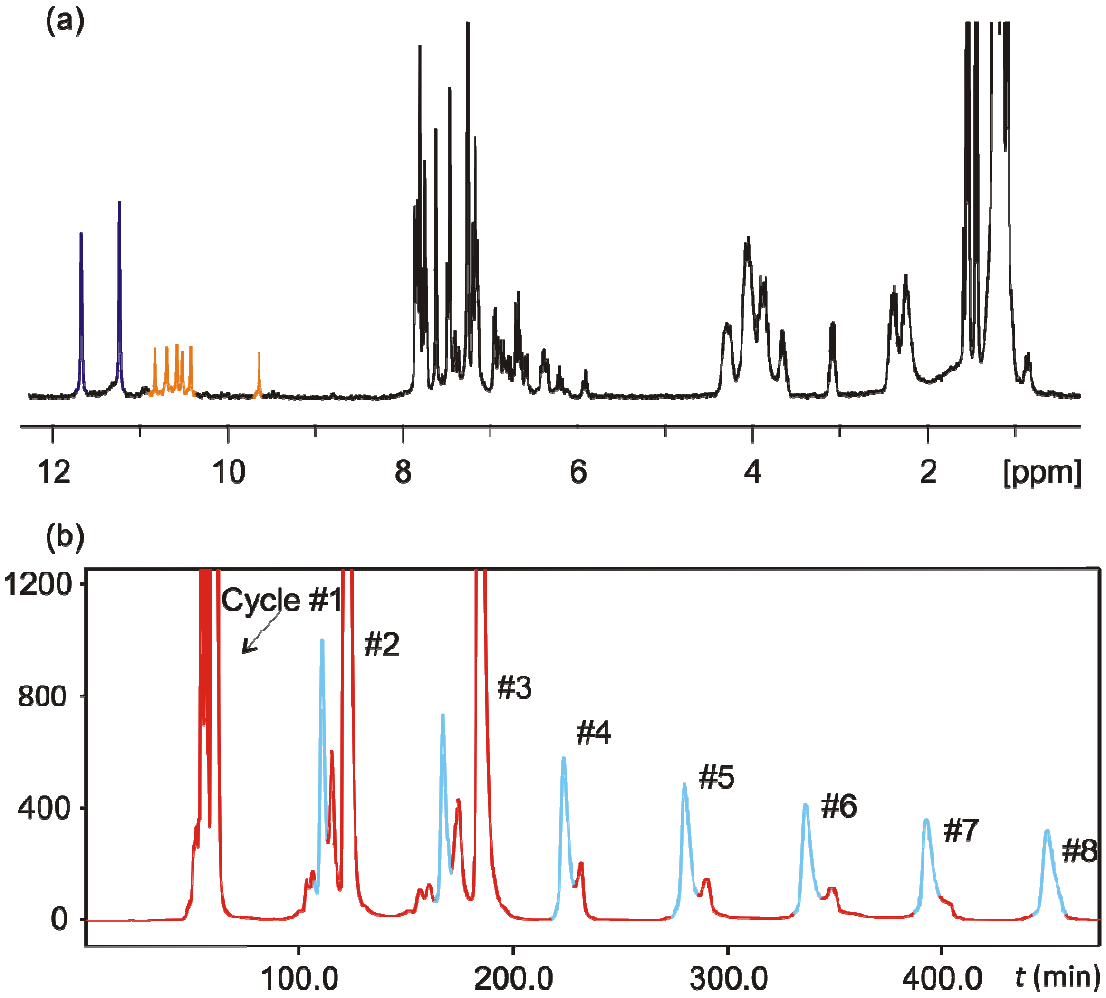

Figure 3: (a) crude ^1H NMR spectrum from the synthesis of 15mer in $CDCl_3$. Starting material has been highlighted in blue and the desired molecule in orange and (b) GPC of the crude mixture. The peak corresponding to the desired product has been highlighted in light blue.

5.2.2. Synthesis of 45mer (2nd coupling step)

Similar coupling conditions were used for the preparation of the 45mer. However, the 15-mer diacid was activated with Ghosez reagent since oxalyl chloride was incompatible with the anhydride functionality, leading to cleavage.

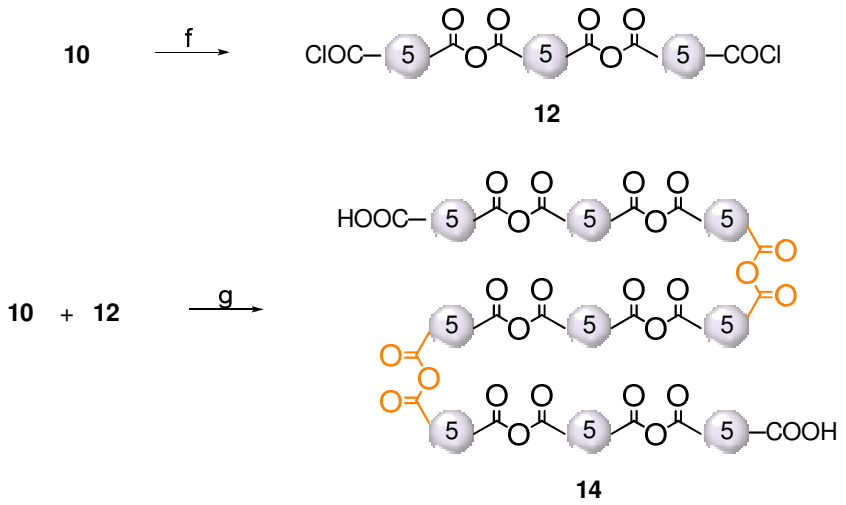

Scheme 9: Activation of 15mer (**10**) and coupling to produce 45mer: (f) Ghosez reagent, $CHCl_3$, r.t., 2 hours and (g) DIPEA, $CHCl_3$, r.t., 48 hours. Newly formed bonds are highlighted in orange.

The acid chloride was then added to a cold solution of 15mer diacid (3 eq.) and base under inert atmosphere (Scheme 9).

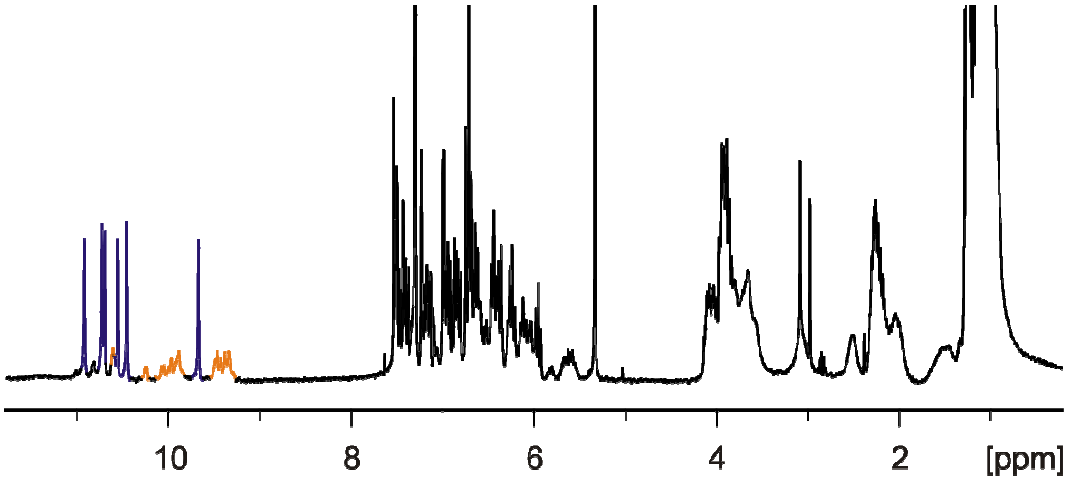

Figure 4: crude ^{1}H NMR spectrum from the synthesis of 45mer in $CDCl_3$. Starting material has been highlighted in blue and the desired molecule in orange.

The reaction resulted in a cloudy solution and ^{1}H NMR (Figure 4) confirmed the formation of the desired compound. Direct filtration of the solid and washing with cold $CHCl_3$, followed by centrifugation of the solid in EtOAc afforded pure 45-mer. The solubility of the 45mer was found to be poor in most organic solvents, property that was exploited for its purification. The identity of the 45mer was validated by MALDI-TOF.

5.3. 'Series 9'

The same segment tripling strategy used with pentameric building blocks was then applied to the nonameric diacid blocks for constructing longer oligomers.

5.3.1. Synthesis of 27mer (1st coupling step)

The nonamer diacid (**7**) was activated with oxalyl chloride to yield the corresponding acid chloride in a clean and quantitative reaction. A solution of the acid chloride was added to a cold solution of the nonamer diacid (3 eq.) and base, under inert atmosphere (Scheme 10).

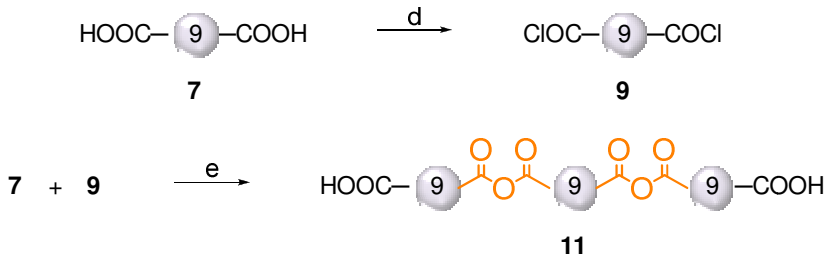

Scheme 10: 1st tripling step in 'Series 9': (d) oxalyl chloride, $CHCl_3$, r.t., 2 hours and (e) DIPEA, $CHCl_3$, r.t., 24 hours. Newly formed bonds are highlighted in orange.

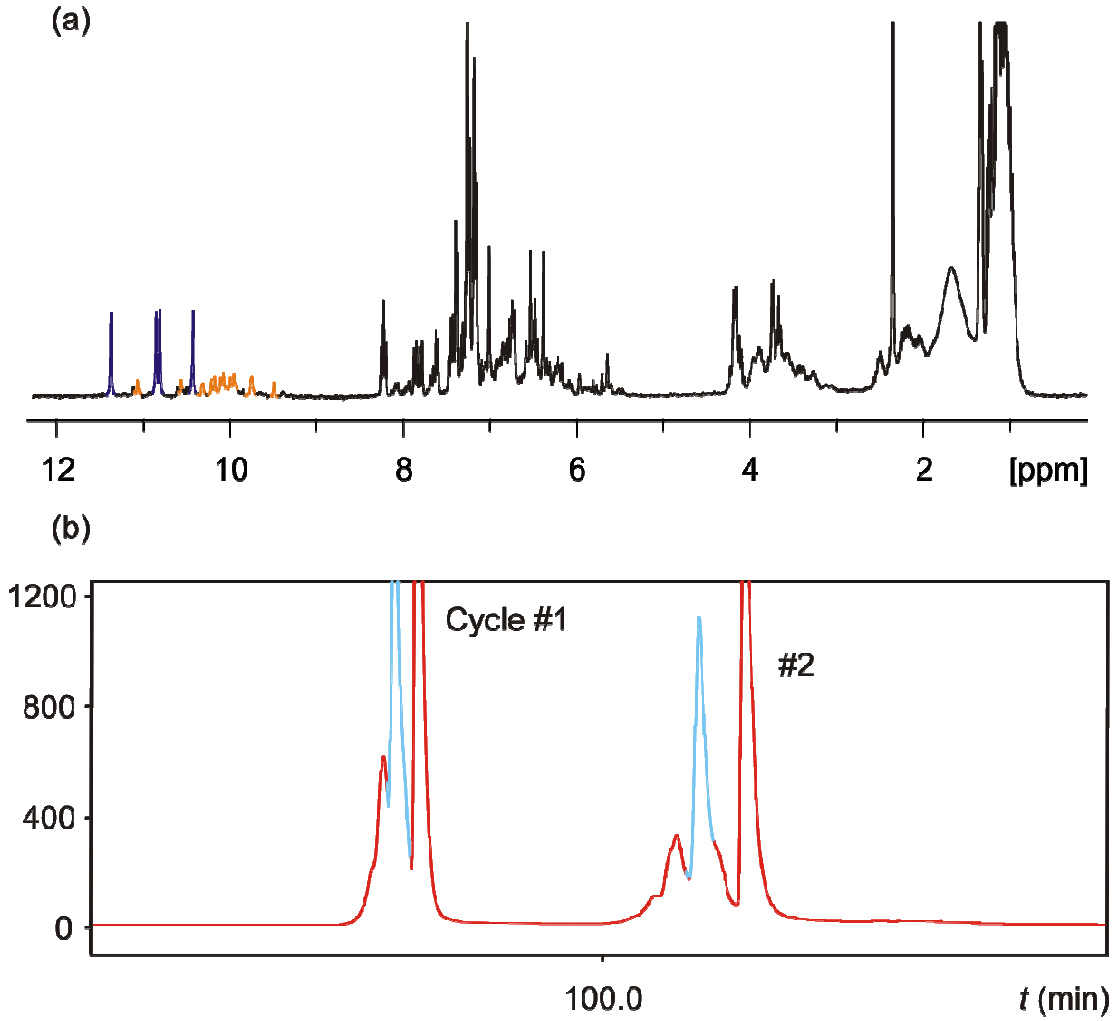

Figure 5: (a) crude ^1H NMR spectrum from the synthesis of 27mer in $CDCl_3$. Starting material has been highlighted in blue and the desired molecule in orange and (b) GPC of the crude mixture. The peak corresponding to the desired product has been highlighted in light blue.

After 24 hours no acid chloride was found to remain as shown by ^{1}H NMR, which also suggested the presence of the desired 27mer, along with several side products (Figure 5a). Purification of the 27mer was again carried out by GPC (Figure 5b) followed by an additional crystallization step (liquid-liquid diffusion of methanol in chloroform) to ensure high purity of the product for the next step.

5.3.2. Synthesis of 81mer (2nd coupling step)

27-mer diacid (**11**) was, for the same reason as the 15mer, activated with Ghosez reagent to yield the corresponding acid chloride (**13**) which was then added to a cold solution containing the 27mer diacid (3 eq.) and base under inert atmosphere in the presence of activated molecular sieves (Scheme 11). The reaction was stirred for 4 days until full consumption of the acid chloride occurred. ^{1}H NMR of the crude (Figure 6a) suggested the presence of the desired 81-mer, which due to its good solubility in chloroform was purified by GPC (Figure 6b).

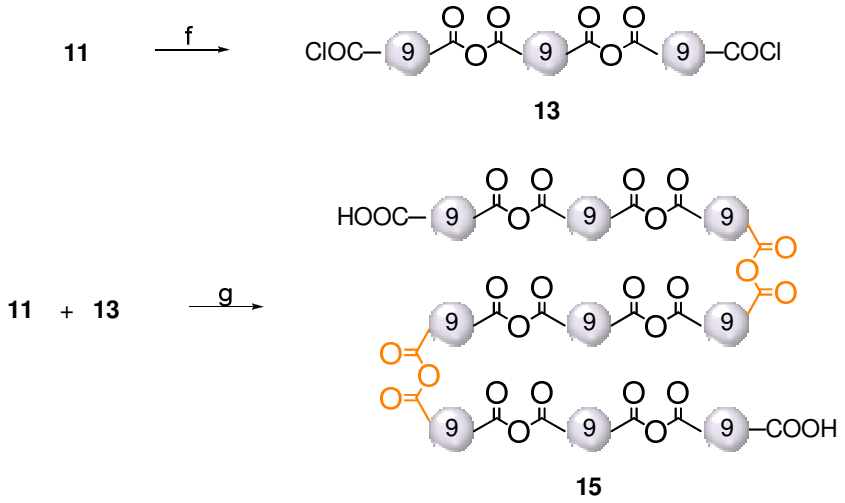

Scheme 11: Activation of 27mer (**11**) and 2nd coupling step for 81mer: (f) Ghosez reagent, $CHCl_3$, r.t., 2 hours and (g) DIPEA, $CHCl_3$, r.t., 96 hours. Newly formed bonds are highlighted in orange.

The chromatogram suggested that the presence of sieves was important to protect the acid chloride against hydrolysis. Additionally, comparison of GPC separation of the 15mer, 27mer and 81mer (Figures 3b, 5b and 6b clearly indicates that the longer the desired foldamer, the easier its separation from the crude, due to the increasing size difference between the products. For example, the 9mer and 27mer have 18 units difference while the 27mer and 81mer have 54 units difference; this is reflected in the number of purification cycles necessary for good separation of the products.

Despite the low yielding nature of these reactions our experiments indicate that the

segment tripling strategy can (although susceptible to different parameters including moisture) be optimized to minimize hydrolysis, and afford increased yields.

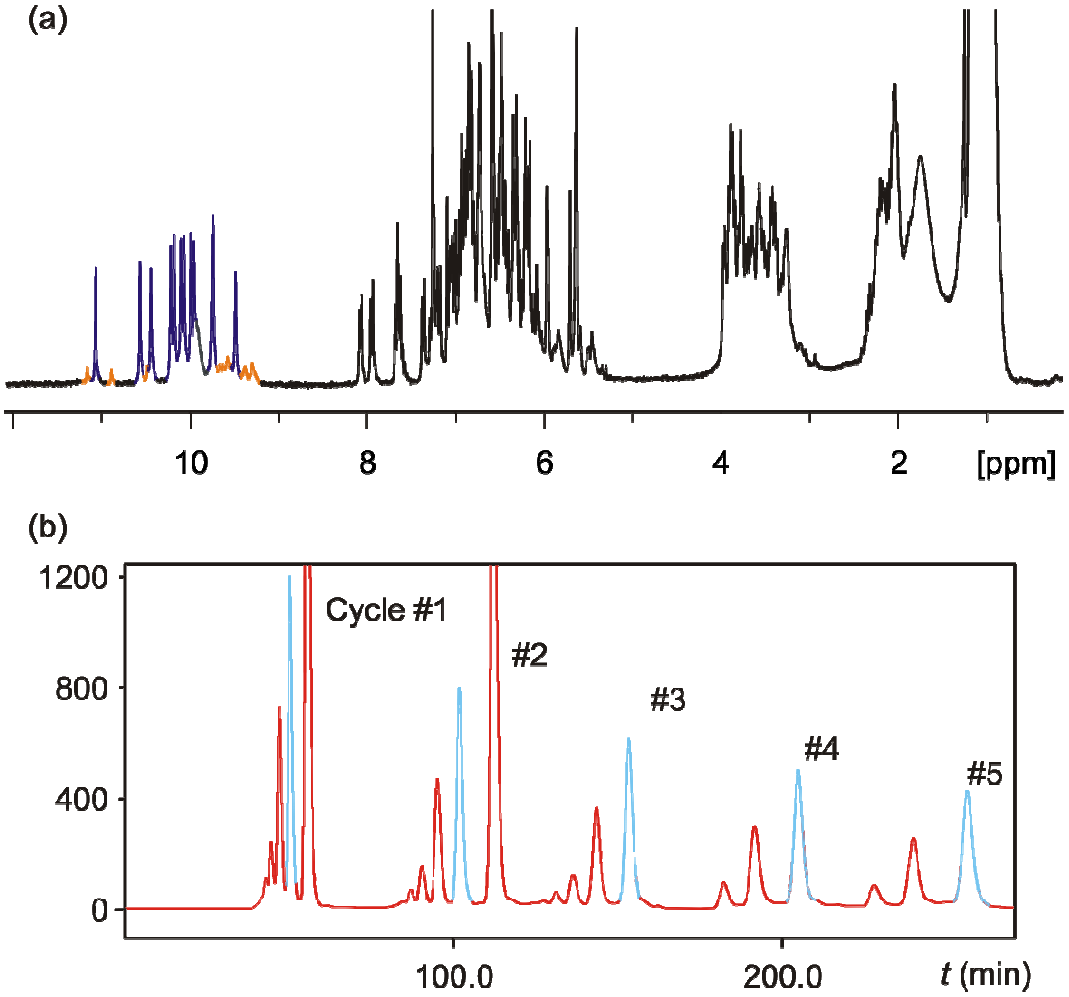

Figure 6: (a) crude ^{1}H NMR spectrum from the synthesis of 81mer in $CDCl_3$. Starting material has been highlighted in blue and the desired molecule in orange and (b) GPC of the crude mixture. The peak corresponding to the desired product has been highlighted in light blue.

5.4. NMR experiments

Despite the polymeric size of the synthesized molecules, they can be characterized by NMR spectroscopy. Indeed, the most striking characteristic in the NMR spectra of these molecules is their sharp peaks, suggesting well-defined conformations even for products composed of 45 or 81 units. Additionally, by looking at the spectra several other observations can be made, including the diastereotopicity of the methylene signals, the extensive overlapping of signals in the same region, as well as the overall upfield shifts as the molecules become longer.

In principle the methylene region provides information about the dynamics of the system; diastereotopicity indicates that the rate of helix handedness inversion is slow on the NMR

time scale, a fact which is in agreement with the well-defined structures, as additionally indicated by the sharp signals observed in the spectra. The extensive overlap of multiple peaks in that region suggests that when the helical architecture becomes long, the differences in environment around the central part of the helical structure become negligible.

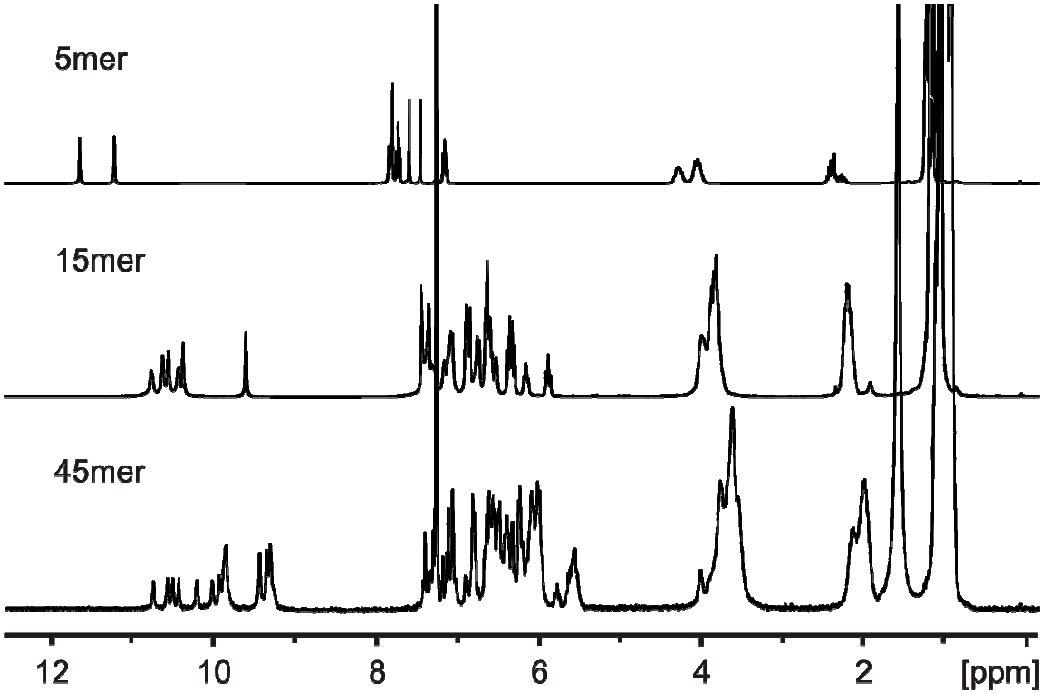

Figure 7: ^{1}H NMR spectra of 5mer, 15mer and 45mer at 25 ^{o}C in $CDCl_3$.

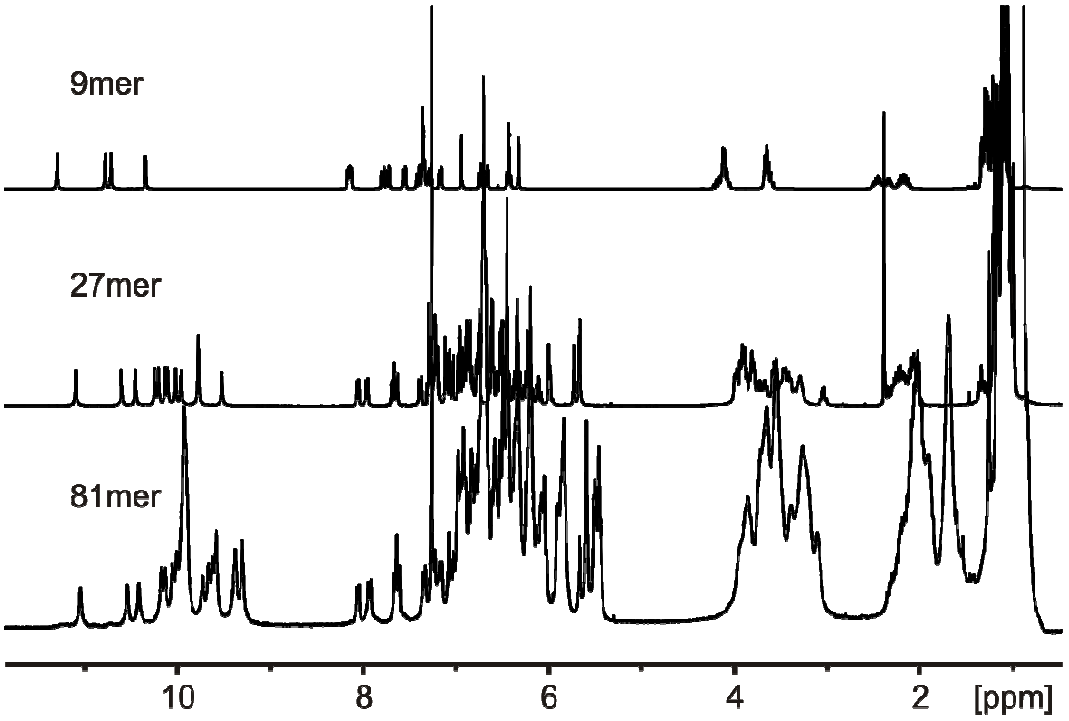

Figure 8: ^{1}H NMR spectra of 9mer, 27mer and 81mer at 25 ^{o}C in $CDCl_3$.

The upfield shifts of the chemical shift values as the oligomer becomes longer, can be

presumably attributed to cumulative ring current effects, as described in the introductory chapter (Chapter 1).

6. X-ray crystallography

Liquid-liquid diffusion provided crystals suitable for X-ray diffraction measurements for the case of the starting oligomers as well as the products after the 1st segment tripling step (15 and 27 monomeric units). Compounds crystallized from slow diffusion of methanol into a chlorinated solvent for 5mer and 15mer diesters, as well as the 27mer diacid. Additionally, slow diffusion of EtOAc into a chlorinated solvent provided good quality crystals for the 9mer diester.

Unfortunately, the oligomer composed of 45 units did not crystallize due to its limited solubility in most organic solvents, resulting in precipitation. Crystals of the 81mer were obtained but their low quality hampered the attempts to solve the crystal structure.

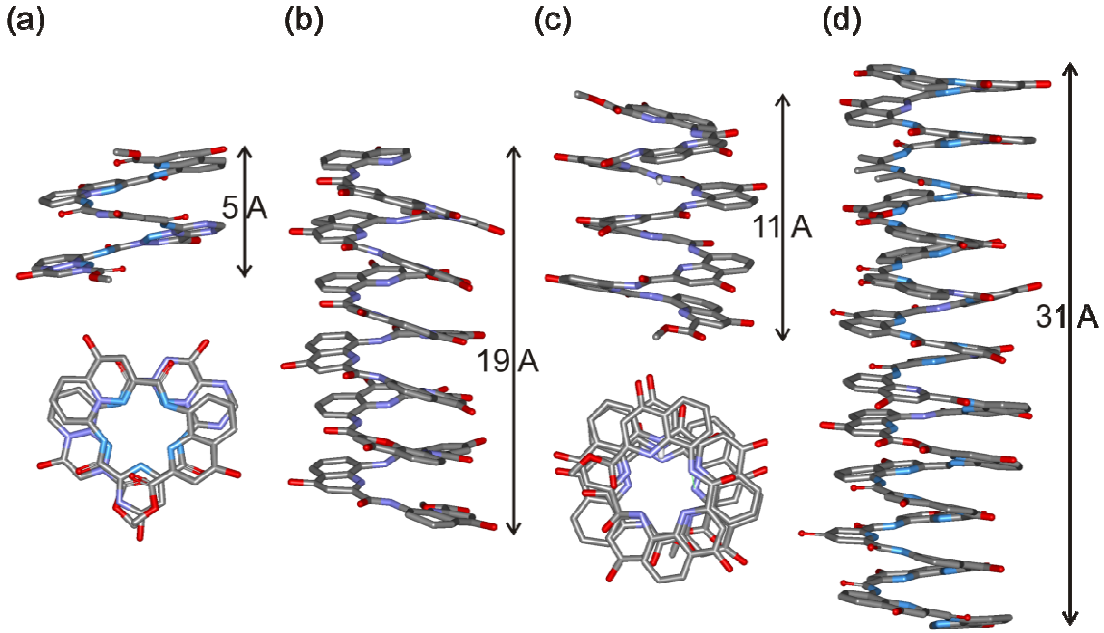

Figure 9: Crystal structures of (a) 5mer diester, (b) 15mer diester, (c) 9mer diester and (d) 27mer diacid.

The crystal structures show well-defined helical architectures for all the oligomers and they confirm the successful utilization of anhydride functions for the generation of long helical rods, by mediating intrahelical head-to-head communication (Figure 9). The 1st coupling step gives rise to molecules that reach 2 nm (15mer) and 3 nm (27mer) in length. From these values and in the absence of structural data of products of the 2nd coupling step, we can safely assume that molecules spanning over 6 and 9 nm long are generated.

The size of these molecules is much bigger than natural helices and they are comparable to small proteins.

Comparison of the all the crystal structures of AOF that contain anhydride functionalities brought to our attention significant differences in the dihedral angles between the two carbonyl oxygen atoms of the anhydride moiety (Figure 10).

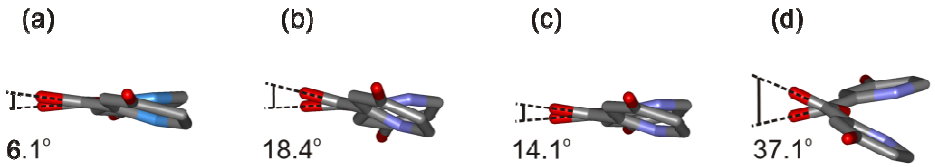

Figure 10: Detail from the crystal structures of (a) 27mer, (b) 15mer, (c) $Q_4COOCOQ_4$ and (d) P'_3A—anh—AP'_3. Q stands for the quinoline monomer equipped with isobutyl side chain.

In particular this angle is very wide in P_3A-anhydride-AP_3 compared to the rest of the candidates. This is presumably due to the methyl group of the anthracene pointing inside the helical cavity. The fluctuations observed in the angles in figure 10 a, b and c may be related to unique stability profiles associated with the helical segments adjacent to the anhydride, a hypothesis that requires further investigation to be confirmed.

7. Conclusions

In the introduction of this chapter several molecules bearing anhydride functionalities were briefly reviewed. Special emphasis was given to polyanhydrides, a class of biodegradable polymers, and their unique characteristics that make them ideal candidates for drug delivery applications.The incorporation of anhydride functionalities in aromatic oligoamide foldamers, as well as their ability to mediate intra-helical communication were described. The first example of a segment tripling strategy was reported leading to the generation of very long, well-defined and monodisperse aromatic helical rods, that bear anhydride functionalities connecting the individual segments. This method constitutes a convergent, protection/deprotection-free strategy for the synthesis of such oligomeric architectures. Several parameters affecting yield were evaluated and optimized, such as concentration and ratio of reactants. Emphasis was given to the purification methods that were used, especially GPC. Further studies need to be carried out to obtain better understanding of the anhydride linkages, for example to explore if different helical segments attached to the anhydride functionality modify parameters like the rate of hydrolysis.

8. Experimental session

Materials and Methods: All reactions were carried out under a dry nitrogen atmosphere. Commercial reagents were purchased from Sigma-Aldrich or Alfa-Aesar and were used without further purification unless otherwise specified. Chloroform and DIPEA were distilled from calcium hydride (CaH_2) prior to use. DCM was dried over solvent purification system (MBRAUN SPS-400). Reactions were monitored by thin layer chromatography (TLC) on Merck silica gel 60-F254 plates and observed under UV light. Silica gel chromatography was carried out on Merck GEDURAN Si60 (40-63 μm). Electrospray ionization mass spectrometric low and high resolution data (ESI MS, HRMS) were obtained from the Mass Spectrometry Laboratory at the European Institute of Chemistry and Biology (IECB), Pessac, France.

Nuclear Magnetic Resonance

^{1}H and ^{13}C NMR spectra were recorded in $CDCl_3$ solutions using a Bruker 300 Ultrashield Advance II spectrometer, ^{1}H operating at 300.13 MHz and ^{13}C operating at 75.46 MHz Chemical shifts are reported in parts per million (ppm, δ) relative to the signal of the NMR solvent used. ^{1}H NMR splitting patterns with observed first-order coupling are designated as singlet (s), doublet (d), triplet (t), or quartet (q). Coupling constants (J) are reported in hertz. Splitting patterns that could not be interpreted or easily visualized are designated as multiplet (m) or broad (br)

Crystallography

Data were collected using a Rigaku FRX microfocus rotating anode generator with Cu-K_α radiation (1.54178 Å) and varimax HF optics. The data collection, unit cell refinement and data reduction were performed using the CrystalClear software package. The positions of non-H atoms were determined by the program SHELX D and the position of the H atoms were deduced from coordinates of the non-H atoms and confirmed by Fourier Synthesis. H atoms were included for structure factor calculations but not refined. Selected single crystal were mounted on a cryoloop under oil and frozen into a N_2 stream at 100 K.

Gel Permeation Chromatography (GPC)

For the GPC experiment an LC-9130G NEXT (Japan Analytical Industry Co., Ltd.) setup was used equipped with two preparative columns (Inner diameter of 20mm and length of 600

mm): a JAIGEL 2.5H and a JAIGEL 3H, in conjugation with UV-600 NEXT UV detector and an FC-3310 fraction collector. The setup is equipped with a column oven that is set at 37 ^{o}C. Chloroform (HPLC grade, ethanol stabilized) was used for the separations.

5mer diester, (**4**): A solution of 4-isobutoxypyridine-2,6-dicarbonyl dichloride (**3**) (957 mg, 4 mmol) in anhydrous $CHCl_3$ (24 mL) was added via a cannula, under N_2 atmosphere, to a solution of methyl 2mer amine (**1**) (4.19 g, 8.1 mmol) and DIPEA (3 eq., 2 mL) in anhydrous $CHCl_3$ (50 mL) and left to react for 18 hours at room temperature. The reaction mixture was diluted in $CHCl_3$ and the organic layer was washed with 5% citric acid (aqueous) and saturated NaCl solution. The organic layer was dried over Na_2SO_4 and the solvent was evaporated under reduced pressure. Purification by column chromatography in EtOAc/cyclohexane (20/80 → 40/60) resulted in pure 5mer as a yellow solid, (**4**) with isolated yield: 72%. ^{1}H NMR ($CDCl_3$): δ 11.79 (2H, s), 11.72 (2H, s), 7.99 (2H, dd, *J* = 7.7, 1.1 Hz), 7.84 (2H, dd, *J* = 8.5, 1.1 Hz), 7.78 (2H, s), 7.68─7.60 (6H, m), 7.36 (2H, s), 7.21 (2H, t, *J* = 8.1 Hz), 7.05 (2H, t, *J* = 8.1 Hz), 4.37─3.94 (10H, m), 3.25 (6H, s), 2.48─2.22 (5H, m), 1.28─1.19 (24H, m), 1.17 (6H, d, *J* = 6.7 Hz). ^{13}C NMR ($CDCl_3$): δ 168.03, 165.05, 163.54, 162.94, 162.29, 161.35, 151.82, 150.29, 146.28, 139.08, 138.49, 134.00, 133.64, 128.18, 127.70, 122.08, 121.90, 116.84, 116.33, 115.56, 111.34, 101.71, 99.60, 75.58, 75.37, 53.60, 52.35, 51.07, 28.46, 28.43, 28.31, 19.50, 19.35. HRMS (ES^+): *m/z* calcd for $C_{69}H_{73}N_9O_{13}$ $[M+H]^+$ 1236.5406 found 1236.5419.

5mer diacid, (**6**): To a solution of 5mer diester (**4**) (3.2 g, 2.58 mmol) in a mixture of THF/MeOH 9:1 (150 mL), KOH was added (20 eq., 3.2 g) as a solution in 30 ml THF/MeOH 9:1. The reaction was complete in 4 hours and it was directly acidified to pH 4 with 5% citric acid aqueous solution. The organic solvents were evaporated, water was added and the solid was filtered resulting in pure material as a pale yellow solid, (**6**) in 96% yield. ^{1}H NMR ($CDCl_3$): δ 11.65 (2H, s), 11.22 (2H, s), 7.84 (2H, dd, *J* = 3.9, 1.1 Hz), 7.81 (2H, dd, *J* = 4.9, 1.1 Hz), 7.80 (2H, s), 7.77─7.69 (4H, m), 7.59 (2H, s), 7.45 (2H, s), 7.16 (2H, t, *J* = 8.1 Hz), 7.14 (2H, t, *J* = 8.0 Hz), 4.35─3.95 (10H, m), 2.49─2.18 (5H, m) 1.22 (24H, t, *J* = 6.3 Hz), 1.14 (6H, d, *J* = 6.7 Hz). ^{13}C NMR ($CDCl_3$): δ 169.09, 164.25, 163.78, 163.27, 161.88, 160.97, 151.40, 149.84, 145.37, 138.19, 137.59, 133.38, 132.88, 129.25, 128.64, 128.42, 128.07, 122.50, 122.07, 117.42, 116.85, 116.15, 112.38, 99.98, 99.62, 75.87, 75.69, 75.64, 28.40, 28.37, 28.26, 19.46, 19.34. HRMS (ES^+): *m/z* calcd for $C_{67}H_{69}N_9O_{13}$ $[M+H]^+$ 1208.5093 found 1208.5106.

5mer diacid chloride, (**8**): To a solution of 5mer diacid (**6**) (1.5 g, 1.24 mmol) in $CHCl_3$ (80 mL) that was placed under N_2 atmosphere, oxalyl chloride was added (10 eq., 1 mL). The reaction was complete after 2 hours yielding quantitatively the desired diacid chloride (**8**) that was dried carefully and used directly for the next step. ^{1}H NMR ($CDCl_3$): δ 11.75 (2H, s), 11.64 (2H, s), 7.93 (2H, dd, *J* = 7.7, 1.1 Hz), 7.82 (2H, dd, *J* = 8.5, 1.0 Hz), 7.78 (2H, s), 7.76 (2H, dd, *J* = 7.8, 1.0 Hz), 7.66 (2H, dd, *J* = 8.0, 1.2 Hz), 7.64 (2H, s), 7.16 (4H, dd, *J* = 17.8, 8.5 Hz), 4.39─3.91(10H, m), 2,49─2.22 (5H, m), 1.28─1.14 (30H, m).

15mer diacid, (**10**): A solution of 5mer diacid chloride (**8**) (1.24 mmol) in anhydrous $CHCl_3$ (60 mL) was added via a cannula, under N_2 atmosphere, to a solution of 5mer diacid (**6**) (4.5 g, 3.7 mmol) and DIPEA (3 eq., 0.7 mL) in anhydrous $CHCl_3$ (120 mL) and left to react for 18 hours at room temperature. The reaction mixture was diluted in $CHCl_3$ and the organic layer was washed with 5% citric acid (aqueous) and saturated NaCl solution. The organic layer was dried over Na_2SO_4 and the solvent was evaporated under reduced pressure. Purification by GPC resulted in pure 15mer as a yellow solid, (**10**) with isolated yield 33%. ^{1}H NMR ($CDCl_3$): δ 10.85 (2H, s), 10.70 (2H, s), 10.59 (2H, s), 10.53 (2H, s), 10.42 (2H, s), 9.63 (2H, s), 7.51─7.34 (12H, m), 7.20─7.12 (6H, m), 6.98─6.56 (26H, m), 6.45─6.30 (6H, m), 6.20 (2H, t, *J* = 8.0 Hz), 5.91 (2H, t, *J* = 8.0 Hz), 4.11─3.78 (30H, m), 2.33─2.12 (15H, m), 1.27─1.04 (90H, m). ^{13}C NMR ($CDCl_3$): δ 168.22, 167.62, 163.65, 163.16, 163.01, 162.19, 162.01, 161.81, 161.75, 161.68, 161.36, 160.54, 160.50, 160.26, 158.16, 157.96, 150.65, 150.58, 149.91, 149.52, 149.06, 144.92, 144.43, 144.38, 137.63, 137.17, 137.03, 136.79, 136.48, 136.14, 132.74, 132.34, 132.18, 131.78, 131.64, 131.46, 127.00, 127.51, 126.82, 126.17, 125.70, 125.34, 121.94, 121.49, 120.27, 120.07, 119.93, 119.87, 117.07, 116.61, 116.58, 115.83, 115.77, 115.69, 115.48, 115.44, 115.05, 114.18, 113.96, 112.93, 112.36, 112.12, 100.84, 100.74, 99.56, 99.53, 99.20, 99.08, 75.46, 75.25, 75.17, 75.06, 74.82, 74.65, 74.48, 45.86, 29.84, 28.40, 28.32, 28.17, 28.07, 19.66, 19.62, 19.53, 19.41, 19.39, 19.37, 19.33, 19.28, 19.27, 8.66. HRMS (ES^+): *m/z* calcd for $C_{201}H_{203}N_{27}O_{37}$ $[M+H]^+$ 3587.4911 found 1795.2564 (z = 2).

15mer diacid chloride, (**12**): To a solution of 15mer diacid (**10**) (100 mg, 0.028 mmol) in $CHCl_3$ (2 mL) that was placed under N_2 atmosphere, Ghosez reagent was added (2.5 eq., 10 μL). The reaction was complete after 2 hours yielding quantitatively the desired diacid chloride (**12**) that was dried carefully and used directly for the next step.

15mer diester, (**16**): A solution of 15mer diacid chloride (**12**) (20mg, 0.005 mmol) in anhydrous $CHCl_3$ was added via a cannula, under N_2 atmosphere, to a solution of anhydrous chloroform (1 mL) containing anhydrous MeOH (25 μL) and DIPEA (12 eq, 9 μL) and left to react for 30 min at room temperature. The crude was dried and it was purified by GPC and pure compound was obtained as a yellow solid (**16**). Isolated yield: 86%. ^{1}H NMR ($CDCl_3$): δ 11.11 (2H, s), 10.94 (2H, s), 10.69 (2H, s), 10.44 (2H, s), 10.43 (2H, s), 9.69 (2H, s), 7.55 (2H, dd, *J* = 7.6, 1.1 Hz), 7.48─7.41 (8H, m), 7.28─7.23 (4H, m), 7.13─7.06 (6H, m), 6.99 (2H, dd, *J* = 7.6, 1.1 Hz), 6.96 (4H, d, *J* = 1.9 Hz), 6.89 (2H, dd, *J* = 8.4, 1.2 Hz), 6.84 (2H, t, *J* = 8.0 Hz), 6.77 (2H, dd, *J* = 8.4, 1.2 Hz), 6.72─6.55 (12H, m), 6.47─6.33 (6H, m), 6.17 (2H, t, *J* = 7.9 Hz), 5.92 (2H, t, *J* = 8.0 Hz), 4.10─3.72 (30H, m), 2.91 (6H, s), 2.35─2.11 (15H, m), 1.27─1.05 (90H, m). ^{13}C NMR ($CDCl_3$): δ 167.85, 167.70, 164.92, 162.94, 162.51, 162.24, 162.08, 161.96, 161.90, 161.77, 161.49, 160.93, 160.67, 160.57, 158.29, 158.16, 151.25, 150.79, 150.77, 150.06, 149.84, 149.78, 146.02, 144.55, 144.48, 138.70, 137.97, 137.18, 136.93, 136.67, 136.31, 133.50, 133.17, 132.45, 131.98, 131.81, 131.61, 127.67, 127.26, 126.83, 126.25, 125.68, 125.32, 121.61, 121.49, 120.38, 120.21, 120.07, 119.97, 116.77, 116.59, 116.12, 115.95, 115.76, 115.68, 115.42, 115.12, 114.28, 114.11, 113.04, 112.21, 111.72, 101.39, 100.92, 100.79, 99.65, 99.44, 99.36, 99.22, 75.37, 75.23, 75.12, 74.89, 74.75, 74.55, 52.14, 32.20, 29.97, 29.63, 28.55, 28.47, 28.40, 28.33, 28.23, 22.96, 19.76, 19.70, 19.68, 19.56, 19.48, 19.42, 14.39, 1.28. HRMS (ES^+): *m/z* calcd for $C_{203}H_{207}N_{27}O_{37}$ $[M+H]^+$ 3615.5124 found 1809.2714 (z = 2).

45mer, (**14**): A solution of 15mer diacid chloride (**12**) (0.028 mmol) in anhydrous $CHCl_3$ (1 mL) was added with a syringe, under N_2 atmosphere, to a solution of 15mer diacid (**11**) (300 mg, 0.084 mmol) and DIPEA (3 eq., 50 μL) in anhydrous $CHCl_3$ (1 mL) and left to react for 2 days at room temperature. The solid was filtered from the reaction mixture and the solid was solubilised by a 50/50 mixture of warm $CHCl_3$/chlorobenzene. The solvents were evaporated and the solid was suspended and sonicated in EtOAc. The suspension was centrifuged and the solid was washed several times with EtOAc and pure 45mer (**14**) was obtained as a light yellow solid. Isolated yield 10%. HRMS (ES^+): *m/z* calcd for $C_{603}H_{605}N_{81}O_{109}$ $[M+H]^+$ 10723.4288 found 2147.1014 (z = 5).

9mer diester, (**5**): A solution of 4-isobutoxypyridine-2,6-dicarbonyl dichloride (**3**) (622 mg, 2.6 mmol) in anhydrous $CHCl_3$ (16 mL) was added via a cannula, under N_2 atmosphere, to a solution of methyl methyl 4mer amine, (**2**) (5.1 g, 5.1 mmol) and DIPEA (3 eq., 1.4 mL) in anhydrous $CHCl_3$ (22 mL) and left to react overnight at room temperature. The reaction mixture was diluted in $CHCl_3$ and the organic layer was washed with 5% citric acid (aqueous)

and saturated NaCl solution. The organic layer was dried over Na_2SO_4 and the solvent was evaporated under reduced pressure. Purification by column chromatography in EtOAc/cyclohexane (20/80 → 40/60) followed by a consecutive crystallization step (slow diffusion of EtOAc in $CHCl_3$) resulted in pure 9mer as a yellow solid, (**6**) with isolated yield 85%. ^{1}H NMR ($CDCl_3$): δ 11.58 (2H, s), 11.34 (2H, s), 10.85 (2H, s), 10.39 (2H, s), 8.19 (2H, dd, *J* = 7.7, 1.2 Hz), 8.13 (2H, dd, *J* = 7.7, 1.2 Hz), 7.84 (2H, dd, *J* = 8.4, 1.2 Hz), 7.72 (2H, dd, *J* = 8.4, 1.2 Hz), 7.61 (1H, dd, *J* = 8.4, 1.3 Hz), 7.43 (2H, t, *J* = 8.1 Hz), 7.42 (2H, s), 7.39 (2H, t, *J* = 8.0 Hz), 7.29 (2H, s), 7.24 (2H, dd, *J* = 5.6, 1.3 Hz), 7.22 (2H, dd, *J* = 5.1, 1.2 Hz), 7.09 (2H, s), 6.78 (2H, dd, *J* = 7.8, 1.3 Hz), 6.76 (2H, t, *J* = 8.1 Hz), 6.48 (2H, s), 6.47 (2H, t, *J* = 8.0 Hz), 6.30 (2H, s), 4.24─4.11 (8H, m), 4.00 (2H, dd, *J* = 9.0, 6.2 Hz), 3.75─3.69 (4H, m), 3.66─3.53 (4H, m) 3.12 (6H, s), 2.58─2.07 (9H, m), 1.37─1.04 (45H, m). ^{13}C NMR ($CDCl_3$): δ 167.17, 163.90, 163.11, 162.96, 162.77, 162.23, 161.98, 160.64, 160.19, 159.61, 150.47, 149.71, 149.63, 148.74, 145.06, 138.81, 138.08, 137.08, 137.04, 133.79, 133.52, 132.57, 132.34, 127.41, 126.93, 126.30, 126.22, 121.88, 121.71, 121.55, 121.19, 116.97, 116.94, 116.57, 116.18, 116.02, 115.55, 115.08, 114.56, 113.00, 100.11, 100.06, 98.67, 97.70, 75.47, 75.35, 75.10, 74.83, 52.23, 28.51, 28.46, 28.43, 28.25, 28.24, 19.65, 19.61, 19.59, 19.55, 19.51, 19.45, 19.42, 19.37. HRMS (ES^+): *m/z* calcd for $C_{125}H_{129}N_{17}O_{21}$ $[M+H]^+$ 2204.9549 found 2205.9691.

9mer diacid, (**7**): To a solution of 9mer diester, (**5**) (6 g, 2.7 mmol) in a mixture of THF/MeOH 9:1 (100 mL), KOH was added (80 eq., 12 g) as a solution in 100 mL THF/MeOH 9:1. The reaction was complete in 6 hours and it was directly acidified to pH 4 with 5% citric acid aqueous solution. The organic solvents were evaporated, water was added and the solid was filtered resulting in pure material as a light yellow solid (**8**) in 98% yield. ^{1}H NMR ($CDCl_3$): δ 11.36 (2H, s), 10.84 (2H, s), 10.79 (2H, s), 10.42 (2H, s), 8.24 (2H, dd, *J* = 6.5, 1.2 Hz), 8.21 (2H, dd, *J* = 6.3, 1.0 Hz), 7.85 (2H, dd, *J* = 8.4, 1.1 Hz), 7.79 (2H, dd, *J* = 8.3, 1.3 Hz), 7.60 (2H, dd, *J* = 8.4, 1.2 Hz), 7.43 (4H, dd, *J* = 16.3, 7.6 Hz) 7.39 (4H, d, *J* = 2.8 Hz), 7.32 (2H, dd, *J* = 8.4, 1.1 Hz), 7.21 (2H, dd, *J* = 7.8, 1.1 Hz), 6.99 (2H, s), 6.77 (2H, t, *J* = 8.0 Hz), 6.72 (2H, dd, *J* = 7.7, 1.0 Hz), 6.53 (2H, s), 6.47 (2H, t, *J* = 8.0 Hz), 6.38 (2H, s), 4.23─4.05 (9H, m), 3.78─3.60 (9H, m), 2.56─2.01 (9H, m), 1.38─1.05 (45H, m). ^{13}C NMR ($CDCl_3$): δ 167.19, 163.60, 163.17, 162.94, 162.69, 161.98, 161.66, 160.41, 160.00, 159.46, 150.40, 150.27, 149.30, 148.18, 144.06, 137.86, 137.21, 136.99, 136.84, 133.20, 132.74, 132.45, 131.96, 127.50, 127.13, 126.40, 125.96, 122.01, 121.73, 121.67, 121.60, 117.95, 117.49, 116.70, 116.60, 115.92, 115.67, 115.59, 114.48, 112.98, 99.75, 99.63, 98.27, 97.71, 75.49, 75.42, 75.32, 75.11, 28.41, 28.39, 28.35, 28.20, 28.13, 19.58, 19.55, 19.51,

19.46, 19.37, 19.36, 19.35, 19.28. HRMS (ES^+): *m/z* calcd for $C_{123}H_{125}N_{17}O_{21}$ $[M+H]^+$ 2176.9236 found 2177.9389.

9mer diacid chloride, (**9**): To a solution of 9mer diacid (**7**) (1.5 g, 0.69 mmol) in $CHCl_3$ (30 mL) that was placed under N_2 atmosphere, oxalyl chloride was added (10 eq., 0.6 mL). The reaction was complete after 2 hours yielding quantitatively the desired diacid chloride (**9**) that was dried carefully and used directly for the next step. ^1H NMR ($CDCl_3$): δ 11.47 (2H, s), 11.14 (2H, s), 10.88 (2H, s), 10.47 (2H, s), 8.26 (2H, dd, *J* = 7.7, 1.1 Hz), 8.22 (2H, dd, *J* = 7.6, 1.0 Hz), 7.85 (2H, dd, *J* = 8.4, 1.1 Hz),7.75 (2H, dd, *J* = 8.4, 1.1 Hz), 7.61 (2H, dd, *J* = 8.4, 1.1 Hz), 7.44 (2H, m), 7.40 (2H, s),7.34 (2H, s), 7.29 (2H, dd, *J* = 8.4, 1.2 Hz), 7.20 (2H, dd, *J* = 7.8, 1.1 Hz), 6.99 (2H, s), 6.77 (2H, t, *J* = 8.0 Hz), 6.74 (2H, dd, *J* = 7.6, 1.1 Hz), 6.54 (2H, s), 6.48 (2H, t, *J* = 7.9 Hz), 6.20 (2H, s), 4.27─4.12 (8H, m), 4.04 (2H, dd, *J* = 6.8, 6.3 Hz), 3.73 (4H, d, *J* = 6.5 Hz), 3.69─3.57 (4H, m), 2.58─2.10 (9H, m), 1.38─1.06 (45H, m).

27mer diacid, (**11**): A solution of 9mer diacid chloride (**9**) (0.69 mmol) in anhydrous $CHCl_3$ (15 mL) was added via a cannula, under N_2 atmosphere, to a solution of 9mer diacid (**7**) (4.5 g, 2.1 mmol) and DIPEA (3eq, 0.4 mL) in anhydrous $CHCl_3$ (45 mL) and left to react overnight at room temperature. The reaction mixture was diluted in $CHCl_3$ and the organic layer was washed with 5% citric acid (aqueous) and saturated NaCl solution. The organic layer was dried over Na_2SO_4 and the solvent was evaporated under reduced pressure. Purification by GPC, followed by a consecutive crystallization step (slow diffusion of MeOH in $CHCl_3$) resulted in pure 27mer as a yellow solid, (**11**) with isolated yield 25%. ^1H NMR ($CDCl_3$): δ 11.05 (2H, s), 10.56 (2H, s), 10.42 (2H, s), 10.20 (2H, s), 10.16 (2H, s), 10.10 (2H, s), 10.06 (2H, s), 9.98 (2H, s), 9.92 (2H, s), 9.74 (4H, s), 9.48 (2H, s), 8.02 (2H, dd, *J* = 7.6, 0.8 Hz), 7.92 (2H, dd, *J* = 7.5, 0.9 Hz), 7.66─7.57 (4H, m), 7.35 (2H, dd, *J* = 8.1, 1.1 Hz), 7.28 ─7.11 (13H, m), 7.09─6.97 (7H, m), 6.95─6.76 (20H, m), 6.75─6.69 (6H, m), 6.61─6.12 (34H, m), 6.06 (2H, t, *J* = 7.8 Hz), 5.99─5.92 (3H, m), 5.69 (2H, s), 5.66─5.60 (5H, m), 3.99─3.18 (52H, m), 3.00 (2H, dd, *J* = 16.3, 7.3 Hz), 2.35─1.97 (27H, m), 1.34─0.88 (162H, m). ^{13}C NMR ($CDCl_3$): δ 166.60, 166.22, 163.26, 162.95, 162.74, 162.49, 162.37, 162.34, 162.15, 162.01, 161.98, 161.44, 161.35, 160.84, 160.81, 160.78, 160.65, 160.22, 159.63, 159.49, 159.45, 159.34, 159.18, 159.00, 158.72, 158.29, 156.61, 149.97, 149.81, 149.71, 149.31, 148.93, 148.91, 148.80, 148.56, 148.46, 148.05, 148.00, 147.93, 144.13, 143.34, 143.23, 138.00, 137.72, 137.12, 136.79, 136.76, 136.72, 136.59, 136.39, 136.31, 136.23, 136.20, 136.12, 136.04, 133.07, 132.62, 132.18, 131.85, 131.72, 131.69, 131.53, 131.40, 131.12, 131.02, 129.17, 128.37, 127.30, 126.86, 126.05, 126.02, 125.72, 125.69, 125.57, 125.51, 125.44, 125.35, 124.60, 124.57, 124.41, 124.39, 121.83, 121.47,

121.29, 121.26, 121.10, 120.74, 120.55, 119.53, 119.40, 117.79, 117.74, 117.27, 117.25, 116.67, 116.63, 116.57, 116.53, 116.51, 116.47, 116.45, 116.43, 116.28, 116.26, 116.04, 115.84, 115.79, 115.76, 115.75, 115.72, 115.67, 115.65, 115.54, 115.45, 115.38, 115.37, 115.28, 115.27, 115.23, 115.21, 115.00, 114.85, 114.75, 114.73, 114.68, 114.66, 114.53, 114.36, 114.33, 114.22, 114.17, 113.68, 113.66, 112.55, 112.19, 111.81, 99.77, 99.50, 99.29, 98.14, 97.58, 97.54, 97.50, 97.35, 75.12, 75.02, 74.80, 74.76, 74.64, 74.54, 74.27, 45.78, 29.84, 28.28, 28.23, 28.17, 28.12, 28.09, 28.05, 28.00, 21.60, 19.59, 19.53, 19.50, 19.46, 19.43, 19.36, 19.33, 19.31, 19.27, 19.22, 19.17, 8.76, 8.03. HRMS (ES^+): *m/z* calcd for $C_{369}H_{371}N_{51}O_{61}$ $[M+H]^+$ 6492.7575 found 2166.2664 (z = 3).

27mer diacid chloride, (**13**): To a solution of 27mer diacid (**11**) (100 mg, 0.015 mmol) in $CHCl_3$ (2 mL) that was placed under N_2 atmosphere, Ghosez reagent was added (2.5 eq., 5 μL). The reaction was complete after 2 hours yielding quantitatively the desired diacid chloride (**13**) that was dried carefully and used directly for the next step.

81mer diacid, (**15**): A solution of 27mer diacid chloride (**13**) (0.015 mmol) in anhydrous $CHCl_3$ (1 mL) was added with a syringe, under N_2 atmosphere, to a solution of 27mer diacid (**11**) (300 mg, 0.045 mmol) and DIPEA (3 eq., 25 μL) in anhydrous $CHCl_3$ (1 mL) and left to react for 4 days at room temperature. The reaction mixture was diluted in $CHCl_3$ and the organic layer was washed with 5% citric acid (aqueous) and saturated NaCl solution. The organic layer was dried over Na_2SO_4 and the solvent was evaporated under reduced pressure. Purification by GPC resulted in pure 81mer as a yellow solid, (**15**) with isolated yield 13%. Mass of the desired compound was confirmed by MALDI-TOF.

9. References

1. J. A. Olmsted, *Journal of Chemical Education*, 1998, **75**, 1261.
2. J. Klose, M. Bienert, C. Mollenkopf, D. Wehle, C.-w. Zhang, L. A. Carpino and P. Henklein, *Chemical Communications (Cambridge)*, 1999, 1847-1848.
3. E. G. Peterson, E. R.Littmann, US1993025, 1935.
4. H. L. Gerhart, US2384085, 1945.
5. R. C. Strand, B. G. Gower, D. L. Marion, R. F. Poss and L. R. Hanson, *Detergent Age*, 1967, **4**, 46, 48, 50.
6. D. J. Kay, R. P. Knipple, US3446783A, 1969.
7. Anon, *Federal Register*, 1970, **35**, 16631.
8. K. Watanabe, K. Koichi, JP01313552A, 1989.
9. A. Pettersson, T. Lundqvist, WO2006103417A1, 2006.
10. A. Pettersson, T. Lundqvist, WO2006103407A2, 2006.

11. S. L. Ali, *Pharmazeutische Zeitung*, 1976, **121**, 201-207.
12. N. Kumar, R. S. Langer and A. J. Domb, *Advanced Drug Delivery Reviews*, 2002, **54**, 889-910.
13. J. E. Bucher and W. C. Slade, *Journal of the American Chemical Society*, 1909, **31**, 1319-1321.
14. E. Marin, M. I. Briceno and C. Caballero-George, *International Journal of Nanomedicine*, 2013, **8**, 3071-3091.
15. K. W. Leong, B. C. Brott and R. Langer, *Journal of Biomedical Materials Research*, 1985, **19**, 941-955.
16. A. J. Domb, C. F. Gallardo and R. Langer, *Macromolecules*, 1989, **22**, 3200-3204.
17. A. J. Domb and R. Langer, *Journal of Polymer Science, Part A: Polym. Chem.*, 1987, **25**, 3373-3386.
18. K. W. Leong, P. D'Amore, M. Marletta and R. Langer, *Journal of Biomedical Materials Research*, 1986, **20**, 51-64.
19. H. Brem, A. Kader, J. I. Epstein, R. J. Tamargo, A. Domb, R. Langer and K. W. Leong, *Selective Cancer Therapeutics*, 1989, **5**, 55-65.
20. C. Laurencin, A. Domb, C. Morris, V. Brown, M. Chasin, R. McConnell, N. Lange and R. Langer, *Journal of Biomedical Materials Research*, 1990, **24**, 1463-1481.
21. H. Brem, M. S. Mahaley, Jr., N. A. Vick, K. L. Black, S. C. Schold, Jr., P. C. Burger, A. H. Friedman, I. S. Ciric, T. W. Eller, J. W. Cozzens and a. et, *Journal of Neurosurgery*, 1991, **74**, 441-446.
22. H. Brem, S. Piantadosi, P. C. Burger, M. Walker, R. Selker, N. A. Vick, K. Black, M. Sisti, S. Brem, G. Mohr and a. et, *Lancet*, 1995, **345**, 1008-1012.
23. S. Valtonen, U. Timonen, P. Toivanen, H. Kalimo, L. Kivipelto, O. Heiskanen, G. Unsgaard and T. Kuurne, *Neurosurgery*, 1997, **41**, 44-48.
24. H. Brem and H. C. Lawson, *Cancer*, 1999, **86**, 197-199.
25. E. Mathiowitz, M. D. Cohen and R. Langer, *Reactive Polymers, Ion Exchange, Sorbents*, 1987, **6**, 275-283.
26. D. Teomim, I. Fishbien, G. Golomb, L. Orloff, M. Mayberg and A. J. Domb, *Journal of Controlled Release*, 1999, **60**, 129-142.
27. M. Chasin, R. Langer and Editors, *Drugs and the Pharmaceutical Sciences, Vol. 45: Biodegradable Polymers as Drug Delivery Systems*, Dekker, 1990.
28. E. Mathiowitz, J. S. Jacob, Y. S. Jong, G. P. Carino, D. E. Chickering, P. Chaturvedi, C. A. Santos, K. Vijayaraghavan, S. Montgomery, M. Bassett and C. Morrell, *Nature*, 1997, **386**, 410-414.
29. M. L. Johnson, R. Casas, D. V. Patwardhan, S. K. Pollack and K. E. Uhrich, *Polymer Preprints (Am. Chem. Soc., Div. Polym. Chem.)*, 2007, **48**, 914-915.
30. A. Prudencio, WO2009026544A1, 2009.
31. S. S. Snyder, A. Mitchell, J. P. O'Connor and K. E. Uhrich, *PMSE Preprints*, 2011.
32. S. E. M. Ibim, K. E. Uhrich, M. Attawia, V. R. Shastri, S. F. El-Amin, R. Bronson, R. Langer and C. T. Laurencin, *Journal of Biomedical Materials Research*, 1998, **43**, 374-379.
33. J. Griffin, R. Delgado-Rivera, S. Meiners and K. E. Uhrich, *Journal of Biomedical Materials Research, Part A*, 2011, **97A**, 230-242.
34. J. Griffin, A. Carbone, R. Delgado-Rivera, S. Meiners and K. E. Uhrich, *Acta Biomaterials*, 2010, **6**, 1917-1924.
35. N. Z. Piracha, M. L. Johnson, J. R. Griffin and K. E. Uhrich, *Polymer Preprints (Am. Chem. Soc., Div. Polym. Chem.)*, 2008, **49**, 1109-1110.
36. K. E. Uhrich, A. Gupta, T. T. Thomas, C. T. Laurencin and R. Langer, *Macromolecules*, 1995, **28**, 2184-2193.
37. R. F. Storey and A. E. Taylor, *Journal of Macromolecular Science: Pure and Applied Chemistry*, 1997, **A34**, 265-280.
38. K. E. Uhrich, S. M. Cannizzaro, R. S. Langer and K. M. Shakesheff, *Chemical Reviews (Washington, D. C.)*, 1999, **99**, 3181-3198.
39. L. Erdmann, C. Campo, D. Palms and K. Uhrich, *Polymer Preprints (Am. Chem. Soc., Div. Polym. Chem.)*, 1997, **38**, 570-571.
40. N. Delsuc, L. Poniman, J.-M. Leger and I. Huc, *Tetrahedron*, 2012, **68**, 4464-4469.
41. C. Dolain, J.-M. Leger, N. Delsuc, H. Gornitzka and I. Huc, *Proceedings of the National Academy of Sciences*

of the United States of America, 2005, **102**, 16146-16151.

42. E. Berni, C. Dolain, B. Kauffmann, J.-M. Leger, C. Zhan and I. Huc, *Journal of Organic Chemistry*, 2008, **73**, 2687-2694.
43. D. Sanchez-Garcia, B. Kauffmann, T. Kawanami, H. Ihara, M. Takafuji, M.-H. Delville and I. Huc, *Journal of the American Chemical Society*, 2009, **131**, 8642-8648.
44. B. Baptiste, C. Douat-Casassus, K. Laxmi-Reddy, F. Godde and I. Huc, *Journal of Organic Chemistry*, 2010, **75**, 7175-7185.
45. T. Qi, T. Deschrijver and I. Huc, *Nature Protocols*, 2013, **8**, 693-708, 616 pp.

Conclusions and Perspectives

In nature, the function of helical structures is associated with their stability at a molecular level. Outside of the overall protein structures, helical peptidic motifs have demonstrated limited stability which has hindered their potential application in the pharmaceutical industry. Aromatic oligoamide foldamers have demonstrated their ability to mimic natural helices in terms of structure; however their future as therapeutic agents or advanced materials is yet to be seen. Herein we have investigated several factors affecting the stability of these helical moieties. We have also demonstrated that very long helical architectures could be synthesized using a labile functionality (i.e. the anhydride) mediating their formation.

A series of aromatic helical compounds was synthesized in order to evaluate the helical propensity of aromatic monomers that have been widely used in aromatic foldamer synthesis; 2,6-diaminopyridine, 2.6-diaminobenzene, 2,6-diaminofluorobenzene, 2,6-diaminochlorobenzene and 2,6-diaminotoluene.

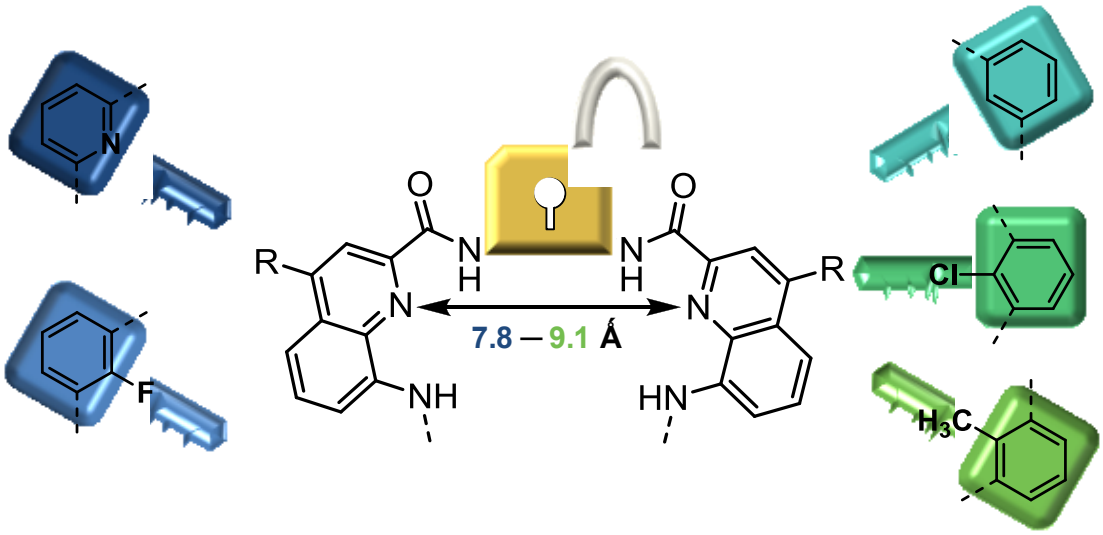

The evaluation of their helical propensity, which was based on NMR and dynamic chiral HPLC experiments, indicated that in principle an aromatic ring bearing a hydrogen bond acceptor, that can be either endocyclic or exocyclic, stabilizes significantly the helical architecture. An important parameter that should be taken into account is the size of the acceptor. If it is bulky, steric hindrance prevails over electrostatics and destabilizes the helix, eg the chlorine atom in chlorobenzene. Furthermore, it was demonstrated that the absence of both attractive and repulsive interactions in the aryl-amide linkage can still result in stable architectures driven by π-π stacking which is increased in the case of homochiral orientation.

Two compounds, a helical motif possessing an intramolecular disulfide bond and two intermolecular bonds connecting two helices together, have been designed and synthesized. These oligomers constitute the first abiotic helical system to explore whether disulfide bridges between side chains could be used to stabilize the helical entities both intra- and intermolecularly. Additionally, their ability to assemble several helices together has been shown. Our results indicated that in both cases disulfide bridges cannot lock the conformations and racemization still occurs. Their racemization kinetics though are significantly slower compared to the non-bridged compounds. We also demonstrated that side-to-side communication takes place in the intermolecularly bridged compound as suggested by chiral HPLC, NP-HPLC and X-ray crystallography.

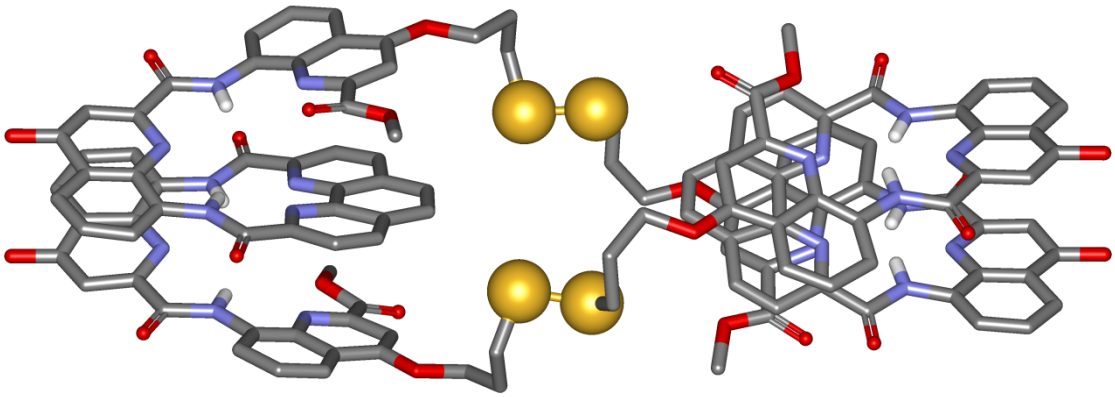

Anhydride functionalities, that have been previously reported to be stable when incorporated into helical aromatic foldamers, have been used as a tool for the synthesis of well-defined helical rods of polymeric dimensions. A segment tripling strategy based on anhydride junctions has been designed and experimentally validated to yield helical AOFs up to 9 nm long in just two steps. Characterization of these nano-sized objects has been carried out by NMR spectroscopy, mass spectrometry and X-ray crystallography.

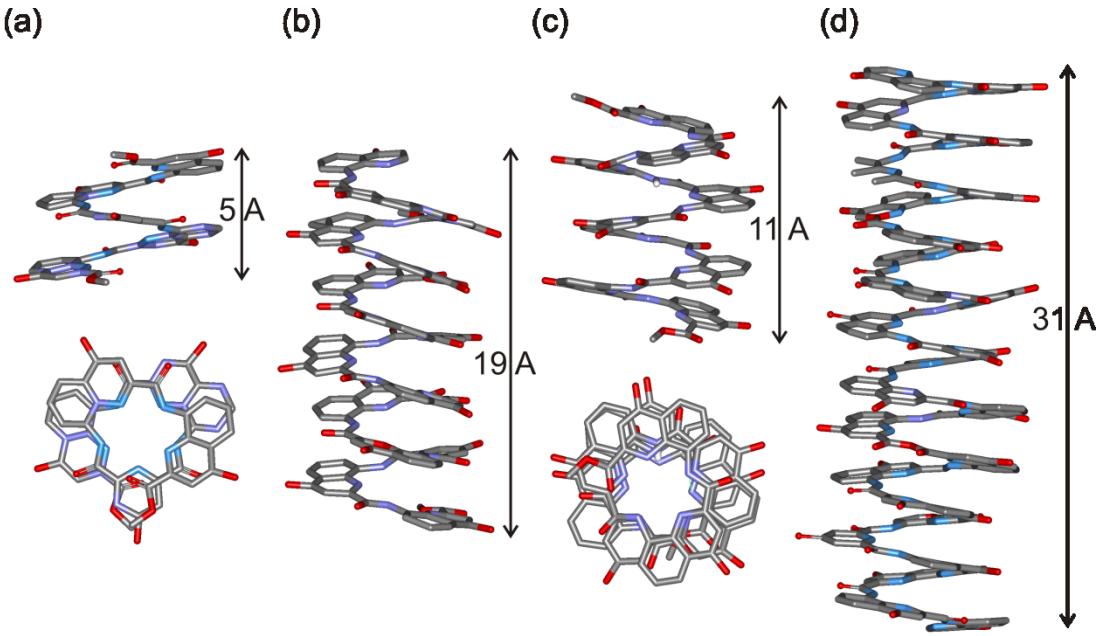

All our efforts in the previous studies demonstrated that stability in aromatic oligoamide foldamers is multi-dimensional, in a sense that it is susceptible to and thus tunable by several parameters. For this reason, further steps towards better understanding of the intrinsic properties of helical foldamers should be done.

- Concerning the effect of aromatic composition, several modifications can be done to these systems that may allow a wider perspective and better understanding of the factors governing folding in aromatic oligoamide foldamers. This would enable the design of molecules with strictly predefined properties:
  - The central diamine can be replaced with a diacid to explore if the polarity of the helical segments has an effect on the stability of the helical architecture.
  - Several other monomers that are used in aromatic foldamer synthesis, such as fluoro-quinoline, anthracene and naphthyridine, can be individually tested to evaluate their unique helical propensity within different backbones.

- Disulfide bridges demonstrated inadequacy to fully inhibit helical dynamics. For this reason they could be used as versatile tools providing insights towards the racemization process in aromatic oligoamide foldamers. Stapling longer and more complex helices in different places can provide structural information about the processes of folding and unfolding

  Additionally, kinetic studies carried out on a mixture of thiol-bearing foldamers (in theory capable of forming several different disulfide bonded species) demonstrated that this class of compounds could be potentially used for the generation of DCLs,

whose characteristics would depend on the properties of the foldamers involved. However, the complexity of the resulting systems could be a limiting factor.

- The anhydride functionality was shown to be a useful linker in the design of the segment tripling strategy enabling the generation of helical rods with polymeric dimensions.
    - Modification of the side chains could possibly resolve solubility problems and result in the successful synthesis of helical nano-sized strings with potential use in materials science.
    - More complex materials can be formed by introducing a different diacid at each coupling step. Materials in which molecules interact with each other to generate networks can be used to make thin films with tunable properties. Additionally such materials can also be tested for their potential application as drug delivery scaffolds.

Titre : Synthèse et étude des relations structure-stabilité de foldamères aromatiques hélicoïdaux

Au niveau moléculaire, les fonctions des motifs hélicoïdaux sont souvent associées à la stabilité de ces architectures. Par exemple, lorsqu'une hélice α est isolée de la structure tertiaire des protéines, celle-ci devient alors flexible et perd son activité. Afin de contrôler la rigidité de ces architectures, différentes approches ont été proposées dont la construction d'édifices moléculaires repliés de façon contrôlée : les foldamères. Notre équipe s'intéresse aux foldamères d'oligoamide aromatique hélicoïdaux et à l'heure actuelle plusieurs études ont déjà été menées afin de comprendre les facteurs influant la stabilité de telles hélices: la longueur de l'oligomère, le solvant et l'effet de l'introduction d'un espaceur aliphatique dans la séquence. Lors de ce travail nous nous sommes tout d'abord intéressés à la capacité de repliement de cinq monomères aromatiques couramment utilisés pour la préparation de foldamères. Leur contribution dans la stabilité hélicoïdale du système a été évaluée par RMN, diffraction des rayons-X et HPLC chirale dynamique. Inspirés par le rôle des ponts disulfure dans les protéines, nous avons décidé d'explorer l'effet d'une telle liaison sur la stabilité des hélices d'oligoamide aromatique. Deux composés contenant une liaison disulfure intramoléculaire ou deux liaisons intermoléculaires ont été synthétisés et leur stabilité étudiée par RMN, HPLC Chiral et Dichroïsme circulaire.
Enfin, la synthèse d'hélices moléculaires de grandes dimensions (assimilables à celles de polymères monodisperses) a été réalisée par une approche convergente de triplement de longueur de segment *via* la formation de liaisons anhydrides entre blocs oligomériques.

Mots clés: Chimie supramoléculaire, Foldamères, Oligoamides aromatiques, Auto-organisation, Stabilité hélicoïdale, Liaison hydrogène, Pont disulfure, Anhydride, Chiralité

Synthesis and structure-stability relationship of Aromatic Helical Foldamers

At the molecular level, the functions of helical patterns are often directly associated with the stability of these architectures, (in α-helices). For example, upon removal of such an entity from the protein's tertiary structure, the peptidic helix becomes flexible and thus inactive. In order to control the rigidity of these architectures, several strategies have been used and the construction of completely artificial well folded molecules known as foldamers is one them. Our group mainly focuses on helical aromatic oligoamide foldamers and to date several studies have been carried out to investigate factors affecting the helical stability; the influence of oligomer length, solvent effects and the effect of aliphatic linkers within a helical aromatic sequence.
In the present study we investigate the helical propensity of five commonly used aromatic monomers in foldamer synthesis and by using NMR spectroscopy, X-ray crystallography and dynamic chiral HPLC we evaluate their contribution in helical stability. Additionally, inspired by the role of disulfide bonds in proteins we decided to explore their effect on helical stability. For this reason intra- and inter-molecularly disulfide bonded compounds were designed and synthesized. Their stability was studied using NMR spectroscopy, chiral HPLC and CD experiments.
Finally, the synthesis of mono-disperse helical strings of polymeric dimensions through a convergent, segment tripling strategy has been developed. This protection/deprotection free synthesis was carried out by connecting oligomeric blocks *via* a labile anhydride functionality.

Keywords: Supramolecular Chemistry, Aromatic Oligoamide Foldamer, Self-organization, Helical stability, Hydrogen bond, Aromatic composition, Disulfide bond, Anhydride, Chirality

Unité de recherche

Institure Européen de Chimie et Biologie (IECB)
Chimie et Biology des Membranes et Nanoobjects (CBMN)

2 rue Robert Escarpit, 33607, PESSAC CEDEX